Structural modifications, metal coordination and self-assembly of quinoline oligoamide foldamers

Jinhua Wang

université de BORDEAUX

THÈSE PRÉSENTÉE

POUR OBTENIR LE GRADE DE

DOCTEUR DE

L'UNIVERSITÉ DE BORDEAUX

ÉCOLE DOCTORALE DES SCIENCES CHIMIQUES

SPÉCIALITÉ CHIMIE ORGANIQUE

Par Jinhua Wang

Modifications structurales, coordination de métaux et auto-assemblage de foldamères d'oligoquinolines carboxamides

Sous la direction de : Ivan HUC & Victor MAURIZOT

Soutenue le 18/07/2019

Membres du jury :

M. BUCHER, Christophe	Directeur de Recherche CNRS, ENS de Lyon	Président du jury
M. CANEVET, David	Maître de conférences, Université d'Angers	Rapporteur
M. HUC, Ivan	Professeur LMU Munich	Examinateur
M. MAURIZOT, Victor	Chargé de Recherche CNRS, Université de Bordeaux	Examinateur

Titre : Modifications structurales, coordination de métaux et auto-assemblage de foldamères d'oligoquinolines carboxamides

Résumé : Les foldamères d'oligoquinoline carboxamide forment des structures hélicoïdales en solution et dans le solide. Ces structures sont stabilisées par liaisons hydrogène, empilement aromatique et interactions électrostatiques. Dans une première partie de ce manuscrit, les fonctions amide connectant les unités quinolines ont été substituées par des fonctions vinylène, isostères de celles-ci. Ces composés quinolynènes-vinylènes, seuls, forment principalement des structures étendues en solution. Toutefois lorsque ces nouvelles unités sont en faible proportion au sein de l'oligomères contenant principalement de connections amides, des architectures hélicoïdales ont pu être obtenues. Dans une seconde partie, des ions Cu (II) ont été introduits au centre des hélices d'oligoquinoline carboxamide. Ces ions sont liés aux atomes d'azote des quinolines, et à ceux des fonctions amides après leur déprotonation. Une organisation linéaire de ces ions a été observée dans le solide. L'auto-assemblage d'hélices, en faisceaux, par empilement aromatique d'unités acridines portées par les chaines latérales a été entrepris dans une troisième partie de ce manuscrit. De faibles associations ont pu être mises en évidence en solution. Dans le solide ces interactions, bien que faibles, ont permis le contrôle de l'organisation des hélices dans le cristal. Dans une dernière partie de ce manuscrit, la coordination de métaux a été utilisée afin de permettre l'assemblage d'hélices d'oligoquinoline carboxamide. Des ligands acridine et pyridine ont été fixés sur la périphérie de l'hélice de façon à permettre la coordination par des métaux de transition tel que le palladium (II). Ces assemblages d'hélices induits par le palladium, ont été caractérisés par RMN en solution et par diffraction des rayons X dans le solide.

Mots clés : Foldamères, Isostères, Auto-organisation, Chimie supramoléculaire, Coordination de métal, Diffraction des rayons X, RMN

Title : Structural modifications, metal coordination and self-assembly of quinoline oligoamide foldamers

Abstract : Oligo-quinolinecarboxamide foldamers form stable helical structures in solution and in the solid state. These helices are stabilized by hydrogen bonds, π-π stacking and electrostatic interactions. In a first part of this manuscript, vinyl functions have been introduced as isosteres of amides. The resulting quinolylene-vinylene oligomers form mainly extended structures in solution. Helical folded conformations can nevertheless be stabilized by attaching two segments of oligoamides at both ends of an oligoquinolylene-vinylene. In a second part, copper (II) ions have been loaded into the single helices of quinolinecarboxamide foldamers. The copper (II) ions coordinate the nitrogen atoms of the quinoline units and also deprotonated amide nitrogen atoms. A one dimensional alignment of the copper (II) ions was observed in the solid state. In a third part, acridine functionalized foldamers were prepared in order to test their self-assembly into bundles through interactions between aromatic functions at the exterior of helices. Associations of the acridine functionalized oligoamides are weak in organic solution. In contrast, in the solid state, interactions between helices are mainly governed by acridine units. In a fourth part, metal coordination has been used to promote helix-helix assembly of quinoline oligoamides foldamers. Acridine and pyridine rings have been attached on the side chains of these oligomers to allow coordination with metals, palladium (II) in this case. The helix-helix assembly of quinoline oligoamides by palladium coordination has been confirmed by NMR and x-ray diffraction.

Keywords : Foldamers, Isosteres, Self-assembly, Supramolecular Chemistry, Metal Coordination, X-ray Diffraction, MNR

Unité de recherche

UMR 5248, Chimie et Biologie des Membranes et des Nano-objets
Institut Européen de Chimie et Biologie (IECB)
2 rue Robert Escarpit 33607 PESSAC

Acknowledgements

First of all, I would like to thank Dr. Ivan HUC for offering me the opportunity to join his lab at that time to start my study in France. The guidance and supports offered by him during this period have made me learn a lot and improve a lot. I also want to thank Dr. Victor MAURIZOT who spends great efforts and enormous amount of time to help me with research and also problems of living in France. Without his endeavors, I won't be able to complete my study and this thesis. The experience of working here with him will be a nice memory of my life. Dr. FERRAND Yann, Dr. FISCHER Lucile, and M. MERLET Eric also helped me a lot and I'm really appreciate them. I also want to thank my collaborators Dr. BASSANI Dario, Dr. Mcclenaghan Nathan and Dr. BUFFETEAU Thierry. Dr. Bassani was always kind and leaded me into the material and physical chemistry related research. Those experiences with them gave me a broader view in science.

I also want to thank Dr. Brice Kauffmann and Dr. Barbara Wicher who solved all the x-ray structures for me. Without their expertise, I wouldn't be able to obtain the results in this thesis. MMe. Axelle Grélard and MMe. Estelle Morvan assisted with NMR measurements which I owe great thanks to them. Dr. Frédéric Rosu and Loïc Klinger offered many helps with mass spectroscopy which I also want to thank them.

Last but not least, I want to thank all the past and present members that I have met in previous HUC's group in IECB and BISE group. The time we spent together not only in labs but also during group events will be a nice memory for me. There are many names, Xiang, Xuesong, Nan, Xiaobo, Markendeya, Pradeep, Daniel, Soumen, Maëlle, Michal, Antoine M., Antoine J., Subrata, Arthur, Sunbum, Albano, Joan, Valentina, Siyuan, Pedro, Daniela, Ko, Aki, Makoto, Sai Reddy, Dragos, Bappaditya, Floriane, Krishnendu, Mathieu, Alice, ChenHao, Victor K., Vincent, Suprahash, Mathilde, Xavier, Camille, Jinqi, Lianjin and those who I might forget. Also, I want to thank many other people that I met here, Jie, Shilin, Cheng, Zhen, Peizhao, Yutaka. The happy time spent with all those people is very pleasant. I also want to thank CSC for granting me the scholarship. Without the financial support, it's not possible for me to finish the study here.

In the end, I want to thank my family who support my study abroad. Their support is the most important thing to keep me continues with my study.

List of Abbreviations

Boc : *tert*-butyloxycarbonyl

C-AFM: conductive atomic force microscopy

COSY: correlated spectroscopy

CPK : Corey, Pauling, Koltune space filling

DCM : dichloromethane

DIPEA or **DIEA** : diisopropylethylamine

DMF : *N*,*N*-dimethylformamide

DIAD: Diisopropyl azodicarboxylate

DOSY: Diffusion ordered spectroscopy

EDC : N-(3-Dimethylaminopropyl)-N'-ethylcarbodiimide hydrochloride

ESI: electrospray ionization

GPC : Gel Permeation Chromatography

Ghosez reagent : 1-chloro-*N*,*N*,2-trimethyl propenylamine

HRMS : high resolution mass spectroscopy

Me: Methyl

MeOH : methanol

MMFFs : Merck Molecular Force Field static

NaOH : sodium hydroxide

NMR : nuclear magnetic resonance

NOESY : Nuclear Overhauser Effect SpectroscopY

PPh_3: Triphenyl phosphine

ppm : parts per million

r.t.: room temperature

TFA : trifluoroacetic acid

THF : tetrahydrofuran

TLC : thin layer chromatography

Table of Contents

General Introduction

Proteins rely on their particular structures, not only the primary compositions but also sophisticated higher order structures, to perform the functions they carry out. Helices, strands and turns are major secondary structural motifs found in proteins. Tertiary and quaternary structures are assembled from those secondary structural motifs through either covalent or non-covalent linkages. The stability of those structures depends on their primary chemical sequences and environments. Synthetic compounds that form structures akin to those found in proteins are interesting not only to expand the tool-box to create various types of structures but also to enable new possibilities towards useful functions. Foldamer chemistry is such a branch of science that investigates the structures of synthetic oligomers.

Over the past few decades, numerous synthetic oligomers have been found to adopt folded conformations in solution and also in solid state. Those oligomers include derivatives from natural building blocks and completely artificial blocks. Structures motifs such as helices, sheets have been found in those oligomers. Tertiary and quaternary structures have also been created. The developments in foldamers have already enabled structural based design to achieve certain functions such as iterative evolution towards selective sugar binding.

In the Huc group, aromatic oligoamide-based foldamers have been constantly pursued. Various monomers of different covertures and diameters have been developed which allow structural evolution of foldamers. Both side chains and main chain can be tuned for the purpose needed. Hydrophobic, hydrophilic, anionic or cationic side chains are all subjected of choices. Diameter and shapes of the foldamers are modulated by the selection of monomers. Depending on the monomers used, single, double or even quadruple helix can be formed. Assemblies of helical foldamers either by covalent bonding or non-covalent interactions have been demonstrated. Developments towards functions such as mediation of electron transport between electron donor and electron acceptor have been demonstrated.

In this thesis, modifications of quinoline oligoamide foldamers towards creating new modes of foldamers and side chain functionalization towards foldamer assemblies have been

described. This thesis is written as following 5 chapters.

Chapter 1 is a short review about foldamers with special attention paid to recent developments towards application in materials and so on. Applications of foldamers as electron transport mediator, self-assembly materials, artificial channels, catalysts, guest recognition and circular polarized luminescence have been surveyed. This short review serves to provide a general background towards materials-oriented applications of foldamers.

Chapter 2 discusses vinylene double bond isosteres of quinoline oligoamide foldamers. Oligomers of quinolylene-vinylene alone do not show strong propensity to form helical folded structures in organic solution. The helical folded conformation, however, can be stabilized by attachment of two segments of oligoamides at both ends.

Chapter 3 shows copper ions can be loaded into single helical quinoline oligoamides. A series of oligomers loaded with copper (II) ions have been synthetized. The copper ions coordinate with nitrogen atoms inside the helices and small structural variations observed.

Chapter 4 discusses the self-organization of acridine functionalized quinoline oligoamide foldamers. Acridine was introduced as side chains which enable π-π interactions between them. The interactions between acridines allowed association of helical foldamers in the solid state. The packing of helices in the solid was strongly guided by acridine units.

Chapter 5 discusses the self-assembly of helical foldamers through metal coordination. Acridine and pyridine units are introduced on the side chains. Upon complexation with palladium (II) ions, helix-helix assemblies have been demonstrated. Due to handedness of the helices and relative orientation of the helices, four possible stereoisomers are observed. By introducing C2 axis into the helices or fixation of the handedness, the possibilities of stereoisomers are reduced.

NB: Each chapter constitutes a distinct scientific topic which can be considered individually. Therefore, this thesis was written as chapters that can be potentially developed into scientific publications. The numbering of sections, figures and references is also restarted in each chapter.

I Recent Developments of Foldamers towards Applications

1.1 Introduction

Foldamer was defined by J. S. Moore as any oligomer that folds into a conformationally ordered state in solution and the structures of which are stabilized by a collection of noncovalent interactions between nonadjacent monomer units.[1] This definition of foldamer emphasizes several aspects about foldamer: 1) foldamer is a chain molecule of several repeating monomers; 2) the ability to fold which implies the conformational dynamics; 3) a small set of conformations has much lower energy than any other reachable conformations; 4) noncovalent interactions are important factors to stabilize the folded conformation and 5) the folded conformation is preserved in solution. Although this definition of foldamers limits the scope to oligomers, helical polymers which have helical structures are considered as a class of foldamers under a broader view point.[2] Another definition of foldamer was given by S. Gellman as any polymer with a strong tendency to adopt a specific compact conformation.[3] This definition includes polymers as foldamers and uses the conformations preferences as main factors to classify a compound as a foldamer or not. As both definitions pointed out, foldamers concern with the structures/conformations and the interactions involved.

Foldamers are considered to be at the interface of covalent and noncovalent chemistry where synthetic efforts to bring the chain molecules and careful control of a collection of intra/intermolecular interactions to bring the folded conformations joint together. Noncovalent interactions such as hydrogen bonds, van der Waals interactions (such as dipole-dipole interactions), electrostatic forces, and π-π stacking work synergistically to drive the folding. Solvophobic effect, hydrophobic effect in particular, is also an important factor involved in the folding. Metal coordination is also used as stabilizing force of foldamers.

Foldamer is inspired by the naturally occurring higher order structures such as helices, sheets and turns found in proteins and nucleic acids. As mimics of peptide structures, peptidomimetics constitute a large family of foldamers. This type of foldamers includes α-peptide, β-peptide, γ-peptide and δ-peptide. Peptoids, azapeptides, azatides, vinylogous

peptides also fall into this category. These foldamers are largely based on the modification of bio-macromolecules or derived from biological systems which also called “top-down” approach of foldamer design. Another family of foldamers is called abiotic foldamers which is based on the “bottom-up” design strategy in which arylamide, oligohydrazide, phenylene ethynylene are included. A simple classification of foldamers into aliphatic and aromatic can be drawn based on aromatic units used or not in the backbone.[4] Foldamers based on “top-down” approach fall often into the aliphatic class where a large number of “bottom-up” designed foldamers belong to aromatic category.

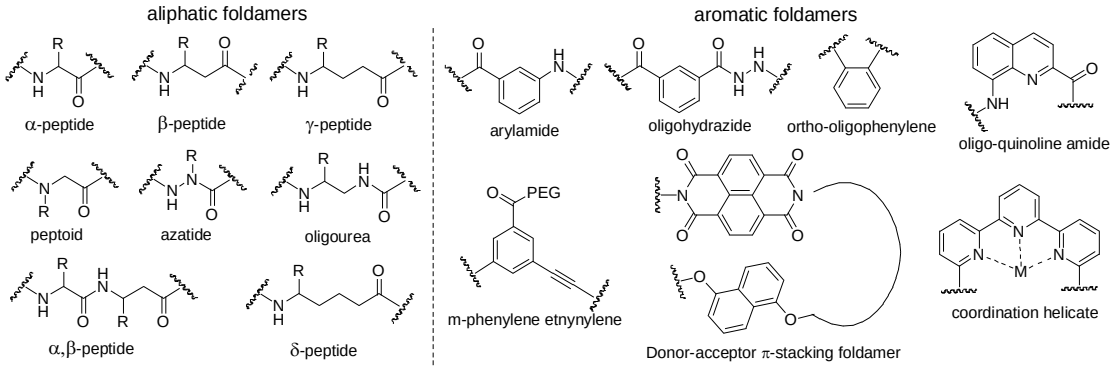

Figure 1-1: Examples of repeating units of aliphatic and aromatic foldamers.

Design, identification and characterization of chain molecules that fold into specific compact structures in solution are central parts of foldamer chemistry. During the past decades, many synthetic oligomers have been found to adopt folded structures akin to the secondary structures of proteins. Tertiary and quaternary folds of oligomers were also developed.[5,6] The vast knowledge accumulated along the path certainly advances the field further. Foldamers with more and more complexed structures have been successfully prepared and applications of foldamers attract more and more attentions. Here, recent progress of the foldamers will be described and the applications of foldamers especially applications towards materials will be stressed.

1.2 Electron transfer across foldamer bridge

Photosynthesis which converts solar energy into chemical energy is the essential source of the energy flowed through biological systems. During photosynthesis, the solar energy

absorbed by chromophores (antenna chlorophylls in photosystem II for instance) in photosynthesis systems is transferred to the reaction center which catalyzes the splitting of water to convert the solar energy to chemical energy and finally stored as carbohydrates.[7,8] The success of this process relies on the long range electron transfer in proteins after photo excitation and charge separation. The detailed mechanism of how electron transport in proteins attracts great attentions due to its importance. Chemical mimics of that process have also been extensively made to study the electron transfer in order to accomplish artificial photosynthesis for the production of renewable energy from solar energy.

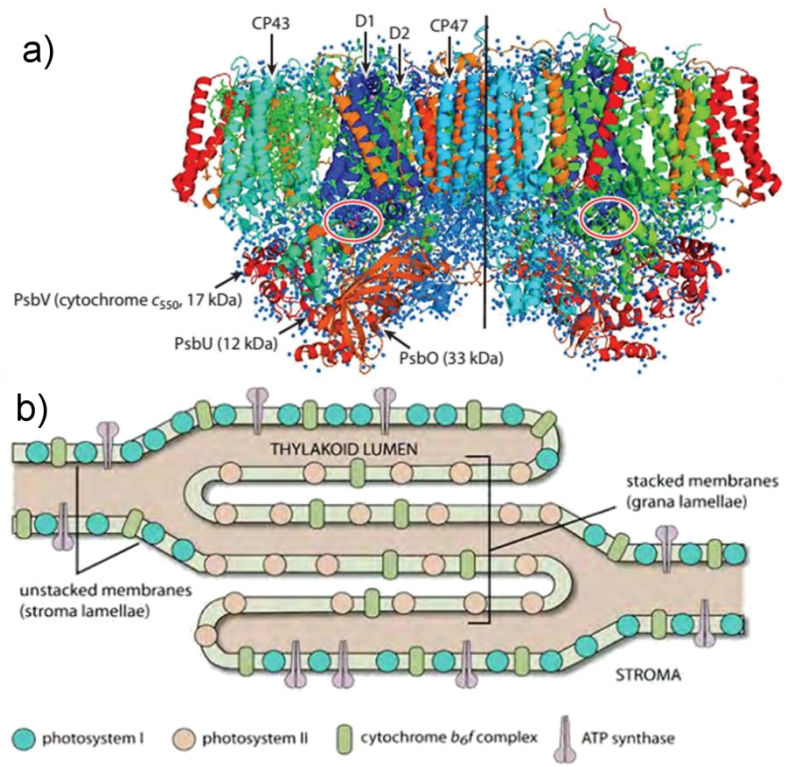

Figure 1-2: a) Crystal structure of photosynthesis system II[9] and b) Spatial arrangements of photosynthesis systems within the thylakoid membrane[10].

Usually, the molecular system that mimics the charge separation and electron transport in photosynthesis comprises electron donor, acceptor and bridge known as donor-bridge-acceptor (D-B-A) dyad. The bridge serves dual role as structural motif to organize the chromophores at well-defined distances and orientations, and as a medium to modulate the electron transfer. The electron transfer rate (k_{et}) is empirically considered to decay exponentially with distance (r).[11]

$$k_{et} = \exp(-2\beta r)$$

Where β is the attenuation coefficient. The value of attenuation coefficient can be varied depending on the chemical nature of the spacer, such as for proteins (1.0-1.4 $Å^{-1}$), saturated hydrocarbons (0.8-1.0 $Å^{-1}$), DNA (0.2-1.4 $Å^{-1}$) and unsaturated phenylene, polyyne, polyene (0.2-0.6 $Å^{-1}$).[12] The dependence of electron transfer rate on the free energy (ΔG_{ET}^{0}), the reorganization energy (λ), and the electronic coupling (H_{DA}) can be expressed as:[11,13]

$$\kappa_{et} = \sqrt{\frac{\pi}{\hbar^2 \lambda \kappa_B T}} H_{DA}^2 \exp\left(-\frac{(\lambda + \Delta G_{ET}^{0})^2}{4\lambda \kappa_B T}\right)$$

The magnitude of electronic coupling between donor and acceptor decreases exponentially with the distance which results the exponentially dependence of the electron transfer rate on the distance.

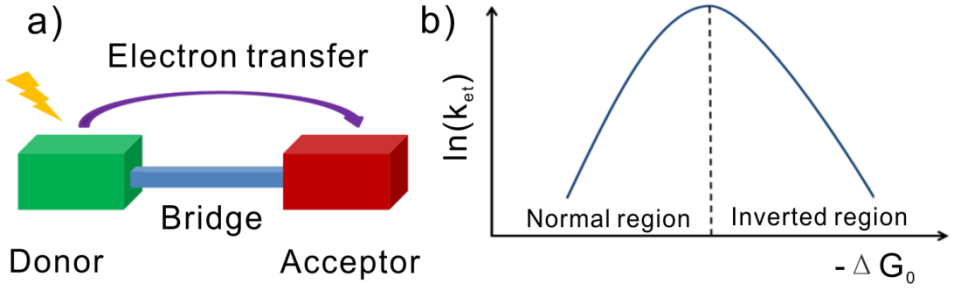

Figure 1-3: a) Cartoon representation of electron transfer between Donor-Bridge-Acceptor system; b) Bell-shaped electron transfer rate dependence on reaction free energy (ΔG_0).

The electron transfer can occur through electron-exchange known as superexchange which is directly relates to the orbital overlap and the energy gap or through oxidation/reduction states involving the bridge known as hopping. The electron transfer through superexchange becomes less important at long distances due to the exponentially dependence on the distance. However, the overall electron transfer rate is not necessary monotonously depending on the free energy as predicted by Marcus theory that inverted region exists (Fig. 1-3b).[13,14] The electron transfer through hopping mechanism is less distance dependent and more effective at long distance.

In the past, many artificial molecular systems[11,15,16] and natural biomolecules such as proteins[17,18] and DNA[19-22] have been studied in order to understand the mechanisms and dependences of the electron transfer rates. For example, the electron transfer through DNA was found to occur through superexchange or hopping mechanisms depending on the energetics of the D-B-A dyad. The superexchange mechanism was only found to occur at

short donor-acceptor distances and at longer distances, hopping mechanism was found to be the major electron transfer process in the Adenine-Thymine (A-T) base pair hairpin motif.[22] Guanine (G) has the lowest ionization potential among four DNA bases (**A**denine, **T**hymine, **G**uanine and **C**ytosine) which makes it the major target during oxidation damage of DNA under oxidative stress and UV irradiation. It was found that electron transfer can occur effectively between the oxidized guanine (guanine radical cation $G^{+\cdot}$ in this case) and guanine rich sequence (GGG for example) at long distance through hopping mechanism where guanines located in between serve as mediation spot.[20]

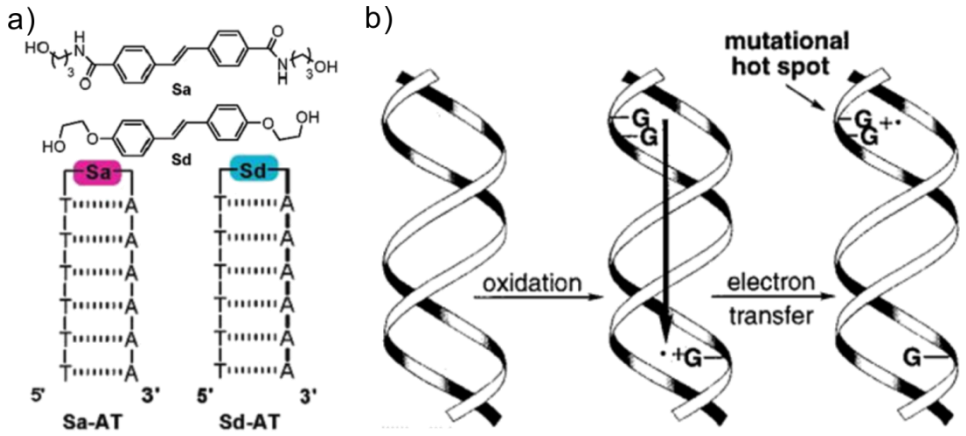

Figure 1-4: a) Stilbene inked A-T hairpin structure motif[22]; b) Electron transfer between oxidized G ($G^{+\cdot}$) and G rich sequence in DNA[20].

The electron transport across quinoline-carboxamide oligomers bridged donor-acceptor dyads was found to be through superexchange mechanism for the short oligomers (oligomers length less than 5 units) but are dominated by hopping mechanism for the oligomers longer than nine by using perylene bis-imide (PB) as acceptor and oligophenylene-vinylene (OPV) as donor.[23,24] It has been found that even if the conjugation through different monomers are relatively weak, the quinoline-carboxamide bridge can mediate very well the electron transport. In a serie of short oligomers, relatively low attenuation coefficient (β = 0.05 Å^{-1}) has been found[23] and for the long oligomers, subnano and nanosecond charge separation as well as long distance over 306 Å charge separation has been found.[24] The electron transfer through quinoline-carboxamide oligomer bridge can be described as a hole injection into the bridge shortly after photoexcitation of PB, the hole hopes along the bridge and is finally trapped by OPV. The charge separated state was found to be very long lived ($\tau > 80\ \mu s$) as

well as the very long life time of charge recombination of triplet state of PB ($\tau > 80\ \mu s$) has been found.[24] In the short oligomers, there are two factors varying between the donor and acceptor: distance and orientation. In the longer oligomers, since the oligomers were chosen to have multiple five units' differences, the orientation of the donor and acceptor was fixed and the only variable was the distance between them.

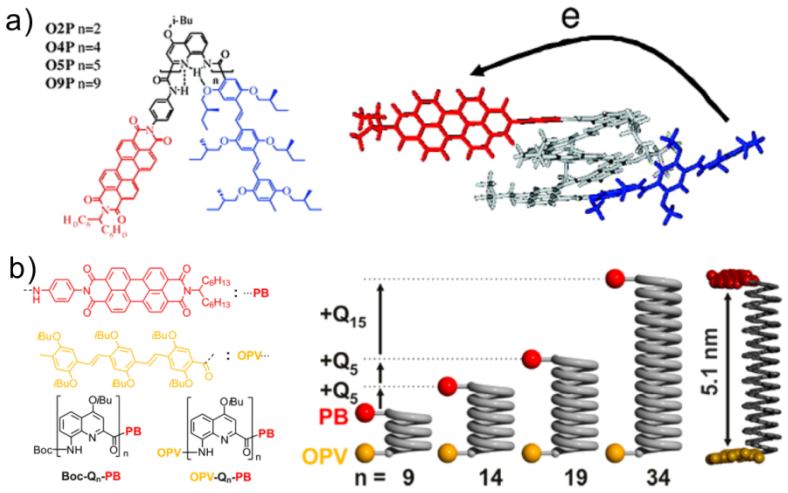

Figure 1-5: a) Photo-electron transfer using short *oligo*-quinolinecarboxamides bridges and b) chemical design of photo-electron transfer with long *oligo*-quinolinecarboxamide bridges.

Direct measurement of electron transfer across *oligo*-quinolinecarboxamide foldamers was realized using conductive atomic force microscopy (C-AFM).[25] Conductive AFM is a technique that is able to measure very small current across a small collection of molecules in contact with the AFM tips. In order to employ this technique, mono-layers of foldamers functionalized with thiol (Fig. 1-6a) were prepared on gold surface. The conductance measured showed increasing resistance with the length of foldamers. The factor of length dependent resistance was found to be small ($\beta = 0.06 \pm 0.015\ \text{Å}^{-1}$) (Fig. 1-6c) which was in accordance with hopping mechanism of the electron transfer across *oligo*-quinolinecarboxamides foldamers. Molecular models revealed that the charge transfer through the foldamers backbone occurred through multiple pathways where through space coupling played more important role than through bond coupling. The horizontal charge transfer through the self-assembled monolayer was not effective and was found to be almost completely insulating.

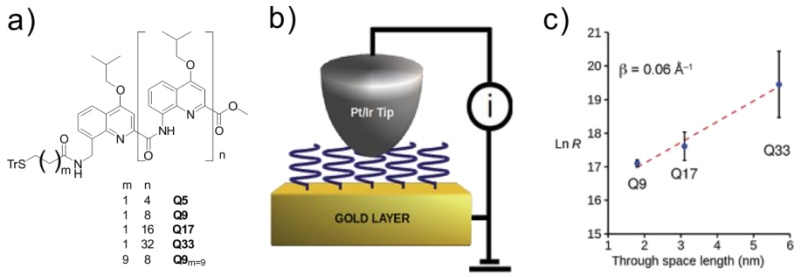

Figure 1-6: a) chemical structures of thiol functionalized oligo-quinolinecarboxamides; b) carton representation of MOM junction prepared using conductive AFM; c) molecular length dependence of vertical resistance (Ω) of **Q9**-**Q33**.

The conductance through other types of foldamers was also measured with C-AFM technique. The electron transfer across oligourea foldamer was investigated using the same method.[26] The oligourea foldamers adopt a 2.5-helix structure as indicated by circular dichroism in solution. Electron transfer across oligourea foldamers showed similar small length depended transfer rate. The distance decay constant (β) is 0.92-0.95 nm^{-1} which indicates electron transport through oligourea via hopping mechanism. Rectification effect, which is the dependence of the electron transfer on the direction of the electron flow in the helix, was observed in oligourea foldamers. Rectification effect normally associates with permanent dipole moment aligned along the direction of electron transfer, i.e. long axis of the helix foldamer. The residue dipole moment of a urea is ~4.7-4.9 D which is bigger than the amide in peptides (~3.5 D). The bigger residue dipole moment is probably the origin of rectification effect observed.

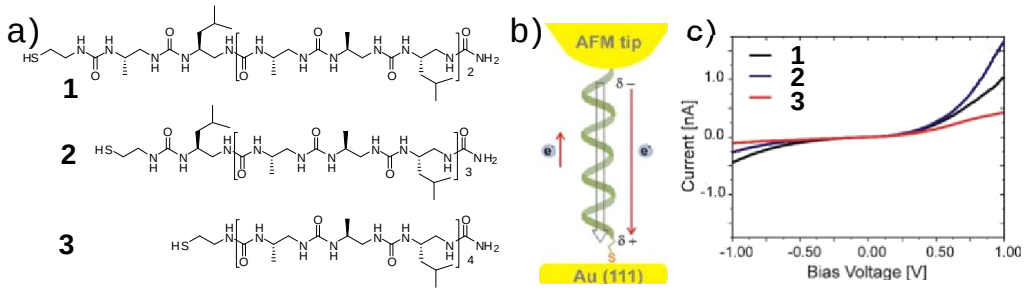

Figure 1-7: a) Chemical structures of thiol functionalized oligourea foldamers; b) cartoon representation of conductivity measurement with C-AFM; c) rectification effect of conductivity through oligourea foldamers.

The effect of copper ion complexation on the conductivity of self-assembled monolayer of tripeptide Gly-Gly-His (glysine-glysine-histidine) was found to be dependent on the

density of the monolayer used.[27] The conductivity of high density monolayer decreased after complexation with copper ions. On the other hand, the conductivity of low density monolayer increased after copper binding. The observation of two different trends was explained by the different conformation changes after copper binding. In the case of high density monolayer, little space was left for any substantial conformational changes of the Gly-Gly-His tripeptide and an insulating layer was formed after binding with copper ions. The formation of this insulating layer caused the decrease of conductivity. On the other hand, the low density monolayer has enough space to allow conformational changes of the tripeptide. The tripeptide in the monolayer changes its conformation to wrap around the copper ion after complexation which changes the work function and increased the conductivity of the monolayer.

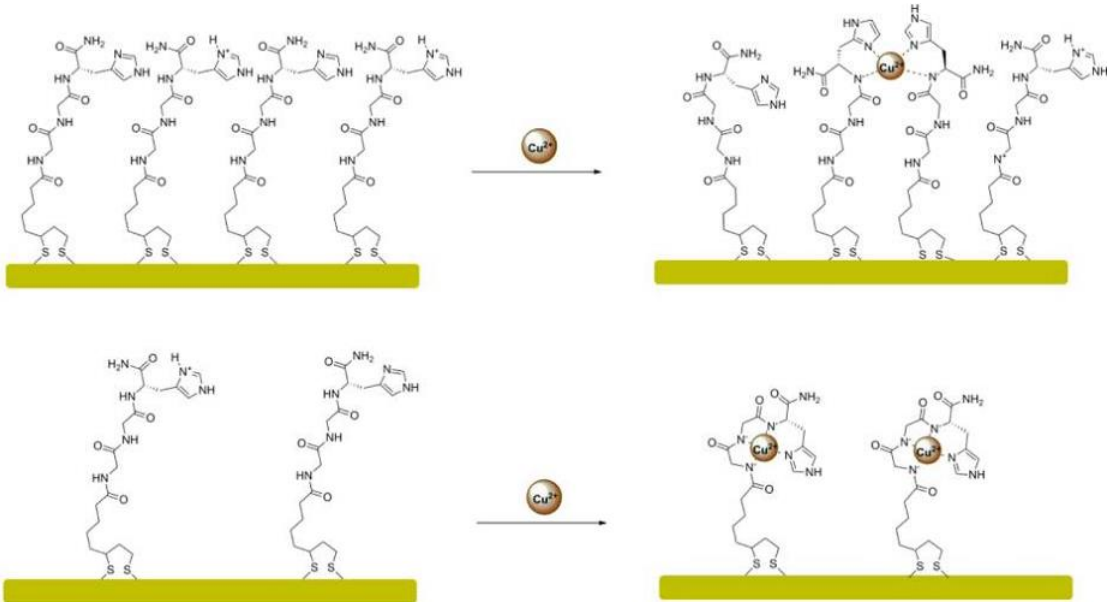

Figure 1-8: The representation of high and low density monolayer of tripeptide Gly-Gly-His and the different conformational changes after complexation with copper ions.

Chirality dependent electron transfer was observed in D/L-12mer peptide Cya-[(D/L-Ala)$_3$-Aib]$_3$-(D/L-Ala)$_2$ (Cya = cysteamine; Ala = alanine and Aib = aminoisobutyric acid).[28] Ferrocene was attached at the N-terminus of the peptide as an electron donor or acceptor depending on the potential applied. When a magnetic field was applied to the self-assembled monolayer of D/L peptide on gold, opposite dependence of the conductivity on the magnetic field was observed. For the D-peptide, the conductivity is about four times smaller when the magnetic field is up than the magnetic field is down. While for

the L-peptide, it is the opposite. The observation of the magnetic dependence on the rate of electron transfer was explained by the magnetization of the system and the spin selective electron transfer through the chiral peptide. The magnetization of the system was confirmed by a ferromagnetic response of the SAM on gold. The spin dependent electron transfer of a chiral molecule is called chiral induced spin selectivity (CISS)[29] which allows the electron with preferred spin to be transferred faster while the electron with opposite spin is transferred slower. In this system, both the magnetic moment of the gold substrate and the ferrocene are parallel to the molecule axis and therefore the electron injected into the peptide has the spin orients to the same direction. Because of the CISS effect, the L-peptide prefers the electron to be transfer through one direction while the D-peptide prefers the opposite direction.

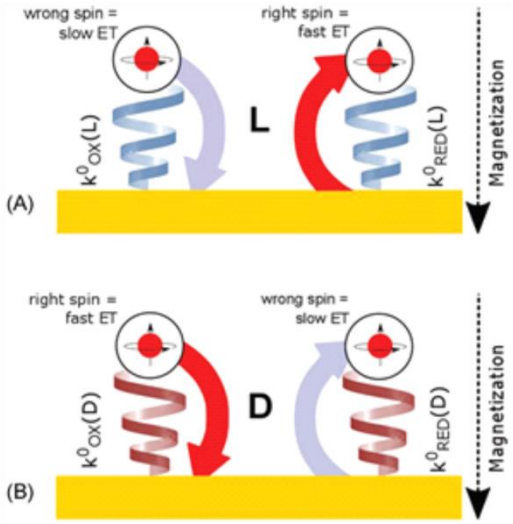

Figure 1-9: Cartoon representation of the asymmetric electron transfer of chiral peptides when magnetic field is applied. The gold is magnetized by the magnetic field which caused the electron with one spin is injected preferentially to the molecule than with the other spin. A) In the case of L-oligopeptide (right handed helix) the electron injected from the gold has a spin aligned parallel to the electron's velocity, which is the preferred spin for the electron transfer. As a result, the electron transfer in this direction (reduction process) is faster than backward. B) In the case of D-oligopeptide (left handed helix), the preferred spin orientation is antiparallel to the electron's velocity; therefore the preferred rate is for the oxidation process.

1.3 Self-assembled nano/macro-materials

1.3.1 Organization in the solid (bulk)

Virus usually has a shell formed by tightly assembled proteins at the surface which served

as protection for the inner nucleic acids. Tobacco mosaic virus, for instance, has a rod like appearance with a capsid made by self-assembly of 2130 copies of proteins. The proteins of the capsid form a helical rod which wrap around the nucleic acid inside.[30] Inspired by the fascinating nano-structures/materials formed by self-assembly of proteins, it is interesting to use self-assembly of proteins/peptides or foldamers to obtain novel nanomaterials. The self-assembly of foldamers to form various types of architectures has been extensively studied by Hee-Seung Lee and co-workers that they named foldectures.[31] Different shapes of nano/micro-objects were obtained by self-assembly of foldamers. Windmill-shaped supramolecular architectures were formed by self-assembly of $ACPC_7$ (ACPC = trans-(S,S)-2-aminocyclopentanecarboxylic acid) heptameric foldamer in distilled water alone. And the shape can be tuned by addition of a nonionic surfactant P123 (Pluronic P123, $(ethylene\ glycol)_{20}$-$(propylene\ glycol)_{70}$-$(ethylene\ glycol)_{20}$). The size distribution of the formed structures was very narrow which is interesting for preparation of homogeneous nano/micro sized materials. Other foldamers such as BocNH-$ACPC_6$-OBn (**4**),[32] BocNH-$ACPC_6$-OH (**5**),[33] BocNH-$(Aib\text{-}ACPC)_3$-Aib-OBn (**6**),[34] BocNH-$(Aib\text{-}ACPC)_3$-OBn (**7**)[35] and BocNH-$ACPC_6Leu_2$-OBn (**8**)[36] were also found to form specific structures as showed in the bellow figure. Detailed analysis of the structures revealed the foldamers formed pseudo-continues packing along the long axis of the helix or formed zigzag alignment along the long axis. Noncovalent interactions between the helices allow the foldamers to align at the same plane in an antiparallel organization.

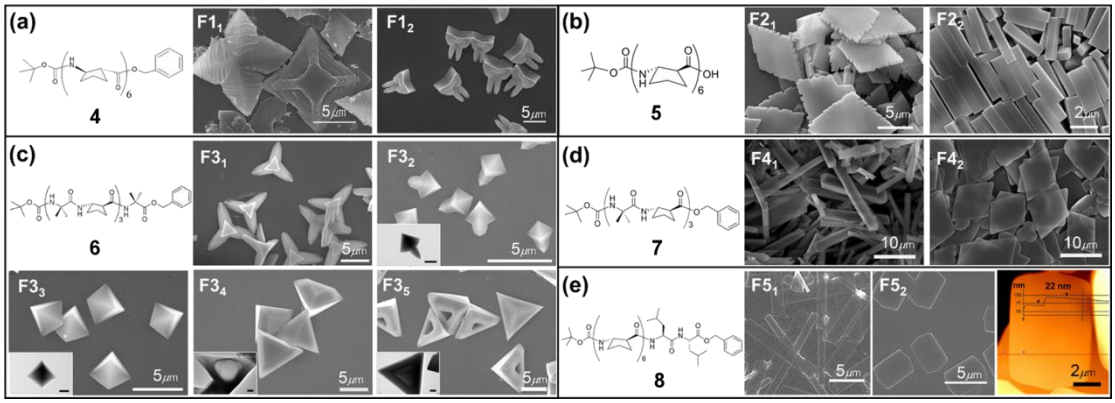

Figure 1-10: Various microstructures formed by self-assembly of foldamers; a)-e) Chemical structures of the foldamers **4**-**8** and the SEM images of the structures formed.

The nano/micro structures formed by self-assembly of foldamers were found to be able to

respond to magnetic field. Usually diamagnetic molecules do not show any effects under magnetic field due to thermal relaxation and random Brownian motion that cancelled the overall magnetic dipole. In order to observe magnetic effects of diamagnetic molecules, ordered alignments of the molecules are necessary to preserve the diamagnetic anisotropy of the materials. Peptide **9** (BocNH-ACPC$_6$-OH) forms rhombic rods and peptide **10** (BocNH-ACPC$_8$-OBn) forms rectangular plates upon injection of the peptide solutions in THF into water containing surfactant P123. When static magnetic field was applied to the aqueous suspensions of these two foldectures, the alignments of the foldectures were observed. The longitudinal axis of rhombic rods of peptide **9** aligned parallel to the magnetic field (Fig. 1-11c) while the rectangular plates of peptide **10** aligned parallel to the magnetic field along their minor axes (Fig. 1-11d). The alignments of the foldectures were due to ordered organization of the diamagnetic dipole moment along the crystalline axes that the overall magnetic moment was not cancelled. Macroscopic movement was achieved also by incorporation of the foldectures into hydrogels as a potential application of those materials.

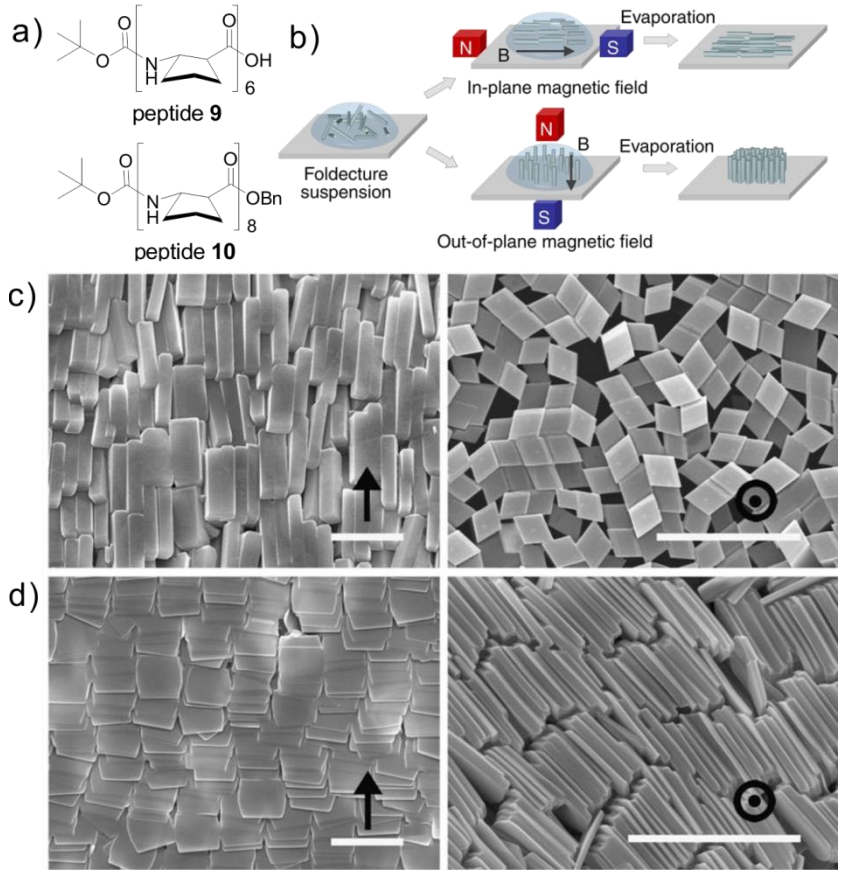

Figure 1-11: a) Chemical structures of ACPC peptides **9** and **10**; b) illustration of magnetic field directed alignments of foldectures; c) SEM images of rhombic rod foldectures deposited on Si

substrates under (left) in-plane magnetic field and (right) out-of-plane magnetic field; d) SEM images of rectangular plate foldectures deposited on Si substrates under (left) in-plane magnetic field and (right) out-of-plane magnetic field. Arrows and circles indicate direction of magnetic field. Scale bars, 5 μm.

1.3.2 Organization on surface

A triaxial supramolecular weave was achieved by self-assembly of perylene-monoimide (PMI) functionalized oligoprolines reported by H. Wennemers and co-workers.[37] Oligoprolines forms a helical structure of three units per turn with a increment of 9 Å along the axis. Perylene-monoimide forms strong aggregates due to large flat aromatic surface which enables π-π interactions. The compound was designed to have the PMIs separated by seven monomers so that the two PMIs are on the same side of the helix of oligoproline. The distance between the PMIs is estimated to be 18 Å based on the helical structure of oligoproline. The self-assembly of this system occurred when water was added into the solution in THF. Highly ordered flat hexagonal structures were formed as observed by transmission electron microscopy (TEM) and atomic force microscopy (AFM). The diameters of the hexagonal structures exceed 1 μm and the heights exceed 100 nm. A regular mesh-like superstructure was observed under higher magnification TEM which has regular hexagonal holes with diameters around 3.0 nm. Detailed analysis of the self-assembled structures reveals that the molecules form head-to-tail π-stacking. It was found out that CH-π interaction in additional to the π-π interactions between the PMIs was important factor to form 60^{o} intercalation of two strands of oligoprolines. Due to the weaving, the structures were quite robust as indicated by Young's modulus (~1.7 Gpa was found).

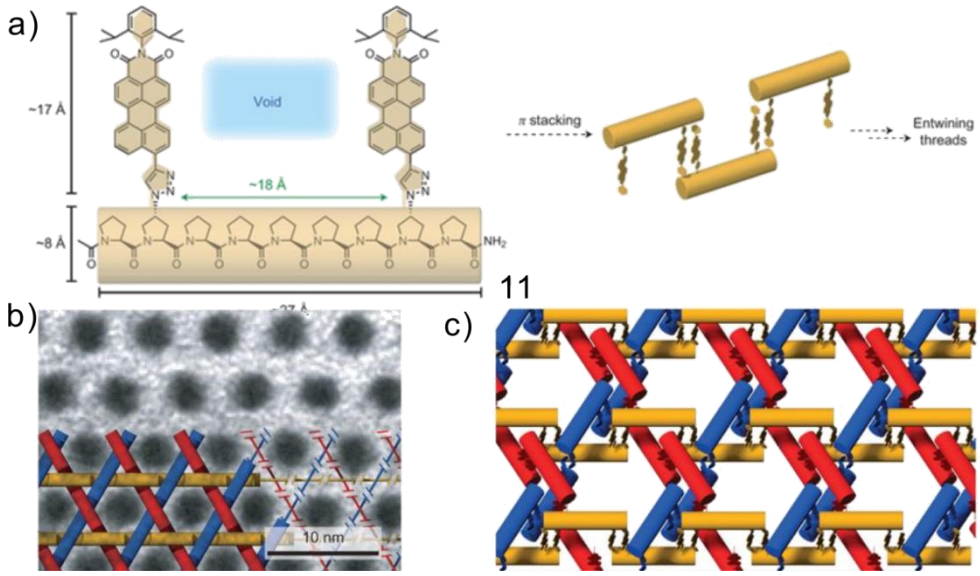

Figure 1-12: a) Chemical structure of the perylene-monoimide functionalized oligoprolines and estimated molecular dimensions and expected mode of self-assembly; b) TEM image of the woven structure and superimposition of proposed molecular organization; c) carton representation of triaxial weave to form the hexagonal structures.

1.4 Foldamer based artificial channels

In nature, the maintenance of ions' concentration inside cell is controlled by groups of membrane pore forming proteins which are able to selectively transport ions out or into the cells. These proteins usually have asymmetric structures with respect to the axis of cell membrane which is essential for governing the direction of ions transport. Inspired by the membrane protein channels as well as the need to develop membranes for practical applications such as seawater desalination, developing water channels and selective ions' channels are interesting. Many foldamers have helical structure with an interior space stabilized by hydrogen bonds which makes them as suitable candidates of channel molecules. Zeng developed extensively oligo-pyridine carboxylic amides foldamers based water channels.[38] In order to avoid labor consuming and low yield synthesis of long oligomers with length over 3.4 nm to across the membrane, "sticky-end" guided stacking of short helical foldamers to form long assembly of helix and to form channels was found to be useful.[39] Oligomer **11** formed nicely assembled 1D channel and a chain of water molecules were aligned inside the channel. Water transporting ability of this channel was supported by size

expansion of large unilamellar vesicles. Osmotic pressure created by pH gradient across the membrane allowed transportation of water though the channel. Alkali metal ions such as Na^+ and K^+ were not transported which might be due to the channels diameter was only around 2.8 Å and lack of interactions to free these ions from their hydration shells.

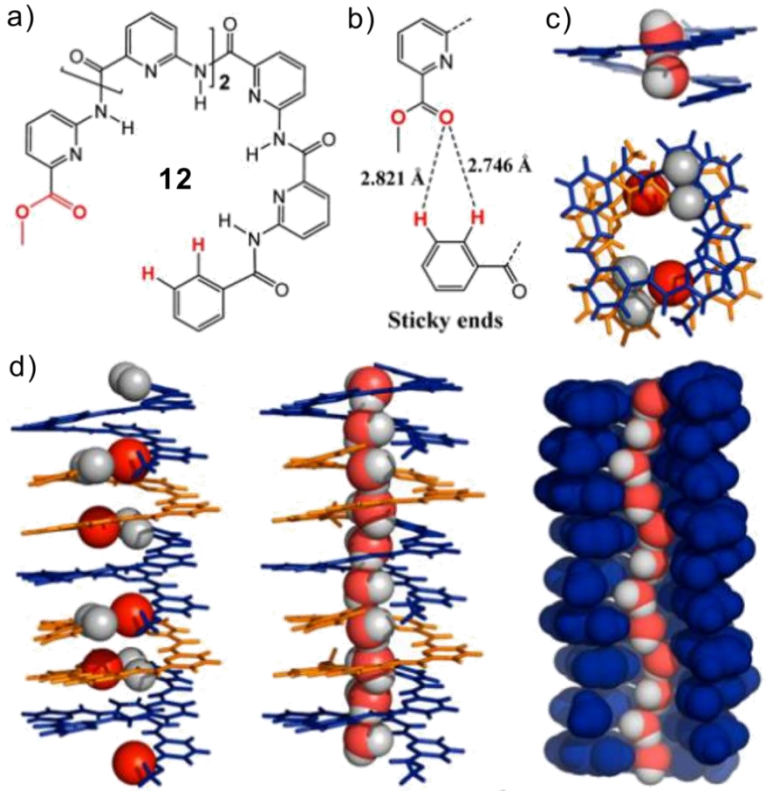

Figure 1-13: a) Chemical structure of foldamer **12**; b) H-bonded "sticky ends" of **12**; c) crystal structure of **12** with water molecules encapsulated in the cavity; d) crystal structure of self-assembled channel of **12** and a chain of water molecules aligned inside the channel.

Similar alignments of helical foldamers were also observed with Indolocarbazole-pyridine (IP) oligomers. These oligomers were also found to form channels with water molecules aligned inside the channels.[40] The IP oligomers formed helical folded structure due to opposite dipoles of the neighboring units and π-stacking interactions. In the crystal structures of hexamer and heptamer, water molecules were found to be enclosed inside the channels of the helices. In the case of heptamer **14**, the stacks of the helices were not aligned and offsets were observed between helices. The helices were packed by alternating P and M helices along the helix axis. An interesting observation was that the hexamer **13** formed a pseudo-continuous helix by aligning one helix on top of another. The water molecules inside the helices were also aligned. The packing of the helices were continuous P

or M of each line of channel. The water or ions transportation performance of this channel was not reported.

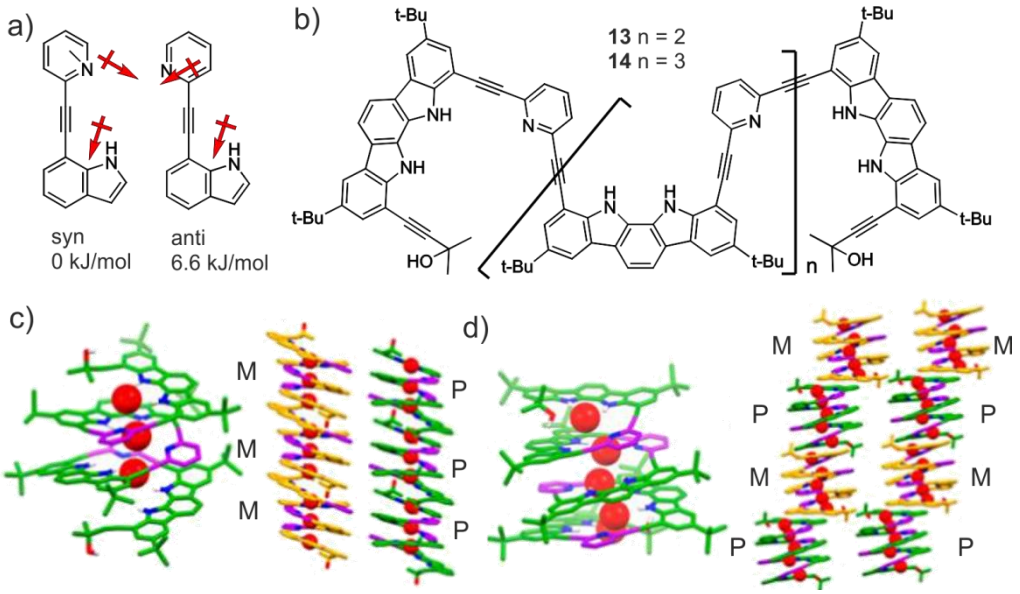

Figure 1-14: a) conformation preference of indolocarbazole–pyridine (IP) conjugates; b) chemical structures of indolocarbazole–pyridine (IP) oligomers **13** and **14**; c) crystal structure of **13** and the channel stacking of single P or M helices in one line with water molecules aligned inside the channels; d) crystal structure of **14** and the channel stacking of alternating P/M helices with water molecules inside the helices.

Helically folded polymers **15** and **16** were also found to form channels.[41] The preparation of these polymers was achieved by post-cyclization of linear polymer precursors. Two polymers with estimated length of 13 and 30 units were tested. The diameter of the polymer channels was estimated to be 5.5 Å which was big enough for hydrated ions to pass through. The ion transport ability were about the same level following the Eisenman sequence III of the ions selectivity ($Rb^+ > K^+ > Cs^+ > Na^+ > Li^+$). Another type of oligomers **17** and **18** were also reported to form channels by the same group.[42] Oligomers **17** and **18** use pyridine instead of 10-methyl-pyrido[3,2-g]quinoline in **15** and **16** as one of the repeating units. The ions selectivity of those oligomers was different to that of polymer **13** and **14**. The following order $Cs^+ \sim Rb^+ > K^+ >> Na^+ > Li^+$ of selectivity was found. It is worth mentioning that the selectivity of K^+ over Na^+ was high (up to 22.5).

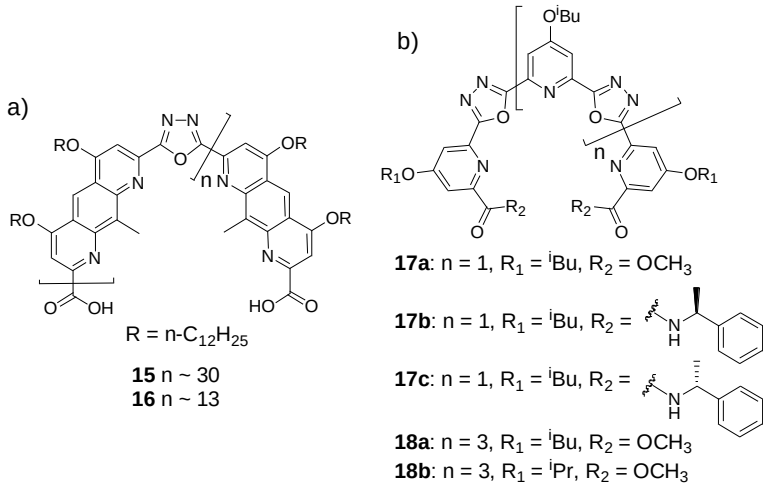

Figure 1-15: Chemical structures of a) helical folded **15** and **16**; b) oligomers **17** and **18**.

1.5 Foldamer catalyst

Enzymes are a class of highly efficient catalysts usually made of proteins and nucleic acids. It is known that multiple interactions with the substrates and specific catalytic pockets are essential for the activity of enzymes. Foldamers are considered to mimic the structures of proteins; it would be interesting to know if foldamers are also able to be designed as catalysts in order to mimic enzymes. Recently, G. Guichard and co-worker reported an excellent example of foldamer-based catalyst (Fig. 1-16).[43] The foldamer catalysts were made from oligoureas which are known to form helical folded structures. The active site of the oligourea catalyst is the urea group at the terminus which is not completely involved in the endo-helical hydrogen bonds networks that stabilize the helical structure of the oligomers. In order to improve the activity of this terminus urea, 3,5-bis(trifluoromethyl)phenyl group was attached at the terminus. Thiourea counterpart was also prepared due to better hydrogen bonding ability. The catalytic activity of the oligourea catalysts was tested for Michael reaction. In the presence of suitable base (DIEA), the oligourea catalysts were able to catalyze Michael reaction with high yields and enantioselectivites. It is remarkable that the turn over number of oligourea catalyst is also very high (over 10^4) which means very small quantity of catalyst is necessary to catalyze the reaction. More importantly, the catalytic activity of the oligourea catalyst can be fine-tuned by structure variations of the oligoureas. The length and sequences of the oligomers can be changed to tune the activity of the catalyst. The ability to fine tune the

foldamers structures offers a unique way to improve and design catalysts.

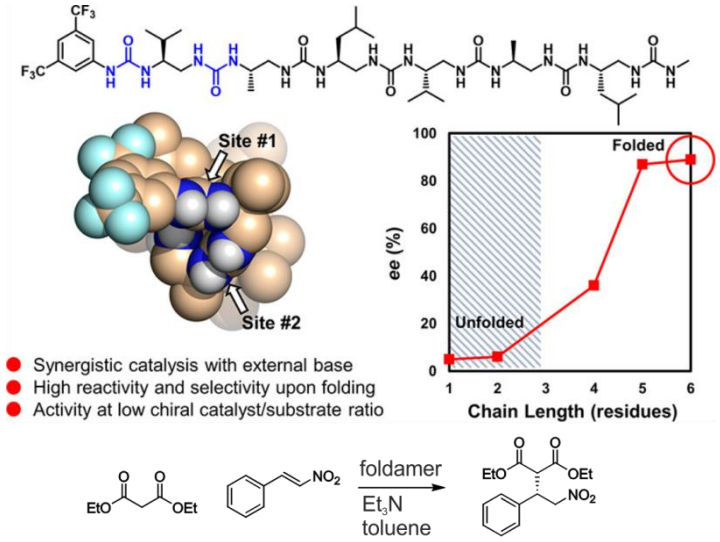

Figure 1-16: Oligourea based highly reactive and enantioselctive catalyst and the model reaction catalyzed by oligourea catalyst.

Another example of foldamer based catalyst was reported by Gellman which also showed the strength of structural modifications of the foldamers to tune the catalytic activities.[44] A serial of oligomers of trans-2-aminocyclopentanecarboxylic acid (ACPC) and 4-amino pyrrolidine-3-carboxylic acid (APC) showed catalytic activity towards aldol reaction (Fig. 1-17). By systematic variation of the positions of the APC residues in the sequences and also inserting α-aminoacids, the catalytic activities were found to vary above 100 times. The APC residue is the catalytic active residue. The distance and angles between two APC residues are tuned by separating them by different units. The catalytic activity of the foldamers is then modulated because the best outcome needs two APC residues to work synergistically to activate the two reactants. The foldamer catalyst with best efficiency was found to be α/β-peptides (1:2 ratio of α and β-peptides) where the two APC residues were separated by 3 residues (peptide **22**). The two active sites (APC residues) are separated by 5.5 Å in space and an angle of 10°. As pointed by the author, the ability of foldamers to access various spatial arrangements of reactive diad will accelerate the searching for optimal arrangements of cooperative catalytic sites. Compared to enzymes which contain hundreds of amino acid residues, foldamer catalysts are simple, yet, they might be a step to understand the origin of enzymes in the prebiotic period.

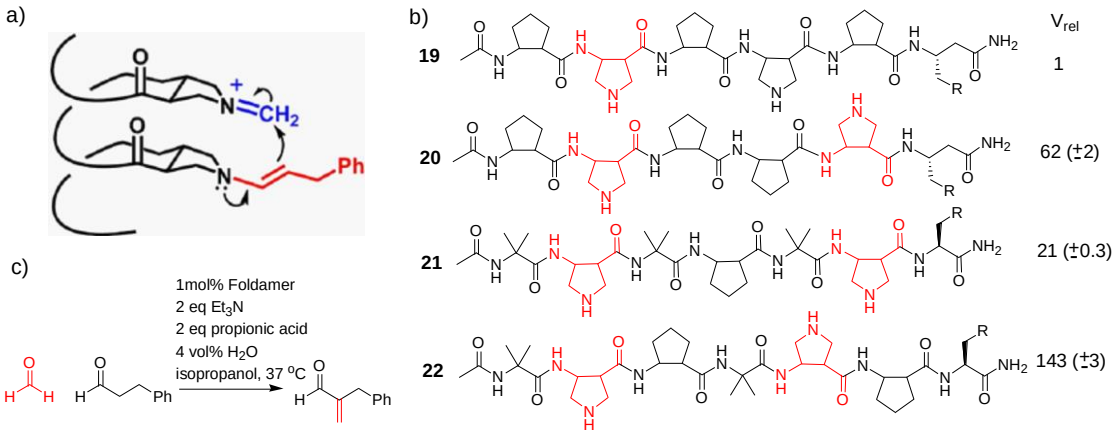

Figure 1-17: a) scheme of the active site of oligo-α/β-peptide catalysts; b) chemical structures of variations of position of active monomer of the oligo-α/β-peptide catalysts and the relative reactivity; c) the crossed aldol reaction catalyzed by these foldamers.

1.6 Some other applications

1.6.1 Foldamer based guest binding

Molecular capsules based on helically folded aromatic amides have been extensively developed in the group.[45] The "capsules" were designed based on the length and angles of different monomers which generate curvature with different diameters. Usually, the monomers that generate small diameters are placed at the terminus position of the oligomers and serve as "caps" to close the capsules. Monomers that generate large diameters are in the middle to create a cavity inside the capsules. Monomers that are able to interact with guest molecules, sugars for instance, are also organized in the middle of the capsule. Those monomers usually form strong hydrogen bonds with the guest molecules. Over the years, capsules of various sizes, binding strengths and selectivity have been prepared. Also structure based design allows for optimizing the capsules for selective binding of one sugar among many others.[46] A very recent example demonstrated the ability to prepare capsules with inner cavity large enough to accommodate disaccharide.[47]

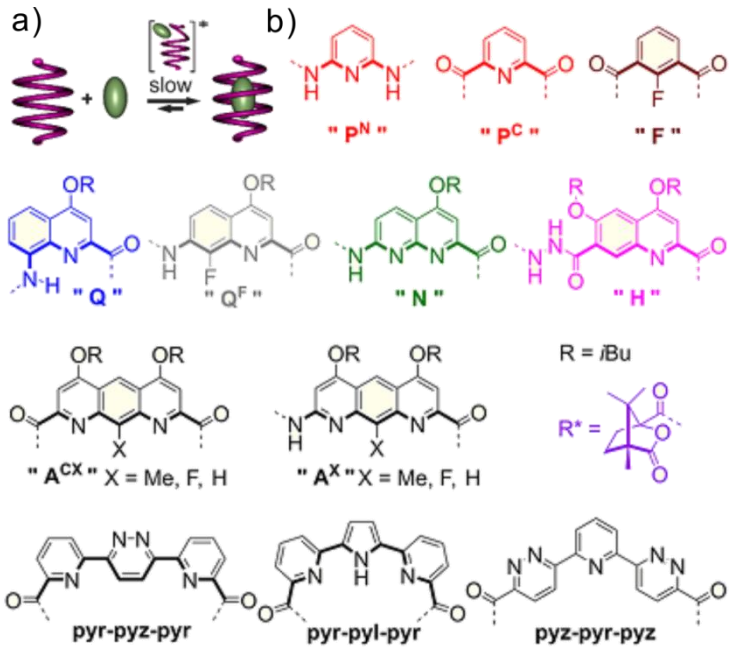

Figure 1-18: a) Capsule like foldamers and binding with guest molecules; b) some typical monomers used in construction of foldamer capsules.

1.6.2 Circularly polarized luminescence of foldamer

Circularly polarized luminescence (CPL) is the emission of light that the intensity of left and right circularly polarized light is different.[48] The difference between left and right circularly polarized light is characterized by anisotropy factor g_{lum} which can be obtained by the intensities of left (I_L) and right-handed (I_R) circularly polarized emissions.

$$g_{lum} = {2(I_L - I_R)}\Big/{(I_L + I_R)}$$

The range of allowed values of g_{lum} is from -2 to +2. The g_{lum} of organic compounds falls in the range of 10^{-5}-10^{-3} which is very small compared to lanthanide complexes (usually within the range of 0.05-0.5). Hence, intense researches were focused on improving the anisotropy factor of chiral organic dyes. Helical folded aromatic foldamers adopt P or M helical structures which might give CPL if enantiomeric pure helices are provided. Indeed, the enantiomeric pure P or M handed foldamers induced by oxazolylanilines showed nice CPL signals.[49] The anisotropy factor was found to be 0.015 which is about one order magnitude higher than usual chiral organic compounds. The $|g_{lum}|$ values of longer oligomers were found

to be higher than the shorter oligomers which might be because of the increased helical aromatic stacks in the longer oligomers.

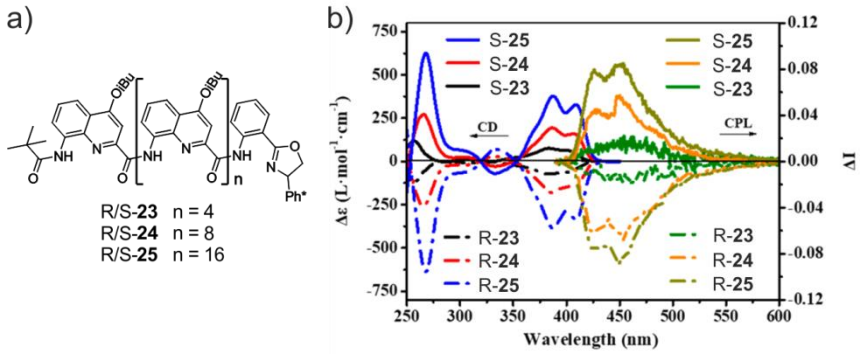

Figure 1-19: a) chemical structures of one handed *oligo*-quinoline carboxamides **23**-**25**; b) CD and CPL spectra of oligomers **23**-**25**.

1.7 Conclusions

The foldamers are inspired by nature. Many abiotic monomers were developed and their oligomers form various types of folded structures such as helix, sheet and turns. Higher structures such as tertiary and quaternary structures of foldamers were also obtained. The developments of new foldamers with functions demonstrate its ability to mimic the structures of proteins. It should not be forget that in proteins, only α-amino acids are used, while a much bigger pool of monomers can be used and developed by chemist. It would be natural to use foldamers beyond what has been seen in proteins and nucleic acids. As described in above the examples of some applications of foldamers, they can play roles in much broader areas such as materials. Predicable structures and structural based designs are among various advantages of foldamers that make them unique candidates of vast applications. Structural based design paves a way to endow functions and also optimizations. Although great developments have been achieved in the foldamers discoveries and applications, still many more questions are pending. How can we achieve large and sophisticated foldamers structures and aggregates akin to the size of proteins through segments assembly? How can the backbone of existing foldamers be modified to endow new functions? How can the foldamers be applied as novel materials? With those questions in mind, we try to develop quinoline carboxamide based foldamers towards materials and new self-assemblies through main chain and side chain modifications.

References

(1) Hill, D. J.; Mio, M. J.; Prince, R. B.; Hughes, T. S.; Moore, J. S. *Chem. Rev.* **2001**, *101*, 3893-4012.

(2) Stefan Hecht, I. H. *Foldamers: Structure, Properties and Applications*, 2007.

(3) Gellman, S. H. *Acc. Chem. Res.* **1998**, *31*, 173-180.

(4) Goodman, C. M.; Choi, S.; Shandler, S.; DeGrado, W. F. *Nat. Chem. Biol.* **2007**, *3*, 252.

(5) Collie, G. W.; Pulka-Ziach, K.; Lombardo, C. M.; Fremaux, J.; Rosu, F.; Decossas, M.; Mauran, L.; Lambert, O.; Gabelica, V.; Mackereth, C. D.; Guichard, G. *Nat. Chem.* **2015**, *7*, 871.

(6) De, S.; Chi, B.; Granier, T.; Qi, T.; Maurizot, V.; Huc, I. *Nat. Chem.* **2017**, *10*, 51.

(7) Brettel, K.; Leibl, W. *Biochimica et Biophysica Acta (BBA) - Bioenergetics* **2001**, *1507*, 100-114.

(8) McConnell, I.; Li, G.; Brudvig, G. W. *Chemistry & Biology* **2010**, *17*, 434-447.

(9) Shen, J.-R. *Annu. Rev. Plant Biol.* **2015**, *66*, 23-48.

(10) Mirkovic, T.; Ostroumov, E. E.; Anna, J. M.; van Grondelle, R.; Govindjee; Scholes, G. D. *Chem. Rev.* **2017**, *117*, 249-293.

(11) Paddon-Row, M. N. *Acc. Chem. Res.* **1994**, *27*, 18-25.

(12) Wasielewski, M. R. *The Journal of Organic Chemistry* **2006**, *71*, 5051-5066.

(13) Marcus, R. A.; Sutin, N. *Biochimica et Biophysica Acta (BBA) - Reviews on Bioenergetics* **1985**, *811*, 265-322.

(14) Brunschwig, B. S.; Ehrenson, S.; Sutin, N. *J. Am. Chem. Soc.* **1984**, *106*, 6858-6859.

(15) Kuss-Petermann, M.; Wenger, O. S. *J. Am. Chem. Soc.* **2016**, *138*, 1349-1358.

(16) Yu, J.; Horsley, J. R.; Abell, A. D. *Acc. Chem. Res.* **2018**, *51*, 2237-2246.

(17) Shih, C.; Museth, A. K.; Abrahamsson, M.; Blanco-Rodriguez, A. M.; Di Bilio, A. J.; Sudhamsu, J.; Crane, B. R.; Ronayne, K. L.; Towrie, M.; Vlček, A.; Richards, J. H.; Winkler, J. R.; Gray, H. B. *Science* **2008**, *320*, 1760-1762.

(18) Wang, H.; Lin, S.; Allen, J. P.; Williams, J. C.; Blankert, S.; Laser, C.; Woodbury, N. W. *Science* **2007**, *316*, 747-750.

(19) Lewis, F. D.; Wu, T.; Zhang, Y.; Letsinger, R. L.; Greenfield, S. R.; Wasielewski, M. R. *Science* **1997**, *277*, 673-676.

(20) Giese, B. *Acc. Chem. Res.* **2000**, *33*, 631-636.

(21) Schuster, G. B. *Acc. Chem. Res.* **2000**, *33*, 253-260.

(22) Lewis, F. D.; Zhu, H.; Daublain, P.; Fiebig, T.; Raytchev, M.; Wang, Q.; Shafirovich, V. *J. Am. Chem. Soc.* **2006**, *128*, 791-800.

(23) Wolffs, M.; Delsuc, N.; Veldman, D.; Anh, N. V.; Williams, R. M.; Meskers, S. C. J.; Janssen, R. A. J.; Huc, I.; Schenning, A. P. H. J. *J. Am. Chem. Soc.* **2009**, *131*, 4819-4829.

(24) Li, X.; Markandeya, N.; Jonusauskas, G.; McClenaghan, N. D.; Maurizot, V.; Denisov, S. A.; Huc, I. *J. Am. Chem. Soc.* **2016**, *138*, 13568-13578.

(25) Méndez-Ardoy, A.; Markandeya, N.; Li, X.; Tsai, Y.-T.; Pecastaings, G.; Buffeteau, T.; Maurizot, V.; Muccioli, L.; Castet, F.; Huc, I.; Bassani, D. M. *Chem. Sci.* **2017**, *8*, 7251-7257.

(26) Pulka-Ziach, K.; Puszko, A. K.; Juhaniewicz-Debinska, J.; Sek, S. *The Journal of Physical*

Chemistry C **2019**, *123*, 1136-1141.

(27) Mervinetsky, E.; Alshanski, I.; Lenfant, S.; Guerin, D.; Medrano Sandonas, L.; Dianat, A.; Gutierrez, R.; Cuniberti, G.; Hurevich, M.; Yitzchaik, S.; Vuillaume, D. *The Journal of Physical Chemistry C* **2019**, *123*, 9600-9608.

(28) Tassinari, F.; Jayarathna, D. R.; Kantor-Uriel, N.; Davis, K. L.; Varade, V.; Achim, C.; Naaman, R. *Adv. Mater.* **2018**, *30*, 1706423.

(29) Naaman, R.; Waldeck, D. H. *Annu. Rev. Phys. Chem.* **2015**, *66*, 263-281.

(30) Namba, K.; Stubbs, G. *Science* **1986**, *231*, 1401-1406.

(31) Yoo, S. H.; Lee, H.-S. *Acc. Chem. Res.* **2017**, *50*, 832-841.

(32) Kwon, S.; Shin, H. S.; Gong, J.; Eom, J.-H.; Jeon, A.; Yoo, S. H.; Chung, I. S.; Cho, S. J.; Lee, H.-S. *J. Am. Chem. Soc.* **2011**, *133*, 17618-17621.

(33) Yoo, S. H.; Eom, T.; Kwon, S.; Gong, J.; Kim, J.; Cho, S. J.; Driver, R. W.; Lee, Y.; Kim, H.; Lee, H.-S. *J. Am. Chem. Soc.* **2015**, *137*, 2159-2162.

(34) Eom, J.-H.; Gong, J.; Kwon, S.; Jeon, A.; Jeong, R.; Driver, R. W.; Lee, H.-S. *Angew. Chem. Int. Ed.* **2015**, *54*, 13204-13207.

(35) Eom, J.-H.; Gong, J.; Jeong, R.; Driver, R. W.; Lee, H.-S. *Solid State Sci.* **2015**, *48*, 39-43.

(36) Yoon, E.; Gong, J.; Jung, Y.; Lee, W.; Driver, R. W.; Lee, H.-S. *Chem. Commun.* **2016**, *52*, 5250-5253.

(37) Lewandowska, U.; Zajaczkowski, W.; Corra, S.; Tanabe, J.; Borrmann, R.; Benetti, E. M.; Stappert, S.; Watanabe, K.; Ochs, N. A. K.; Schaeublin, R.; Li, C.; Yashima, E.; Pisula, W.; Müllen, K.; Wennemers, H. *Nat. Chem.* **2017**, *9*, 1068.

(38) Huo, Y.; Zeng, H. *Acc. Chem. Res.* **2016**, *49*, 922-930.

(39) Zhao, H.; Sheng, S.; Hong, Y.; Zeng, H. *J. Am. Chem. Soc.* **2014**, *136*, 14270-14276.

(40) Jeon, H.-G.; Jung, J. Y.; Kang, P.; Choi, M.-G.; Jeong, K.-S. *J. Am. Chem. Soc.* **2016**, *138*, 92-95.

(41) Lang, C.; Li, W.; Dong, Z.; Zhang, X.; Yang, F.; Yang, B.; Deng, X.; Zhang, C.; Xu, J.; Liu, J. *Angew. Chem. Int. Ed.* **2016**, *55*, 9723-9727.

(42) Lang, C.; Deng, X.; Yang, F.; Yang, B.; Wang, W.; Qi, S.; Zhang, X.; Zhang, C.; Dong, Z.; Liu, J. *Angew. Chem. Int. Ed.* **2017**, *56*, 12668-12671.

(43) Bécart, D.; Diemer, V.; Salaün, A.; Oiarbide, M.; Nelli, Y. R.; Kauffmann, B.; Fischer, L.; Palomo, C.; Guichard, G. *J. Am. Chem. Soc.* **2017**, *139*, 12524-12532.

(44) Girvin, Z. C.; Gellman, S. H. *J. Am. Chem. Soc.* **2018**, *140*, 12476-12483.

(45) Ferrand, Y.; Huc, I. *Acc. Chem. Res.* **2018**, *51*, 970-977.

(46) Chandramouli, N.; Ferrand, Y.; Lautrette, G.; Kauffmann, B.; Mackereth, C. D.; Laguerre, M.; Dubreuil, D.; Huc, I. *Nat. Chem.* **2015**, *7*, 334.

(47) Saha, S.; Kauffmann, B.; Ferrand, Y.; Huc, I. *Angew. Chem. Int. Ed.* **2018**, *57*, 13542-13546.

(48) Kumar, J.; Nakashima, T.; Kawai, T. *J. Phys. Chem. Lett.* **2015**, *6*, 3445-3452.

(49) Zheng, D.; Zheng, L.; Yu, C.; Zhan, Y.; Wang, Y.; Jiang, H. *Org. Lett.* **2019**, *21*, 2555-2559.

II Quinolylene-vinylene as *oligo*-Quinoline Carboxamide Foldamer Isostere

2.1 Introduction

The foldamer chemistry[1,2] has long been inspired by the naturally occurring higher order structures prevailing through the biomacromolecules, such as proteins and nucleic acids. The structure features noted other than the chemical compositions like helix, sheet and β-turn are the structural basis of the functions that those biomacromolecules preform. The evolution allows nature to choose the building blocks and molecules that form precisely the required structures and thus the functions they play. However, novel building blocks that beyond those found in nature can be developed by the ever new synthetic techniques and unlimited designs. The foldamer chemistry is such an example that expands the scopes and possibilities of the nature's inspirations.

The aromatic foldamers stand out among other biomimetic compounds that they are not only resemblance to the structures of biomolecules but also their functions. For example, different types of structures such as helix,[3] double helix[4,5] and β-sheets[6,7] have been reported by several groups. Also, several functions, such as sugar recognition[8] and information communication[9], have also been proved. Nevertheless, those foldamers were mostly based on the oligoamides which were found in proteins. The ease of synthetic efforts and the abilities of acting as both hydrogen bond donor and acceptor to stabilize the folded conformation are among the advantages of using amide as propagation linkage group. However, in order to achieve more diverse structures and functions, the sole use of amide linkage might be a limitation. The efforts of using different connecting groups which served as isosteres of peptides[10,11] have been proven as interesting and promising methods to probe the structures of peptides[12-14] as well as the mechanism[15] behind their functions. Also, the potential abilities to resist enzyme degradation makes them suitable candidates as small peptide drugs which may

have long term efficiency.[16,17]

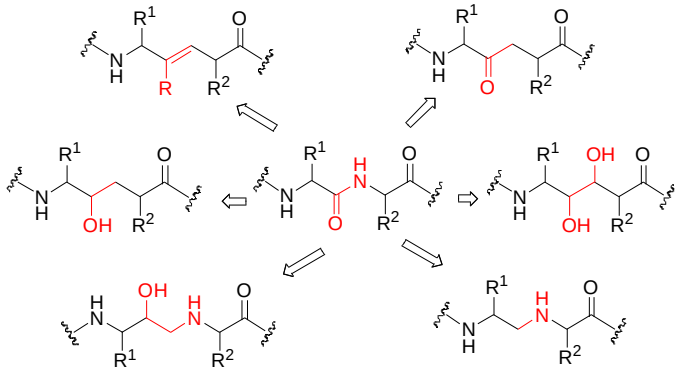

Many type of isosteres for peptides have been proposed in the last few decades. Wipf [18,19] and Fujii[16,17,20,21] have developed extensively tri-substituted E-alkene peptide isosteres. Other types of peptide bond mimetics such as ketomethylene[22,23], (di)hydroxyethylene[24-27], hydroxyethylamine[28] and methyleneamine[29-31] have also been proposed. The vinyl bond is one of the most studied surrogates of amide bond because of structural similarities between them. On the other hand, vinyl can improve the conjugation between the adjacent moieties which may affect the electron orbital energy levels and the photophysical properties. In recent years, large π-conjugated compounds have been extensively studied in the field of optical-electronic organic materials.[32-34]

The *oligo*-quinoline carboxamides forms a stable helical folded structure in solution and in the solid state. The helical structure of the oligo-quinoiline carboxamides are stabilized by the endo-helical H-bond chains and electron repulsion of the adjacent polar groups as well as the π-π stacking effects of the aromatics of quinoline rings. What will happen if the amide bonds which play a central role to stabilize the structures are replaced with bonds that are not able to form H-bonds? What will be the preferred conformation? In order to answer those questions, we prepared a serie of aromatic foldamers using vinyl bond as linkage which replaced the amide bond and a detailed structure analysis of these oligomers was conducted.

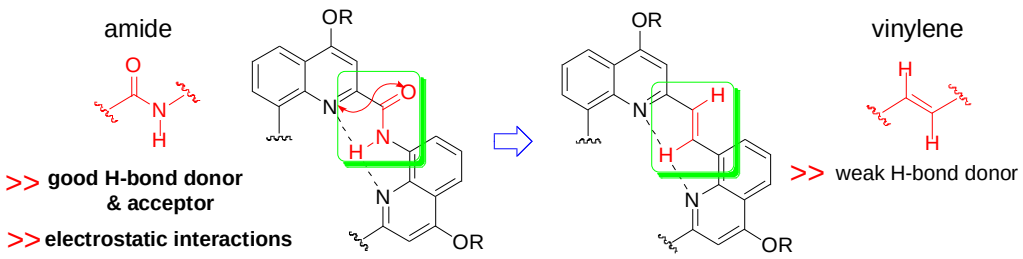

Figure 2-1: Chemical structure of the parts of quinoline amide oligomers and vinylene isotere.

2.2 Compounds design

Vinylene double bond has been long considered as a good choice of isosteres for peptide bond. The amide and vinylene double bond are similar in the geometry and spatial arrangements of substituents attached to them. There is only one atom difference (nitrogen atom in the amide changed to carbon atom in vinylene double bond) in the main chain between these two bonds. Only small structural differences are then expected by replacing the amide bond to vinylene double bond. As showed in above figure 2-1, the amide bond of 8-aminoquinoline-2-carboxamide is replaced with vinylene double bond as an isostere. It should be noted that the intermolecular interactions between vinylene double bond and amide bond are different. The amide bond is good hydrogen bond donor and acceptor while vinylene double bond is only a very week hydrogen bond donor. The electrostatic interaction of vinylene double bond is also very weak compared to amide. So, it is interesting to know how the vinylene isostere behaves and what the preferred structures of those isosteres are. The vinylene isostere will also bring us some additional physical properties because of the enhanced conjugation compared to the amide bonds. For example, fluorescence which is weak in the *oligo*-quinolinecarboxylamides might become strong in the vinylene isostere.

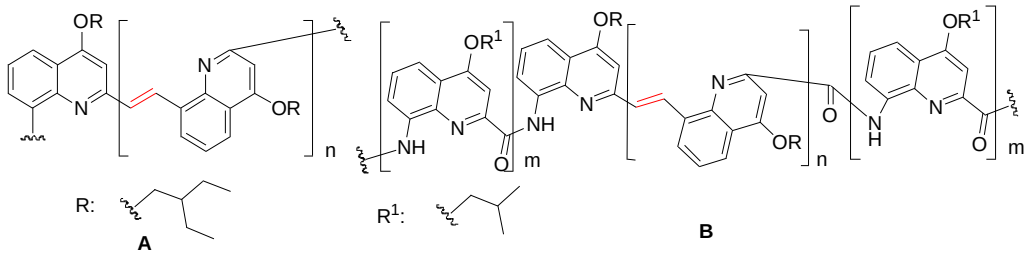

Figure 2-2: Chemical structure of quinolylene-vinylene oligomers (**A**) and quinoline carboxamide-quinolylene-vinylene hybrid-oligomers (**B**).

The quinolylene-vinylene oligomers (**A** in figure 2-2) are the isosteres of *oligo*-quinoline carboxamides that the amide bonds are replaced by vinylene double bond. A hexyl side chain is selected over isobutyl side chain to avoid possible solubility issue during synthesis. An oligomer length of quinolylene-vinylenes of seven is targeted which is long enough to know the structure preferences of those oligomers. On the other hand, in order to combine the amide oligomer and vinylene oligomer together, a hybrid oligomers composed of both sequences

were synthetized. (**B** in figure 2-2) The hybrid oligomers are composed of two short amide oligomers at both ends and in the middle a segment of vinylene oligomers of different length. A quinoline carboxamide tetramer is used for the oligoamide segments which form stable helical folded structure and it is simple to obtain. The hybrid oligomers allowed us to know if the vinylene oligomers maintain the similar helical structure inside the quinoline amide oligomers. Also, in the case that the vinylene oligomers alone did not form stable helically folded structures, it is interesting to know how the amide oligomers affect the structure of the vinylene oligomer part and induce its folding.

2.3 Results and discussions

2.3.1 Compounds synthesis

The synthesis of quinolylene-vinylene oligomers were achieved according to the route showed in scheme 2-1. The monomer **1** was prepared from *o*-toluidine according to our previous procedures[35] with minor changes. Selective transformation of **1** resulted in two key intermediates, the aldehyde **3** and phosphonate ester **5**. The aldehyde **3** was obtained via two steps transformations. The monomer **1** was first reduced to alcohol **2** which was then re-oxidized to corresponding aldehyde **3** by using SIBX[36] as a selective oxidation reagent. The phosphonate ester **5** was also synthesized via two steps' transformations. A Br-substituted intermediate **4** was obtained by free radical bromination using N-bromosuccinimide (NBS). A subsequent nucleophilic substitution reaction yielded the desired phosphonate ester **5**. The subsequent Horner-Wadsworth-Emmons (HWE) reaction furnished the formation of vinylene bond using NaH as the base. However, under the condition used, saponification of methylester of **5** occurred as a major unwanted side reaction due to trace of moisture. An additional step of re-esterification was performed to obtain the desired oligomers. The elongation of the oligomers was achieved by stepwise addition of one monomer each time under similar conditions. The longest oligomer we prepared was the heptamer **11a**. Further elongation of the oligomers according to this method was not trivial due to formation of side products (partial transformation of aldehyde reagent to corresponding carboxylic acid of

unknown reason) during the HWE reaction which hampered efficient purification of the products. Another serie of oligomers (**15a**-**19a**) bearing Boc-amide terminal functional group was also prepared according to the same procedures. (Scheme. 2-1) These oligomers allowed them to be inserted into amide analogs

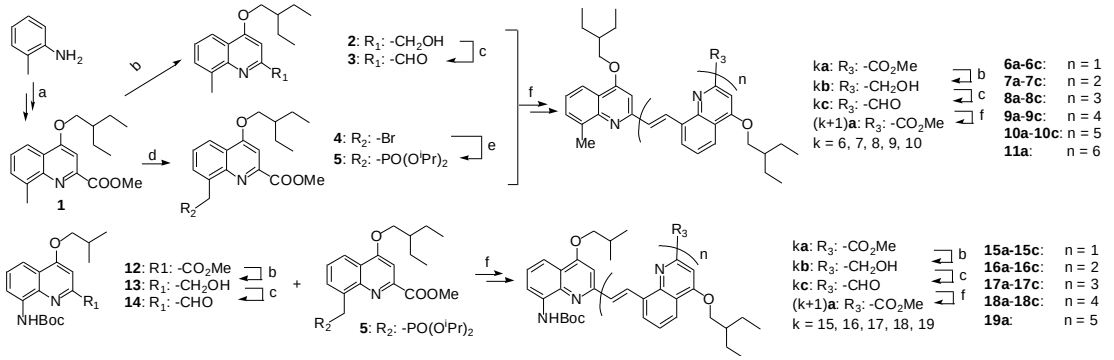

a: 1) dimethyl acetylenedicarboxylate, MeOH, 2) Ph_2O, 260 ℃; 3) DIAD, THF, PPh_3, 2-ethylbutanol; b: $NaBH_4$, THF, 60 ℃; c: SIBX, THF, 60 ℃; d: NBS, CCl_4, reflux; e: $P(O^iPr)_3$, 70 ℃; f: 1) NaH, 15-crown-5, THF; 2) K_2CO_3, MeI, acetone.

Scheme 2-1: Synthesis of the quinolylene-vinylene oligomers.

The hybrid amide and vinylene oligomers were prepared by acid chloride activation of the proper acid and coupled with the amine functionalized oligomers. The synthetic scheme was displayed in scheme 2-2. Briefly, the Boc-protected vinylene oligomers of different lengths (dimer, tetramer and hexamer) were treated with sodium hydroxide to obtain the carboxylic acids which were activated to their corresponding acid chlorides with 1-chloro-N,N,2-trimethyl-1-propenylamine (Ghosez's reagent) and coupled with quinoline *oligo*-carboxamide tetramer amine. This intermediate was then treated with TFA to afford the free amine and then coupled with quinoline *oligo*-carboxamide tetramer acid chloride to afford the designed hybrid oligomers. Compound **21** (scheme 2-2) which has only one double bond and one short amide oligomer at one end was prepared as a short model compound. Compounds **27**, **28**, and **29** all have a tetramer oligoamide at both ends differing with the number of central vinylene linkers which are 1, 3 and 5 double bonds respectively. Another hybrid oligomer **30** was also prepared which shared the same central units of **27** with a single double bond in the middle and a longer amide segments (quinoline *oligo*-amide octamer).

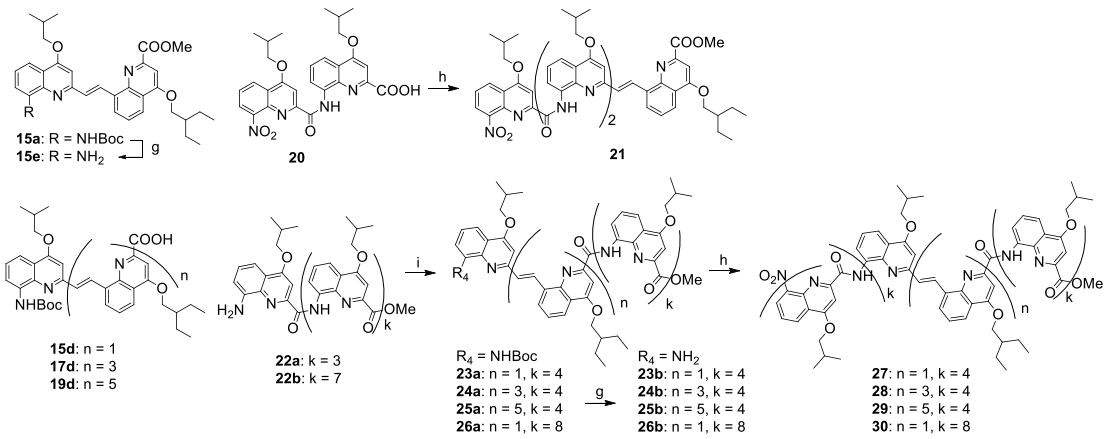

g: TFA, DCM, r.t.; h: 1) oxalyl chloride, DCM, 2) DIEA, $CHCl_3$; i: 1) 1-chloro-N,N,2-trimethyl-1-propenylamine, DCM, 2) DIEA, $CHCl_3$.

Scheme 2-2: Synthesis of the quinolylene-vinylene amide hybrid oligomers.

2.3.2 Conformation study of the oligomers

The proton NMR spectra of the oligomers (**6a**-**11a** and **15a**-**19a**) are shown in figure 2-3 and 2-4 and reflected their conformations in solution. For the oligomers **6a**-**11a**, the proton signals of the -CH_3 and -$COOCH_3$ were separated from others and hence were easily recognized. The chemical shifts of those two groups can be useful to indicate the possible conformations of the oligomers in solution due to dramatic changes of the chemical shifts between different conformations. The observed evolution of those two signals showed, first, an upfield shift caused by the deshielding effect of the aromatic rings and then downfield shift when oligomer length exceeding four (from **8a** to **11a**). The chemical shift differences between **10a** and **11a** was actually negligible (about 0.001 ppm for -CH_3 and 0.006 ppm for -OCH_3). The two stage evolution of chemical shifts indicates that multiple effects might take places. The downfield shifting of the –CH_3 signal from **8a** to **11a** indicate that the folding is weak in chloroform solution otherwise dramatic upper field shifts of the signals should be observed. The upfield shift from **6a** to **8a** might be caused by increased conjugation in those oligomers. In the aromatic region, the H^3 protons (Figure 2-3) of the quinoline rings did not shift to upper field which is also consistent with the fact that helical folding is not the major conformation in solution. In the helical folded conformation, the H^3 proton should

consistently shifts to upper field due to the enhancement of π-π stacking upon increase of the oligomer length.[3] One of the vinylene protons (H^{α} in figure 2-5) was separated from the other signals and could clearly be identified, because of its large coupling constant (around 16.6 Hz). The overlapping of this signal in **10a** and **11a** also reflect a similar environment of these protons. The trend of evaluation of the chemical shifts of the ester protons in the Boc-amide functionalized oligomers **15a-19a** was similar to the previous oligomers and two stage shifts were observed (figure 2-4).

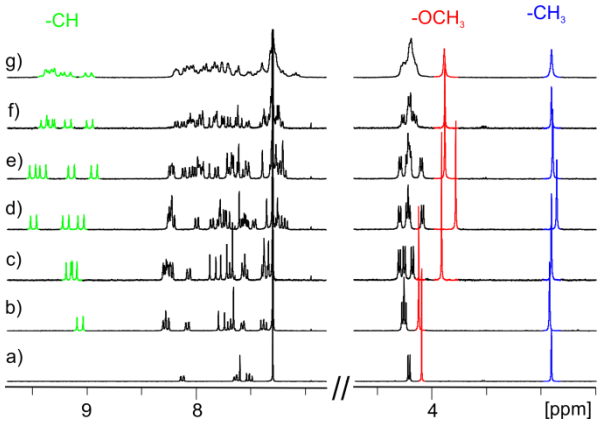

Figure 2-3: Parts of the ^{1}H NMR spectra (300 MHz) of **1** and **6a-11a** showing the vinyl (green), aromatic and terminal groups of $–OCH_3$ (red) and $–CH_3$ (blue) at 298 K for a) **1**, b) **6a**, c) **7a**, d) **8a**, e) **9a**, f) **10a**, g) **11a**.

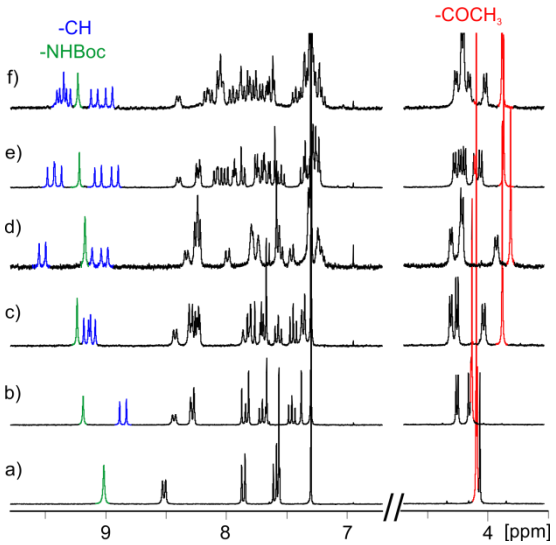

Figure 2-4: Parts of the ^{1}H NMR spectra (300 MHz) of **12** and **15a-19a** showing the vinyl (blue), aromatic and terminal groups $–OCH_3$ (red) and BocNH- (green) at 298 K for a) **12**, b) **15a**, c) **16a**, d) **17a**, e) **18a**, f) **19a**.

The dimer **6a** which has only one vinylene bonds was used as a model compound to

analyze the possible conformations of this type of oligomers. By subsequently flipping the orientation of the double bonds, four possible conformations can be drawn as shown in the figure 2-5. Among the four conformations, two of them (**B** and **D**) were compatible with structure of helical folding, while the other two (**A** and **C**) gave a sheet structure upon extending the segments. For each double bond, the same number of possible conformation can be generated. If we count the number of double bond in a given oligomer as n, the number of conformations will be 4^n. In order to find out the conformations of those oligomers in solution, we measured the NOESY spectrum of **6a**. The four possible conformations of **6a** gave four sets of correlations between H^3, H^7 and H^α, H^β protons as summarized in figure 2-5. For example, in the conformation of **A**, only H^3-H^β, H^7-H^α correlations were expected. As showed in figure 2-5, the observed NOESY spectrum of **6a** in $CDCl_3$ showed strong correlations between H^3-H^α and H^7-H^β which correspond to the conformation **C** in figure 2-5. However, a set of weaker correction was also observed (H^3-H^β and H^7-H^α) which indicated the presence of other conformations. The observation of four correlations can be explained by coexistence of the four possible conformations which underdo fast exchange in solution. The relative intensity of the different sets of corrections reflected the relative population of the possible conformations which in our case implied that conformation **C** was the major one in chloroform solution. We also checked the NOESY spectrum in CD_2Cl_2 which gave similar results. The similar conformation behavior also holds for the longer oligomers as indicated by the NOESY spectrum of **8a** in $CDCl_3$ (Fig. 2-6).

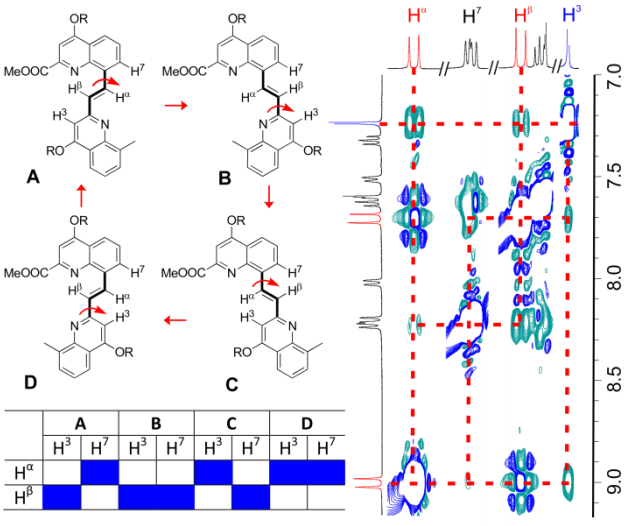

Figure 2-5: The four possible conformations of the **6a** and the expected ^{1}H-^{1}H NOESY correlations and

excerpt from ^{1}H-^{1}H NOESY spectrum of **6a** in $CDCl_3$ at 298 K (400 MHz).

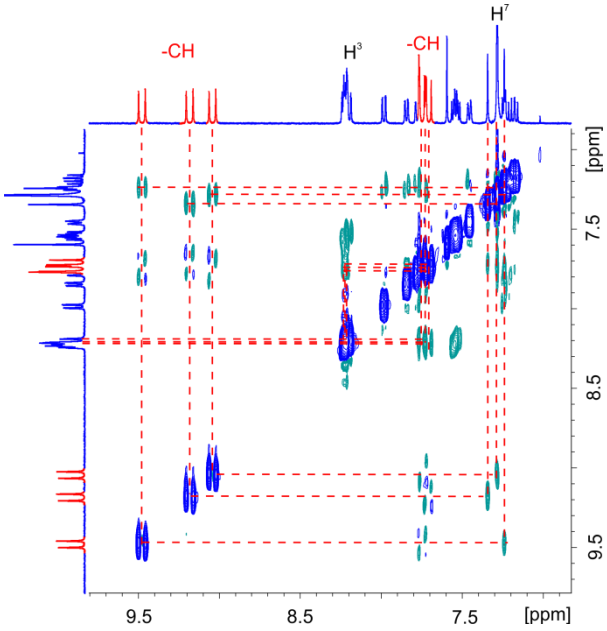

Figure 2-6: Excerpt from ^{1}H-^{1}H NOESY spectrum of **8a** in $CDCl_3$ at 298 K (400 MHz) indicating the correlations between vinyl protons and aromatic protons.

The extended conformation of the quinolylene-vinylene oligomers in solution reflected the conformational flexibility of those oligomers. In order to favor the helical folded conformation, a segment of quinoline carboxamide oligomers may be helpful to induce the helical shape of vinylene segments. As a starting point, we tried to elucidate the conformation of tetramer **21** in solution which is composed of only two amides and one vinylene bonds. The signal of the two vinylene protons of **21** were greatly shifted to upper field compared to the dimer **6a**. The shifts are in agreement with a shielding effect of the aromatic rings that come from the quinoline carboxylamide trimer segments. However, the vinylene bond is still capable to cause different conformations similar to those depicted in figure 2-5. The part of oligoamide trimer was known to adopt a helically folded conformation in solution.[3] The quinoline that connected though vinylene bond with the oligoamide trimer could have four possible positions related to the helical shaped trimer. Among them, two are compatible with the helically folded conformation while the other two are not. Nevertheless, the vinylene protons of all four possible conformations are positioned at the deshielding region of the helix trimer as observed in our energy minimized models of four conformations. (Figure 2-9) The dynamic behavior of the vinylene bond was also reflected by the proton NMR spectra. The signal of $-OCH_2-$ on the iso-butyoxyl side chain (δ 3.09 ppm, side chain of N-terminus

quinoline) is broad at 298 K which became a sharp doublet at 323 K. This signal became broader upon cooling and at 238 K, the signal almost disappeared and splits as two broad peaks at 228 K. (Figure 2-7) Those changes reflected the dynamic exchange rates of these signals are fast at elevated temperature and slow at low temperature at the NMR time scale. This behavior can be caused by the slow dynamics of P/M handedness exchange of the helical folded **21** which also known as anisochronous signals. The 2D NOESY spectrum of **21** in chloroform showed similar pattern as compound **6a** that is a set of strong correlations which correspond to the linear conformation of the vinylene part, together with a set of minor correlations that could indicate the helically folded conformation in solution. As showed in figure 2-8, a major set of correlations between H^3-H^{α} and H^7-H^{β} was observed while a minor set of correlation between H^3-H^{β} and H^7-H^{α} was also observed. The dynamic conformation behavior and especially the major unfolded conformation indicated that amide oligomer at only one end might not be sufficient to template the folding the vinylene segments.

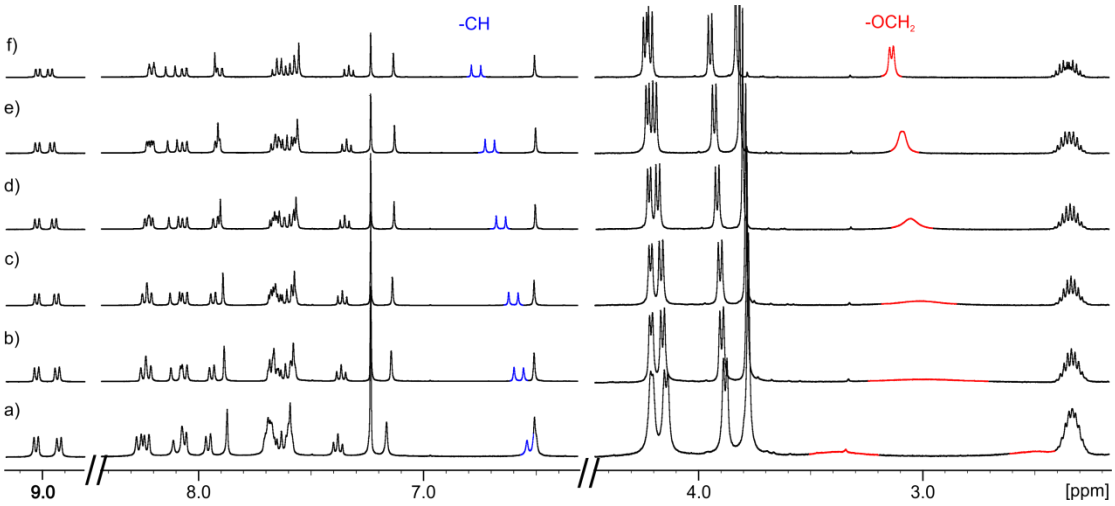

Figure 2-7: parts of the variable temperature ^{1}H NMR spectra of **21** showing the amide, aromatic and side chain region, a) 228 K, b) 248 K, c) 258 K, d) 278 K, e) 298 K and f) 323 K.

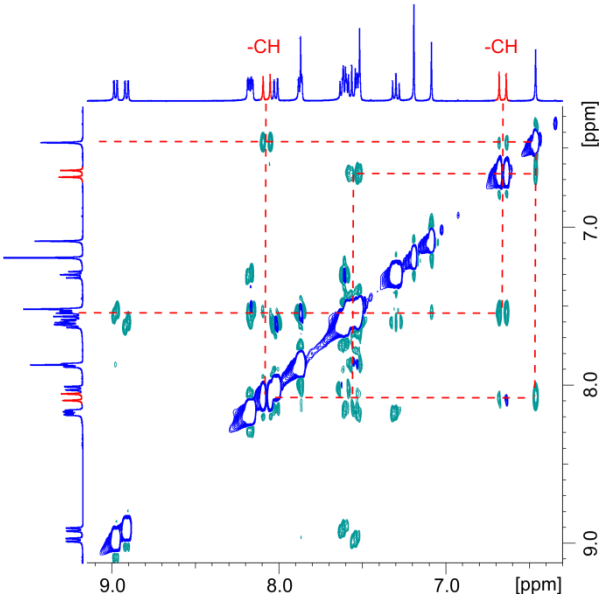

Figure 2-8: Excerpt from ^{1}H-^{1}H NOESY spectrum of **21** in $CDCl_3$ at 25 ℃ (400 MHz) indicating the correlations between vinyl protons and aromatic protons.

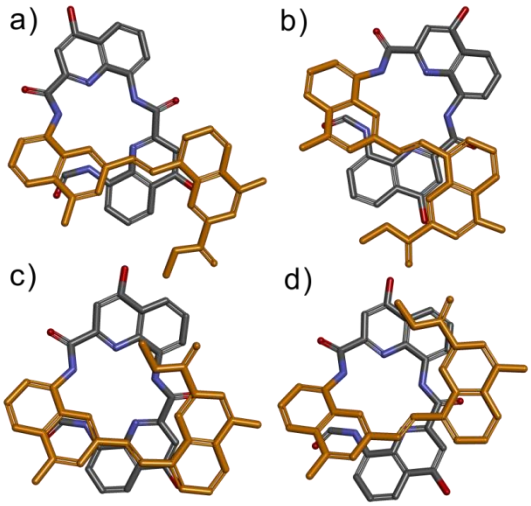

Figure 2-9: Energy minimized molecular models of four conformations of **21**. The models were produced with Maestro software package, using MFFS force field, chloroform as solvent and PRCG as minimization method.

The lack of sufficient induced folding effect of only one oligoamide segment at one end of the vinylene oligomers guide us to add another segment of oligoamide at the other end of the vinylene oligomers. The compounds, **27**, **28** and **29** were prepared and all shared the same oligo-tetrameric quinoline carboxamide segments at both end of the quinolylene-vinylene oligomers. Complicated NMR spectra are observed for all three compounds in $CDCl_3$ showing more than one set of signals. The coexistence of different sets of signals reflected that different conformations are in slow exchange at the NMR time scale. As showed in the

figure 2-10, the proportion of conformers of **27** and **28** are solvent dependent. In $CDCl_3$, **27** which has one vinyl bond gives two sets of signals at 298 K in which one is the major. We attributed the major set of signals to the helically folded conformation. The minor set of signals, on the other hand, was difficult to assign. The proportion of the two set of signals were dependent on the solvents. The minor set of signals almost disappeared in CD_2Cl_2, and observable but tiny in acetone-d6. Upon addition of ten percent of methanol in chloroform, the minor set of signals decrease which indicated that methanol as a solvent favors the major helical conformation. The proton NMR of **28** which possess three vinyl bond in chloroform is much more complicated than **27**. The solvent dependent NMR is similar to **27** except that proportion of the minor set of signals are higher than **27**. As showed in figure 2-10, two sets of signals of similar intensity coexist in $CDCl_3$. One set of signals became smaller upon addition of large amount of methanol (up to 40 vol%). In dichloromethane, there is a major set of signals that coexist with some small signals while two sets of similar intensity signals coexist in acetone-D6. The proton NMR spectroscopy of **29** is too complicated to allow interpretation of NMR data. However, several sets of signals reflecting coexistence of more than two conformations are observed.

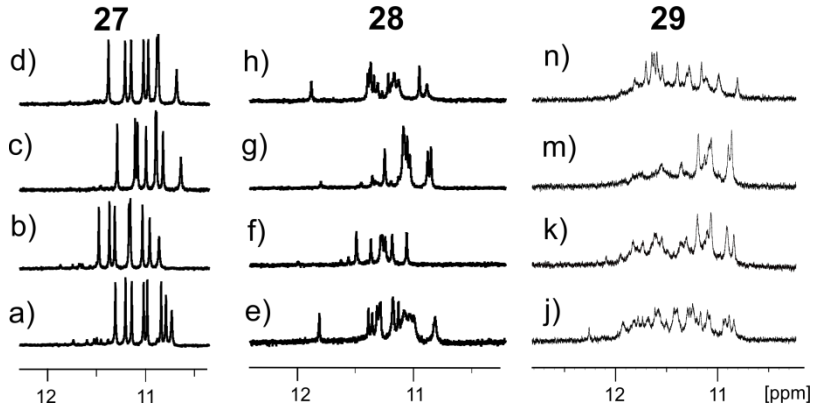

Figure 2-10: Parts of the ^1H NMR spectra (300 MHz) of **27** and **28** showing the amide in different solvents at 25 ℃ for a) **27** in $CDCl_3$, b) **27** in $CDCl_3/CD_3OD$ (9/1), c) **27** in CD_2Cl_2, d) **27** in acetone-D6, e) **28** in $CDCl_3$, f) **28** in $CDCl_3/CD_3OD$ (6/4), g) **28** in CD_2Cl_2, h) **28** in acetone-D6; j) **29** in $CDCl_3$; k) **29** in CD_2Cl_2; m) **29** in CD_2Cl_2/CD_3OD (8/2) and n) **29** in acetone-d6.

The conformations of the aforementioned compounds were further analyzed with multiple techniques. The variable temperature proton NMR of **27** in dichloromethane showed that a different conformation appeared upon cooling to 253 K (Figure 2-11). Upon cooling,

the minor signals which came from a minor conformation at room temperature did not change significantly until the temperature decreased to 253 K and then disappeared in favor to a new set of minor signals. This change is attributed to a conformation change upon cooling. We suspect that the new set of peaks could belong to another conformation that is compatible with a helical folding. The new set of signals was independent to the concentration which implied that this set of peaks is not caused by aggregation behavior. We also checked the variable temperature proton NMR of **27** at high temperature in $C_2D_2Cl_4$. Upon heating the sample from 268 K to 343 K, we observed changes of the chemical shifts of most of the signals. The interesting part is that at higher temperature, some of the signals which were difficult to observe at room temperature became sharper. Especially the most important signals of one of the vinylene proton could only be observed at higher temperature at 4.72 ppm at 343 K (figure 2-12). The other vinylene proton was identified by COSY spectrum to be at 7.80 ppm (343 K). The substantial upfield shifts of those two peaks compared to **6a** could be explained by the shielding of quinoline rings from both upper and lower side in the helix. After identification of the vinylene protons, we performed 2D NOESY experiment which gives only the correlation of one vinylene proton with both H^3 and H^7 proton in the aromatics which correspond to the folded conformation **B** in figure 2-5. (Figure 2-13) Herein, we showed that the addition of two short oligoamide segments at both end of the vinylene oligomers could induce the folding of the vinylene oligomers.

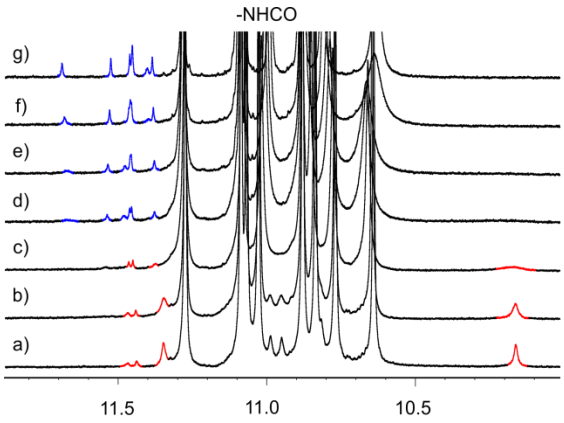

Figure 2-11: Part of the ^{1}H NMR spectra (700 MHz) of **27** in CD_2Cl_2 showing the amide and aromatic at different temperature for a) 233 K, b) 238 K, c) 253 K, d) 263 K, e) 268 K, f) 283 K and g) 298 K.

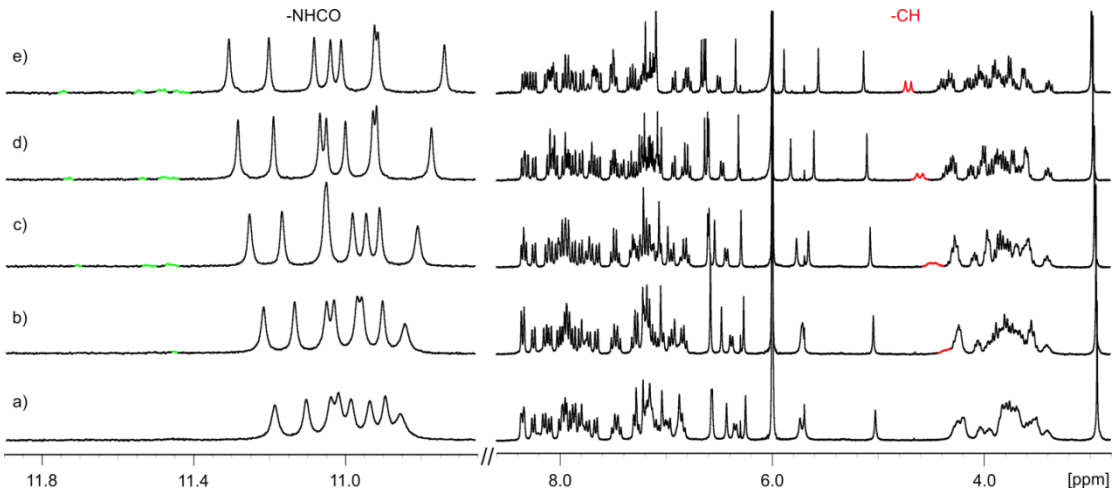

Figure 2-12: Part of the ^{1}H NMR spectra (300 MHz) of **27** in $C_2D_2Cl_4$ showing the amide and aromatic at different temperature for a) 268 K, b) 283 K, c) 303 K, d) 323 K, e) 343 K.

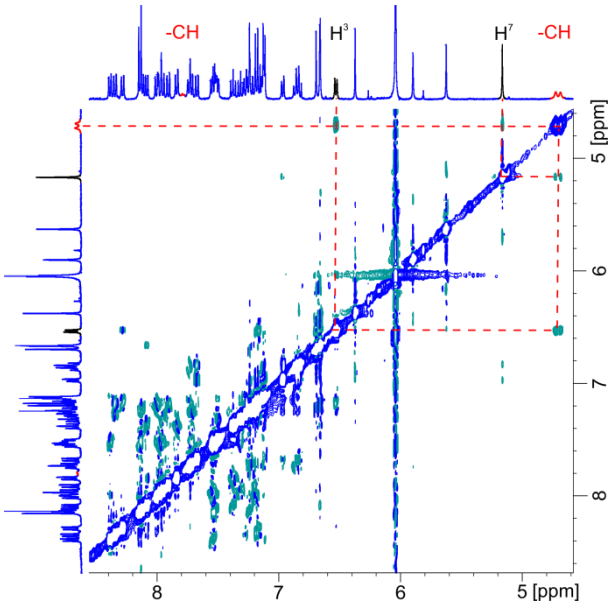

Figure 2-13: Excerpt from ^{1}H-^{1}H NOESY spectrum of **27** in $C_2D_2Cl_4$ at 333 K (400 MHz) indicating the correlations between vinyl protons and aromatic protons.

This observation is also confirmed by the X-ray single crystal structures. We obtained single crystals suitable for X-ray analysis for **6a**, **27** and **28**. All structures show the helical conformation of the vinylene segment (conformation **B** in figure 2-5). The structure of **6a**, whose crystal was obtained by slow diffusion of methanol into dichloromethane solution, showed different conformation compared with the solution data. This is probably reflecting that different conformations coexist in solution in which the one compatible with folding were easier than the others to crystallize in the mixture of dichloromethane/methanol. The structure of **6a** was almost flat on the side view, the dihedral angle of the two aromatic ring is only 8.6 °

which was expected due to the maximum conjugation of the two aromatic rings. However, in the structure of **27** and **28**, the two consecutive quinoline rings connected with vinylene bonds are no longer coplanar and have large dihedral angles of 17.5 °in **27** and 18.3 °, 15.5 °and 14.1 ° in **28** respectively. The distortion of the conjugation was a result of the steric effect from the helical structure. From a top view of **28**, a triangular shape of the central vinylene tetramer part could be observed in which the fourth quinoline ring sit on the top of the first one. This shape will give a helix structure of three units per turn which is slightly larger than the 2.5 units per turn of quinoline oligoamides.[3] The slight conformation differences can be also observed from the side views of the two different oligomers.

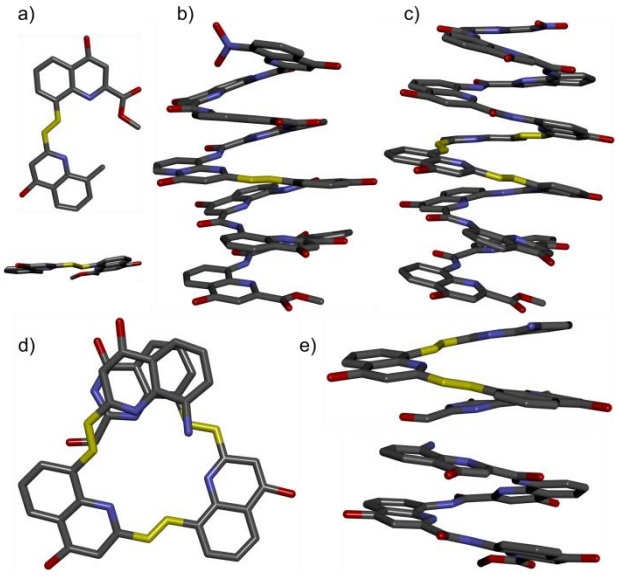

Figure 2-14: The X-ray structure of the **6a**, **27** and **28** for a) front and side view of **6a**, b) side view of **27**, c) side view of **28**, d) front view of the central part of **28** showing the three double bonds, e) side view of **28** showing the central part and end part, the double bond was marked as yellow, hydrogen atoms and side chains were removed for clarity.

The ^{1}H NMR of **27** after immediately dissolving the crystal which was found to have the folded conformation displayed two sets of signals in $CDCl_3$ which showed no evolution with time at room temperature. This observation implied that the conformation equilibrium was completed within few minutes. As discussed above, the two sets of signals are associated with two isomers of **27**. The compound **27** is composed by two segments of helical oligoamides and a central vinylene. The helical oligoamides can be either P or M-helix. The central vinylene has four possible conformations as showed in figure 2-5. In order to change from one conformation to another, a flipping around the double bond is required. However, this

flipping results overlapping of the two helical oligoamides. The change of conformation is then possible that the handedness of one of the helical oligoamide segments changes at the same time. The rate of handedness inversion is highly dependent on the length of the oligomers. The handedness inversion rate of longer oligomers is lower than the shorter oligomers. Hence, in order to slow down the kinetics of handedness inversion, similar compound **30** with longer oligoamide segments (quinoline carboxylamide octamer in this case) was prepared. The crystal structure of **30** showed similar folded conformation as **27**. As expected, compound **30** showed two sets of signals in $CDCl_3$ similar to **27**. However, the NMR spectrum after immediately dissolving the crystals showed only one set of signals which corresponds to the major set of signals at equilibrium. The proton NMR slowly evolved to display another set of minor peaks after standing at room temperature for few hours and the proportion stopped changing after about one day. The observation of slowing kinetics of the oligomer with longer amide segments also justified our hypothesis about the conformational dynamics of the oligomers in solution.

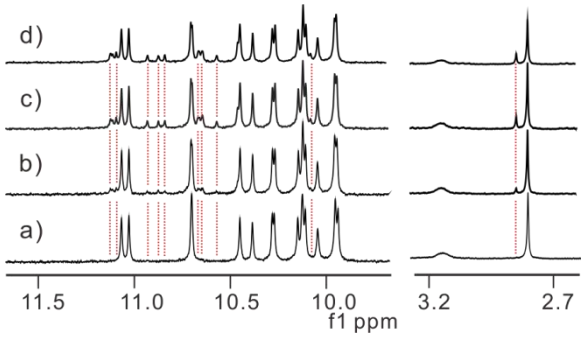

Figure 2-15: Part of ^{1}H NMR spectra of **30** of dissolving the crystal measured after a) 6 minutes, b) 5 hours, c) 21 hours and d) 72 hours, only the amide region and methyl ester region were shown in here.

2.3.3 Absorption and emission

The absorption and emission spectra of **6a-11a** were measured in chloroform. Compared to the monomer **1**, the UV-Vis absorption spectra of **6a-11a** all had a distinct absorbance at longer wavelength (around 360 nm) which was attributed to the effect of conjugation through the double bonds. The continually bathochromic shift of the absorption band from **6a** to **11a** indicated the elongation of the conjugation which lowering the π–π* transition energies. It is interesting to note that the absorbance by the number of double bonds dropped from **6a** to **11a**.

The absorption spectra of **21**, **27**, **30** and **28** were also measured to compare with **6a** and **8a**. Compared with **6a**, the absorption of **21**, **27** and **30** all have bigger absorbance and the absorption peaks shift to short wavelength. The absorption spectra of **28** and **8a** also show similar differences. The fluorescence emission spectra of **6a-11a** were measured in chloroform at the concentration of 10 μM as showed in figure 2-16. The compound **1** was measured as a reference which has very weak emission. The intensity of the emission increased as the order of **6a** < **7a** < **11a** < **10a** < **8a** < **9a** (measured at the same condition). The decreasing of the intensity from **9a** to **11a** could be attributed to the saturation of conjugation effect. The small shifts of emission maximum also reflected the saturation of the conjugation as the emission peak shift little form **7a** to **11a** show in the normalized emission spectra.

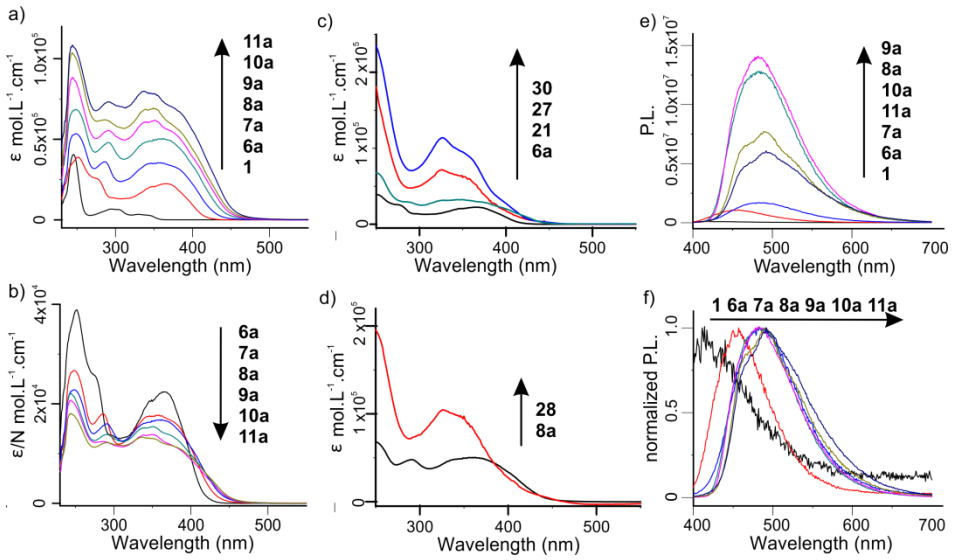

Figure 2-16: The UV-Vis absorption spectra of **1**, **6a-11a**, **21**, **27**, **28** and **30** and fluorescence spectra of **1** and **6a-11a**. a) UV-Vis spectra of **1** and **6a-11a**; b) molar extinction coefficients of **1** and **6a-11a** divided by number of double bonds; c) UV-Vis spectra of 6a and **21**, **27**, **28** and **30**; d) UV-Vis spectra of **8a** and **28**; e) fluorescence spectra of **1** and **6a-11a** and f) normalized fluorescence spectra of **1** and **6a-11a**.

2.4 Conclusions and perspectives

We have successfully synthetized the quinolylene-vinylene oligomers by developing a Horner-Wadsworth-Emmons (HWE) reaction strategy. In solution, those oligomers showed distinct conformations from their oligoamide analogs. The flexibility of the conformation of

those oligomers could be attributed to the lack of stabilizing forces that drive the conformation to a preferential one which was rather strong in the carboxamide analogs. The quinolylene-vinylene oligomers do not have strong tendency to form helical folded conformation alone. *Oligo*-quinoline carboxamides are necessary to induce the helical structures of quinolylene-vinylene oligomers, yet, several conformers exist. The population of the helical conformation is solvent dependent and addition of polar solvent such as methanol favors it. The lack of stable folding structure might undermine their usability as building blocks as foldamers. Also, if we consider that the vinylene is an isostere of amide, the results indicated the importance of the amide to maintain the helical folded conformation.

The flexibility of this type of oligomers might open another avenue to the design oligomers where structure rigidity wasn't necessary. The replacement of the amide bond with vinylene bond, itself, changes not only the structure but also the properties. The nature of conjugation of the vinylene linkage was sure to affect the nature of the backbone of the oligomers in terms of electronic behaviors as already indicated by the absorption and emission spectra. The investments of the electron transport properties of the oligomers with vinylene bonds are hence very interesting to know. The electron transport properties can be studied by attaching electron donor and acceptor. Ultrafast absorption and emission spectroscopy is a well suited technique to study the photo-electron transport of donor-bridge-acceptor systems. Two proposed compounds are showed in below figure 2-17 (**P1** and **P2**). Another interesting future plan of the quinolylene-vinylene oligomers is the water soluble version of them. A short side chain with amine group (Figure 2-17 **P3**) is proposed which brings the water solubility and also compatible with growing crystals. In aqueous phase, the strong hydrophobic effect might force the aromatic rings of quinolines to stay close in order to bury as much as possible of hydrophobic surfaces. The aromatic rings also form π-π stacking to further stabilize the folded structures.

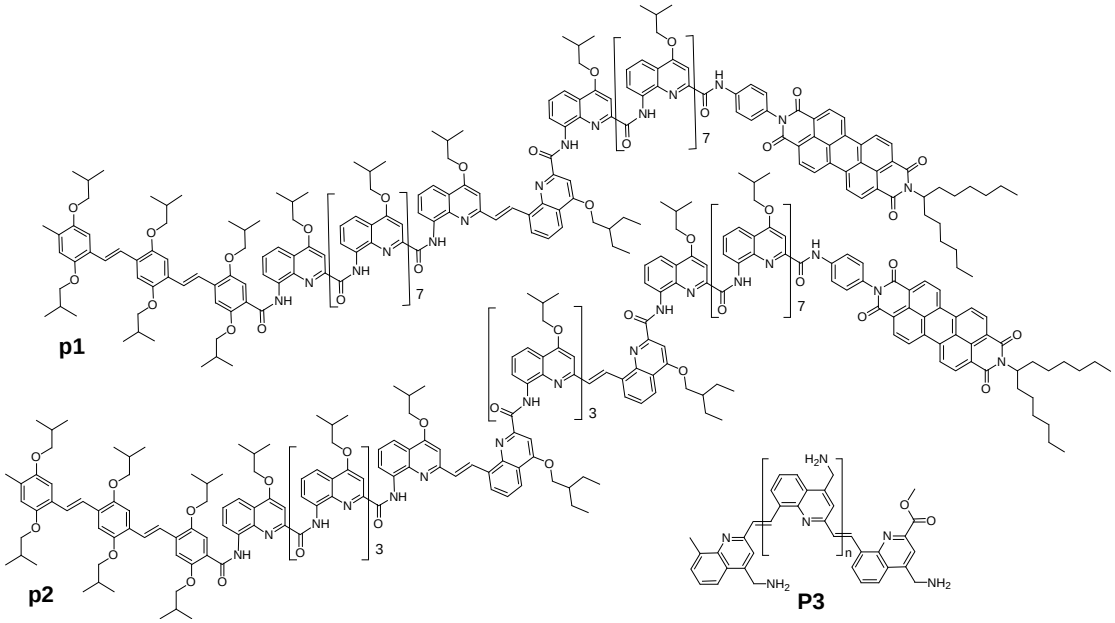

Figure 2-17: Proposed compounds P1 and P2 attached with electron donor (OPV) and electron acceptor (PB) for the purpose to study the photo-electron transfer and the proposed oligomers with water soluble side chains to investigate the structure in water.

2.5 Experimental section

2.5.1 General remarks

All the solvents and reagents were used as received unless otherwise specified. Dry THF was obtained from distillation over sodium/benzophenone. ^{1}H NMR, ^{13}C NMR and 2D NMR were recorded on 300 MHz, 400 MHz or 700 MHz Bruker Avance 300, 400 and 700 spectrometer. Reactions were monitored by thin layer chromatography (TLC) on Merck silica gel 60-F254 plates and observed under UV light. Column chromatography purifications were carried out on Merck GEDURAN Si60 (40-63 μm). ESI mass spectra were obtained from the Mass Spectrometry Laboratory at the European Institute of Chemistry and Biology (UMS 3033 - IECB), Pessac, France. UV-Vis spectra were recorded on Varian® Cary 300 Scan UV-Visible spectrophotometer at room temperature. Fluorescence spectra were recorded on HORIBA FluoroMax-4 spectrofluorometer at room temperature.

2.5.2 X-ray crystallography

The single crystals were obtained by slow diffusion of acetonitrile or hexane into the stock solution in chloroform. Typically, the crystals were obtained in around 1 to 2 weeks and suitable crystals were picked for X-ray diffraction.

2.5.3 Compounds synthesis

Synthesis of **1**: To a 250 mL flask was added triphenylphosphine (7.97 g, 30.4 mmol), **S2** (6.00 g, 27.6 mmol). Then the flask was filled with N_2. Dry THF (45 mL) and 2-ethylbutanol (3.7 mL, 30.4 mmol) were added through syringe. DIAD (6.0 mL, 30.4 mmol) was slowly added into the flask through a dropping funnel during 20 minutes. The resulting mixture was then stirred for 17 hours. The reaction mixture was concentrated and 50 mL methanol was added in to the resulting slurry and cooled down to form white precipitate. The solid was filtrated off and washed with methanol and dried to yield white solid (5.8 g, 69.6%). ^{1}H NMR (300 MHz, $CDCl_3$): δ 8.09 (d, *J* = 8.3 Hz, 1 H), 7.60 (d, *J* = 5.6 Hz, 1 H), 7.56 (s, 1 H), 7.47 (t, *J* = 7.7 Hz, 1 H), 4.17 (d, *J* = 5.6 Hz, 2 H), 4.06 (s, 3 H), 2.87 (s, 3 H), 1.86 (m, 1 H), 1.64-1.53 (m, 4 H), 0.99 (t, *J* = 7.4 Hz, 6 H) ppm; ^{13}C NMR (84 MHz, $CDCl_3$): δ 166.8, 163.1, 148.0, 147.8, 138.3, 130.7, 127.3, 122.6, 119.7, 100.6, 70.9, 53.2, 41.0, 23.7, 18.2, 11.4 ppm, HRMS (ESI) m/z: calcd for $C_{18}H_{24}NO_3$ $[M+H]^+$ 302.1750, found 320.1748.

Synthesis of oligomers

General procedure for the synthesis of methylene alcohol: To a 100 mL flask was added with methyl ester (1 eq.) and $NaBH_4$ (10 eq.), THF was added and heated at 50 ℃, and then MeOH was added slowly. After the reaction completed, water was added to quench the unreacted $NaBH_4$. Then dichloromethane was added to extract the compound and then washed with brine. The organic layer was dried over Na_2SO_4 and then filtrated and removed the solvent to give a white solid. This was used without further purification.

General procedure for the preparation of aldehydes: To a 50 mL flask was added with methylene alcohol (1 eq.) and SIBX (1.2 eq.), then the flask was filled with N_2. Dry THF was added through syringe. Then the mixture was heated under reflux for 1 hour under N_2.

Heating was stopped and the mixture was cooled down to room temperature; a saturated $Na_2S_2O_3$ solution was added. Dichloromethane was added to extract the compound and then washed three times with saturated Na_2CO_3 solution. The organic layer was dried over Na_2SO_4 and then filtrated and the solvent was removed. Hexane was added to precipitate the compound. The precipitate was filtrated off to give the aldehyde.

Synthesis of **4**: To a 100 mL flask was added **1** (2.10 g, 7.0 mmol), NBS (1.37 g, 7.7 mmol) and AIBN (22 mg, 0.14 mmol). The air inside was replaced with N_2 three times. Then 40 mL of CCl_4 was added through a syringe. The mixture was heated under N_2 at 75 ℃ overnight. The reaction mixture was cooled down to room temperature and washed with brine three times. The organic layer was dried over Na_2SO_4, filtrated and the solvent was removed. Cyclohexane was added to form a white needle like precipitate. The solid was filtrated to obtain a white solid (1.85 g, 69.0%). ^{1}H NMR (300 MHz, $CDCl_3$): δ 8.21 (dd, *J* = 8.4, 1.5 Hz, 1 H), 7.90 (dd, *J* = 7.2, 1.5 Hz, 1 H), 7.58 (s, 1 H), 7.56 (t, *J* = 7.7 Hz, 1 H), 5.31 (s, 2 H), 4.18 (d, *J* = 5.6 Hz, 2 H), 4.06 (s, 3 H), 1.86 (m, 1 H), 1.64-1.53 (m, 4 H), 0.99 (t, *J* = 7.4 Hz, 6 H) ppm; ^{13}C NMR (75 MHz, $CDCl_3$): δ 166.5, 163.0, 148.8, 146.0, 137.0, 131.7, 127.2, 122.6, 101.0, 71.1, 53.1, 40.8, 29.5, 23.6, 11.3 ppm, HRMS (ESI) m/z: calcd for $C_{18}H_{23}BrNO_3$ $[M+H]^+$ 380.0856, found 380.0852.

Synthesis of **5**: To a 50 mL flask was added **4** (2.36 g, 6.2 mmol). The air inside was replaced with N_2 and triisopropanylphosphine (3.0 mL, 12.4 mmol) was added. The mixture was heated at 70 ℃ for 3 hours under N_2. The reaction mixture was cooled down to room temperature. Toluene was added to remove the excess of triisopropanylphosphine by co-evaporating under reduced pressure. The slurry was dried under high vacuum to give a white solid (2.52 g, quant). ^{1}H NMR (300 MHz, $CDCl_3$): δ 8.13 (d, *J* = 8.5 Hz, 1 H), 7.93 (dd, *J* = 7.3, 3.4 Hz, 1 H), 7.53 (s, 1 H), 7.54 (t, *J* = 8.2 Hz, 1 H), 4.74-4.63 (m, 2 H), 4.16 (d, *J* = 5.4 Hz, 2 H), 4.06 (d, *J* = 22.3 Hz, 2 H), 1.84 (m, 1 H), 1.61-1.53 (m, 4 H), 1.22 (d, *J* = 6.4 Hz, 6 H), 1.09 (d, *J* = 6.4 Hz, 6 H), 0.99 (t, *J* = 7.2 Hz, 6 H) ppm; ^{13}C NMR (75 MHz, $CDCl_3$): δ 163.1, 148.1, 146.9, 146.8, 132.7, 132.6, 131.6, 131.5, 127.2, 127.1, 122.7, 122.6, 120.8, 120.7, 100.6, 70.7, 52.9, 41.0, 29.2, 27.3, 24.2, 23.9, 23.7, 11.4 ppm; ^{31}P NMR (121 MHz, $CDCl_3$): δ 25.2 ppm, HRMS (ESI) m/z: calcd for $C_{24}H_{37}NO_6P$ $[M+H]^+$ 466.2353, found 466.2348.

General procedure for the coupling: To a 50 mL flask was added with the aldehyde (1 eq.), **5** (1.1 eq.) and NaH (2 eq.). The flask was then connected with vacuum and then filled with N_2. Dry THF and 15-rown-5 (1 eq.) were added through syringes. The mixture was stirred at room temperature for 2 hours. The reaction was quenched by adding water and dichloromethane. The compound was extracted with dichloromethane and dried over Na_2SO_4. The salt was filtrated off and the solvent was removed under vacuum. The residue was dried under high vacuum. K_2CO_3 (1.5 eq.) and acetone was added. The mixture was stirred at room temperature for about 10 minutes before adding MeI (2 eq.). The mixture was stirred at room temperature for 5 hours. Dichloromethane was added and the solution was washed with brine three times. The organic layer was dried with Na_2SO_4 and then filtrated and the solvent was removed. The residue was purified with column.

2: ^{1}H NMR (300 MHz, $CDCl_3$): δ 8.04 (d, *J* = 8.5 Hz, 1 H), 7.54 (d, *J* = 8.5 Hz, 1 H), 6.57 (s, 1 H), 4.96 (s, 1 H), 4.84 (s, 2 H), 4.07 (d, *J* = 5.5 Hz, 2 H), 2.78 (s, 3 H), 1.85 (m, 1 H), 1.64-1.53 (m, 4 H), 0.98 (t, *J* = 7.4 Hz, 6 H) ppm; ^{13}C NMR (75 MHz, $CDCl_3$): δ 162.7, 158.7, 146.4, 136.0, 130.4, 125.1, 121.2, 120.0, 97.0, 70.7, 64.2, 41.0, 23.7, 18.3, 11.4 ppm, HRMS (ESI) m/z: calcd for $C_{17}H_{24}NO_2$ $[M+H]^+$ 274.1802, found 274.1798.

3: ^{1}H NMR (300 MHz, $CDCl_3$): δ 10.16 (s, 1 H), 8.11 (d, *J* = 8.5 Hz, 1 H), 7.63 (d, *J* = 7.2 Hz, 1 H), 7.51 (t, *J* = 7.7 Hz, 1 H), 7.38 (s, 1 H), 4.17 (d, *J* = 5.6 Hz, 2 H), 2.87 (s, 3 H), 1.86 (m, 1 H), 1.64-1.54 (m, 4 H), 0.99 (t, *J* = 7.3 Hz, 6 H) ppm; ^{13}C NMR (75 MHz, $CDCl_3$): δ 194.9, 163.1, 153.1, 148.1, 138.5, 130.7, 127.9, 123.3, 120.0, 96.3, 71.1, 40.9, 23.7, 18.3, 11.3 ppm, HRMS (ESI) m/z: calcd for $C_{17}H_{22}NO_2$ $[M+H]^+$ 272.1645, found 272.1642.

6a: ^{1}H NMR (300 MHz, $CDCl_3$): δ 9.03 (d, *J* = 16.8 Hz, 1 H), 8.25 (d, *J* = 7.6 Hz, 1 H), 8.21 (d, *J* = 7.8 Hz, 1 H), 8.04 (d, *J* = 8.4 Hz, 1 H), 7.74 (d, *J* = 16.8 Hz, 1 H), 7.64 (t, *J* = 7.8 Hz, 1 H), 7.62 (s, 1 H), 7.53 (d, *J* = 7.4 Hz, 1 H), 7.34 (t, *J* = 7.6 Hz, 1 H, 7.26 (s, 1 H), 4.23 (d, *J* = 5.9 Hz, 2 H), 4.21 (d, *J* = 5.8 Hz, 2 H), 4.08 (s, 3 H), 2.89 (s, 3 H), 1.93-1.84 (m, 2 H), 1.68-1.55 (m, 8 H), 1.03 (t, *J* = 5.5 Hz, 6 H), 1.01 (t, *J* = 5.7 Hz, 6 H) ppm; ^{13}C NMR (75 MHz, $CDCl_3$): δ 166.7, 163.2, 162.1, 156.4, 148.4, 148.3, 146.4, 137.0, 136.0, 133.0, 130.1, 129.2, 127.5, 127.2, 124.9, 122.9, 122.0, 121.0, 119.7, 100.8, 98.4, 71.2, 70.4, 53.0, 41.1, 41.0, 23.8, 23.7, 18.4, 11.4, 11.3 ppm, HRMS (ESI) m/z: calcd for $C_{35}H_{43}N_2O_4$ $[M+H]^+$ 555.3217, found 555.3212.

6b: ^{1}H NMR (300 MHz, $CDCl_3$): δ 9.01 (d, *J* = 16.5 Hz, 1 H), 8.19 (d, *J* = 8.2 Hz, 2 H), 8.03 (d, *J* = 8.2 Hz, 1 H), 7.56 (d, *J* = 16.5 Hz, 1 H), 7.58 (d, *J* = 6.2 Hz, 1 H), 7.52 (t, *J* = 4.8 Hz, 1 H), 7.34 (t, *J* = 7.3 Hz, 1 H), 7.12 (s, 1 H), 6.64 (s, 1 H), 4.91 (s, 2 H), 4.19 (d, *J* = 5.5 Hz, 2 H), 4.11 (d, *J* = 5.6 Hz, 2 H), 2.87 (s, 3 H), 1.90-1.83 (m, 2 H), 1.69-1.55 (m, 8 H), 1.04-0.98 (m, 12 H) ppm, HRMS (ESI) m/z: calcd for $C_{34}H_{43}N_2O_3$ $[M+H]^+$ 527.3268, found 527.3266.

6c: ^{1}H NMR (300 MHz, $CDCl_3$): δ 10.26 (s, 1 H), 9.07 (d, *J* = 16.6 Hz, 1 H), 8.27 (d, *J* = 7.8 Hz, 1 H), 8.25 (d, *J* = 8.2 Hz, 1 H), 8.05 (d, *J* = 7.8 Hz, 1 H), 7.70 (d, *J* = 16.6 Hz, 1 H), 7.68 (t, *J* = 7.4 Hz, 1 H), 7.55 (d, *J* = 7.2 Hz, 1 H), 7.43 (s, 1 H), 7.35 (t, *J* = 8.2 Hz, 1 H), 7.21 (s, 1 H), 4.22 (d, *J* = 5.5 Hz, 2 H), 4.20 (d, *J* = 5.8 Hz, 2 H), 2.88 (s, 3 H), 1.91-1.84 (m, 2 H), 1.70-1.53 (m, 4 H), 1.06-0.98 (m, 12 H) ppm; ^{13}C NMR (75 MHz, $CDCl_3$): δ 194.6, 163.2, 162.3, 156.2, 153.2, 148.4, 146.8, 137.0, 136.2, 133.0, 130.2, 129.0, 128.1, 127.2, 125.0, 123.7, 122.3, 121.1, 119.7, 98.4, 96.6, 71.3, 70.4, 41.1, 41.0, 23.9, 23.8, 18.4, 11.5, 11.4 ppm, HRMS (ESI) m/z: calcd for $C_{34}H_{41}N_2O_3$ $[M+H]^+$ 525.3112, found 525.3108.

7a: ^{1}H NMR (300 MHz, $CDCl_3$): δ 9.12 (d, *J* = 16.6 Hz, 1 H), 9.08 (d, *J* = 16.6 Hz, 1 H), 8.24-8.18 (m, 4 H), 8.03 (d, *J* = 7.8 Hz, 1 H), 7.80 (d, *J* = 16.6 Hz, 1 H), 7.70 (d, *J* = 16.6 Hz, 1 H), 7.64 (m, 2 H), 7.53 (d, *J* = 7.4 Hz, 1 H), 7.52 (t, *J* = 7.4 Hz, 1 H), 7.34 (s, 1 H), 7.33 (t, *J* = 7.8 Hz, 1 H), 7.30 (s, 1 H), 4.26 (d, *J* = 5.4 Hz, 2 H), 4.21 (d, *J* = 5.8 Hz, 2 H), 4.14 (d, *J* = 5.8 Hz, 2 H), 3.87 (s, 3 H), 2.87 (s, 3 H), 1.85-1.70 (m, 3 H), 1.68-1.43 (m, 12 H), 1.05 (t, *J* = 7.5 Hz, 6 H), 1.02 (t, *J* = 7.6 Hz, 6 H), 0.92 (t, *J* = 7.5 Hz, 6 H) ppm; ^{13}C NMR (75 MHz, $CDCl_3$): δ 166.7, 163.2, 162.2, 162.1, 157.1, 156.8, 148.4, 147.0, 146.4, 136.9, 136.1, 134.7, 133.0, 131.9, 130.2, 130.0, 129.9, 127.5, 127.4, 126.7, 125.2, 124.8, 123.0, 122.2, 121.6, 121.0, 119.7, 101.0, 98.9, 98.1, 71.2, 70.5, 53.0, 41.1, 41.0, 40.9, 23.9, 23.8, 23.6, 18.5, 11.5, 11.4, 11.3 ppm, HRMS (ESI) m/z: calcd for $C_{52}H_{62}N_3O_5$ $[M+H]^+$ 808.4684, found 808.4674.

7b: ^{1}H NMR (300 MHz, $CDCl_3$): δ 9.07 (d, *J* = 16.6 Hz, 1 H), 8.90 (d, *J* = 16.6 Hz, 1 H), 8.22-8.16 (m, 4 H), 8.03 (d, *J* = 7.5 Hz, 1 H), 7.69 (d, *J* = 16.6 Hz, 1 H), 7.68 (d, *J* = 16.6 Hz, 1 H), 7.58-7.49 (m, 3 H), 7.33 (t, *J* = 7.5 Hz, 1 H), 7.31 (s, 1 H), 7.24 (s, 1 H), 6.67 (s, 1 H), 4.86 (d, *J* = 3.6 Hz, 2 H), 4.50 (t, *J* = 3.6 Hz, 1 H), 4.24 (d, *J* = 5.4 Hz, 2 H), 4.18 (d, *J* = 5.6 Hz, 2 H), 4.12 (d, *J* = 5.5 Hz, 2 H), 2.86 (s, 3 H), 1.91-1.77 (m, 3 H), 1.70-1.49 (m, 12 H), 1.06-0.93 (m, 18 H) ppm.

7c: ^{1}H NMR (300 MHz, $CDCl_3$): δ 10.16 (s, 1 H), 9.11 (d, *J* = 16.5 Hz, 1 H), 9.08 (d, *J* = 16.5 Hz, 1 H), 8.27 (d, *J* = 8.3Hz, 1 H), 8.25 (d, *J* = 7.2 Hz, 1 H), 8.19 (d, *J* = 7.8 Hz, 2 H), 8.03 (d, *J* = 7.8 Hz, 1 H), 7.80 (d, *J* = 16.5 Hz, 1 H), 7.69 (d, *J* = 16.5 Hz, 1 H), 7.69 (t, *J* = 7.6 Hz, 1 H), 7.52 (t, *J* = 7.3 Hz, 1 H), 7.51 (d, *J* = 5.8 Hz, 1 H), 7.43 (s, 1 H), 7.33 (t, *J* = 7.6 Hz, 1 H), 7.28 (s, 1 H), 7.27 (s, 1 H), 4.26 (d, *J* = 5.2 Hz, 2 H), 4.21 (d, *J* = 5.7 Hz, 2 H), 4.15 (d, *J* = 5.4 Hz, 2 H), 2.86 (s, 3 H), 1.92-1.78 (m, 3 H), 1.68-1.47 (m, 12 H), 1.05 (t, *J* = 7.4 Hz, 6 H), 1.02 (t, *J* = 7.4 Hz, 6 H), 0.94 (t, *J* = 7.4 Hz, 6 H) ppm; ^{13}C NMR (75 MHz, $CDCl_3$): δ 194.4, 163.2, 162.3, 162.2, 156.9, 156.7, 153.4, 148.4, 147.1, 146.8, 136.9, 136.3, 134.8, 133.2, 132.1, 130.2, 130.1, 129.8, 128.1, 127.5, 126.9, 125.3, 124.8, 123.7, 122.5, 122.2, 121.6, 121.0, 119.7, 98.6, 98.3, 96.7, 71.3, 70.6, 70.5, 41.0, 41.0, 23.9, 23.8, 23.7, 18.5, 11.5, 11.4 ppm, HRMS (ESI) m/z: calcd for $C_{51}H_{60}N_3O_4$ $[M+H]^+$ 778.4578, found 778.4569.

8a: ^{1}H NMR (300 MHz, $CDCl_3$): δ 9.45 (d, *J* = 16.6 Hz, 1 H), 9.16 (d, *J* = 16.8 Hz, 1 H), 9.02 (d, *J* = 16.7 Hz, 1 H), 8.22-8.16 (m, 4 H), 7.96 (dd, *J* = 8.3, 1.1 Hz, 1 H), 7.82 (d, *J* = 7.4 H, 1 H), 7.76 (d, *J* = 5.3 Hz, 1 H), 7.72 (d, *J* = 16.4 Hz, 1 H), 7.71 (d, *J* = 16.4 Hz, 1 H), 7.68 (d, *J* = 16.4 Hz, 1 H), 7.57 (s, 1 H), 7.53 (dd, *J* = 7.8, 3.5 Hz, 1 H), 7.50 (dd, *J* = 7.7, 3.5 Hz, 1 H), 7.43 (d, *J* = 6.6 Hz, 1 H), 7.32 (s, 1 H), 7.22 (s, 1 H), 7.23-7.13 (m, 2 H), 4.26 (d, *J* = 5.5 Hz, 2 H), 4.19 (d, *J* = 5.3 Hz, 2 H), 4.17 (d, *J* = 5.3 Hz, 2 H), 4.05 (d, *J* = 5.9 Hz, 2 H), 3.74 (s, 3 H), 2.82 (s, 3 H), 1.94-1.81 (m, 4 H), 1.71-1.51 (m, 8 H), 1.05 (t, *J* = 7.5 Hz, 6 H), 1.03 (t, *J* = 7.6 Hz, 6 H), 0.97 (t, *J* = 7.5 Hz, 6 H), 0.84 (t, *J* = 7.4 Hz, 6 H) ppm; ^{13}C NMR (75 MHz, $CDCl_3$): δ 166.6, 163.0, 162.2, 161.9, 157.0, 157.0, 156.9, 148.1, 148.0, 147.1, 136.6, 135.4, 134.6, 134.5, 132.4, 131.8, 131.2, 130.8, 130.3, 130.1, 129.7, 127.2, 127.1, 126.8, 126.6, 125.1, 125.0, 124.4, 122.6, 122.4, 122.1, 121.8, 121.5, 121.4, 120.8, 119.5, 100.8, 99.6, 99.1, 97.8, 71.0, 70.6, 70.5, 70.5, 52.8, 41.1, 41.0, 40.9, 40.7, 23.8, 23.7, 23.6, 23.3, 18.5, 11.4, 11.4, 11.3, 11.2 ppm, HRMS (ESI) m/z: calcd for $C_{69}H_{81}N_4O_6$ $[M+H]^+$ 1061.6151, found 1061.6142.

8b: ^{1}H NMR (300 MHz, $CDCl_3$): δ 9.45 (d, *J* = 16.5 Hz, 1 H), 8.66 (d, *J* = 16.9 Hz, 1 H), 8.85 (d, *J* = 16.6 Hz, 1 H), 8.22-8.16 (m, 4 H), 7.91 (dd, *J* = 8.2, 1.2 Hz, 1 H), 7.70 (d, *J* = 16.8 Hz, 1 H), 7.67 (d, *J* = 16.4 Hz, 1 H), 7.58 (d, *J* = 16.6 Hz, 1 H), 7.73 (m, 2 H), 7.54-7.47 (m, 2 H), 7.40 (d, *J* = 7.0 Hz, 1 H), 7.32 (s, 1 H), 7.19 (s, 1 H), 7.17 (s, 1 H), 7.11 (m, 2 H), 6.59 (s, 1 H), 4.76 (s, 2 H), 4.51 (w, 1 H), 4.23 (d, *J* = 5.3 Hz, 2 H), 4.25 (d, *J* = 5.5 Hz, 2 H),

4.08 (d, *J* = 5.5 Hz, 2 H), 4.02 (d, *J* = 5.9 Hz, 2 H), 2.80 (s, 3 H), 1.89-1.83 (m, 4 H), 1.68-1.54 (m, 8 H), 1.04 (t, *J* = 7.05 Hz, 6 H), 1.02 (t, *J* = 6.6 Hz, 6 H), 0.99 (t, *J* = 6.9 Hz, 6 H), 0.81 (t, *J* = 7.4 Hz, 6 H) ppm.

8c: ^{1}H NMR (300 MHz, $CDCl_3$): δ 9.88 (s, 1 H), 9.64 (d, *J* = 16.2 Hz, 1 H), 9.17 (d, *J* = 16.9 Hz, 1 H), 9.14 (d, *J* = 16.5 Hz, 1 H), 8.22-8.14 (m, 4 H), 7.82 (dd, *J* = 8.3, 1.1 Hz, 1 H), 7.72-7.61 (m, 4 H), 7.56-7.48 (m, 4 H), 7.36 (d, *J* = 6.6 Hz, 1 H), 7.31 (s, 1 H), 7.14 (s, 1 H), 7.09 (s, 1 H), 7.12-7.05 (m, 3 H), 4.24 (d, *J* = 5.4 Hz, 2 H), 4.19 (d, *J* = 6.0 Hz, 2 H), 4.17 (d, *J* = 5.9 Hz, 2 H), 3.94 (d, *J* = 6.0 Hz, 2 H), 2.71 (s, 3 H), 1.94-1.83 (m, 4 H), 1.71-1.56 (m, 8 H), 1.06 (t, *J* = 6.8 Hz, 6 H), 1.03 (t, *J* = 7.9 Hz, 6 H), 1.01 (t, *J* = 7.5 Hz, 6 H), 0.76 (t, *J* = 7.4 Hz, 6 H) ppm; ^{13}C NMR (75 MHz, $CDCl_3$): δ 194.5, 162.8, 162.4, 162.3, 161.6, 156.8, 156.6, 1156.5, 153.0, 147.9, 147.4, 147.1, 146.3, 136.6, 135.1, 134.9, 134.3, 131.8, 131.6, 131.4, 130.4, 130.3, 130.0, 129.5, 127.2, 126.9, 126.8, 126.5, 125.1, 125.0, 124.2, 123.1, 122.3, 122.2, 121.8, 121.5, 121.4, 120.7, 119.4, 100.3, 99.6, 97.6, 96.4, 71.1, 70.6, 41.1, 41.0, 41.0, 40.6, 23.9, 23.8, 23.7, 23.2, 18.4, 11.5, 11.4, 11.4, 11.1 ppm, HRMS (ESI) m/z: calcd for $C_{68}H_{79}N_4O_5$ $[M+H]^+$ 1031.6045, found 1031.6037.

9a: ^{1}H NMR (300 MHz, $CDCl_3$): δ 9.46 (d, *J* = 16.4 Hz, 1 H), 9.36 (d, *J* = 16.6 Hz, 1 H), 9.10 (d, *J* = 16.8 Hz, 1 H), 8.89 (d, *J* = 16.6 Hz, 1 H), 8.21-8.17 (m, 2 H), 8.07 (d, *J* = 6.8 Hz, 1 H), 8.01 (d, *J* = 8.3 Hz, 1 H), 7.96 (d, *J* = 7.9 Hz, 1 H), 7.94 (d, *J* = 5.9 Hz, 1 H), 7.92 (d, *J* = 6.0 Hz, 1 H), 7.87 (d, *J* = 16.6 Hz, 1 H), 7.77 (d, *J* = 7.3 Hz, 1 H), 7.67-7.48 (m, 7 H), 7.35 (s, 1 H), 7.24-7.14 (m, 5 H), 4.25 (d, *J* = 5.5 Hz, 2 H), 2.20-4.15 (m, 6 H), 4.06 (d, *J* = 5.7 Hz, 2 H), 3.84 (s, 3 H), 2.85 (s, 3 H), 1.95-1.37 (m, 15 H), 1.06 (t, *J* = 7.4 Hz, 6 H), 0.99 (t, *J* = 7.4 Hz, 12 H), 0.92 (t, *J* = 7.5 Hz, 6 H), 0.89 (t, *J* = 7.5 Hz, 6 H) ppm; ^{13}C NMR (75 MHz, $CDCl_3$): δ 166.7, 163.0, 162.3, 162.0, 162.0, 161.9, 157.1, 157.0, 157.0, 156.9, 148.3, 148.0, 147.3, 147.0, 146.8, 146.1, 136.7, 135.4, 134.5, 134.4, 134.2, 132.9, 131.7, 131.5, 131.4, 131.2, 130.2, 130.1, 129.8, 129.7, 127.2, 127.1, 126.4, 126.2, 124.8, 124.7, 124.5, 122.6, 122.3, 122.1, 121.8, 121.7, 121.4, 121.3, 120.9, 119.7, 100.7, 100.0, 99.2, 98.6, 97.9, 71.1, 70.6, 70.5, 70.4, 53.6, 52.8, 41.2, 41.0, 40.9, 40.9, 40.8, 23.8, 23.7, 23.6, 23.6, 23.5, 18.6, 11.5, 11.4, 11.3, 11.2 ppm, HRMS (ESI) m/z: calcd for $C_{86}H_{100}N_5O_7$ $[M+H]^+$ 1314.7617, found 1314.7641.

9b: ^{1}H NMR (300 MHz, $CDCl_3$): δ 9.44 (d, *J* = 16.5 Hz, 1 H), 9.37 (d, *J* = 16.5 Hz, 1 H),

9.08 (d, *J* = 16.5 Hz, 1 H), 8.75 (d, *J* = 16.5 Hz, 1 H), 8.20 (t, *J* = 7.3 Hz, 2 H), 8.06 (d, *J* = 7.3 Hz, 1 H), 8.00 (d, *J* = 8.8 Hz, 1 H), 7.92 (d, *J* = 8.6 Hz, 2 H), 7.85 (d, *J* = 16.5 Hz, 1 H), 7.76 (d, *J* = 8.8 Hz, 1 H), 7.64-7.45 (m, 5 H), 7.34 (s, 1 H), 7.26-7.14 (m, 4 H), 7.05 (t, *J* = 8.0 Hz, 1 H), 6.6 (s, 1 H), 4.82 (s, 2 H), 4.22 (d, *J* = 4.7 Hz, 2 H), 4.21 (d, *J* = 5.3 Hz, 2 H), 4.16 (d, *J* = 5.3 Hz, 2 H), 4.06 (d, *J* = 5.3 Hz, 2 H), 4.04 (d, *J* = 5.9 Hz, 2 H), 2.85 (s, 3 H), 1.89-1.41 (m, 15 H), 1.05 (t, *J* = 7.5 Hz, 6 H), 1.01 (t, *J* = 7.5 Hz, 6 H), 0.99 (t, *J* = 7.7 Hz, 6 H), 0.92 (t, *J* = 7.6 Hz, 6 H), 0.88 (t, *J* = 7.8 Hz, 6 H) ppm.

9c: ^{1}H NMR (300 MHz, $CDCl_3$): δ9.98 (s, 1 H), 9.61 (d, *J* = Hz, 1 H), 9.39 (d, *J* = Hz, 1 H), 9.01 (d, *J* = Hz, 1 H), 8.21 (d, *J* = Hz, 1 H), 8.14 (d, *J* = Hz, 1 H), 8.01 (d, *J* = Hz, 1 H), 7.96 (d, *J* = Hz, 1 H), 7.93 (d, *J* = Hz, 2 H), 7.86 (d, *J* = Hz, 1 H), 7.76 (d, *J* = Hz, 1 H), 7.67 (d, *J* = Hz, 1 H), 7.59-7.45 (m, 6 H), 7.29-7.24 (m, 2 H), 7.21-7.08 (m, 4 H), 7.06 (s, 1 H), 7.05 (s, 1 H), 4.23 (d, *J* = Hz, 2 H), 4.19 (d, *J* = Hz, 2 H), 4.17 (d, *J* = Hz, 2 H), 4.09 (d, *J* = Hz, 2 H), 3.95 (d, *J* = Hz, 2 H), 2.83 (s, 3 H), 1.96-1.35 (m, 15 H), 1.06 (t, *J* = Hz, 6 H), 1.02 (t, *J* = Hz, 6 H), 0.94 (t, *J* = Hz, 6 H), 0.92 (t, *J* = Hz, 6 H), 0.86 (t, *J* = Hz, 6 H) ppm; ^{13}C NMR (75 MHz, $CDCl_3$): δ 194.7, 162.8, 162.4, 162.1, 161.8, 161.7, 157.0, 156.7, 156.6, 156.5, 152.9, 148.2, 147.4, 147.1, 146.6, 146.3, 136.7, 135.2, 134.3, 134.3, 132.1, 131.7, 131.4, 131.3, 130.0, 129.8, 129.8, 129.7, 127.5, 127.2, 126.7, 126.2, 124.8, 124.7, 124.4, 124.3, 123.1, 122.4, 122.0, 121.8, 121.7, 121.4, 121.2, 121.1, 120.9, 100.7, 99.3, 99.2, 97.8, 96.3, 71.2, 70.5, 70.4, 41.1, 41.0, 40.8, 40.8, 40.7, 23.8, 23.8, 23.5, 23.5, 23.4, 18.6, 11.5, 11.4, 11.3, 11.2, 11.2 ppm, HRMS (ESI) m/z: calcd for $C_{85}H_{98}N_5O_6$ $[M+H]^+$ 1284.7512, found 1284.7537.

10a: ^{1}H NMR (300 MHz, $CDCl_3$): δ 9.36 (d, *J* = 16.4 Hz, 1 H), 9.30 (d, *J* = 16.4 Hz, 1 H), 9.29 (d, *J* = 16.4 Hz, 1 H), 9.13 (d, *J* = 16.4 Hz, 1 H), 8.94 (d, *J* = 16.5 Hz, 1 H), 8.14 (d, *J* = 5.9 Hz, 1 H), 8.08 (d, *J* = 7.1 Hz, 1 H), 8.04-7.90 (m, 7 H), 7.84-7.70 (m, 5 H), 7.66 (d, *J* = 6.8 Hz, 1 H), 7.60-7.54 (m, 2 H), 7.49 (d, *J* = 6.6 Hz, 1 H), 7.37- 7.29 (m, 4 H), 7.24-7.16 (m, 4 H), 4.22 (d, *J* = 5.8 Hz, 2 H), 4.17-4.10 (m, 10 H), 3.84 (s, 3 H), 2.87 (s, 3 H), 1.91-1.44 (m, 18 H), 1.03 (t, *J* = 7.3 Hz, 6 H), 0.99 (t, *J* = 7.4 Hz, 12 H), 0.96 (t, *J* = 7.4 Hz, 6 H), 0.93 (t, *J* = 7.4 Hz, 6 H), 0.90 (t, *J* = 7.4 Hz, 6 H) ppm; ^{13}C NMR (75 MHz, $CDCl_3$): δ 166.7, 163.0, 162.0, 157.1, 157.0, 156.8, 148.1, 147.1, 146.9, 146.1, 163.7, 135.5, 134.4, 134.2, 134.1, 133.0, 131.6, 131.4, 131.3, 131.1, 131.0, 130.8, 130.2, 129.8, 129.6, 127.3, 127.1, 126.7,

126.5, 126.2, 124.9, 124.5, 122.7, 122.0, 121.8, 121.4, 120.9, 119.7, 100.8, 99.5, 99.3, 99.0, 98.5, 98.0, 71.1, 70.6, 70.5, 52.9, 41.0, 40.9, 40.8, 23.7, 23.7, 23.6, 23.5, 18.6, 11.4, 11.3, 11.3 ppm, HRMS (ESI) m/z: calcd for $C_{103}H_{119}N_6O_8$ $[M+H]^+$ 1568.9118, found 1568.9151.

10b: ^{1}H NMR (300 MHz, $CDCl_3$): δ 9.38 (d, *J* = 16.4 Hz, 1 H), 9.33 (d, *J* = 16.4 Hz, 1 H), 9.23 (d, *J* = 16.4 Hz, 1 H), 9.13 (d, *J* = 16.4 Hz, 1 H), 8.81 (d, *J* = 16.4 Hz, 1 H), 8.14 (d, *J* = 7.8 Hz, 1 H), 8.07 (d, *J* = 7.8 Hz, 1 H), 8.02-7.86 (m, 4 H), 7.79-7.72 (m, 2 H), 7.69-7.47 (m, 3 H), 7.33 (s, 1 H), 7.22-7.11 (m, 5 H), 6.63 (s, 1 H), 4.83 (s, 2 H), 4.22-4.07 (m, 12 H), 2.86 (s, 3 H), 1.89-1.43 (m, 18 H), 1.05-0.85 (m, 36 H) ppm.

10c: ^{1}H NMR (300 MHz, $CDCl_3$): δ 10.00 (s, 1 H), 9.31 (d, *J* = 16.1 Hz, 1 H), 9.36 (d, *J* = 16.4 Hz, 1 H), 9.18 (d, *J* = 16.4 Hz, 1 H), 9.11 (d, *J* = 16.4 Hz, 1 H), 9.02 (d, *J* = 16.4 Hz, 1 H), 8.13 (d, *J* = 7.8 Hz, 1 H), 8.05-7.88 (m, 6 H), 7.82-7.80 (m, 2 H), 7.75-7.64 (m, 3 H), 7.59-7.49 (m, 3 H), 7.37 (t, *J* = 7.9 Hz, 1 H), 7.32 (s, 2 H), 7.25-7.15 (m, 5 H), 7.10 (s, 1 H), 7.08 (s, 1 H), 4.20-4.09 (m, 10 H), 4.02 (d, *J* = 5.8 Hz, 2 H), 2.88 (s, 3 H), 1.89-1.40 (m, 18 H), 1.04-0.86 (m, 36 H) ppm; ^{13}C NMR (75 MHz, $CDCl_3$): δ 194.6, 162.9, 162.2, 162.1, 161.9, 161.8, 157.1, 157.0, 156.7, 156.5, 153.0, 148.3, 147.2, 147.1, 147.0, 146.4, 136.7, 135.4, 134.4, 134.0, 132.4, 131.6, 131.3, 131.1, 130.9, 130.5, 129.8, 129.7, 127.6, 126.8, 126.7, 126.5, 126.3, 124.8, 124.5, 124.3, 123.2, 122.0, 121.4, 121.2, 120.9, 119.7, 100.0, 99.6, 99.0, 98.9, 98.1, 96.4, 71.3, 70.5, 41.1, 41.0, 40.9, 40.8, 40.7, 31.7, 23.8, 23.7, 23.6, 23.5, 22.8, 18.6, 14.2, 11.4, 11.4, 11.3, 11.2, HRMS (ESI) m/z: calcd for $C_{102}H_{117}N_6O_7$ $[M+H]^+$ 1538.9012, found 1538.9036.

11a: ^{1}H NMR (300 MHz, $CDCl_3$): δ 9.34-9.26 (m, 4 H), 9.23 (d, *J* = 16.4 Hz, 1 H), 9.14 (d, *J* = 16.4 Hz, 1 H), 8.95 (d, *J* = 16.6 Hz, 1 H), 8.15 (m, 2 H), 8.07-1.96 (m, 5 H), 7.92-7.36 (m, 16 H), 7.20-7.02 (m, 3 H), 4.24-4.15 (m, 14 H), 3.85 (s, 3 H), 2.86 (s, 3 H), 1.90-1.77 (m, 7 H), 1.62-1.43 (m, 28 H), 1.12-0.93 (m, 42 H) ppm, HRMS (ESI) m/z: calcd for $C_{120}H_{138}N_7O_9$ $[M+H]^+$ 1822.0584, found 1822.0619.

13: ^{1}H NMR (300 MHz, $CDCl_3$): δ 8.72 (s, 1 H), 8.43 (d, *J* = 7.8 Hz, 1 H), 7.80 (d, *J* = 7.8 Hz, 1 H), 7.44 (t, *J* = 8.0 Hz, 1 H), 6.66 (s, 1 H), 4.87 (s, 2 H), 3.95 (d, *J* = 6.4 Hz, 2 H), 3.66 (w, 1 H), 2.27 (m, 1 H), 1,58 (s, 9 H), 1.13 (d, *J* = 6.6 Hz, 6 H) ppm; ^{13}C NMR (75 MHz, $CDCl_3$): δ 162.7, 158.9, 153.0, 137.7, 134.4, 126.0, 120.9, 115.7, 114.7, 98.0, 80.7, 77.6, 77.2, 76.7, 75.0, 65.0, 28.6, 28.3, 19.4 ppm.

14: ^{1}H NMR (300 MHz, $CDCl_3$): δ 10.17 (s, 1 H), 9.00 (s, 1 H), 8.49 (d, *J* = 7.8 Hz, 1 H), 7.84 (d, *J* = 7.8 Hz, 1 H), 7.59 (t, *J* = 7.8 Hz, 1 H), 7.36 (s, 1 H), 4.04 (d, *J* = 6.5 Hz, 2 H), 2.28 (m, 1 H), 1.60 (s, 9 H), 1.13 (d, *J* = 6.6 Hz, 6 H) ppm; ^{13}C NMR (75 MHz, $CDCl_3$): δ 193.7, 163.1, 152.8, 151.7, 138.7, 136.0, 129.2, 123.1, 115.7, 114.5, 96.9, 81.0, 77.6, 77.2, 76.7, 75.4, 28.5, 28.3, 19.4 ppm.

15a: ^{1}H NMR (300 MHz, $CDCl_3$): δ 9.15 (s, 1 H), 8.81 (d, *J* = 16.6 Hz, 1 H), 8.39 (d, *J* = 7.8 Hz, 1 H), 8.25-8.23 (m, 2 H), 7.80 (d, *J* = 16.6 Hz, 1 H), 7.78 (d, *J* = 7.8 Hz, 1 H), 7.66 (t, *J* = 7.8 Hz, 1 H), 7.62 (s, 1 H), 7.42 (t, *J* = 8.0 Hz, 1 H), 7.34 (s, 1 H), 4.21 (d, *J* = 5.6 Hz, 2 H), 4.11 (d, *J* = 6.4 Hz, 2 H), 4.09 (s, 3 H), 2.40-2.26 (m, 1 H), 1.93-1.81 (m, 1 H), 1.69-1.54 (m, 2 H), 1.60 (s, 9 H), 1.18 (d, *J* = 6.3 Hz, 6 H), 1.01 (t, *J* = 7.2 Hz, 6 H) ppm; ^{13}C NMR (75 MHz, $CDCl_3$): δ 166.6, 163.2, 162.1, 155.8, 153.1, 148.3, 146.3, 139.0, 135.7, 135.0, 132.8, 129.6, 127.6, 127.5, 126.0, 123.0, 122.3, 120.8, 115.0, 114.4, 100.9, 98.2, 80.4, 74.8, 71.2, 53.1, 41.0, 28.6, 28.4, 23.8, 19.5, 11.4 ppm, HRMS (ESI) m/z: calcd for $C_{37}H_{46}N_3O_6$ $[M+H]^+$ 628.3381, found 628.3380.

15b: ^{1}H NMR (300 MHz, $CDCl_3$): δ 9.14 (s, 1 H), 8.82 (d, *J* = 16.7 Hz, 1 H), 8.39 (d, *J* = 7.5 Hz, 1 H), 8.21-8.17 (m, 2 H), 7.78 (d, *J* = 8.3 Hz, 1 H), 7.56 (d, *J* = 16.7 Hz, 1 H), 7.55 (t, *J* = 7.8 Hz, 1 H), 7.41 (t, *J* = 8.0 Hz, 1 H), 7.17 (s, 1 H), 6.67 (s, 1 H), 4.91 (s, 2 H), 4.11 (d, *J* = 5.6 Hz, 2H), 4.07 (d, *J* = 6.4 Hz, 2 H), 2.35-2.26 (m, 1 H), 1.88-1.81 (m, 1 H), 1.60 (s, 9 H), 1.65-1.52 (m, 4 H), 1.16 (d, *J* = 6.7 Hz, 6 H), 1.00 (t, *J* = 7.4 Hz, 6 H) ppm; ^{13}C NMR (75 MHz, $CDCl_3$): δ 162.7, 162.3, 159.8, 155.6, 153.1, 145.3, 139.0, 134.9, 134.0, 131.6, 129.8, 127.0, 126.0, 125.4, 122.7, 121.7, 120.8, 115.0, 114.4, 98.5, 97.6, 80.4, 74.7, 70.9, 64.7, 41.0, 28.6, 28.4, 23.8, 19.5, 11.4 ppm.

15c: ^{1}H NMR (300 MHz, $CDCl_3$): δ 10.27 (s, 1 H), 9.19 (s, 1 H), 9.08 (d, *J* = 16.7 Hz, 1 H), 8.42 (d, *J* = 7.32 Hz, 1 H), 8.28-8.25 (m, 2 H), 7.79 (d, *J* = 8.4 Hz, 1 H), 7.70 (t, *J* = 7.8 Hz, 1 H), 7.66 (d, *J* = 16.7 Hz, 1 H), 7.43 (t, *J* = 8.1 Hz, 1 H), 7.43 (s, 1 H), 7.16 (s, 1 H), 4.21 (d, *J* = 5.6 Hz, 2 H), 4.08 (d, *J* = 6.33 Hz, 2 H), 2.37-2.28 (m, 1 H), 1.93-1.83 (m, 1 H), 1.61 (s, 9 H), 1.64-1.61 (m, 4 H), 1.18 (d, *J* = 6.6 Hz, 6 H), 1.01 (t, *J* = 7.4 Hz, 6 H) ppm; ^{13}C NMR (75 MHz, $CDCl_3$): δ 194.5, 163.2, 162.4, 155.2, 153.3, 153.1, 146.7, 139.1, 135.9, 135.0, 131.9, 129.3, 128.1, 127.1, 126.1, 123.8, 122.6, 120.8, 115.1, 114.4, 99.3, 96.7, 80.5, 74.8, 71.3, 40.9, 28.6, 28.4, 23.7, 19.5, 11.4 ppm, HRMS (ESI) m/z: calcd for $C_{36}H_{44}N_3O_5$

$[M+H]^+$ 598.3276, found 598.3275.

16a: ^{1}H NMR (300 MHz, $CDCl_3$): δ 9.20 (s, 1 H), 9.11 (d, *J* = 16.6 Hz, 1 H), 9.07 (d, *J* = 16.6 Hz, 1 H), 8.38 (d, *J* = 7.6 Hz, 1 H), 8.27-8.18 (m, 4 H), 7.82-7.76 (m, 2 H), 7.69 (d, *J* = 16.8 Hz, 1 H), 7.65 (t, *J* = 7.6 Hz, 1 H), 7.63 (s, 1 H), 7.53 (t, *J* = 7.7 Hz, 1 H), 7.40 (t, *J* = 8.1 Hz, 1 H), 7.34 (s, 1 H), 7.31 (s, 1 H), 4.27 (d, *J* = 5.3 Hz, 2 H), 4.21 (d, *J* = 5.5 Hz, 2 H), 3.99 (d, *J* = 6.5 Hz, 2 H), 3.84 (s, 3 H), 2.22-2.11 (m, 1 H), 1.96-1.84 (m, 2 H), 1.75-1.55 (m, 8 H), 1.55 (s, 9 H), 1.05 (t, *J* = 7.6 Hz, 6 H), 1.02 (t, *J* = 7.3 Hz, 6 H), 1.01 (d, *J* = 7.1 Hz, 6 H) ppm; ^{13}C NMR (75 MHz, $CDCl_3$): δ 166.6, 163.2, 162.3, 162.1, 157.0, 156.1, 153.2, 148.4, 146.4, 139.0, 136.0, 134.9, 134.4, 132.7, 131.2, 130.6, 130.1, 127.5, 127.4, 126.9, 125.8, 125.2, 123.0, 122.5, 122.3, 121.6, 120.7, 115.0, 114.4, 101.0, 98.9, 98.7, 80.3, 74.7, 71.2, 70.6, 53.0, 41.1, 41.0, 28.6, 28.3, 23.8, 23.7, 19.3, 11.5, 11.4 ppm, HRMS (ESI) m/z: calcd for $C_{54}H_{65}N_4O_7$ $[M+H]^+$ 881.4849, found 881.4847.

16b: ^{1}H NMR (300 MHz, $CDCl_3$): δ 9.19 (s, 1 H), 8.99 (d, *J* = 16.8 Hz, 1 H), 8.92 (d, *J* = 16.6 Hz, 1 H), 8.37 (d, *J* = 7.2 Hz, 1 H), 8.21-8.16 (m, 4 H), 7.77 (dd, *J* = 8.3, 1.2 Hz, 1 H), 7.69 (d, *J* = 16.6 Hz, 1 H), 7.67 (d, *J* = 16.8 Hz, 1 H), 7.54 (t, *J* = 7.1 Hz, 1 H), 7.52 (t, *J* = 7.1 Hz, 1 H), 7.39 (d, *J* = 16.1 Hz, 1 H), 7.30 (s, 1 H), 7.24 (s, 1 H), 6.67 (s, 1 H), 4.83 (s, 2 H), 4.24 (d, *J* = 5.4 Hz, 2 H), 4.11 (d, *J* = 5.5 Hz, 1 H), 4.04 (d, *J* = 6.4 Hz, 2 H), 2.32-1.98 (m, 2 H), 1.74-1.54 (m, 12 H), 1.53 (s, 9 H), 1.07 (d, *J* = 6.8 Hz, 6 H), 1.03 (t, *J* = 7.9 Hz, 6 H), 1.00 (t, *J* = 7.4 Hz, 6 H) ppm.

16c: ^{1}H NMR (300 MHz, $CDCl_3$): δ 10.13 (s, 1 H), 9.19 (s, 1 H), 9.12 (d, *J* = 16.5 Hz, 1 H), 9.03 (d, *J* = 16.7 Hz, 1 H), 8.38 (d, *J* = 7.4 Hz, 1 H), 8.27 (d, *J* = 8.3 Hz, 1 H), 8.28 (d, *J* = 7.1 Hz, 1 H), 8.21 (d, *J* = 6.9, 1 H), 8.18 (d, *J* = 7.6 Hz, 1 H), 7.80 (d, *J* = 16.8Hz, 1 H), 7.78 (d, *J* = 4.7 Hz, 1 H), 7.70 (d, *J* = 16.7 Hz, 1 H), 7.69 (t, *J* = 7.9, 1 H), 7.53 (t, *J* = 15.6 Hz, 1 H), 7.41 (t, *J* = 8.0 Hz, 1 H), 7.42 (s, 1 H), 7.29 (s, 1 H), 7.28 (s, 1 H), 4.02 (d, *J* = 6.4 Hz, 2 H), 4.27 (d, *J* = 5.5 Hz, 2 H), 4.21 (d, *J* = 5.6 Hz, 2 H), 2.27-2.19 (m, 1 H), 1.94-1.84 (m, 2 H), 1.68-1.51 (m, 8 H), 1.51 (s, 9 H), 1.08 (d, *J* = 6.7 Hz, 6 H), 1.06 (t, *J* = 7.4 Hz, 6 H), 1.01 (t, *J* = 7.4 Hz, 6 H) ppm; ^{13}C NMR (75 MHz, $CDCl_3$): δ 194.3, 163.2, 162.3, 162.2, 156.9, 156.0, 153.3, 153.1, 147.1, 146.8, 139.0, 136.1, 134.9, 134.6, 132.9, 131.4, 130.7, 129.8, 128.1, 127.4, 127.1, 125.8, 125.3, 123.7, 122.6, 122.5, 121.6, 120.7, 115.0, 114.4, 98.8, 98.6, 96.7, 80.2, 74.7, 71.3, 70.6, 41.1, 40.9, 28.5, 28.4, 23.9, 23.7, 19.4, 11.5, 11.3 ppm, HRMS (ESI)

m/z: calcd for $C_{53}H_{63}N_4O_6$ $[M+H]^+$ 851.4742, found 851.4741.

17a: ^{1}H NMR (300 MHz, $CDCl_3$): δ 9.48 (d, *J* = 16.5 Hz, 1 H), 9.13 (s, 1 H), 9.10 (d, *J* = 17.9 Hz, 1 H), 8.97 (d, *J* = 16.9 Hz, 1 H), 8.29 (d, *J* = 7.3 Hz, 1 H), 8.22-8.18 (m, 4 H), 7.95 (d, *J* = 8.1 Hz, 1 H), 7.75-7.70 (m, 4 H), 7.54-7.50 (m, 4 H), 7.42 (d, *J* = 7.9 Hz, 1 H), 7.29 (s, 1 H), 7.22-7.15 (m, 3 H), 4.27 (d, *J* = 5.1 Hz, 2 H), 4.18-4.16 (m, 4 H), 3.89 (d, *J* = 6.2 Hz, 2 H), 3.77 (s, 3 H), 2.17-2.07 (m, 1 H), 1.94-1.80 (m, 3 H), 1.74-1.51 (m, 12 H), 1.57 (s, 9 H), 1.05 (t, *J* = 7.5 Hz, 6 H), 1.02 (t, *J* = 7.4 Hz, 6 H), 0.98 (t, *J* = 7.4 Hz, 6 H), 0.90 (d, *J* = 6.6 Hz, 6 H) ppm; ^{13}C NMR (75 MHz, $CDCl_3$): δ 166.6, 163.0, 162.3, 161.9, 157.1, 157.0, 156.0, 153.2, 148.0, 146.1, 138.8, 135.2, 134.7, 132.4, 131.4, 131.2, 130.5, 127.4, 127.1, 126.7, 125.4, 125.1, 125.0, 122.6, 122.5, 122.4, 122.0, 121.6, 121.5, 120.5, 114.8, 113.4, 100.7, 99.8, 99.0, 98.4, 80.2, 74.4, 71.2, 70.7, 70.6, 52.8, 41.1, 41.0, 40.9, 28.6, 28.2, 23.8, 23.7, 23.7, 19.2, 11.4, 11.4 ppm, HRMS (ESI) m/z: calcd for $C_{71}H_{84}N_5O_8$ $[M+H]^+$ 1134.6314, found 1134.6331.

17c: ^{1}H NMR (300 MHz, $CDCl_3$): δ 9.91 (s, 1 H), 9.61 (d, *J* = 16.3 Hz, 1 H), 9.10 (d, *J* = 16.7 Hz, 1 H), 9.04 (d, *J* = 19.8 Hz, 1 H), 8.25-8.13 (m, 4 H), 7.85 (d, *J* = 7.8 Hz, 1 H), 7.71-7.50 (m, 5 H), 7.33 (d, *J* = 7.8 Hz, 1 H), 7.29 (s, 1 H), 7.18-7.10 (m, 4 H), 4.25 (d, *J* = 5.5 Hz, 2 H), 4.20 (d, *J* = 5.6 Hz, 2 H), 4.16 (d, *J* = 5.9 Hz, 2 H), 3.80 (d, *J* = 6.7 Hz, 2 H), 2.06-1.84 (m, 4 H), 1.70-1.54 (m, 12 H), 1.56 (s, 9 H), 1.06 (t, *J* = 7.4 Hz, 6 H), 1.02 (t, *J* = 7.4 Hz, 6 H), 1.01 (t, *J* = 7.4 Hz, 6 H), 0.83 (d, *J* = 6.7 Hz, 6 H) ppm; ^{13}C NMR (75 MHz, $CDCl_3$): δ 194.6, 162.9, 162.4, 162.3, 161.6, 156.7, 155.9, 153.1, 153.0, 147.4, 147.1, 146.4, 138.6, 135.0, 134.8, 134.7, 134.0, 131.8, 131.5, 131.1, 130.6, 130.4, 130.2, 127.4, 127.0, 126.9, 126.6, 125.2, 125.1, 124.9, 123.2, 122.5, 122.4, 122.0, 121.5, 120.4, 114.6, 114.2, 100.4, 99.4, 98.2, 96.4, 80.2, 74.2, 71.4, 70.6, 70.6, 41.0, 41.0, 40.7, 28.6, 28.2, 23.9, 23.8, 23.7, 23.6, 19.2, 19.1, 11.5, 11.4, 11.4, 11.3 ppm, HRMS (ESI) m/z: calcd for $C_{70}H_{82}N_5O_7$ $[M+H]^+$ 1104.6209, found 1104.6226.

18a: ^{1}H NMR (300 MHz, $CDCl_3$): δ 9.42 (d, *J* = 16.6 Hz, 1 H), 9.35 (d, *J* = 16.4 Hz, 1 H), 9.18 (s, 1 H), 9.02 (d, *J* = 16.8 Hz, 1 H), 8.88 (d, *J* = 16.7 Hz, 1 H), 8.36 (d, *J* = 7.2 Hz, 1 H), 8.21-8.18 (m, 2 H), 8.05 (d, *J* = 7.3 Hz, 1 H), 8.02 (d, *J* = 8.4 Hz, 1 H), 7.96 (d, *J* = 8.2 Hz, 1 H), 7.90-7.80 (m, 3 H), 7.72-7.60 (m, 5 H), 7.56 (s, 1 H), 7.51 (t, *J* = 7.8 Hz, 1 H), 7.35-7.18 (m, 9 H), 4.24 (d, *J* = 5.6 Hz, 2 H), 4.19 (d, *J* =5.6 Hz, 2 H), 4.15 (d, *J* = 5.7 Hz, 2 H), 4.07 (d,

J = 5.8 Hz, 2 H), 4.02 (d, *J* = 6.5 Hz, 2 H), 3.83 (s, 3 H), 2.25-2.17 (m, 1 H), 1.96-1.54 (m, 20 H), 1.58 (s, 9 H), 1.08-0.83 (m, 30 H) ppm; ^{13}C NMR (75 MHz, $CDCl_3$): δ 166.7, 163.0, 162.3, 162.1, 162.0, 157.2, 157.1, 156.9, 156.2, 153.2, 148.0, 147.3, 147.0, 146.8, 146.1, 138.9, 135.4, 134.8, 134.4, 134.2, 134.1, 132.9, 131.5, 131.3, 130.9, 130.7, 130.4, 129.9, 127.3, 127.2, 126.6, 126.4, 125.5, 124.8, 124.5, 122.6, 122.4, 122.2, 122.1, 121.8, 121.5, 121.3, 120.6, 114.8, 114.4, 100.7, 99.9, 99.3, 98.7, 98.4, 80.2, 74.6, 71.1, 70.7, 70.6, 52.8, 41.0, 41.0, 40.9, 40.8, 28.6, 28.3, 23.8, 23.7, 23.7, 23.5, 19.3, 11.4, 11.4, 11.3, 11.3 ppm, HRMS (ESI) m/z: calcd for $C_{88}H_{103}N_6O_9$ $[M+H]^+$ 1387.7781, found 1387.7816.

18b: ^{1}H NMR (300 MHz, $CDCl_3$): δ 9.40 (d, *J* = 16.5 Hz, 1 H), 9.38 (d, *J* = 16.5 Hz, 1 H), 9.18 (s, 1 H), 9.01 (d, *J* = 16.8 Hz, 1 H), 8.74 (d, *J* = 16.6 Hz, 1 H), 8.34 (d, *J* = 7.7 Hz, 1 H), 8.20 (d, *J* = 8.2 Hz, 1 H), 8.19 (d, *J* = 7.5 Hz, 1 H), 8.03 (d, *J* = 5.4 Hz, 1 H), 8.01 (d, *J* = 6.9 Hz, 1 H), 7.93 (d, *J* = 8.2 Hz, 1 H), 7.88 (d, *J* = 5.5 Hz, 1 H), 7.84 (d, *J* = 16.5 Hz, 1 H), 7.81 (d, *J* = 8.1 Hz, 1 H), 7.67-7.47 (m, 6 H), 7.32 (t, *J* = 8.1 Hz, 1 H), 7.27 (s, 1 H), 7.23-7.16 (m, 5 H), 7.10 (t, *J* = 7.8 Hz, 1 H), 6.61 (s, 1 H), 4.81 (s, 2 H), 4.21 (d, *J* = 5.5 Hz, 4 H), 4.07 (d, *J* = 5.3 Hz, 2 H), 4.05 (d, *J* = 4.7 Hz, 2 H), 4.00 (d, *J* = 6.6 Hz, 2 H), 2.27-2.18 (m, 1 H), 1.92-1.49 (m, 20 H), 1.07-0.96 (m, 24 H), 0.89 (t, *J* = 7.4 Hz, 6 H) ppm.

18c: ^{1}H NMR (300 MHz, $CDCl_3$): δ 9.98 (s, 1 H), 9.54 (d, *J* = 16.3 Hz, 1 H), 9.34 (d, *J* = 16.6 Hz, 1 H), 9.15 (s, 1 H), 8.99 (d, *J* = 16.6 Hz, 1 H), 8.92 (d, *J* = 16.8 Hz, 1H), 8.35 (d, *J* = 7.0 Hz, 1 H), 8.22 (d, *J* = 8.2 Hz, 1 H), 8.14 (d, *J* = 6.5 Hz, 1 H), 7.99 (d, *J* = 7.9 Hz, 2 H), 7.90 (d, *J* = 6.3 Hz, 1 H), 7.87 (d, *J* = 7.2 Hz, 1 H), 7.78 (d, *J* = 16.4 Hz, 1 H), 7.73 (d, *J* = 8.2 Hz, 1 H), 7.64-7.48 (m, 6 H), 7.33 (t, *J* = 8.0 Hz, 1 H), 7.31 (s, 1 H), 7.26-7.13 (m, 3 H), 7.11 (s, 1 H), 7.09 (s, 1 H), 7.07 (s, 1 H), 4.22 (d, *J* = 5.9 Hz, 2 H), 4.20 (d, *J* = 5.9 Hz, 2 H), 4.09 (d, *J* = 5.8 Hz, 2 H), 4.02 (d, *J* = 6.6 Hz, 2 H), 3.98 (d, *J* = 5.8 Hz, 2 H), 2.28-2.17 (m, 1 H), 1.94-1.38 (m, 20 H), 1.59 (s, 9 H), 1.08-0.99 (m, 18 H), 0.95 (t, *J* = 7.4 Hz, 6 H), 0.87 (t, *J* = 7.4 Hz, 6 H) ppm; ^{13}C NMR (75 MHz, $CDCl_3$): δ 194.6, 162.8, 162.4, 162.2, 161.9, 161.8, 157.0, 156.8, 156.5, 156.2, 153.2, 153.0, 147.4, 147.1, 146.6, 146.4, 138.9, 135.9, 135.3, 134.8, 134.3, 134.0, 132.2, 131.7, 131.4, 131.2, 130.7, 130.6, 130.1, 129.8, 127.5, 127.3, 127.0, 126.4, 125.7, 125.4, 124.8, 124.3, 123.2, 122.5, 122.2, 122.0, 121.9, 121.5, 121.3, 121.2, 120.6, 114.8, 114.4, 100.4, 99.4, 99.2, 98.3, 96.4, 80.2, 74.6, 71.3, 70.6, 41.0, 40.9, 40.8, 34.4, 30.5, 29.6, 28.6, 28.4, 23.8, 23.5, 23.4, 21.3, 19.3, 11.4, 11.4, 11.3, 11.2 ppm,

HRMS (ESI) m/z: calcd for $C_{87}H_{101}N_6O_8$ $[M+H]^+$ 1357.7675, found 1357.7717.

19a: ^{1}H NMR (300 MHz, $CDCl_3$): δ 9.34 (d, *J* = 16.6 Hz, 1 H), 9.31 (d, *J* = 16.2 Hz, 1 H), 9.28 (d, *J* = 16.4 Hz, 1 H), 9.19 (s, 1 H), 9.06 (d, *J* = 16.7 Hz, 1 H), 8.93 (d, *J* = 16.7 Hz, 1 H), 8.36 (d, *J* = 6.5 Hz, 1 H), 8.13 (d, *J* = 6.8 Hz, 1 H), 8.09 (d, *J* = 6.7 Hz, 1 H), 8.03-7.99 (m, 4 H), 7.94-7.56 (m, 12 H), 7.39 (d, *J* = 15.7 Hz, 1 H), 7.34-7.15 (m, 12 H), 4.23 (d, *J* = 5.8 Hz, 2 H), 4.17 (d, *J* = 5.5 Hz, 6 H), 4.12 (d, *J* = 5.6 Hz, 2 H), 3.98 (d, *J* = 6.4 Hz, 2 H), 3.84 (s, 3 H),2.21-2.12 (m, 1 H), 1.93-1.77 (m, 5 H), 1.66-1.44 (m, 29 H), 1.08-0.86 (m, 36 H) ppm; ^{13}C NMR (75 MHz, $CDCl_3$): δ 166.6, 162.1, 157.2, 156.9, 156.2, 153.2, 148.1, 147.0, 146.2, 134.8, 134.3, 131.5, 130.9, 127.2, 127.1, 126.7, 125.5, 124.7, 122.4, 122.1, 121.8, 121.2, 120.7, 114.8, 114.4, 100.8, 99.4, 98.4, 80.2, 74.6, 71.2, 70.7, 52.9, 40.9, 28.6, 28.3, 23.7, 23.6, 22.8, 19.3, 11.4, 11.3 ppm, HRMS (ESI) m/z: calcd for $C_{105}H_{122}N_7O_{10}$ $[M+H]^+$ 1641.9281, found 1641.9285.

15e: ^{1}H NMR (300 MHz, $CDCl_3$): δ 8.92 (d, *J* = 16.Hz, 1 H), 8.22 (d, *J* = 8.2 Hz, 1 H), 8.21 (d, *J* = 7.2 Hz, 1 H), 7.69 (d, *J* = 16.7Hz, 1 H), 7.64 (t, *J* = 7.7 Hz, 1 H), 7.62 (s, 1 H), 7.52 (d, *J* = 8.2 Hz, 1 H), 7.25 (t, *J* = 8.7 Hz, 1 H), 7.22 (s, 1 H), 6.93 (d, *J* = 7.4 Hz, 1 H), 4.21 (d, *J* = 5.6 Hz, 2 H), 4.08 (d, *J* = 6.1 Hz, 2 H), 4.08 (s, 3 H), 2.36-2.27 (m, 1 H), 1.90-1.84 (m, 1 H), 1.66-1.54 (m, 4 H), 1.17 (d, *J* = 6.7 Hz, 6 H), 1.01 (t, *J* = 7.4 Hz, 6 H) ppm.

21: ^{1}H NMR (300 MHz, $CDCl_3$): δ 12.41 (s, 1 H), 12.29 (s, 1 H), 9.05 (d, *J* = 7.7 Hz, 1 H), 8.98 (d, *J* = 7.7 Hz, 1 H), 8.25 (d, *J* = 8.32 Hz, 1 H), 8.24 (d, *J* = 7.9 Hz, 1 H), 8.14 (d, *J* = 16.8 Hz, 1 H), 8.09 (d, *J* = 8.4 Hz, 1 H), 7.94 (d, *J* = 8.3 Hz, 1 H), 7.94 (s, 1 H), 7.71-7.58 (m, 5 H), 7.58 (s, 1 H), 7.34 (t, *J* = 7.9 Hz, 1 H), 7.16 (s, 1 H), 6.73 (d, *J* = 16.7 Hz, 1 H), 6.54 (s, 1 H), 4.22 (d, *J* = 5.6 Hz, 2 H), 4.19 (d, *J* = 6.4 Hz, 2 H), 3.93 (d, *J* = 6.4 Hz, 2 H), 3.81 (s, 3 H), 3.09 (d, *J* = 6.9 Hz, 2 H), 2.40-2.24 (m, 2 H), 1.95-1.85 (m, 1 H), 1.69-1.58 (m, 5 H), 1.21 (d, *J* = 6.7 Hz, 6 H), 1.18 (d, *J* = 6.8 Hz, 6 H), 1.04 (t, *J* = 7.4 Hz, 6 H), 0.78 (d, *J* = 6.7 Hz, 6 H) ppm.

15d: ^{1}H NMR (300 MHz, $CDCl_3$): δ 9.12 (s, 1 H), 8.76 (d, *J* = 16.4 Hz, 1 H), 8.43 (d, *J* = 7.8 Hz, 1 H), 8.29 (d, *J* = 9.5 Hz, 1 H), 8.26 (d, *J* = 7.2 Hz, 1 H), 7.80 (d, *J* = 8.3 Hz, 1 H), 7.71 (t, *J* = 7.9 Hz, 1 H), 7.71 (s, 1 H), 7.55 (d, *J* = 16.4 Hz, 1 H), 7.44 (t, *J* = 8.1 Hz, 1 H), 7.08 (s, 1 H), 4.25 (d, *J* =5.6 Hz, 2 H), 4.07 (d, *J* = 6.4 Hz, 2 H), 2.34-2.28 (m, 1 H), 1.94-1.82

(m, 1 H), 1.68-1.51 (m, 13 H), 1.17 (d, *J* = 6.7 Hz, 6 H), 1.02 (t, *J* = 7.4 Hz, 6 H) ppm, HRMS (ESI) m/z: calcd for $C_{36}H_{42}N_3O_6$ $[M-H]^-$ 612.3068, found 612.3063.

23a: ^{1}H NMR (300 MHz, $CDCl_3$): δ 11.91 (s, 1H), 11.82 (s, 1 H), 11.72 (s, 1 H), 11.49 (s, 1 H), 8.64 (s, 1 H), 8.50 (d, *J* = 6.7 Hz, 1 H), 8.36 (d, *J* = 7.8 Hz, 1 H), 8.32 (d, *J* = 8.6 Hz, 1 H), 8.28 (d, *J* = 7.4 Hz, 1 H), 8.23 (d, *J* = 7.3 Hz, 1 H), 8.09 (d, *J* = 8.5 Hz, 1 H), 8.06 (d, *J* = 7.6 Hz, 1 H), 7.85 (d, *J* = 6.8 Hz, 1 H), 7.80 (d, *J* = 8.5 Hz, 1 H), 7.67 (d, *J* = 7.6 Hz, 1 H), 7.62 (d, *J* = 7.5 Hz, 2 H), 7.47 (d, *J* = 16.2 Hz, 1 H), 7.40-7.19 (m, 6 H), 7.09-6.98 (m, 2 H), 6.87 (s, 1 H), 6.82 (s, 1 H), 6.62 (d, *J* = 16.6 Hz, 1 H), 6.47 (s, 1 H), 6.20 (s, 1 H), 4.54-4.49 (m, 1 H), 4.51 (d, *J* = 9.0 Hz, 2 H), 4.33-4.27 (m, 2 H), 4.11-3.93 (m, 5 H), 3.68 (d, *J* = 6.6 Hz, 2 H), 3.17 (s, 3 H), 2.57-2.07 (m, 6 H), 1.85-1.71 (m, 4 H), 1.59 (s, 9 H), 1.34-1.07 (m, 30 H), 0.70 (d, *J* =6.6 Hz, 3 H), 0.59 (d, *J* = 6.7 Hz, 3 H) ppm, HRMS (ESI) m/z: calcd for $C_{93}H_{102}N_{11}O_{14}$ $[M+H]^+$ 1597.7636, found 1597.7646.

23b: ^{1}H NMR (300 MHz, $CDCl_3$): δ 11.93 (s, 1 H), 11.89 (s, 1 H), 11.76 (s, 1 H), 11.58 (s, 1 H), 8.54 (d, *J* = 8.0 Hz, 1 H), 8.40 (d, *J* = 7.6 Hz, 1 H), 8.29 (d, *J* = 7.6 Hz, 1 H), 8.24 (d, *J* = 8.1 Hz, 1 H), 8.08 (d, *J* = 8.4 Hz, 1 H), 8.05 (d, *J* = 8.5 Hz, 1 H), 7.83 (d, *J* = 6.0 Hz, 1 H), 7.81 (d, *J* = 7.1 Hz, 1 H), 7.74 (d, *J* = 16.8 Hz, 1 H), 7.64 (t, *J* = 7.9 Hz, 1 H), 7.48 (t, *J* = 7.9 Hz, 1 H), 7.40 (t, *J* = 8.1 Hz, 1 H), 7.39 (s, 1 H), 7.36-7.28 (m, 2 H), 7.23 (s, 1H), 7.20-7.10 (m, 1 H), 7.02 (t, *J* = 7.9 Hz, 1 H), 6.85 (s, 1H), 6.81 (s, 1H), 6.74 (d, *J* = 7.4 Hz, 1 H), 6.50 (d, *J* = 16.5 Hz, 1 H), 6.48 (s, 1 H), 6.22 (s, 1H), 4.55-4.47 (m, 3 H), 4.35-4.27 (m, 2 H), 4.12-3.92 (m, 5 H), 3.68 (d, *J* = 6.3 Hz, 2 H), 3.18 (s, 3 H), 2.57-2.08 (m, 6 H), 1.87-1.70 (m, 4 H), 1.37-1.23 (m, 18 H), 1.19-1.13 (m, 6 H), 1.10 (t, *J* = 6.3 Hz, 6 H), 0.70 (d, *J* = 6.7 Hz, 3 H), 0.60 (d, *J* = 6.7 Hz, 3 H) ppm.

27: ^{1}H NMR (400 MHz, $CDCl_3$): δ 11.30 (s, 1 H), 11.20 (s, 1 H), 11.14 (s, 1 H), 11.01 (s, 1 H), 10.97 (s, 1 H), 10.84 (s, 1 H), 10.78 (s, 1 H), 10.72 (s, 1 H), 8.24 (d, *J* = 8.2 Hz, 1 H), 8.19 (d, *J* = 7.5 Hz, 1 H), 8.15 (d, *J* = 7.7 Hz, 1 H), 8.14 (d, *J* = 7.5 Hz, 1 H), 8.07 (d, *J* = 7.5 Hz, 1 H), 7.96 (d, *J* = 8.3 Hz, 1 H), 7.91 (d, *J* = 7.5 Hz, 1 H), 7.84 (d, *J* = 8.2 Hz, 1 H), 7.53 (d, *J* = 7.9 Hz, 1 H), 7.40 (d, *J* = 7.7 Hz, 1 H), 7.38 (d, *J* = 7.9 Hz, 1 H), 7.30 (t, *J* = 7.8 Hz, 1 H), 7.01 (s, 1 H), 6.63 (s,1 H), 6.61 (s, 1 H), 6.50 (s, 1 H), 6.27 (s, 1 H), 5.88 (s, 1 H), 5.40 (s, 1 H), 5.08 (s, 1 H), 2.94 (s, 3 H), 1.04 (t, *J* = 7.9 Hz, 6 H) ppm; ^{13}C NMR (200 MHz, $CDCl_3$): δ 163.9, 163.5, 163.3, 163.2, 163.2, 163.0, 162.9, 162.4, 162.1, 161.8, 161.6,

161.0, 161.0, 160.8, 160.8, 160.6, 160.2, 159.8, 159.8, 153.4, 150.6, 150.4, 150.0, 149.2, 148.8, 148.6, 148.2, 145.4, 145.0, 144.6, 139.9, 139.1, 139.1, 139.0, 138.6, 138.4, 138.3, 137.9, 137.8, 137.2, 134.6, 133.9, 133.8, 133.8, 133.7, 133.7, 133.5, 133.3, 132.6, 128.3, 127.6, 127.3, 127.2, 126.8, 126.7, 126.2, 126.1, 125.3, 124.6, 124.4, 124.0, 123.3, 122.6, 122.4, 122.1, 121.9, 121.8, 121.6, 121.3, 120.7, 117.4, 117.4, 117.3, 117.2, 116.9, 116.8, 116.5, 116.4, 116.4, 116.3, 116.1, 115.6, 115.2, 114.8, 100.4, 100.4, 100.0, 99.5, 98.8, 98.1, 98.0, 97.9, 97.8, 76.0, 75.8, 75.7, 75.6, 75.5, 75.2, 75.0, 74.9, 71.8, 52.0, 41.6, 28.8, 28.8, 28.8, 28.7, 28.7, 28.6, 28.5, 28.5, 24.2, 24.1, 19.6, 19.6, 19.6, 19.6, 19.5, 19.5, 19.4, 19.4, 19.3, 19.3, 19.2, 19.2, 11.6 ppm, HRMS (ESI) m/z: calcd for $C_{144}H_{148}N_{19}O_{22}$ $[M+H]^+$ 2496.1074, found 2496.1087.

17d: ^{1}H NMR (300 MHz, $CDCl_3$): δ 9.68 (d, *J* = 16.2 Hz, 1 H), 9.10 (d, *J* = 16.9 Hz, 1 H), 8.93 (s, 1H), 8.79 (d, *J* = 16.1 Hz, 1 H), 8.21 (d, *J* = 7.2 Hz, 4 H), 8.13 (d, *J* = 7.4 Hz, 1 H), 7.81 (d, *J* = 8.3 Hz, 1 H), 7.65 (d, *J* = 16.3 Hz, 1 H), 7.60-7.49 (m, 6 H), 7.43 (d, *J* = 16.3 Hz, 1 H), 7.30 (d, *J* = 8.1 Hz, 1 H), 7.13-7.02 (m, 6 H), 4.24-4.19 (m, 6 H), 3.73 (d, *J* = 6.7 Hz, 2 H), 1.97-1.88 (m, 4 H), 1.68-1.58 (m, 12 H), 1.07-0.99 (m, 18 H), 0.78 (d, *J* = 6.7 Hz, 6 H) ppm, HRMS (ESI) m/z: calcd for $C_{70}H_{82}N_5O_8$ $[M+H]^+$ 1120.6158, found 1120.6208.

19d: ^{1}H NMR (300 MHz, $CDCl_3$): δ 9.38 (d, *J* = 16.5 Hz, 1 H), 9.36 (d, *J* = 16.3 Hz, 1 H), 9.16 (d, *J* = 16.2 Hz, 1 H), 9.18 (s, 1 H), 8.99 (d, *J* = 16.8 Hz, 1 H), 8.72 (d, *J* = 16.4 Hz, 1 H), 8.35 (d, *J* = 6.8 Hz, 1 H), 8.11 (d, *J* = 6.6 Hz, 1 H), 7.97 (d, *J* = 6.7 Hz, 4 H), 7.87 (d, *J* = 7.4 Hz, 1 H), 7.82 (d, *J* = 6.5 Hz, 1 H), 7.74 (d, *J* = 7.8 Hz, 1 H), 7.68-7.30 (m, 11 H), 7.22-7.07 (m, 5 H), 7.00 (s, 1 H), 6.97 (s, 1 H), 6.91 (s, 1 H), 4.19-4.12 (m, 8 H), 3.96 (d, *J* = 6.0 Hz, 4 H), 2.20-2.11 (m, 1 H), 1.92-1.82 (m, 5 H), 1.66-1.37 (m, 31 H), 1.02-0.83 (m, 36 H) ppm, HRMS (ESI) m/z: calcd for $C_{104}H_{120}N_7O_{10}$ $[M+H]^+$ 1627.9125, found 1627.9177.

24a: ^{1}H NMR (300 MHz, $CDCl_3$): δ 11.62 (s, 1 H), 11.60 (s, 1 H), 11.47 (s, 1 H), 11.36 (s, 1H), 8.82 (s, 1 H), 8.70 (d, *J* = 16.3 Hz, 1 H), 8.50 (d, *J* = 16.7 Hz, 1 H), 8.33 (d, *J* = 7.4 Hz, 1 H), 8.22-8.08 (m, 4 H), 8.01-7.91 (m, 3 H), 7.84 (d, *J* = 7.3 Hz, 1 H), 7.74-7.60 (m, 3 H), 7.54-7.34 (m, 6 H), 7.24-7.06 (m, 6 H), 6.98 (t, *J* = 7.9 Hz, 1 H), 6.87 (s, 1 H), 6.80 (d, *J* = 6.1 Hz, 1 H), 6.75 (d, *J* = 7.9 Hz, 1 H), 6.67 (s, 1 H), 6.58 (s, 1 H), 6.40 (s, 1 H), 6.22 (s, 1 H), 6.07 (s, 1 H), 4.47-4.42 (m, 1 H), 4.24-3.68 (m, 12 H), 3.66-3.62 (m, 2 H), 3.46-3.41 (m, 1 H), 3.02 (s,3 H), 2.52-2.12 (m, 7 H), 1.92-1.56 (m, 15 H), 1.37-1.34 (m, 6 H), 1.29-0.98 (m,

42 H), 0.56 (d, J = 6.4 Hz, 3 H), 0.34 (d, J = 6.3 Hz, 3 H), HRMS (ESI) m/z: calcd for $C_{127}H_{140}N_{13}O_{16}$ $[M+H]^+$ 2104.0569, found 2104.0586.

28: HRMS (ESI) m/z: calcd for C178H186N21O24 $[M+H]^+$ 3003.4041, found 3003.4087.

25a: HRMS (ESI) m/z: calcd for C161H178N15O18 $[M+H]^+$ 2610.3502, found 2610.3562.

29: HRMS (ESI) m/z: calcd for C212H224N23O26 $[M+2H]^{2+}$ 1755.3524, found 1755.3685.

References

(1) Guichard, G.; Huc, I. *Chem. Commun.* **2011**, *47*, 5933-5941.

(2) Huc, I. *Eur. J. Org. Chem.* **2004**, *2004*, 17-29.

(3) Jiang, H.; Léger, J.-M.; Huc, I. *J. Am. Chem. Soc.* **2003**, *125*, 3448-3449.

(4) Jiang, H.; Maurizot, V.; Huc, I. *Tetrahedron* **2004**, *60*, 10029-10038.

(5) Haldar, D.; Jiang, H.; Léger, J.-M.; Huc, I. *Angew. Chem. Int. Ed.* **2006**, *45*, 5483-5486.

(6) Sebaoun, L.; Maurizot, V.; Granier, T.; Kauffmann, B.; Huc, I. *J. Am. Chem. Soc.* **2014**, *136*, 2168-2174.

(7) Sebaoun, L.; Kauffmann, B.; Delclos, T.; Maurizot, V.; Huc, I. *Org. Lett.* **2014**, *16*, 2326-2329.

(8) Chandramouli, N.; Ferrand, Y.; Lautrette, G.; Kauffmann, B.; Mackereth, C. D.; Laguerre, M.; Dubreuil, D.; Huc, I. *Nat. Chem.* **2015**, *7*, 334-341.

(9) Gan, Q.; Wang, X.; Kauffmann, B.; Rosu, F.; Ferrand, Y.; Huc, I. *Nat Nano* **2017**, *12*, 447-452.

(10) Gante, J. *Angew. Chem. Int. Ed. Eng.* **1994**, *33*, 1699-1720.

(11) Choudhary, A.; Raines, R. T. *ChemBioChem* **2011**, *12*, 1801-1807.

(12) Dai, N.; Etzkorn, F. A. *J. Am. Chem. Soc.* **2009**, *131*, 13728-13732.

(13) Dai, N.; Wang, X. J.; Etzkorn, F. A. *J. Am. Chem. Soc.* **2008**, *130*, 5396-5397.

(14) Gardner, R. R.; Liang, G.-B.; Gellman, S. H. *J. Am. Chem. Soc.* **1995**, *117*, 3280-3281.

(15) Vasbinder, M. M.; Jarvo, E. R.; Miller, S. J. *Angew. Chem. Int. Ed.* **2001**, *40*, 2824-2827.

(16) Narumi, T.; Hayashi, R.; Tomita, K.; Kobayashi, K.; Tanahara, N.; Ohno, H.; Naito, T.; Kodama, E.; Matsuoka, M.; Oishi, S.; Fujii, N. *Org. Biomol. Chem.* **2010**, *8*, 616-621.

(17) Oishi, S.; Kamitani, H.; Kodera, Y.; Watanabe, K.; Kobayashi, K.; Narumi, T.; Tomita, K.; Ohno, H.; Naito, T.; Kodama, E.; Matsuoka, M.; Fujii, N. *Org. Biomol. Chem.* **2009**, *7*, 2872-2877.

(18) Xiao, J.; Weisblum, B.; Wipf, P. *J. Am. Chem. Soc.* **2005**, *127*, 5742-5743.

(19) Wipf, P.; Henninger, T. C.; Geib, S. J. *J. Org. Chem.* **1998**, *63*, 6088-6089.

(20) Niida, A.; Tomita, K.; Mizumoto, M.; Tanigaki, H.; Terada, T.; Oishi, S.; Otaka, A.; Inui, K.-i.; Fujii, N. *Org. Lett.* **2006**, *8*, 613-616.

(21) Oishi, S.; Kamano, T.; Niida, A.; Odagaki, Y.; Hamanaka, N.; Yamamoto, M.; Ajito, K.;

Tamamura, H.; Otaka, A.; Fujii, N. *J. Org. Chem.* **2002**, *67*, 6162-6173.

(22) Våbenø, J.; Lejon, T.; Nielsen, C. U.; Steffansen, B.; Chen, W.; Ouyang, H.; Borchardt, R. T.; Luthman, K. *J. Med. Chem.* **2004**, *47*, 1060-1069.

(23) Dondoni, A.; Perrone, D. *Tetrahedron Lett.* **1992**, *33*, 7259-7262.

(24) Lama, T.; Del Valle, S. E.; Genest, N.; Lubell, W. D. *Int. J. Pept. Res. Ther.* **2007**, *13*, 355-366.

(25) Myers, A. G.; Barbay, J. K.; Zhong, B. *J. Am. Chem. Soc.* **2001**, *123*, 7207-7219.

(26) Aoyagi, Y.; Williams, R. M. *Tetrahedron* **1998**, *54*, 10419-10433.

(27) Righi, G.; Ronconi, S.; Bonini, C. *Eur. J. Org. Chem.* **2002**, *2002*, 1573-1577.

(28) Gilligan, P. J.; Robertson, D. W.; Zaczek, R. *J. Med. Chem.* **2000**, *43*, 1641-1660.

(29) Leftheris, K.; Kline, T.; Vite, G. D.; Cho, Y. H.; Bhide, R. S.; Patel, D. V.; Patel, M. M.; Schmidt, R. J.; Weller, H. N.; Andahazy, M. L.; Carboni, J. M.; Gullo-Brown, J. L.; Lee, F. Y. F.; Ricca, C.; Rose, W. C.; Yan, N.; Barbacid, M.; Hunt, J. T.; Meyers, C. A.; Seizinger, B. R.; Zahler, R.; Manne, V. *J. Med. Chem.* **1996**, *39*, 224-236.

(30) Zanda, M. *New J. Chem.* **2004**, *28*, 1401-1411.

(31) Li, C. S.; Deschenes, D.; Desmarais, S.; Falgueyret, J.-P.; Gauthier, J. Y.; Kimmel, D. B.; Léger, S.; Massé, F.; McGrath, M. E.; McKay, D. J.; Percival, M. D.; Riendeau, D.; Rodan, S. B.; Thérien, M.; Truong, V.-L.; Wesolowski, G.; Zamboni, R.; Black, W. C. *Bioorganic & Medicinal Chemistry Letters* **2006**, *16*, 1985-1989.

(32) Huang, H.; Zhou, N.; Ortiz, R. P.; Chen, Z.; Loser, S.; Zhang, S.; Guo, X.; Casado, J.; López Navarrete, J. T.; Yu, X.; Facchetti, A.; Marks, T. J. *Adv. Funct. Mater.* **2014**, *24*, 2782-2793.

(33) Tanase, C.; Wildeman, J.; Blom, P. W. M. *Adv. Funct. Mater.* **2005**, *15*, 2011-2015.

(34) Burroughes, J. H.; Bradley, D. D. C.; Brown, A. R.; Marks, R. N.; Mackay, K.; Friend, R. H.; Burns, P. L.; Holmes, A. B. *Nature* **1990**, *347*, 539-541.

(35) Qi, T.; Deschrijver, T.; Huc, I. *Nat. Protocols* **2013**, *8*, 693-708.

(36) Ozanne, A.; Pouységu, L.; Depernet, D.; François, B.; Quideau, S. *Org. Lett.* **2003**, *5*, 2903-2906.

III Copper (II) Loaded Quinoline Carboxamide Foldamers

3.1 Introduction

Helices are extensively observed in nature such as in proteins and nucleic acids.[1-3] Those helical structures serve not only as structural components but also as functional units. Inspired by the helices found in bio-macromolecules, mimics of those helical structure motifs are pursued. Among all different kinds of mimics, helicates, which were introduced by Lehn to describe helical metal coordination complexes,[4] stand out as a very important and interesting class of compounds. Usually, helicates are composed with multiple metal centers (at least 2 metal centers) and various number strand ligands. Based on the number of strands, single/double/triple-stranded helicates are produced.[5] There are many advantages to prepare helicates such as many metal ions can be chosen and the geometry requirements of each metal ions are well established which allow bottom-up design based on those knowledge. The helical structure is governed by the coordination of the metal center which results in the helical arrangement of the ligand that surround the metal. A great number of helicates has been prepared before, such as double stranded helicates,[4-7] triple stranded helicates.[8,9] The nature of ligands and the metals are varied, nevertheless, they all share a common feature that the ligands are oligomers composed of several monomers that have the site for coordination. By changing the metal and ligand, literally infinite number of helicates can be made which allows design of different kinds of functions such as muscle like extension/contraction movements.[10,11] However, limitations are also found such as the difficulty to synthesize very long ligands.[12] One possible solution to that problem is the spontaneous polymerization of the ligand and coordination which was elegantly demonstrated recently by Nitschke et al. by taken advantage of imine condensation and metal coordination.[9,13] Although, this method can reach very long helicate, the control of the exact length is less powerful.

In our group, metal helicates were prepared by the coordination of copper (II) ions and with oligopyridine dicarboxamide previously.[14] In these helicates, the coordination was

between metal ions and the nitrogen atoms of pyridine rings and the deprotonated amide bonds. Two molecules of oligopyridine dicarboxamide were wrapped around multiple copper (II) ions to form a double helix. The coordination geometry of Cu (II) ions inside the double helix is pseudo-square planar (with distortion). The metal centers are not completely aligned inside the double helix.

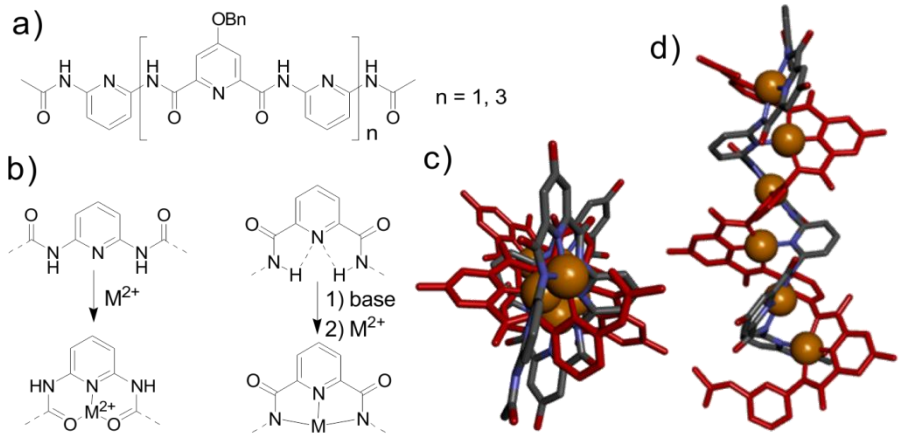

Figure 3-1: a) Chemical structures of oligopyridine dicarboxamides; b) expected metal coordination modes of 2,6-bis(carbonylamino)pyridines and 2,6-pyridinedicarboxamides; c) top view and d) side view of crystal structure of helicate.

Metal coordination was also used to help the formation of closed molecular capsules and guest binding.[15-17] Pyridazine-pyridine-pyridazine (Pyz-Pyr-Pyz) prefers the anti-anti conformation over syn-syn conformation in its native state. The conformation preference of it can be altered to syn-syn by coordination with suitable metal ions, such as copper and silver.[17] The conformation switching of Pyz-Pyr-Pyz was successfully used to construct molecular container by connecting two units of conical segments with it. The two conical segments were separated due to the preferred anti-anti conformation of Pyz-Pyr-Pyz unit. After complexation with metals such as Cu (I), Cu (II), Silver (I)[17] and even alkali/alkaline-earth metals such as Na^+, K^+, Ca^{2+} and Mg^{2+},[15,16] a closed capsule like molecules formed by switching the conformation of Pyz-Pyr-Pyz to syn-syn conformation. Strong binding with carbohydrate guests was found with the metal containing capsules which the binding of guests was mediated with the coordination.[15]

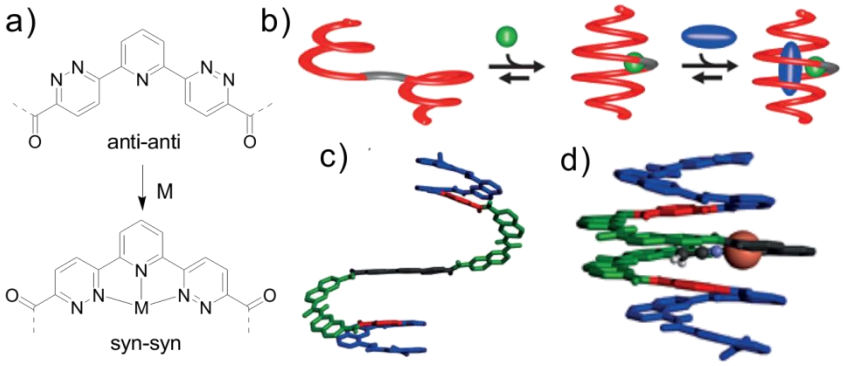

Figure 3-2: a) Conformation preferences of Pyz-Pyr-Pyz before and after metal coordination; b) representation of helical-capsule folding upon metal coordination and guest binding; c) crystal structure of helical-capsule before metal coordination and d) crystal structure of helical-capsule after metal coordination.

Quinoline carboxamide oligomers are studied extensively and are found to form stable helical structure both in solution and in the solid state.[18] The outside of the helices are surrounded by aliphatic side chains which allowed good solubility in organic solvents, whereas inside the helices, well organized hydrogen bonding network ensured the stability of helical structure. The diameter of the inner cavity of the helices is small which does not allow any organic molecules to be encapsulated as this segment is used as end cap in the design of capsules.[19] However, the small cavity may allow single atom such as metal ion to reside in. The quinoline as well as amide upon deprotonation is suitable coordination sites for metal ions. The coordination of de-protonated amide was also proved previously.[14,20-22] Herein, we tried to load metal ions into the helices which will replace the hydrogen bonds to coordination bonds as the major stabilization factors while maintaining the helical structure.

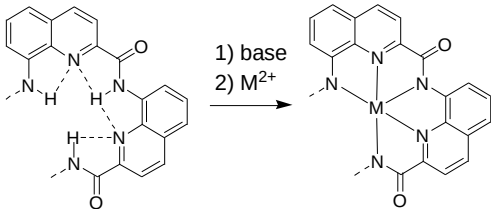

Figure 3-3: Expected metal coordination mode of 8-aminoquinoline-1-carboxamide.

3.2 Results and discussions

The quinolinecarboxylate amide oligomers have been reported before and were prepared accordingly.[18,23] Here, we choose oligomers with odd number of monomers in length in order

to fulfil the requirement of coordination numbers determined by the metal ions (chemical structures of the oligomers showed below in scheme 3-1). For each oligomer with length of 2n+1, the available coordination sites are 4n+1 in which 2n comes from the deprotonated amide bonds and 2n+1 from the quinolines. The total number of coordination sites is suitable for a number of n metal ions to complete their coordination spheres (4 coordination sites are necessary for each metal center). Hence, n metal ions are expected if all the coordination sites of the oligomer with length of 2n+1 are occupied. For example, Q_3 can accommodate one copper ion and Q_5 can accommodate two copper ions and so on.

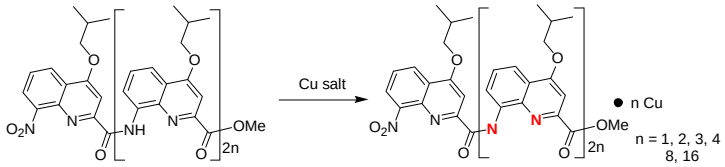

Scheme 3-1: The reaction scheme to load copper ions inside the quinolinecarboxylate amide oligomers.

We started testing our hypothesis by mixing quinolinecarboxylate amide trimer (Q_3) with copper (II) acetate in the mixture of chloroform and methanol (1/1, v/v) at room temperature. After mixing the solution of Q_3 and $Cu(OAc)_2$, the color of the solution immediately changed from light yellow to green. The immediate color changing serves as a good indication of the formation of complex which might be a result of the metal-to-ligand charge transfer (MLCT). Since, copper acetate was able to form complex with Q_3 immediately, UV-Vis titration of Q_3 with Cu (II) at room temperature was performed in chloroform/methanol mixture (1/1, v/v) which allowed us to extract a binding constant of 9.7×10^5 L/mol (Fig. 3-4b) based on 1 to 1 binding stoichiometry. As showed in figure 3-4a of the titration curve, the two absorption peaks at 323 nm and 355 nm of the Q_3 gradually decreased and shifted to longer wavelength. New peaks appeared at 345 nm at the end of titration which might be a result of red shift of the 323 nm absorption of Q_3. The gradually increasing shoulder peak above 420 nm was attributed to metal to ligand charge transfer absorption which is a clear evidence of the complexation. Isosbestic point at 348 nm was clearly observed which indicated two species equilibrium during titration. The high binding constant extracted from the titration curve indicated strong binding between Cu (II) ion and Q_3 which proved our assumption that quinolinecarboxylate amide oligomer can serve as ligand for suitable metal ions.

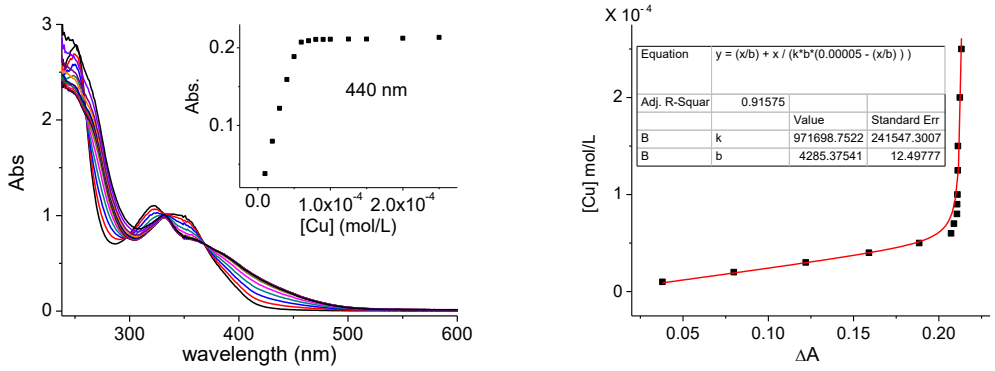

Figure 3-4: a) UV-Vis titration of $Cu(OAc)_2$ into Q_3, $[Q_3] = 5\times10^{-5}$ M, solvent: $CHCl_3$/MeOH (1/1, v/v), the inset was the evolution of absorbance at 440 nm upon addition of $Cu(OAc)_2$; b) nonlinear fitting curve of the absorbance at 440 nm, the fitting equation was based on the 1 to 1 binding model.

Other metal acetates salts, including Co (II), Zn (II), Ni (II), Pd (II), were also tested, however, the color changing were not obvious shortly after mixing at room temperature. This might be because of slow complexation or not at all or complexation with those metals did not cause any color changing. Nevertheless, for Zn (II) and Pd (II), it is possible to check NMR as a method to follow the complex formation because they are diamagnetic metal ions. As showed in Fig. 3-5, after mixing Q_3 with $Zn(OAc)_2$ (1 to 1 ratio) at room temperature in $CHCl_3$/MeOH, a new set of peaks corresponding to the complex slowly appeared. After 16 hours at room temperature, the complex formed was calculated to be around 1/3 conversion of the starting Q_3 by integrating the peaks in the ^{1}H NMR spectrum (Fig. 3-5b). Luckily, after standing the mixture at room temperature for about 2 to 3 days, crystal slowly grows in the mixture of chloroform/methanol which was the pure complex as indicated by the proton NMR after dissolving the crystal (Fig. 3-5c). The complex was stable in chloroform solution at room temperature as followed by ^{1}H NMR spectroscopy (data not shown). Compared to the ^{1}H NMR spectrum of Q_3, the resonances from amide protons completely disappear in the complex which indicates complete deprotonation of the amides in the complex. The ^{1}H NMR spectrum of the complex show broadness of some peaks while others are relatively sharp which indicated small structural dynamics at room temperature in chloroform. The resonances in the aromatic region are shifted to upper field region compared to Q_3. In the region of side chains (3.5 to 4.5 ppm), anisochronous signals were observed (Fig. 3-5c) indicating slow exchanging of those signals at the NMR time scale.

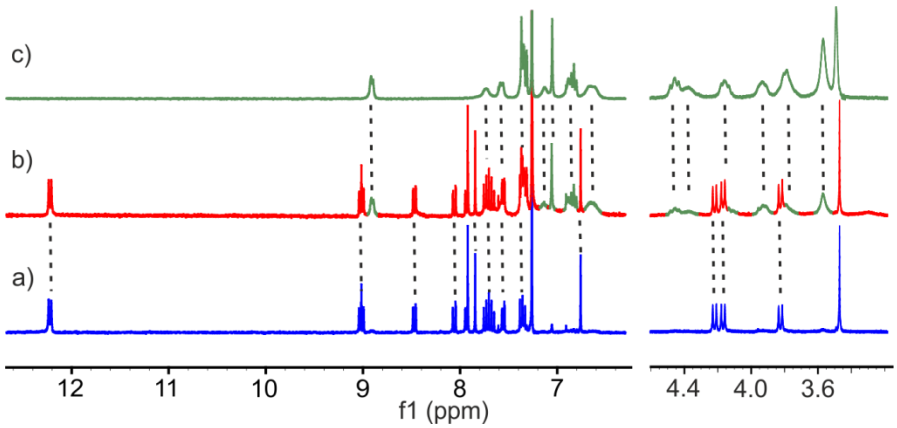

Figure 3-5: Part of ^{1}H NMR (300 MHz) spectra of a) Q_3, b) Q_3 mixed with 1 equivalent of $Zn(OAc)_2$ at room temperature after 16 hours, c) redissolve crystal of Q_3-Zn complex, the solvent is $CDCl_3$ for all three spectra.

The complex formation between Q_3 and $Pd(OAc)_2$ was also tested in the same manner as zinc. The Q_3 and $Pd(OAc)_2$ were mixed in chloroform/methanol (8/2, v/v) at a 1 to 1 ratio. After 4 hours at room temperature, a small new set of peaks was observed in ^{1}H NMR spectrum (Fig. 3-6b) and this new set of peaks kept growing until almost complete conversion of starting Q_3 after 7 days at room temperature (Fig. 3-6c). This clearly showed the formation of complex between Q_3 and $Pd(OAc)_2$, however, as indicated by the NMR spectra, the conversion was not exclusive and some small peaks can be spotted which might be corresponding to other complex than the major one. Also, it is important to note that the presence of methanol was necessary to observe the formation of complex. No NMR change was observed when pure chloroform was used (data not shown).

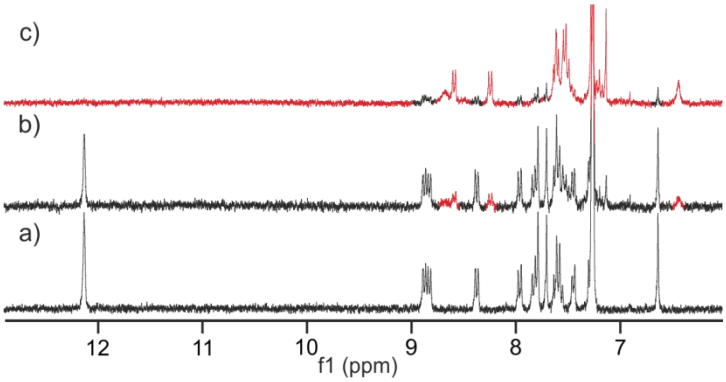

Figure 3-6: Part of ^{1}H NMR (300 MHz) spectra of a) Q_3 and Q_3 mixed with 1 equivalent of $Pd(OAc)_2$ standing at r.t. after b) 4 hours and c) 7 days, [Q_3] = 1 mM, the solvent is $CDCl_3$/MeOD (8/2, v/v).

As previously mentioned, the complex formed between Q_3 and zinc was successfully

crystalized and crystal suitable for X-ray diffraction was obtained. To our surprise, the crystal showed dimeric complex between Q_3 and zinc as showed in figure 3-7. Two antiparallel strands of Q_3 wrapped around two zinc cation which formed a double-stranded helicate. The Q_3 oligomer was partially unfolded and adopted a "Z" conformation which is very different from its folded conformation. The unfolding of Q_3 was a result of the deprotonation which undermine hydrogen bonds of the folded conformation and more importantly as a result of the geometry requirement for the zinc coordination. The two zinc cation adopted tetrahedral coordination geometry. The bond length between zinc and nitrogen were in the range between 2.003 to 2.096 Å which indicated strong bonding. The distance between two zinc atoms is 3.545 Å which is too long to allow interactions between them. The dimeric complex was also confirmed by mass spectroscopy where the peak with m/z 1705.533 was exclusively found which corresponding to the dimeric complex. The isotope distribution was also matched with the calculated one.

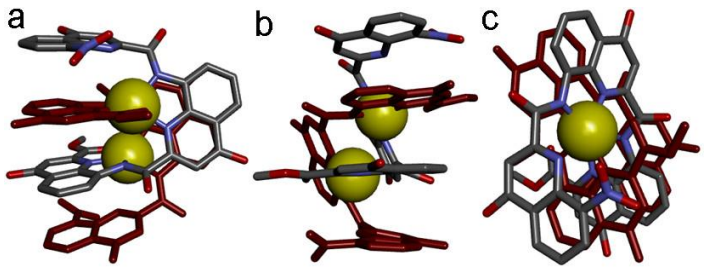

Figure 3-7: Crystal structure of Q_3Zn, a) side view, b) front view and c) top view; the Zn atoms were showed in CPK and all the hydrogens as well as the side chains were removed for clarity.

We next investigated the complexation of different metals with longer oligomers. When different metal salts were mixed with Q_5 which is two units longer than Q_3, we only observed nicely formed complex with $Cu(OAc)_2$ as indicated by TLC, with other salts such as $Zn(OAc)_2$, $Pd(OAc)_2$, $Co(OAc)_2$ and $Ni(OAc)_2$, we only found partial formation of complex or not at all as followed by NMR spectroscopy. Hence, we focused on copper to make complexes with longer oligomers. After mixing $Cu(OAc)_2$ with Q_5 at the same condition as for Q_3, we noticed that the kinetics to form the complex was much slower compared to Q_3. The decreasing of kinetics was expected with increasing the length of oligomers that the energy barriers to form the complexes increased with longer oligomers which was also indicated by the slowing down of handedness inversion with increasing the oligomer length.[24]

For longer oligomers, the helical conformation is more stable than the shorter ones. The deprotonation of the amide bonds inside the helices and insertion of copper ions into the helices are also more difficult for the longer oligomers than the shorter ones. The binding constant between Q_5 and copper was difficult to determine with titration experiment, however, we were interested in following the kinetics of complexation with UV-Vis spectroscopy. By following the evolution of UV-Vis spectra with time, similar changes of the spectra were observed as in the titration of copper with Q_3. The absorption peaks of Q_5 at 325 and 360 nm slowly decreased while new peak above 420 nm increased slowly with time. Isosbestic points at 260, 305 and 365 nm were observed. By plotting the absorbance at 472 nm as a function of time, we were able to find out that the complete formation of complex requires around 95 hours at room temperature at 50 μM concentration. The half conversion time was around 26 hours. The obvious decrease of reaction kinetics upon increasing the length from trimer to pentamer suggested harsher conditions might necessary in order to load copper ions into the longer oligomers.

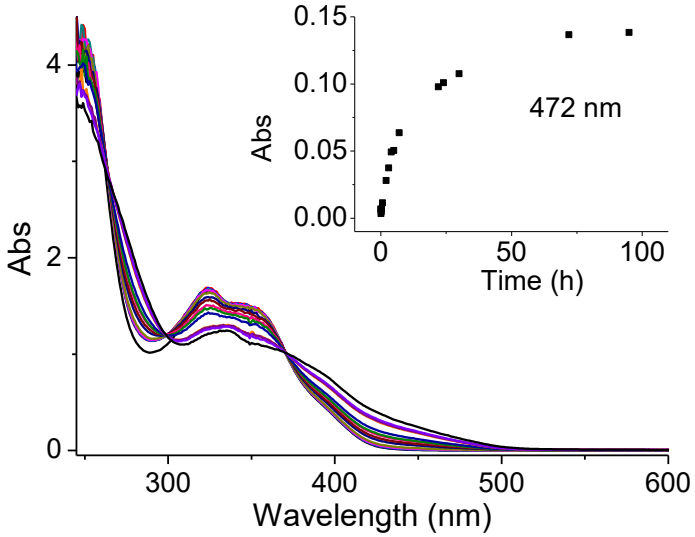

Figure 3-8: The kinetics of the formation of complex with Q_5 at room temperature followed by UV-Vis spectrum, the inset was the changes of absorbance at 472 nm with time, $[Q_5] = 5\times10^{-5}$ M, [Cu] = 1×10^{-4} M, solvent is $CHCl_3$/MeOH (v/v 1/1).

In order to increase the kinetics, we tried to heat the mixture of Q_5 and $Cu(OAc)_2$ in chloroform/methanol (1/1 V/V) at 60 ^{o}C. Indeed, by increasing the temperature, the complexation of Q_5 with $Cu(OAc)_2$ was complete in around 6 hours. The desired complex

was confirmed by HRMS that we found m/z 1397.3640 which corresponded to the calculated complex of Q_5Cu_2 (Fig. 3-10b). For longer oligomers, the formation of complexes especially the fully loaded complexes that metal ions occupy all the available coordinating sites of the quinoline carboxamide oligomers (n metal ions for an oligomer of 2n+1 units) may become challenging as the energy barriers of complexation are expected to increase with the length of the oligomers. For Q_7 and Q_9, the complete formation of fully loaded complexes required heating at 65 ^oC for about one day. Also, excess of $Cu(OAc)_2$ was required (around 5 equivalents for loading of one copper) in order to obtain the fully loaded complexes. The formation of fully loaded complexes was confirmed by HRMS. For Q_7, the peak with m/z 1942.4888 which corresponded to the expected fully loaded complex Q_7Cu_3 was found (Fig. 3-10c); and for Q_9, the peak with m/z 1245.3118 (z equal 2) which corresponded to the fully loaded complex Q_9Cu_4 was found (Fig. 3-10d). The observed isotope distributions of both complexes were also in agreement with the calculated ones which further confirmed the successful formation of the expected fully loaded complexes.

With the success of above copper fully loaded complexes, we decided to test with more ambitious oligomers, Q_{17} and Q_{33}. The estimated length of the two oligomers is 2.4 nm and 4.6 nm respectively. Upon completely loading of copper ions, 8 and 16 metal centers are expected to insert in the backbone of Q_{17} and Q_{33}, respectively. We first applied similar method used above to load copper ions inside Q_{17}. However, we only obtained complicated intermediate complexes with partially loaded oligomers as indicated by HRMS. Peaks corresponding to loading of different number of copper ions ranging from 3 to 8 into Q_{17} were observed. Complete conversion to copper fully loaded helices was failed even after long reaction time and higher temperature (refluxing temperature). The major product was 4-copper loaded Q_{17}, with some fully loaded compound (very minor product) and other partially loaded compounds. Further heating the reaction was not helpful since degradation of the oligomers might happen as indicated by complicated mass spectrum. These observations indicated that the energy and kinetic barriers to form the completely loaded complexes with Q_{17} and Q_{33} were much higher than that of Q_9. In order to overcome those barriers, we decided to heat the reaction at much higher temperature but below the temperature that substantial decomposition happens. We changed the solvent to DMF which is also a solvent

that destabilize the helical conformation of the quinoline oligomers which allow us to increase the temperature up to around 150 °C. However, to our disappointment, after heating at 130 °C, we only observed a mixture of partially and fully loaded complexes even after few hours of heating before decomposition became obvious. Increasing the excess of copper salt ($Cu(OAc)_2$ in this case) was also not helpful (up to 80 equivalents used).

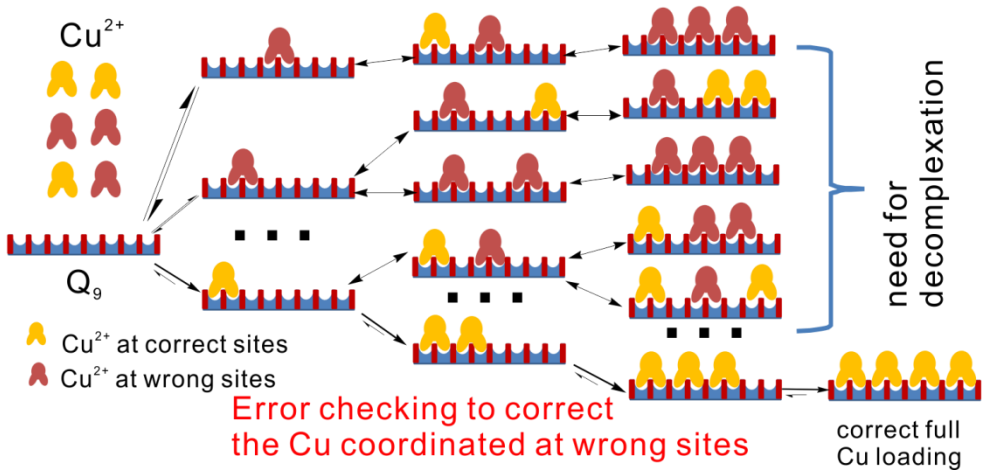

Figure 3-9: Representation of error checking process (take Q_9 as example) in order to obtain the fully loaded Cu (II) complex.

To our surprise, by simply changing the salt from $Cu(OAc)_2$ to $Cu(BF_4)_2$, the loading of copper was much faster and the fully loaded complexes of Q_{17} was obtained after heating in DMF at 120 °C for about 15 minutes. The expected Cu (II) fully loaded Q_{17} was confirmed with HRMS that the expected m/z 2337.0618 (z equals 2) was found to be the major peak (Fig. 3-10e). Compared to acetate, tetrafluoroborate was known to be much weaker coordinating counter anion which might accelerate the reaction by reducing the energy barrier required to dissociate the copper ion from its coordination with counter ions. Another possible reason might be the superacidity of the hydrogen tetrafluoroborate which was generated as a side product during the reaction. Acid was responsible for reverse reaction that protonate the amide bond and removal of copper ions form the helix to restore its original oligomer. The small amount of hydrogen tetrafluoroborate acted as an error correcting reagent that catalyze the reverse reaction to remove the copper ions that coordinate at wrong positions and allow all the copper ions positioned at the right position by fast trial-and-error process (some possible intermediates of Cu-coordination at wrong positions are showed in fig. 3-9). This error

checking process is important for such a long oligomer which allows many different number of possible coordination. If the error checking process is slow, tremendous time is required to screen all the possible ways of coordination and find the most stable fully loaded complex. The slow error checking process can account for much slower kinetics of longer oligomers. The fully loaded Q_{33} was also obtained with similar conditions as confirmed by HRMS of the expected m/z 3014.7144 (z equals 3) was found (Fig. 3-10f).

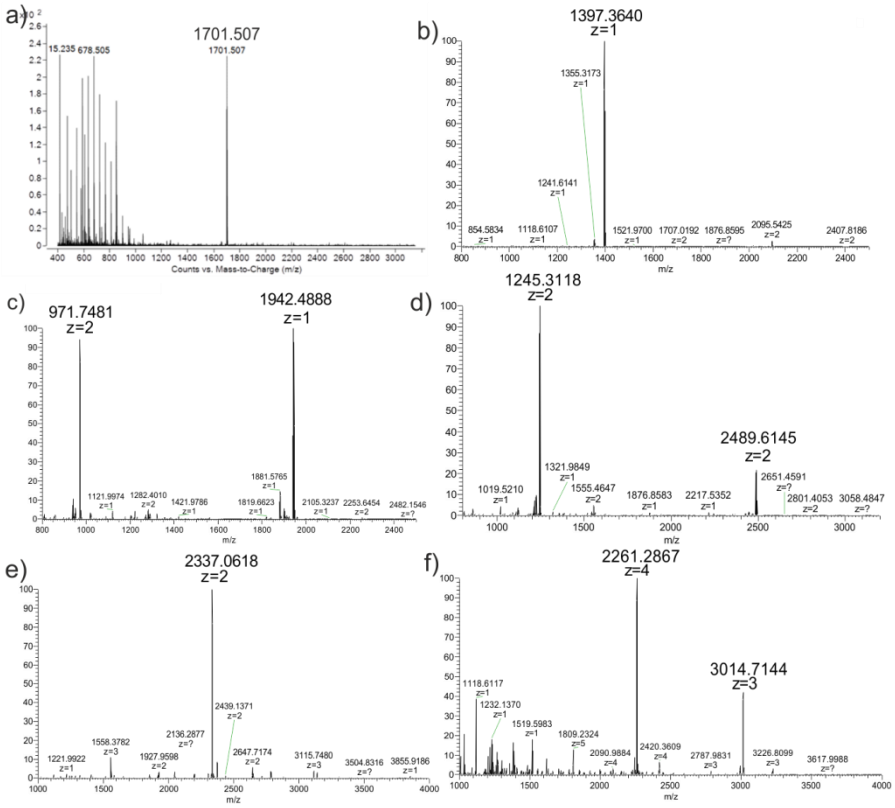

Figure 3-10：ESI+ HRMS spectra of a) Q_3Cu, b) Q_5Cu_2, c) Q_7Cu_3, d) Q_9Cu_4, e) $Q_{17}Cu_8$ and f) $Q_{33}Cu_{16}$.

The UV-Vis spectra of the copper fully loaded helices were showed in figure 3-11. The overall shapes of the spectra of the copper loaded helices were similar which have absorption peaks around 385, 335 and 255 nm. From Q_3Cu to $Q_{33}Cu_{16}$, the molar absorption coefficients increase as the oligomers become longer. However, the molar absorption coefficients were not increasing linearly with the number of quinoline units as showed in the inset figure which was attributed to hypochromic effect found also in the oligomers without copper loading. For the shortest one, Q_3Cu, the peaks at 385 and 335 nm were rather weak and can be barely seen. We suspected that this might be results from the lack of Cu-Cu interaction in Q_3Cu since there is only one copper. Compared with the quinoline oligomers before copper loading, the spectra

showed similar changes among all the oligomers that the rising of absorption over 400 nm and decreasing the absorption around 350 nm. The rising of absorption over 400 nm might be originated from the metal to ligand charge transfer (MLCT) as discussed above.

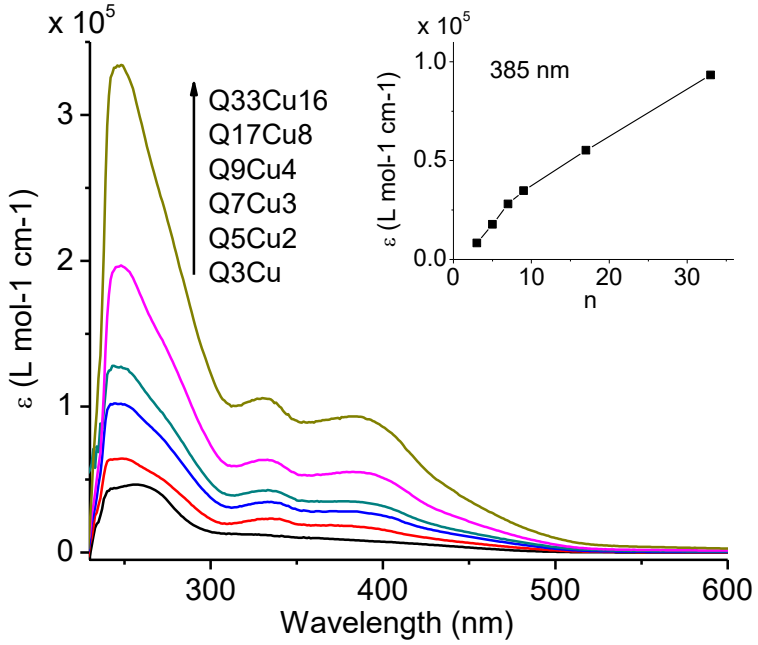

Figure 3-11: UV-Vis spectra of Q_3Cu, Q_5Cu_2, Q_7Cu_3, Q_9Cu_4, $Q_{17}Cu_8$ and $Q_{33}Cu_{16}$, all the spectra were measured in $CHCl_3$ solution at room temperature, inset was the absorbance at 385 nm of the copper loaded oligomers against the number of quinoline units.

The FTIR spectra of the copper fully loaded oligomers were shown in figure 3-12. Compared with the FTIR spectra of the oligomers without copper loading, the peak at 3400 cm^{-1} which is the -NH vibration from amide bond was completely disappeared indicating deprotonation of the amide bond after formation of the complexes. The carbonyl vibrations of the amide bonds shifted from 1700 cm^{-1} to 1600 cm^{-1} in the complexes. The amide I and II resonances also changed a lot after copper loading. The clear changes in the FTIR spectra confirmed again the formation of complexes.

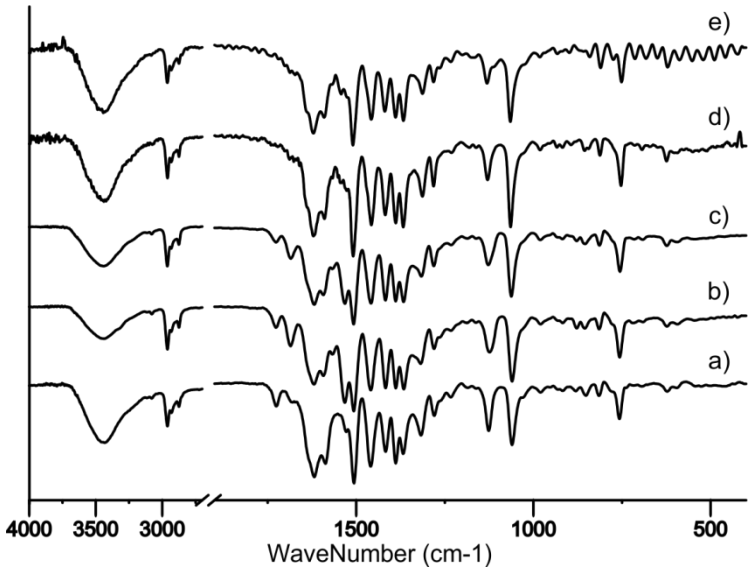

Figure 3-12: FTIR spectra of a) Q_5Cu_2, b) Q_7Cu_3, c) Q_9Cu_4, d) $Q_{17}Cu_8$ and e) $Q_{33}Cu_{16}$.

Single crystals of Q_5Cu_2, Q_7Cu_3 and Q_9Cu_4 suitable for x-ray diffraction were obtained either by slow evaporation of a solution in $CHCl_3$/MeOH mixture (for Q_5Cu_2 and Q_7Cu_3) or by slow diffusion of methanol to the solution in chloroform (for Q_9Cu_4). The single helical structure of the quinolinecarboxylate amide oligomers was maintained as can be seen in the crystal structures, all three compounds were single helical with 2, 3, and 4 copper ions coordinated inside a single strand helices of Q_5, Q_7 and Q_9 respectively. By overlapping the crystal structure of Q_9Cu_4 and Q_8, we were able to find out that after copper coordination, the overall helical shape become tighter than the original helices which have 2.5 units per turn. Q_5Cu_2 spanned more than 2 turns and Q_9Cu_4 completed almost four turns which require less units per turn than the non-copper loaded helices. This reflected the trend that the helices became tighter as the oligomers became longer. Unlike similar oligomers made form pyridine units that upon complexation with copper, double stranded helicates were formed.[14] The quinoline oligomers forms stable single helical structure even after complexation with metal ions reflected its robustness and the space and curvature predefined by the local conformation are well suitable for single helical structure.

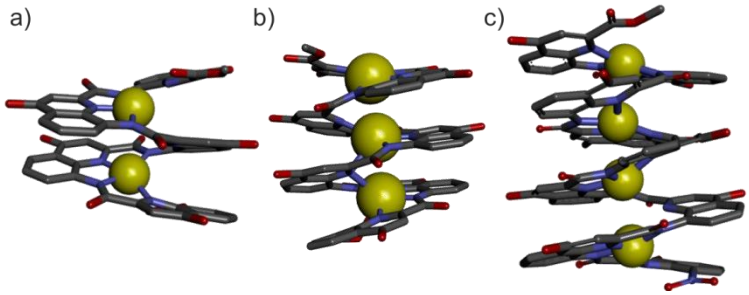

Figure 3-13: Single crystal structure of a) Q5Cu2, b) Q7Cu3 and c) Q9Cu4, all the side chain and hydrogen were removed for clarity.

In the crystal structures, the principle coordination atoms are nitrogen from quinoline rings and the deprotonated amides with bond lengths between 1.87 to 2.11 Å which indicated strong binding. Weak coordination was found between the copper ions at the nitro-extremity in all cases (bond length around 2.6 Å). The coordination geometries of all copper ions were distorted from ideal tetrahedral or octahedral geometry which were caused by the single helical structure of the foldamers. If all the weak coordinations are counted, coordination numbers of 4, 5 and 6 were found. The formation of stable complexes with copper ion with such distorted geometry can be explained with Jahn-Teller effect of d^9 configuration of Cu (II) ions.[25] The Jahn-Teller effect allows distortion form ideal octahedral yet to have small gain of stabilization. The distances between adjacent copper ion in Q_5Cu_2 is 3.372 Å, whereas in Q_7Cu_3, the distances between adjacent copper ions are 3.242 and 3.322 Å; in Q_9Cu_4, the distances are 3.318, 3.019 and 2.999 Å. The distances between adjacent copper ions decrease with the increase of the length of oligomers, which indicates intramolecular stabilization forces such as aromatic π-π stacking increased with increasing the oligomer length.

After carefully checking the coordination of copper ions in the structures, we are now able to understand how other metals, such as Pd (II), Co (III), Ni (II) and Zn (II), were failed on our hands. In order to form stable complexes, the ligands are better to be positioned according to the geometries determined by the metal ions which allows maximum overlapping the orbitals of the metals and ligands. In our case, the geometries of the ligands are determined by the helical structure of the foldamers which are not suitable for most metal ions in a way that they distorted form ideal square planar for Pd (II), tetrahedral for Ni (II) or octahedral for Co (III) and Zn (II) and Ni (II). One way to force the adequate positions of the coordination atoms of the ligands into ideal geometry is to completely unfold the

quinolinecarboxamide oligomers as found in Q_3Zn. However, the energy cost for unfolding the structures is simply too high to allow coordination happens in the case of longer oligomers. Copper, on the other hand, allows a certain flexibility in the coordination geometry and also copper normally forms stronger coordination bonds with nitrogen than other metals which makes it easier to outcompete the energy lose for structure reorganization.

As stated above, the copper ions were aligned inside the helices in the crystal. The alignments of copper ions were found to be macroscopic also. As showed in figures 3-14 and 3-15 of the crystal packing of Q_7Cu_3 and Q_9Cu_4, the helices were aligned along the long axis of the foldamers which formed a pseudo-continuous helical structure. In the case of Q_5Cu_2, similar packing pattern was not found. In the crystal structures of Q_7Cu_3 and Q_9Cu_4, the helices were sitting on top of each other and form a long stack of helices along c-axis in both cases. This organization allows the alignment of the copper ions not only inside the helices on the molecular level but also long range alignment on the macroscopic level which spanned to the dimension of the crystals. The alignments of copper ions in one dimension allow us to form molecular wires on macroscopic level with only relative short oligomers. This type of alignment found in Q_7Cu_3 and Q_9Cu_4 but not in Q_5Cu_2 probably indicated the importance of aspect ratio in the crystal packing. With even longer oligomer, $Q_{17}Cu_8$, we were unable to obtain high resolution diffraction data to solve the structure. Nevertheless, from the electron density map, we were able to observe similar pseudo-continues organization of helices and alignment of copper ions in long range.

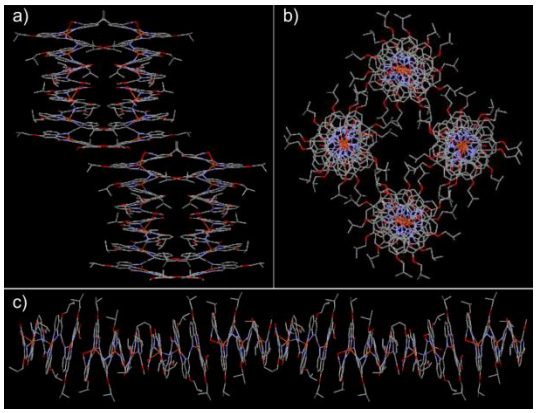

Figure 3-14: Crystal packing pattern of Q_7Cu_3, a) viewed form a-axis, b) viewed form b-axis and c) viewed form c-axis.

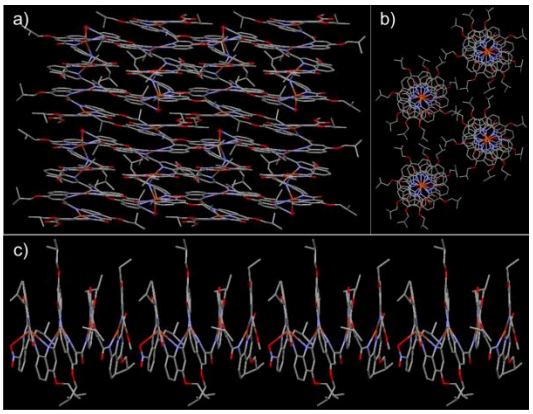

Figure 3-15: Crystal packing pattern of Q_9Cu_4, a) viewed form a-axis, b) viewed from b-axis and c) viewed form c-axis.

Partial loading of Q_7 with copper ions was tried in order to understand the mechanism of copper ions insertion into helices. For Q_7, three copper ions are necessary to form the fully loaded helix. By mixing Q_7 and copper acetate at equal mole ratio at room temperature in chloroform/methanol, partially loaded oligomers were expected. After heating at 60 ^{o}C for 3 hours, oligomers with different loading number of copper ions were obtained as indicated by TLC. To our surprise, this mixture could easily give crystals suitable for x-ray diffraction analysis. The x-ray structure showed Q_7 with 1, 2, and 3 copper ions in the same unit cell with partial occupancy of the copper ions. The crystal could grow despite the different number of copper loading reflecting that small structural differences arise from different copper loading. The copper ions coordinate at the ester end of Q_7 of the single copper loaded helix. The double copper loaded helix has copper at the ester terminus also and leaves the nitro terminus coordination sites open. This probably indicated that the coordination sites at the nitro terminus were less stable than the ester terminus. This hypothesis was further supported by selectively remove one copper ions from the fully loaded Q_7. After completely loading of three copper ions into Q_7, one copper ion can be selectively removed with trace amount of acetic acid. The crystal structure of the one copper removing happened at the nitro terminus of the helix as showed in figure 3-16a. The partial loading and removal of copper ions showed that the nitro terminus was less favored for copper loading than the ester terminus. The single loaded helix showed copper coordinated at the ester terminus indicated that the loading of copper form ester terminus might be favored over the nitro terminus.

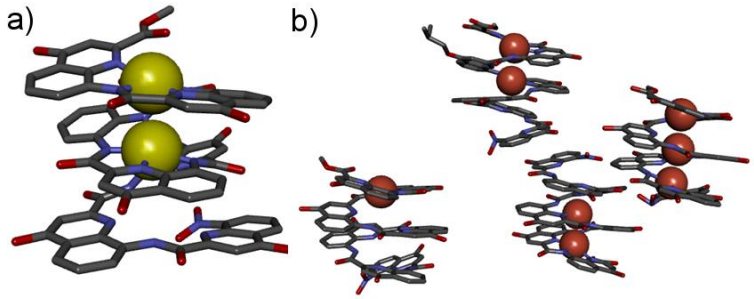

Figure 3-16: a) single crystal structure of Q_7Cu_2; b) the crystal structure of partially copper loaded Q_7 with 1, 2 and 3 copper ions of partial occupancy in the same unit cell, all side chains and hydrogen atoms were removed for clarity.

3.3 Conclusions and perspectives

In conclusion, we successfully prepared a new type of Cu (II) ion loaded foldamers which is a different form of helicates. We have successfully prepared oligomers containing up to 16 copper ions inside a single helix composed of 33 quinoline units. The crystal structures clearly showed that the copper ions coordinated inside the helices and the helical structures of the foldamers were preserved. The coordination geometries of the copper (II) ions were highly distorted due to the helical conformation of the foldamers which was made possible due to the Jahn-Teller distortion of the copper (II) ions. The copper (II) ions were aligned not only inside the helices but also in the macroscopy level due to pseudo-continues packing of the helices. We are expecting the macroscopic molecular wires made from simple oligomers will show novel electronic properties.

For perspectives, pseudo-continues packing of helices and one dimensional alignment of copper ions are found in the crystals. It is interesting to directly measure the conductivity of the crystals to see if the one dimensional aligned copper ions could be served as molecular wires. Another perspective about the copper loaded helices is to use them to form monolayer on the surface which will allow us to measure conductivity and other physical properties. A cartoon for the monolayer on gold is showed below.

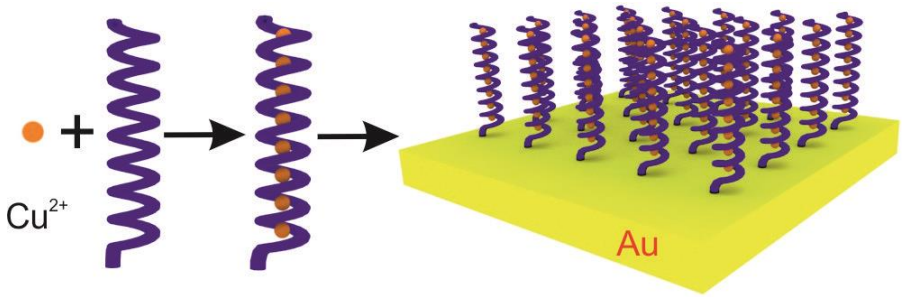

Figure 3-17: Cartoon representation of copper loaded helices and the formation of monolayer on gold surface.

3.4 Experiments

3.4.1 General remarks

All the solvents and reagents were used as received from commercial sources unless otherwise specified. Dichloromethane (CH_2Cl_2) was dried over alumina columns; chloroform ($CHCl_3$) and diisopropylethylamine (DIEA) were distilled over calcium hydride (CaH_2) prior to use. Reactions were monitored by thin layer chromatography (TLC) on Merck silica gel 60-F254 plates and observed under UV light. Column chromatography purifications were carried out on Merck GEDURAN Si60 (40-63 µm). ESI mass spectra were obtained from the Mass Spectrometry Laboratory at the European Institute of Chemistry and Biology (UMS 3033 - IECB), Pessac, France. Preparative recycling Gel Permeation Chromatography (GPC) was performed on a JAI LC-9130G NEXT using two JAIGEL 20×600 mm columns (Japan Analytical Industry) with 0.5 % NEt_3 and 1% ethanol in chloroform (HPLC grade, ethanol stabilized), as mobile phase, with a flow rate of 7 mL/min. UV-Vis spectroscopy was recorded on Varian® Cary 300 Scan UV-Visible spectrophotometer at room temperature. FTIR spectroscopy was recorded on Bruker IRFT IFS 55 infrared spectrometer using KBr to make the pallet and the spectrum was recorded at room temperature.

3.4.2 Oligomer synthesis

The quinolinecarboxylate amide oligomers (Q_3 to Q_9) were prepared according to previous established methods with minor changes.[26] The longer oligomers (Q_{17} and Q_{33}) were

prepared by segment doubling methods and purified with GPC.[23]

3.4.3 Complexation with metals

For metal ions like Zn (II) and Pd (II) that are diamagnetic, NMR was used as a tool to follow the reaction. Typically, an amount of calculated by 1 mM solution of 0.5 mL of the quinolinecarboxylate amide oligomers was added into a NMR tube and 1 equivalent amount of the metal salts were added. Then 0.5 mL of solvents, typically $CDCl_3$ or mixture of $CDCl_3$ and MeOD depending on the solubility, was added. Then NMR spectra were taken after waiting certain period of time either at room temperature or at elevated temperature depending on the reaction kinetics. For metal ions like Cu (II) where NMR was not suitable due to the paramagnetic nature of the Cu (II) ion, the reaction was followed by UV-Vis spectra where significant differences of absorption were observed. Typically, an amount of 15 mg of the quinolinecarboxylate amide oligomers (form Q_3 to Q_9) was added into a flask and dissolved in around 2-3 mL of chloroform. Then an amount of $Cu(OAc)_2$ of calculated around 2-3 equivalents of per copper loading was dissolved in least amount of methanol. The copper acetate solution was added into the quinolinecarboxylate amide solution and the resulting mixture was stirred either at room temperature (for Q_3 and Q_5) or at 65 ^oC (for Q_5 to Q_9). The reaction was quenched after completion of full loading of the copper ions by washing with water after diluting with dichloromethane. The organic layer was separated and the solvent was removed to result a dark green solid. For longer oligomers, like Q_{17} and Q_{33}, the reaction was carried out in dry DMF (for Q_{17}) or dry NMP (for Q_{33}). For both oligomers, the copper salt used was copper tetrafluoroborate that was pre-dried under high vacuum. For Q_{17}, an amount of 15 mg of Q_{17} was added in a dry flask and about 30 mg of $Cu(BF_4)_2$ was added and then 3 mL of dry DMF was added. The mixture was heated at 120 ^oC for 15 minutes and cooled down to room temperature. Dichloromethane was added into the mixture and washed with water. The organic layer was separated and the solvent was removed to yield a dark solid. For Q_{33}, the reaction was similar except the solvent changed to NMP and heated at 150 ^oC for about 7 minutes before cooling down.

3.4.4 X-ray crystallography

Single crystals suitable for X-ray diffraction analysis were obtained by either slow evaporation of the complexes in co-solvent of chloroform and methanol or by slow diffusion of methanol in to the solution of complexes in chloroform.

References

(1) Huang, Y.; Huang, J.; Chen, Y. *Protein & Cell* **2010**, *1*, 143-152.

(2) Tossi, A.; Sandri, L.; Giangaspero, A. *Pept. Sci.* **2000**, *55*, 4-30.

(3) Howson, S. E.; Bolhuis, A.; Brabec, V.; Clarkson, G. J.; Malina, J.; Rodger, A.; Scott, P. *Nat. Chem.* **2012**, *4*, 31.

(4) Lehn, J. M.; Rigault, A.; Siegel, J.; Harrowfield, J.; Chevrier, B.; Moras, D. *Proceedings of the National Academy of Sciences* **1987**, *84*, 2565-2569.

(5) Piguet, C.; Bernardinelli, G.; Hopfgartner, G. *Chem. Rev.* **1997**, *97*, 2005-2062.

(6) Zarges, W.; Hall, J.; Lehn, J.-M.; Bolm, C. *Helv. Chim. Acta* **1991**, *74*, 1843-1852.

(7) Potts, K. T.; Keshavarz-K, M.; Tham, F. S.; Abruna, H. D.; Arana, C. *Inorg. Chem.* **1993**, *32*, 4436-4449.

(8) Jana, B.; Cera, L.; Akhuli, B.; Naskar, S.; Schalley, C. A.; Ghosh, P. *Inorg. Chem.* **2017**, *56*, 12505-12513.

(9) Greenfield, J. L.; Evans, E. W.; Di Nuzzo, D.; Di Antonio, M.; Friend, R. H.; Nitschke, J. R. *J. Am. Chem. Soc.* **2018**, *140*, 10344-10353.

(10) Miwa, K.; Furusho, Y.; Yashima, E. *Nat. Chem.* **2010**, *2*, 444.

(11) Ousaka, N.; Shimizu, K.; Suzuki, Y.; Iwata, T.; Itakura, M.; Taura, D.; Iida, H.; Furusho, Y.; Mori, T.; Yashima, E. *J. Am. Chem. Soc.* **2018**, *140*, 17027-17039.

(12) Bera, J. K.; Dunbar, K. R. *Angew. Chem. Int. Ed.* **2002**, *41*, 4453-4457.

(13) Greenfield, J. L.; Rizzuto, F. J.; Goldberga, I.; Nitschke, J. R. *Angew. Chem. Int. Ed.* **2017**, *56*, 7541-7545.

(14) Maurizot, V.; Linti, G.; Huc, I. *Chem. Commun.* **2004**, 924-925.

(15) Mateus, P.; Wicher, B.; Ferrand, Y.; Huc, I. *Chem. Commun.* **2018**, *54*, 5078-5081.

(16) Mateus, P.; Wicher, B.; Ferrand, Y.; Huc, I. *Chem. Commun.* **2017**, *53*, 9300-9303.

(17) Horeau, M.; Lautrette, G.; Wicher, B.; Blot, V.; Lebreton, J.; Pipelier, M.; Dubreuil, D.; Ferrand, Y.; Huc, I. *Angew. Chem. Int. Ed.* **2017**, *56*, 6823-6827.

(18) Jiang, H.; Léger, J.-M.; Huc, I. *J. Am. Chem. Soc.* **2003**, *125*, 3448-3449.

(19) Ferrand, Y.; Huc, I. *Acc. Chem. Res.* **2018**, *51*, 970-977.

(20) Kawamoto, T.; Hammes, B. S.; Haggerty, B.; Yap, G. P. A.; Rheingold, A. L.; Borovik, A. S. *J. Am. Chem. Soc.* **1996**, *118*, 285-286.

(21) Kawamoto, T.; Prakash, O.; Ostrander, R.; Rheingold, A. L.; Borovik, A. S. *Inorg. Chem.* **1995**, *34*, 4294-4295.

(22) Kawamoto, T.; Hammes, B. S.; Ostrander, R.; Rheingold, A. L.; Borovik, A. S. *Inorg. Chem.*

1998, *37*, 3424-3427.

(23) Li, X.; Qi, T.; Srinivas, K.; Massip, S.; Maurizot, V.; Huc, I. *Org. Lett.* **2016**, *18*, 1044-1047.

(24) Delsuc, N.; Kawanami, T.; Lefeuvre, J.; Shundo, A.; Ihara, H.; Takafuji, M.; Huc, I. *ChemPhysChem* **2008**, *9*, 1882-1890.

(25) Jahn, H. A.; Teller, E.; Donnan, F. G. *Proceedings of the Royal Society of London. Series A - Mathematical and Physical Sciences* **1937**, *161*, 220-235.

(26) Qi, T.; Deschrijver, T.; Huc, I. *Nat. Protoc.* **2013**, *8*, 693.

IV Self-assembly of Acridine Functionalized Quinoline Oligoamide Foldamers

4.1 Introduction

Self-assembly is a powerful technique to form large objects ranging from nanometer to micrometer size by using relative small and simple building blocks. Nature is a master of this technique. For instance, many proteins are the assembly of several copies of small peptides or sub-unit proteins. Even for some small proteins, their structures are an ensemble of multiple simple structural motifs such as helix, sheet and turn. The assembly of proteins is governed by several type of interactions between the interfaces of sub-units such as hydrophobic effects, metal binding and disulfide bond formation.[1] The formation of intricate and complicated assembles of proteins and peptides enable them to perform sophisticated functions.[2]

Protein engineering and *de novo* protein design have created numerous assembles of proteins beyond the tertiary folds of natural proteins as well as diverse chemical functionalities.[3] Tetrahedron assembly of coiled-coil peptides,[2] cyclic closed architectures from α-helical tandem repeat proteins[4] and cages[5,6] have been prepared. The self-assembly of proteins/peptides has also been used to make nanomaterials such as fibrils, nanotubes and nanospheres.[7,8] Although great progresses have been made in *de novo* protein design, most of the current designs are heavily relied on the structures motifs and folds that found in nature.[2,9] Usually, the design was assisted by computation. Modular structural elements have also been used extensively to facilitate the design. Coiled-coil is probably one of the most studied and well understood structural motifs. Coiled-coil is known to form dimeric or higher assemblies characterized by a heptad repeat helix normally designated as abcdefg.[10] The coiled-coil is mostly stabilized by hydrophobic effects of a and d residues as well as electrostatic interactions between e and g residues of the heptad repeat. Although coiled-coil has been extensively applied in de novo protein design, it has been pointed out that at least three types

of coiled-coil elements are required to form two- or three-dimensional assemblies.[2]

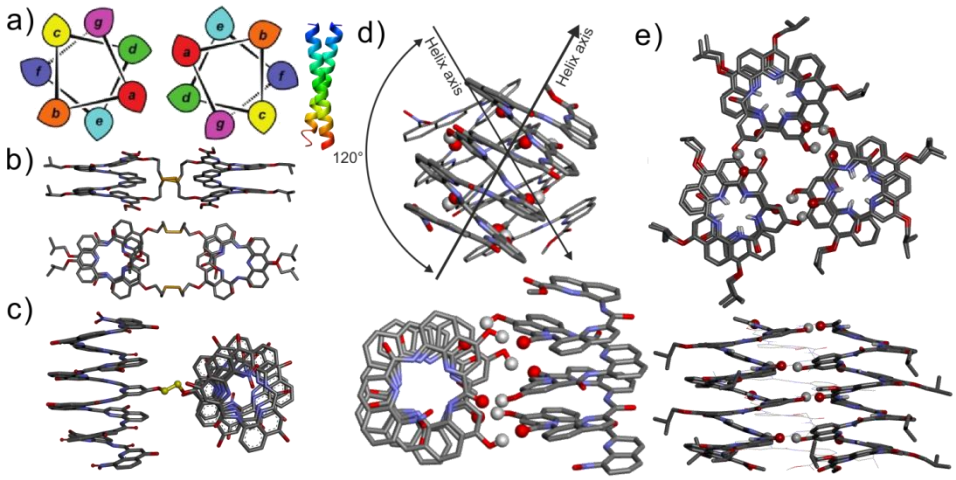

Figure 4-1: a) The heptad repeat (abcdefg) of coiled-coil; b) disulfide bond directed helix-helix structures; c) covalent linked helix-helix structures; d) dimeric helix bundles and e) trimeric helix bundles.

Foldamers, which were inspired by nature, adopt specific folded structures such as helix and sheets. It would be naturally to design not only the secondary structures of foldamers but also tertiary and higher structures as found in proteins. In the lab, helix-helix structures have been prepared based on covalent linkage and non-covalent assembly. Helix-helix motif was first made by covalent link through side chains. By connecting two helical foldamers through flexible alkyl sidechains, the two helices was found to adopt crossing structure and weak chiral communication occurred between the two helices.[11] Disulfide assisted dynamic assembly of helical foldamers has also been reported and remote handedness communication was found.[12] Helix-helix structure was also prepared with covalent linkage through the main chain. Different type of helix-helix structures were found such as “U” shape and anti-shape. Chiral communication was also found. With proper design of hydrogen bonding motifs, helix-helix bundles through non-covalent linkage was achieved. Hydroxyl functional group was designed on the same face of *oligo*-quinolinecarboxamides which was able to form hydrogen bonds as hydrogen bond donors with complementary hydrogen bond acceptors such as carbonyl of the amide bond. The ratio of dimeric and trimeric bundles was found to be solvent dependent.[13] The complex equilibrium found of the assembly bundles of non-covalent interactions indicated complicated behaviors due to the weak and less-directional nature of non-covalent interactions. Hydrogen bond was thought to be directional and stronger than

other non-covalent interactions in organic solvents such as electrostatic and dispersion interactions. However, complete control of those interactions is still challenge.

Here, we decided to use aromatic interactions to form helix-helix assemblies. Aromatic interactions such as π-π stacking, CH-π interaction are commonly encountered in aromatic compounds. These interactions can be found in a large variety of solvents ranging from nonpolar to polar solvents and water also. Flat π aromatic compounds especially electron poor and electron rich pairs are usually found to stack on top of each other. So, we want to take advantages of the stacking of flat aromatic moieties to create helix bundles. Acridine functionalized quinoline oligoamides are presented and helix-helix organization have been achieved by the interactions of acridine units.

4.2 Compounds design

The *oligo*-quinolinecarboxamides form stable single helical structure both in solution and solid state. The pitch of the helix is about 3.5 nm which spans 2.5 units of monomers. The shape of the helix can be represented with a five-star where every corner is a side chain. (Fig 4-2a) From the five-star model, the possible ways to form helix-helix bundle dimers are through interactions of one corner (Fig. 4-2b) or two adjacent corners (Fig. 4-2c). Simultaneous contacts with three corners are not feasible unless specifically long armed sidechains are made at the two non-adjacent corners. The bundles formed through simultaneous contacts with two adjacent corners are more stable because of more contacts are presented than the single corner connection if all those interactions are attractive interactions. Also, contacts are expected every five units because i and i+5 units have side chains that point in the dame direction. Cooperative multidentate interactions can be envisaged by placing proper functional groups every five units. The strength of the interaction between two helices can be tuned by changing the length of the helices which varies the number of contacts between the two helices. Attractive interactions can be designed and placed into the sequence to hold the helices closely. The other units that are not responsible for the interactions in the sequence are selected to improve the solubility or prevent further non-specific aggregations.

Many different types of interactions are available such as hydrogen bonds, halogen bonds, electro-static interactions, coordination bonds, etc., and in aqueous solution, hydrophobic collapse is an important effect yet difficult to control. Strong, directional and well-understood interactions can be chosen as a good starting point to design the bundles. As discussed in the introduction, hydrogen bond between hydroxyl and carbonyl was used to design tertiary structures of foldamers.

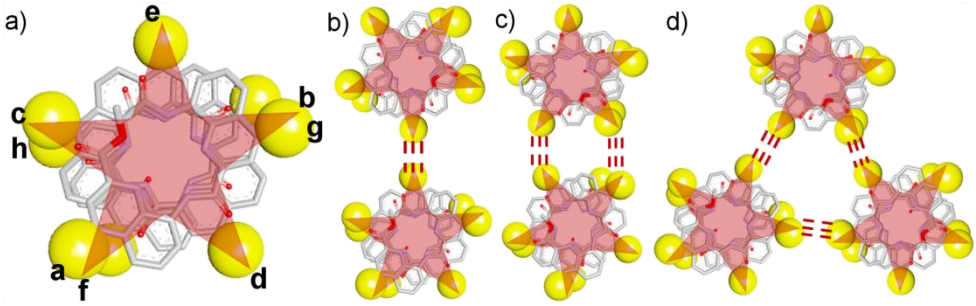

Figure 4-2：a) Five-star representation of the side chain positions of quinocarboxamide oligomers, the yellow ball stands for the oxygen of the side chains, an oligomer of abcdefgh follows the order showed in the figure to place the side chains, where a and f (b and g, c and h as well) which separated by five units have side chains at the same corner of the five star; b) carton representation for two helices interact through only one corner; c) carton representation for two helices interact through two adjacent corners; d) carton representation of three helices interact through adjacent corners.

Here, we decided to use aromatic interactions to form assembly of foldamers. As a choice of interaction units, we have choosed acridine. Acridine is a well-known fluorescent dye found to have vast applications in biology. It is probably the first dye molecules found to be able to intercalate into double strand DNA.[14-16] The flat aromatic surface and dipole moment caused by the 9-endocyclic nitrogen make acridine attracting functional group which may lead to interesting properties. Acetylene was used as linker between acridine and the backbone of quinoline oligoamide foldamers. The rigidity and linear shape of acetylene can fix the orientation and position of acridine units. The acridine units were connected to acetylene at position 9 to avoid complication of free rotation along the connection. Based on the five-star model of the *oligo*-quinolinecarboxamides (Figure 4-2a), different modes of interactions between helices can be imaged. As showed in figure 4-2, helix-helix association through side chains on single face (Fig. 4-2b); dimeric helix-helix association through side chains on two adjacent faces (Fig. 4-2c) and trimeric helix-helix association through side

chains on two adjacent faces are possible (Fig. 4-2d).

The chemical structures of the designed compounds are listed in figure 4-3. Compound **7** is the key monomer that functionalized with acridine at the 4-position of quionline. The acridine is connected to quinoline through a triple bond which reduces the possibility of conformational isomers due to the rotation through the connections. Two series of acridine functionalized oligomers were designed. One series of the oligomers can be represented as $(Q_2Q^aQ_2)_n$ (n = 1, 2, 3; oligomers **1a**-**1c** in figure 4-3a) which bear acridine side chains at a single corner of the surface. The other series of oligomers can be expressed as $Q_2Q^aQQ^a$ and $(Q_2Q^aQQ^a)_nQ_2Q^aQ_2$ (n = 1, 2; oligomers **2a**-**2c** in figure 4-3a) which bear acridine side chains at two adjacent corner of the helices. The oligomers **1a**-**1c** have 1, 2 and 3 acridine side chains respectively. This series of oligomers was designed to form helix-helix structure by interactions at a single corner of the helical surface. As showed in the molecular model of **1c**, two molecules of **1c** are designed to interact with each other through acridine units which form a stack of aromatic rings (Fig. 4-3b and 4-3c). The oligomers **2a**-**2c** bear acridine side chains at two corners of the helices. In this case, interactions between three helices are possible. As showed in figure 4-3d and 4-3e, a possible trimeric bundle can be imaged through stacking of acridine units between these helices.

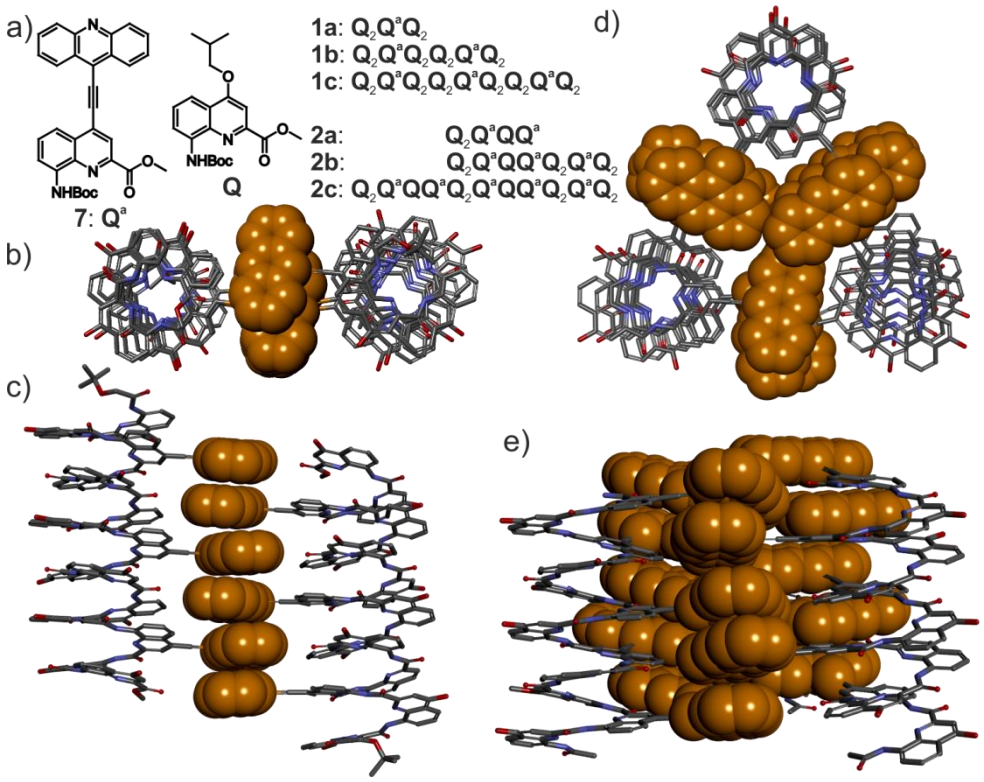

Figure 4-3: a) Chemical structure of acridine functionalized monomer **7** (Q^a) and quinoline monomer (Q) and sequences of two series of oligomers **1a**-**1c** and **2a**-**2c**; Energy minimized molecular model of dimer stack by the acridine units of **1c** showing b) top view and c) side view; Energy minimized molecular model of trimer stack by the acridine units of **2c** showing d) top view and e) side view. The models were produced with Maestro software package, using MFFS force field, chloroform as solvent and PRCG as minimization method.

4.3 Results and discussions

4.3.1 Compounds synthesis

The key monomer with acridine side chain was prepared according to scheme 4-1. The commercially available 9-chloroacridine was converted to 9-ethynylacridine by first Sonogashira coupling with 2-hydroxypropyl-protected acetylene and then deprotection with potassium hydroxide and potassium phosphate with moderate yields. The 4-bromo-8-nitroquinoline **4** was reduced with iron powder and acetic acid which was followed by Boc-protection to afford compound **6**. The monomer **7** was obtained by Sonogashira reaction of precursors **6** and **3** under typical coupling condition with good yield.

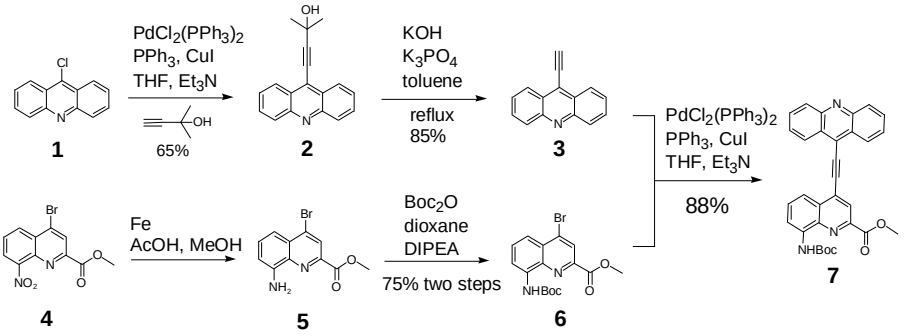

Scheme 4-1: Synthetic scheme of the acridine functionalized quinoline monomer **7**.

Oligomers **1a**-**1c** were prepared according to convergent synthetic route showed in scheme 4-2. The short oligomer $Q_2Q^aQ_2$ (**1a**) was prepared as a precursor block to obtain longer oligomers **1b** and **1c**. Saponification of monomer **7** with sodium hydroxide afford the carboxylic acid monomer **8** which was then activated as acid chloride and coupled with quinoline dimer amine **9**. The product Q^aQ_2 (**10**) was converted to the free amine compound **11** by treatment with TFA and was coupled with quinoline dimer acid **12** via acid chloride activation. The product of this coupling was the short oligomer **1a**. Oligomer **1a** was then separated into two parts. One part was treated with TFA to afford the free amine **13**. The other part was reacted with sodium hydroxide which gave the carboxylic acid **14**. After converting **14** to its corresponding acid chloride using Ghosez's reagent to the corresponding acid chloride, this pentamer was coupled with the amine **13**, oligomer **1b** was obtained after column purification. The longest oligomer **1c** was obtained similarly by coupling the acid chloride of **14** with the free amine of **1b** afforded by Boc-deprotection with TFA. The final oligomer **1c** was purified by GPC and silica gel column chromatography. It is worth mentioning that the activation of carboxylic acid **14** with Ghosez's reagent takes overnight to complete. It is not clear why the activation of **14** to corresponding acid chloride takes such a long time.

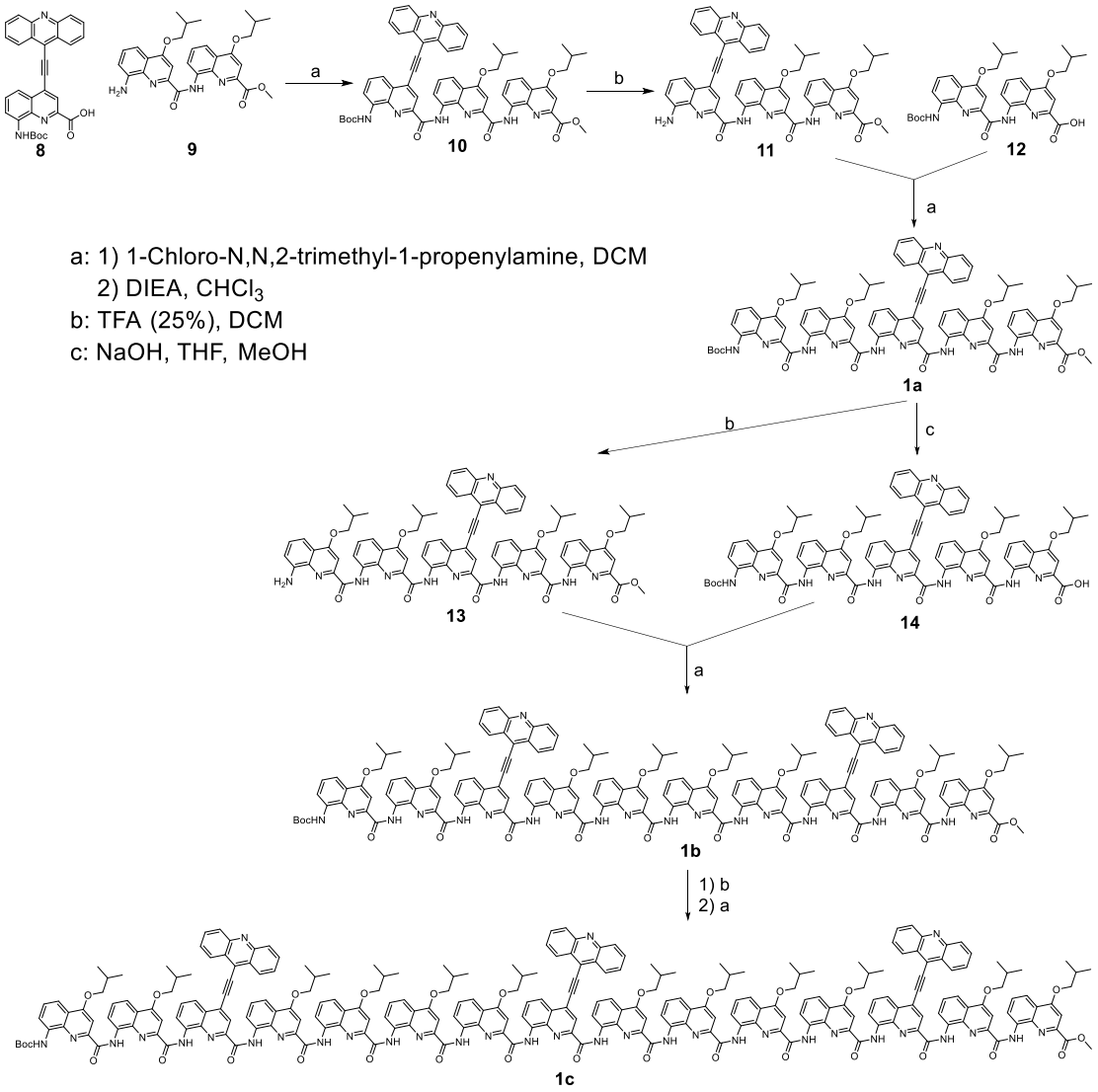

Scheme 4-2: Synthetic route for the acridine functionalized oligomers **1a**-**1c**.

The synthesis of oligomers **2a**-**2c** was a bit more complicated. The convergent synthetic route was displayed in scheme 4-3. Oligomer $Q_2Q^aQQ^a$ (**2a**) was prepared as a segment to synthesis the longer oligomers. Quinoline monomer carboxylic acid **15** was activated as acid chloride with Ghosez's reagent which was then coupled with the Q^a amine **16** to afford QQ^a dimer **17**. The **17** was then treated with TFA to remove the Boc-protecting group and then coupled with Q^a acid chloride to obtain Q^aQQ^a trimer **18**. After Boc-deprotection of **18** and then coupled with Q_2 acid chloride, oligomer $Q_2Q^aQQ^a$ (**2a**) was obtained. The corresponding carboxylic acid of **2a** was obtained by saponification with sodium hydroxide. The carboxylic acid **19** was then activated to corresponding acid chloride and coupled with amine **13** to afford the oligomer $Q_2Q^aQQ^aQ_2Q^aQ_2$ (**2a**). The activation of carboxylic acid **19** to the

corresponding acid chloride was again slow and required overnight reaction. However, the reaction between the acid chloride of **19** and the amine **13** was complicated which gave the desired product with several side products. It was difficult to identify the side products generated during the reaction. Nevertheless, it was possible to obtain small amount of pure oligomer **2a**. However, it was difficult to continue the synthesis of longer oligomer **2c** which only leaded to complicated mixtures.

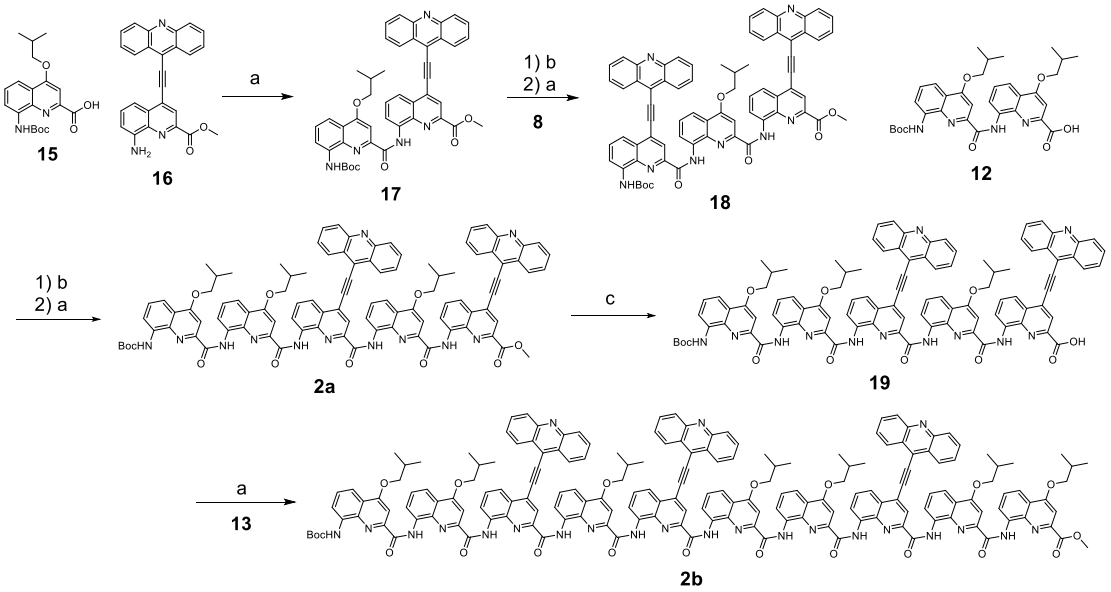

a: 1) 1-Chloro-N,N,2-trimethyl-1-propenylamine, DCM, 2) DIEA, $CHCl_3$
b: TFA (25%), DCM; c: NaOH, THF, MeOH

Scheme 4-3: The synthetic route for oligomers **2a** and **2b**.

In order to obtain the long oligomer **2c**, linear synthetic route was tried which is showed in scheme 4-4. In order to reduce synthetic steps, Q^aQ dimer **21** was made as a carboxylic acid **22** and used as a building block. The whole synthesis was started from $Q_2Q^aQ_2$ amine (**13**). The final compound was obtained by sequencing coupling with appropriate acid chloride and boc-deprotection. To be short, Q^a acid **8**, Q^aQ acid **22**, quinoline monomer acid **15**, Q^aQ acid **22**, Q^aQ acid **22** and quinoline dimer acid **12** were subsequently activated as acid chloride and couple to the corresponding amine to afford the oligomer **2c**. The final compound was purified by cyclic repeating GPC.

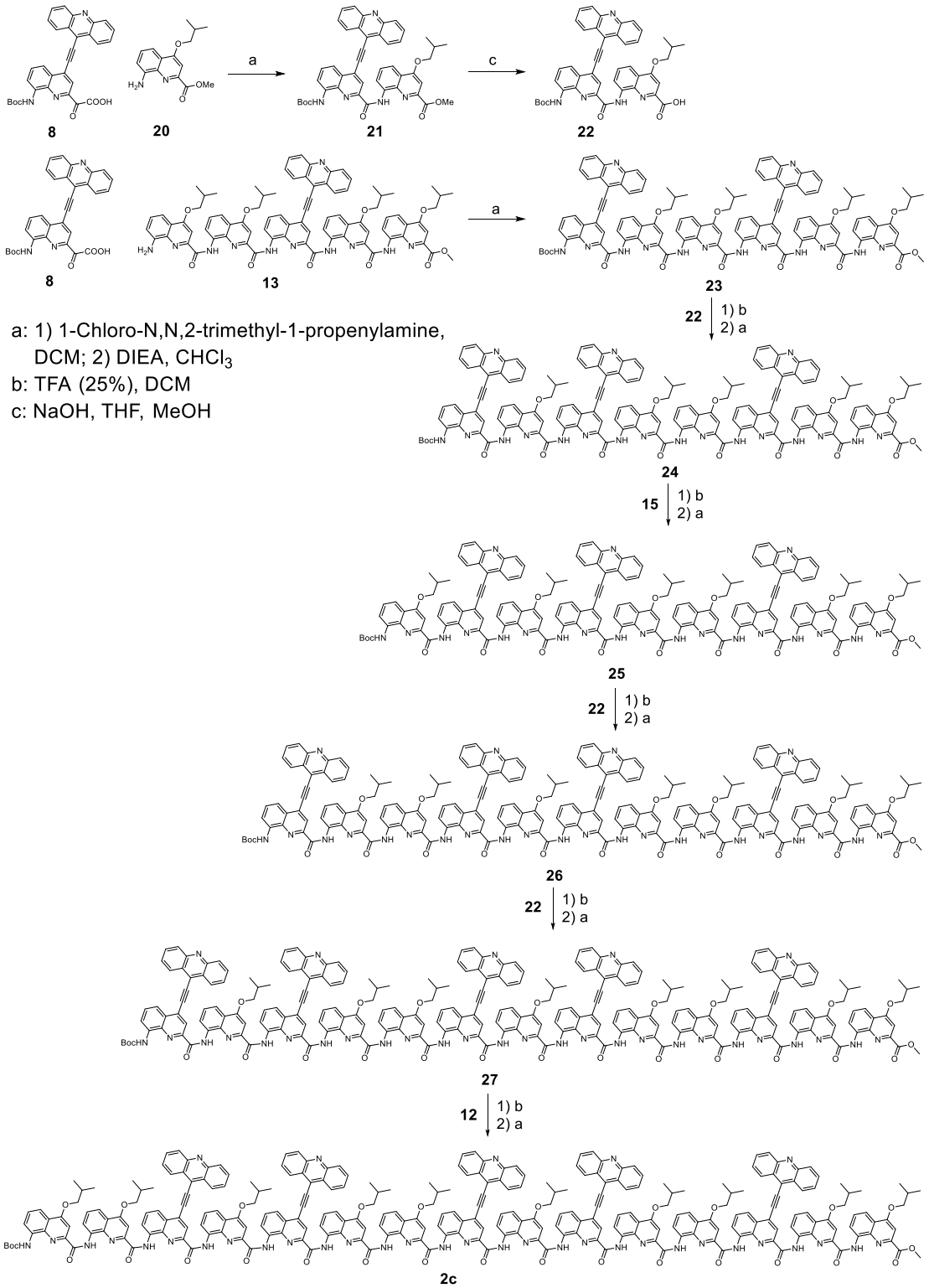

Scheme 4-4: Linear synthetic route for the acridine functionalized oligomers **2c**.

4.3.2 Aggregation of oligomers with acridine units on one face

All three compounds **1a**-**1c** showed sharp single set of peaks in chloroform which

indicated well defined species presented for those compounds in solution at room temperature. The proton NMR spectra of these oligomers with acridine side chain on one side of the helices were well defined and could be separated into different regions similar to the *oligo*-quinolinecarboxamides.[17] As showed in Fig. 4-4, the ^{1}H NMR spectra of **1a**-**1c** showed separated amide region (12 - 10 ppm), aromatic region (9 - 6 ppm) and aliphatic region (below 4.5 ppm). Those peaks spaced into large chemical shift area which clearly indicate helical folding of the oligomers. From **1a** to **1c**, signals are consistently shifted to upper field which is caused by the increased helical stacks with the oligomer length. The amide resonances are all well-resolved and the number of peaks can be clearly counted as the expected number even for the longest oligomer **1c**. In the aromatic region, the peaks were well resolved except for **1c** which showed overlapping of signals. Signals from acridine units were mostly hidden in the aromatic region except one signal which appeared at the lowest field part of the aromatic region. This signal was attributed to the acridine based on its coupling constants. Those acridine signals were clearly shifted to the upper field form 8.76 ppm in **1a** to 8.54 ppm in **1b** and 8.46 ppm in **1c**. The upper field shift of acridine signals were consistent with increasing the strength of pi-pi interactions as the length increased even outside of the helix. In the aliphatic region, diastereotopic proton signals (4.5 – 3.5 ppm) were observed for all three oligomers which were due to right and left handedness of the helical conformation. Methyl ester signals clearly distinguished from other signals and undergo upper field shift as expected for helical folding of the oligomers.

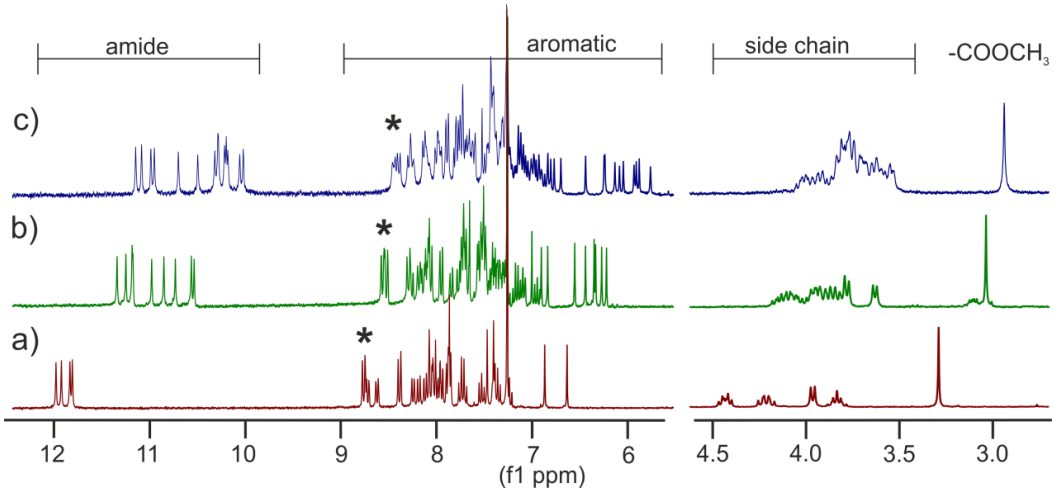

Figure 4-4: Part of ^{1}H NMR (300 MHz, $CDCl_3$) of acridine functionalized oligomers a) **1a**, b) **1b** and c) **1c**.

Concentration dependent NMR spectra were measured in chloroform, which is an informative method to demonstrate the aggregation behavior of a compound in solution. As showed in figures 4-5 and 4-6, the concentration dependent ^{1}H NMR spectra of **1b** and **1c** were recorded from 10 mM solution to 0.1 mM. As observed in the figure, from low concentration to high concentration, both compounds displayed only one set of peaks which indicated that either there is only one species in solution or there is fast exchange between different possible species. Chemical shifts variations were observed in both cases. Upon increasing the concentration, upper field shifts of signals were observed which was consistent with aggregation formation at higher concentration. In the case of **1b**, the peaks corresponding to protons from acridine at 8.62 ppm at 0.1 mM concentration shifted to 8.61 ppm at 10 mM which accounted for very small chemical shifts variations. The longer oligomer **1c** showed bigger chemical shifts variations than **1b**. In the amide region, obvious shifting of some of the signals was observed as marked in the figure 4-6. Also, the resonances corresponding to protons on acridines shifted form 8.51 ppm at 0.1 mM concentration to 8.37 ppm at 15 mM concentration which was more obvious than **1b**. Upon increasing the concentration, some broadening of the signals was also noticed which indicated nonspecific aggregation behavior at higher concentration. Comparing **1b** to **1c**, **1c** has a higher propensity to aggregate in solution. This result is not surprising since **1c** has one more acridine side chain than **1b**. The lack of major chemical shifts variations or appearance of another set of signals observed in both **1b** and **1c** upon changing concentration in $CDCl_3$ indicated that weak or only nonspecific aggregation of those two oligomers in chloroform.

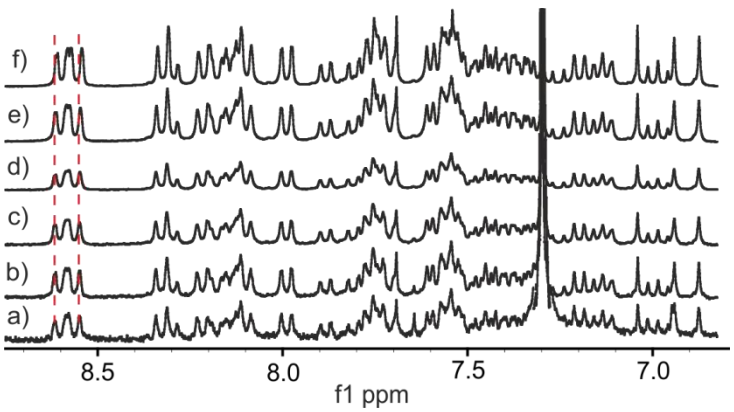

Figure 4-5: Part of the concentration dependent ^{1}H NMR spectra of **1b** showing the aromatic region, a)

0.1 mM, b) 0.5 mM, c) 1 mM, d) 2.5 mM, e) 5 mM and f) 10 mM in $CDCl_3$.

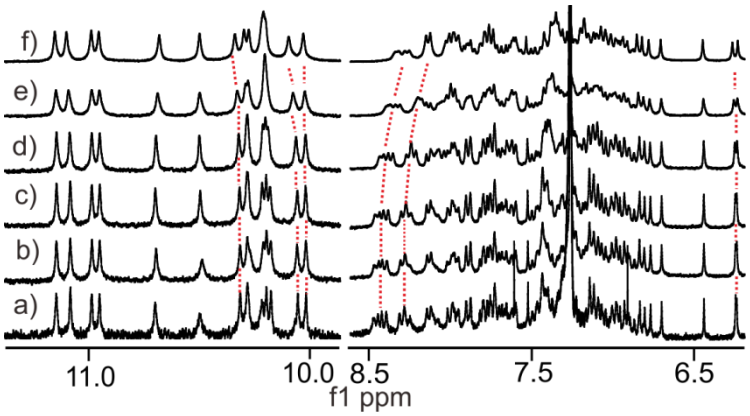

Figure 4-6: Part of the concentration dependent ^{1}H NMR spectra of **1c** showing the amide and aromatic region, a) 0.1 mM, b) 0.5 mM, c) 1 mM, d) 2.5 mM, e) 5 mM and f) 15 mM in $CDCl_3$.

Single crystals suitable for X-ray diffraction of both **1b** and **1c** were obtained by slow diffusion of acetonitrile into a stock solution of **1b** or **1c** in chloroform. As showed in figures 4-7 and 4-8, the acridine side chains of both oligomers are indeed positioned at single face of the helices as designed. The acridine side chains are almost parallel with each other although small angles between them are observed. In the case of **1b**, the two acridine planes had an angle of 8.5^o and both of the two acridines are not perpendicular to the axis of the helix. Similar arrangements of the acridine with respect to the axis of helix are found in **1c** too. The angles between the acridine planes are 9.3^o, 0.5^o (measured between the acridines at the ester end and middle ones; Boc-amide end and middles ones respectively). The distances between the acridines planes is 7.1 Å in the case of **1b** (Fig. 4-7), and 6.8 Å and 7.2 Å in the case of **1c** (Fig. 4-8). The distances between 4-position of the quinolines which acridine side chains are attached are 6.9 Å in **1b** and 6.7 Å, 6.9 Å in **1c** which are all slightly shorter than the distances between the acridines. It was noticed that in **1c**, the triple bond connecting the acridine and quinoline at the Boc-amide end was severely distorted from ideal 180^o bond angle (155^o was found which was 25^o less than the ideal bond angle). The extreme distortion of this triple bond was an indication of some steric hindrance might exist in the crystal. Other triple bond linkages also showed slight bending (bond angles around 172^o were observed) which are in the normal deviation range.

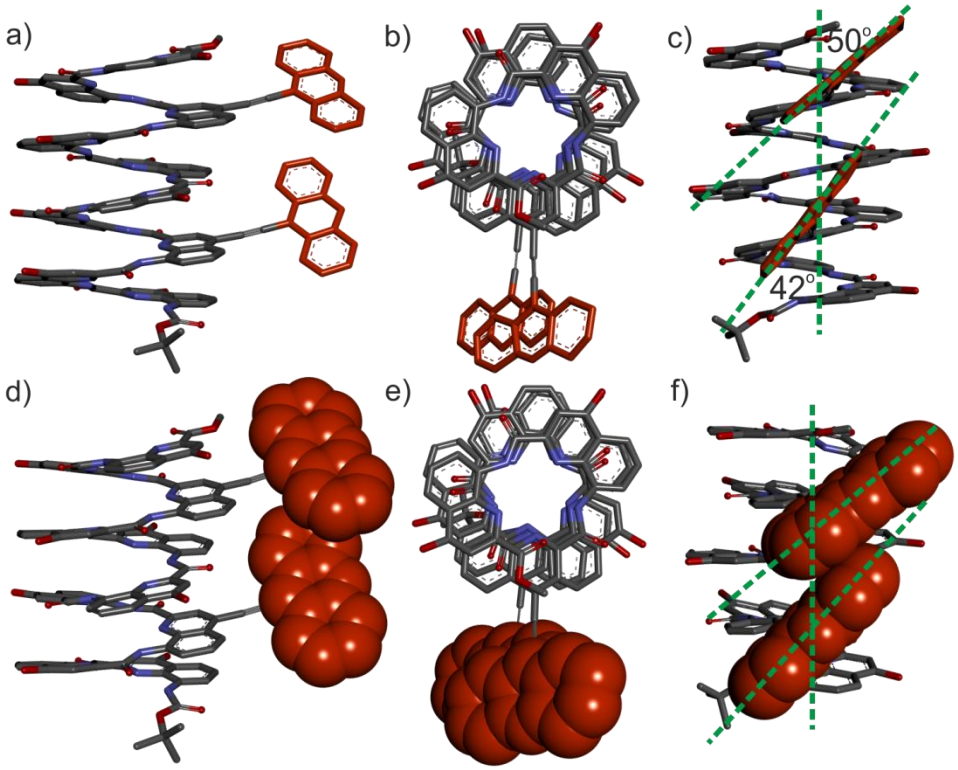

Figure 4-7: Single crystal x-ray structure of **1b**, a) side view form the helix axis; b) top view form the helix axis; c) side view to show relative orientation of the acridine rings with respect to the axis of helix; CPK view of acridine rings of d) side view; e) top view and f) side view to show the relative orientations.

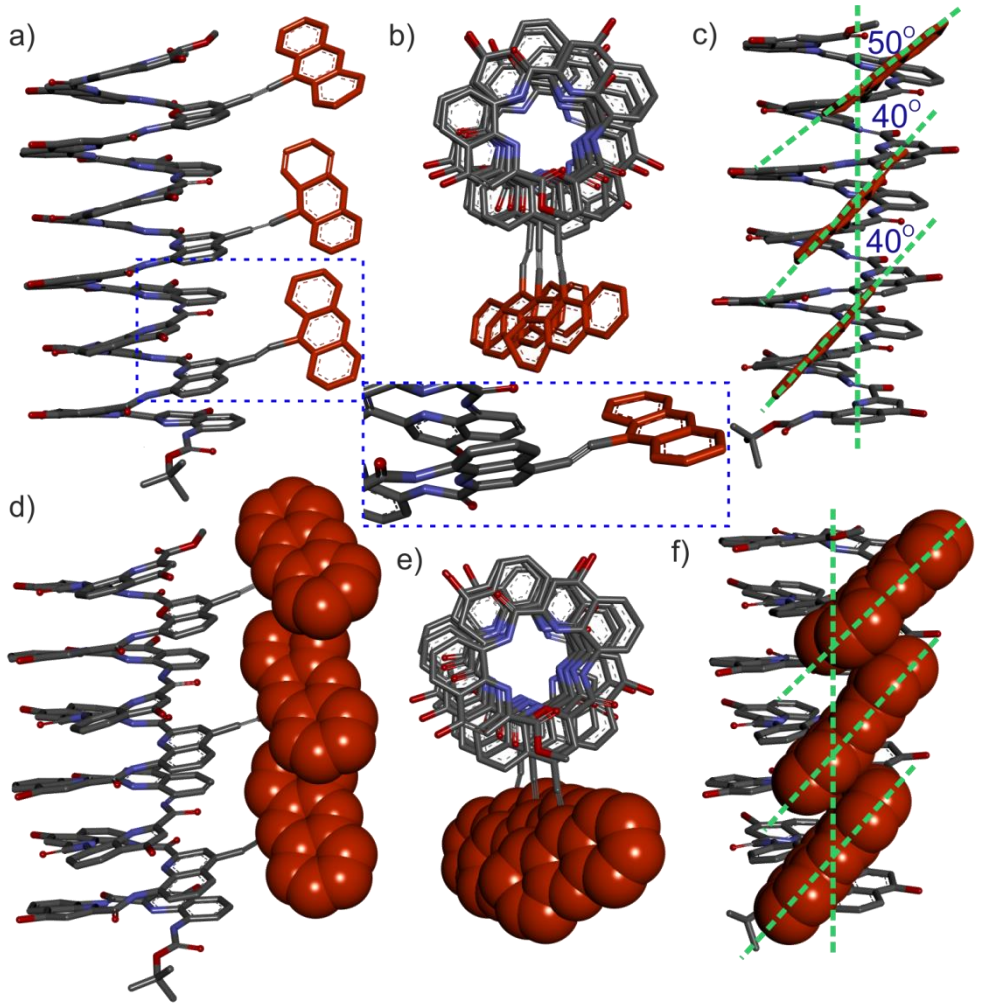

Figure 4-8: Single crystal x-ray structure of **1c**, a) side view form the helix axis, in the blue box is the zoom of the acetylene that have significant distortion; b) top view form the helix axis; c) side view to show relative orientation of the acridine rings with respect to the axis of helix; CPK view of acridine rings of d) side view; e) top view and f) side view to show the relative orientations.

In the crystal structures of **1b** and **1c**, interactions between helices were observed. As showed in figure 4-9, two molecules of **1b** interacted with each other through acridine units. A P-helix of **1b** interacts with another antiparallel M-helix of **1b** in the crystal (Fig. 4-9a). The acridine units of the two helices form π-stacks to associate these helices. Several aromatic CH-π interactions of 3.26 Å to 3.34 Å between acridines have been observed. The distance between an acridine unit to acridine unit of another helix is about 3.4 Å which indicated strong π-stacking effect between them (Fig. 4-9e). From the side view of the acridine stacks (Fig. 4-9b and 4-9e), these acridine units have offsets between adjacent acridine units which are distinct from the design that all acridine units are stacked on top of each other. From the

top view (Fig. 4-9a, 9c and 9d), substantial overlapping of aromatic surfaces of the acridine units can still be observed.

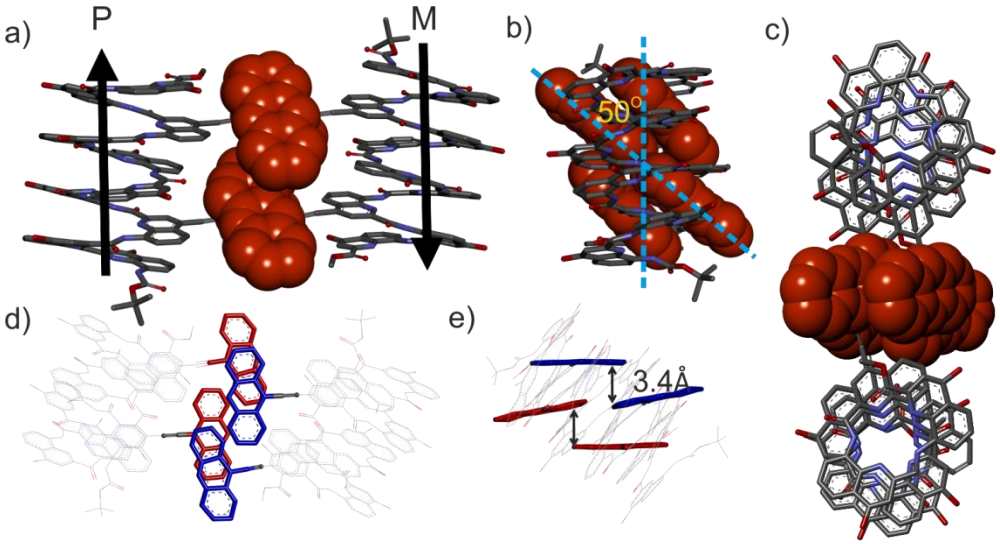

Figure 4-9: The interactions of **1b** in the solid state. a) Side view of two helices that interact with each other through acridine units, the two helices are P and M in an antiparallel orientation; b) side view to show the angle of acridine rings with respect to the axis of helices; c) top view of the two helices that associated together; d) top view to highlight the overlapping of acridine surfaces; e) side view of acridine rings to show the stacking pattern of them, the blue and red color indicate those acridines are belong to the same helix.

In the crystal of **1c**, the interactions between helices are quite similar to **1b**. The two helices that interact with each other are P and M helices. The orientation of the two helices is antiparallel (Fig. 4-10c). The acridine units form moderate π-stacks with distance around 3.6, 3.7 and 3.6 Å (Fig. 4-10f). Strong aromatic CH-π interactions with distance of 3.10 Å was observed. The middle acridines (H^2 proton) also form hydrogen bond with amide carbonyl oxygen (3.17 Å) of the other helix. Significant offset between acridine rings were observed instead of piling up of acridine units as showed in the design (Fig. 4-10b, 10d and 10e). In the top view (Fig. 4-10a), the acridine units of two helices do not intercalate into each other. In the side view (Fig. 4-10d), adjacent acridine units have some overlapping of the aromatic surfaces which indicate aromatic interactions between them. A clear ladder of stacks of acridine rings can be observed in the side view (Fig. 4-10f). Those observations indicate π-π interactions through acridine units play important role to bring two helices together. Although intercalating of acridine rings are not observed, the interactions between acridine rings already able to guide the association of helices.

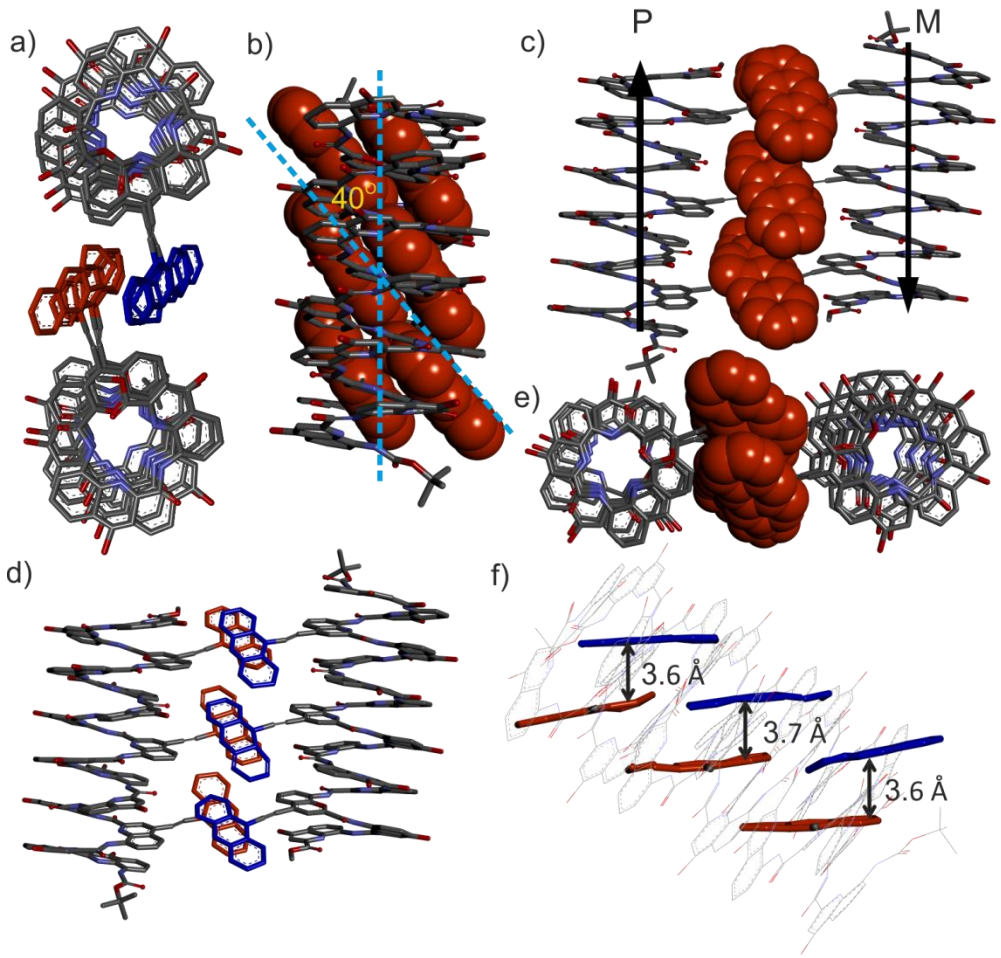

Figure 4-10: The interactions of **1b** in the solid state. a) top view through the helices; b) side view to show the angle of acridine rings with respect to the axis of helices; c) Side view of two helices that interact with each other through acridine units, the two helices are P and M in an antiparallel orientation; d) side view of acridine rings to show the overlapping of aromatic surfaces of adjacent acridine rings; e) top view of the two helices that associated together; f) side view of acridine rings to show the stacking pattern of them, the blue and red color indicate those acridines are belong to the same helix.

4.3.3 Aggregation of oligomers with acridine units on two faces

The proton NMR of oligomers **2a**-**2c** with acridine side chains at two corners of the helices are presented in figure 4-11. NMR of these three oligomers displayed sharp proton NMR spectra with separated regions for amide, aromatic and aliphatic spaced on large chemical shift range similar as the oligomers **1a**-**1c** in agreement with the helical folded structures. The proton NMR spectra of **2a**-**2c** had some over-lapping of signals especially for **2c** in the amide and aromatic regions. In **2a**, parts of the acridine proton signals can be found

at 8.74 and 8.37 ppm. In **2b**, the signals at 8.55 and 8.44 ppm were attributed to acridine units. In **2c**, signals at 8.43 and 8.23 ppm were assigned to acridine units. All three compounds showed only one set of signals same as **1a**-**1c**.

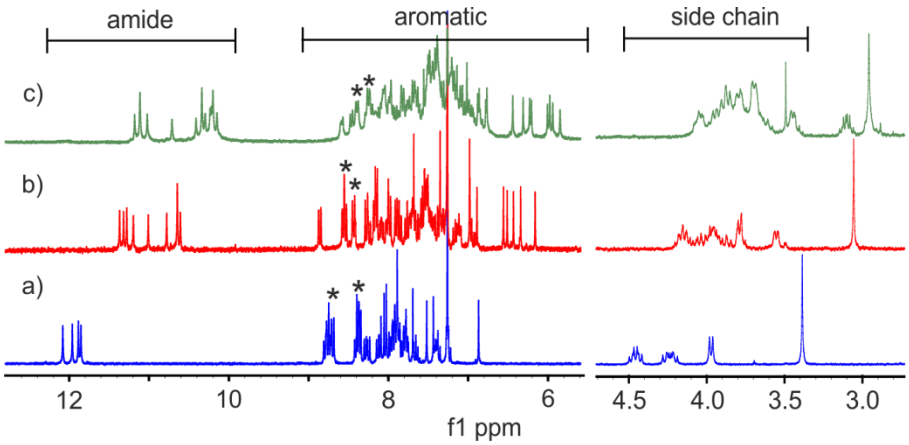

Figure 4-11: Parts of the ^{1}H NMR spectra (300 MHz) of **2a**-**2c** in CDCl3, a) **2a**, b) **2b** and c) **2c**, stars indicate those signals are from acridine units.

Concentration dependent NMR spectra of oligomer **18** ($Q^{a}QQ^{a}$) and **2a** ($Q_2Q^{a}QQ^{a}$) were checked from 0.1 mM to 10 mM concentration. For both compounds, the NMR spectra were sharp at all concentrations and only minor chemical shifts variations were observed. Both oligomers showed more obvious chemical shifts variation than **1b** which have the same acridine side chains. In the case of **18**, the two amide peaks shifted from 12.52 ppm and 12.50 ppm at 0.1 mM to 12.47 ppm and 12.45 ppm at 10 mM respectively. The peaks of the aromatic region also shifted, for example, the doublet at 8.32 ppm shifted to 8.26 ppm by increasing the concentration from 0.1 mM to 10 mM. One interesting feature was that the doublet at 8.38 ppm (two of the acridine proton signals) at 0.1 mM concentration shifted slightly to upper field and separated as two doublets of at 10 mM. Other acridine protons did not show much chemical shift variations, the doublets of acridines at 8.77 and 8.69 ppm at 0.1 mM shifted only slightly to 8.75 and 8.66 ppm at 10 mM respectively.

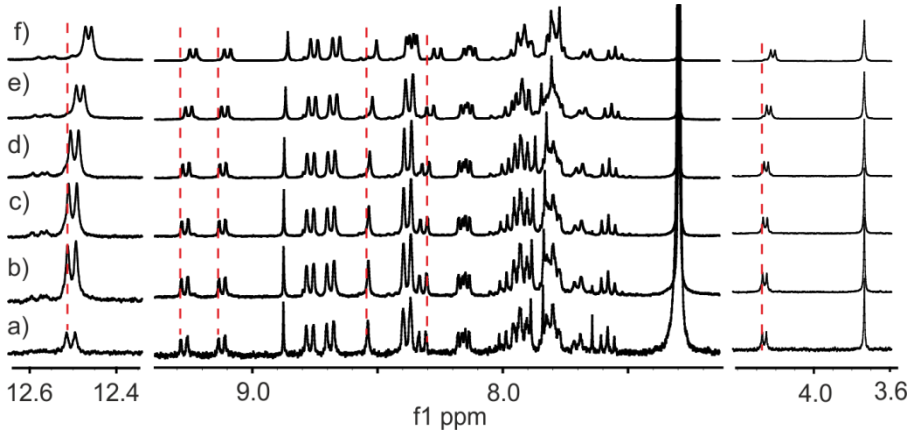

Figure 4-12: Parts of the concentration dependent ^{1}H NMR spectra of **18** (QaQQa) in chloroform, a) 0.1 mM; b) 0.5 mM, c) 1 mM, d) 2.5 mM, e) 5 mM and f) 10 mM.

In the case of oligomer **2a**, the chemical shifts variations were smaller than **18** upon increasing concentration from 0.1 mM to 10 mM. In the amide region, all four amide peaks show around 0.02 to 0.03 ppm of upper filed chemical shifts variations. Similar upper field shifts of the signals in aromatic region also observed. For example, the singlet at 6.91 ppm (0.1 mM concentration) shifted to 6.87 ppm (10 mM concentration). One of the acridine proton signals at 8.74 ppm (0.1 mM concentration) shifted to 8.71 ppm (10 mM concentration). Another acridine proton signal shifted from 8.39 ppm to 8.37 ppm upon increasing concentration from 0.1 mM to 10 mM. Minor chemical shifts variation observed in both **18** and **2a** indicated weak association of these two oligomers in solution.

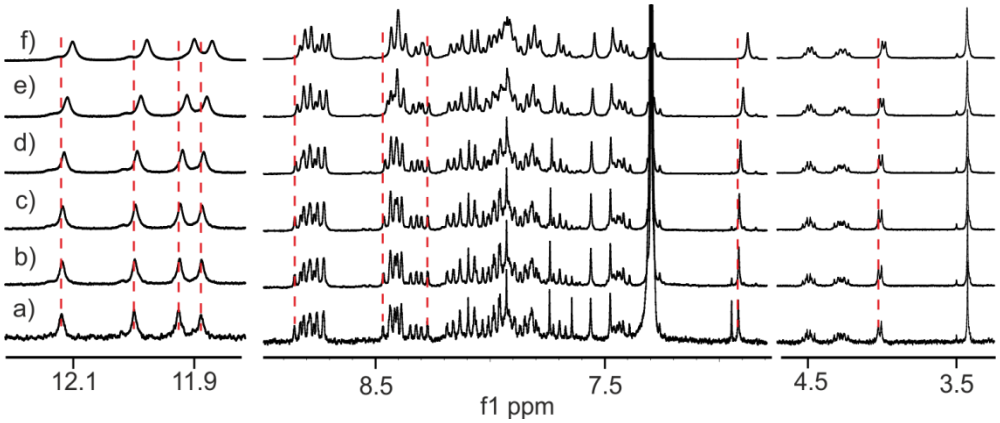

Figure 4-13: Parts of the concentration dependent ^{1}H NMR spectra of **2a** in chloroform, a) 0.1 mM; b) b) 0.5 mM, c) 1 mM, d) 2.5 mM, e) 5 mM and f) 10 mM.

The oligomer **2c** which bears 5 acridine side chains out of 15 side chains was designed to have higher propensity to aggregate. Unlike oligomer **2a** and **18** for which almost all proton

NMR signals displayed upper field shift upon increasing concentration, in oligomer **2c**, showed some proton signals undergo upper field shift and others lower field shift. In the amide region, for example, the peaks at 11.21 ppm (0.1 mM concentration) shifted to 11.23 ppm (10 mM concentration), the peaks at 10.37 ppm and 10.32 ppm all shifted to lower field and almost converged at 10.39 ppm. Three peaks around 10.24 ppm also shifted to lower field and converged as a broad peak at 10.28 ppm at 10 mM concentration. In the region between 5.8 to 6.5 ppm, the singlets of the H^3 proton of quinoline units all shifted to lower field upon changing concentration from 0.1 mM to 10 mM. The doublet at 8.43, 8.28 and 8.08 ppm which are acridine proton signals all showed significant upper field shifts. Chemical shifts variations of 0.17, 0.16 and 0.10 ppm were observed for those three signals respectively. Due to overlapping of signals and some broadening of the peaks, some chemical shifts variations were difficult to follow. The observed chemicals variations and changes in the NMR spectra in **2c** are much bigger than **1a**-**1c** and **2a** which indicated strong propensity to aggregate for **2c**.

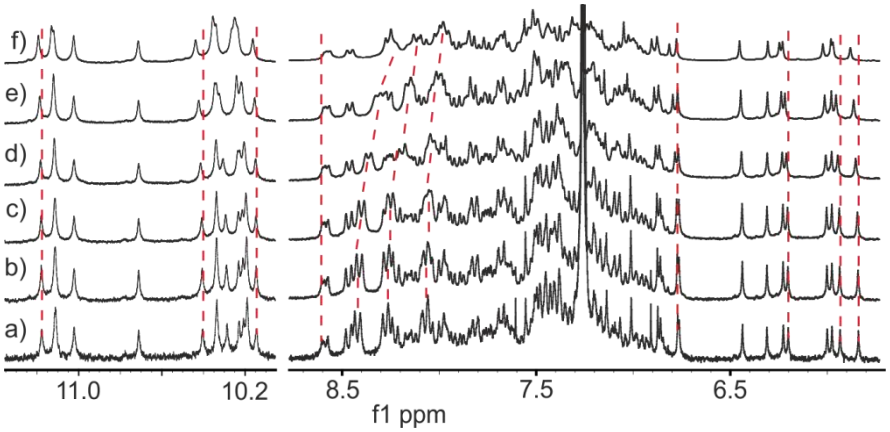

Figure 4-14: Parts of concentration dependent ^{1}H NMR spectra of **2c** in chloroform showing the amide and aromatic region, a) 0.1 mM; b) 0.5 mM, c) 1 mM, d) 2.5 mM, e) 5 mM and f) 10 mM.

The single crystal of **2b** suitable for X-ray diffraction was obtained by layer diffusion of hexane to the stock solution in chloroform. As clearly showed in the top view, the acridine side chains were indeed at two faces of the helices as designed. The angle between the two arms is around 60^o as we wanted. The two acridines (*acr1* and *acr3* in Fig. 4-15) at the same side of the helix were not parallel. The angle between the two acridine planes was 36.4^o which was much bigger than was found in **1b** and **1c**. Two acridine planes (*acr2* and *acr3*) were not

perpendicular to the helix axis as observed in **1b** and **1c**. These two acridine rings have an angle about 55° to the axis of the helix. The *acr1* is almost perpendicular to the axis of helix.

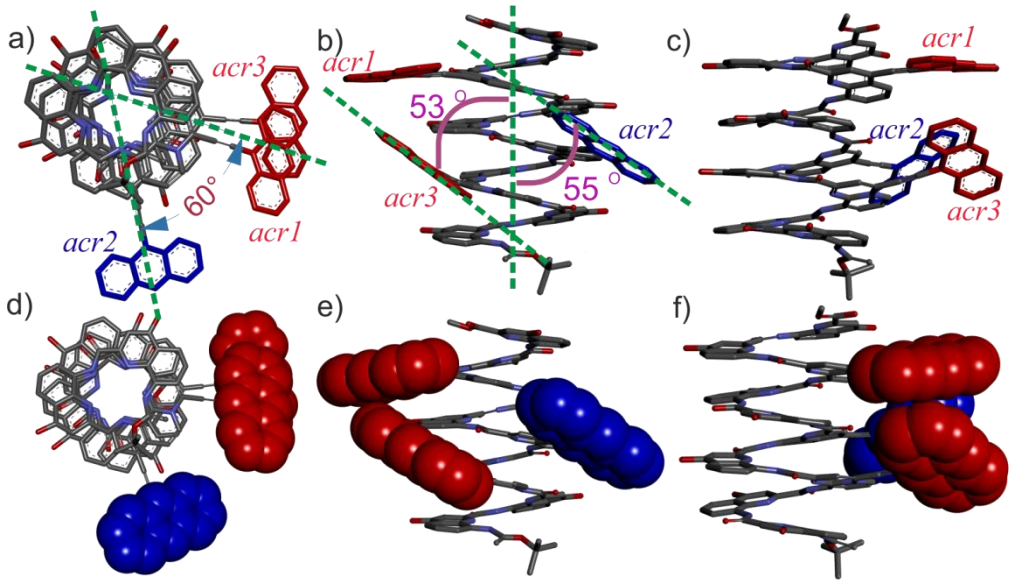

Figure 4-15: The crystal structure of **2b**, a) top view through the helix; b) side views to show the relative position of acr2 and acr3; c) side view to show the relative position of acr1 to the other two acridine units; CPK view of acridine units of d) top view; e) and f) side view. Red color indicate that those two acridines are on the same face of the helix, blue color indicate the face of a single acridine unit. The name of acridine units are followed from the ester end to the Boc-amide terminus of the helix.

The interactions of helices in the crystal of **2b** were different compared to **1b** and **1c**. As showed in figure 4-16, substantial overlapping of the aromatic surfaces can be observed among the acridine units. A P-helix interacts with an antiparallel M-helix similar to **1b** and **1c** (Fig. 4-16b). From the side view (Fig. 4-16d), a nice stack of four acridine rings can be observed. These four acridine units are the *acr2* (*acr2'*) and *acr3* (*acr3'*) from both helices. The two *acr1* (*acr1'*) units did not form parallel stacks with *acr2* and *acr3* as showed in side view (Fig. 4-16d, 16e, 16f). The surfaces of the four acridine rings that stack with each other have an angle around 55° with respect to the helix axis (Fig. 4-16d). The distances between these four acridine rings are about 3.4 Å, 3.3 Å and 3.4 Å (Fig. 4-16e). The *acr3* and *acr3'* form strong π-stacking interactions with each other. Several aromatic CH-π interactions with distance from 3.32 Å to 3.37 Å have been observed between these two acridine rings. The *acr2* (*acr2'*) only forms weak π-stacking interaction with *acr3'* (*acr3*). Only partial surface overlapping between *acr2* (*acr2'*) and *acr3'* (*acr3*) has been observed (Fig. 4-16f). The overall interactions observed between acridine rings indicate those helices are able to

associate together in the solid state.

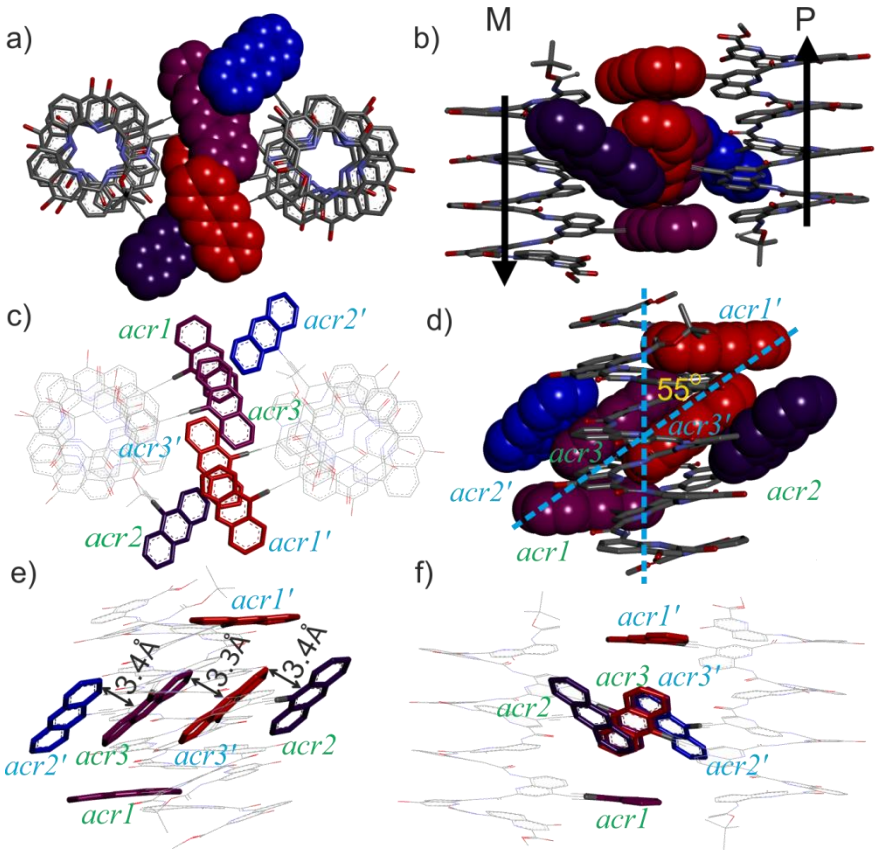

Figure 4-16: The interactions between two helices of **2b**, a) top view through the helices; b) Side view of two helices that interact with each other through acridine units, the two helices are P and M in an antiparallel orientation; c) side view of acridine rings to show the overlapping of aromatic surfaces of adjacent acridine rings; d) side view to show the angle of acridine rings with respect to the axis of helices; e) and f) side view of acridine rings to show the stacking pattern of them, the purple and red color indicate those acridines are belong to the face of helices that have two acridine rings. The names of acridine units are the same as in figure 15.

The packing pattern of **2b** in the crystal structures are displayed in figure 4-17. The acridine units form a continuous ladder of π-stacks in between two lines of helices. From the top view (Fig. 4-17a), a line of P helices standing outward the surface interact with a line of M helices of opposite orientation. The acridine units in between the two lines of helices form a zigzag shaped ladder (Fig. 4-17a). From the side view (Fig. 4-17b), the acridine units that stack with each other are (-*acr3-acr3'-acr2-acr2''*-)$_n$. For any given helix of **2b** in the crystal, its *acr3* interacts with *acr3* of an antiparallel helix at left (right) opposite line, and its *acr2* interacts with *acr2* of another antiparallel helix at right (left) opposite line. Propagating this arrangement forms the continuous stacking of acridine units as showed in figure 4-17. This

packing pattern is different from the design showed in figure 4-2d. A chain like arrangement was observed instead of a cyclic closed ring as designed.

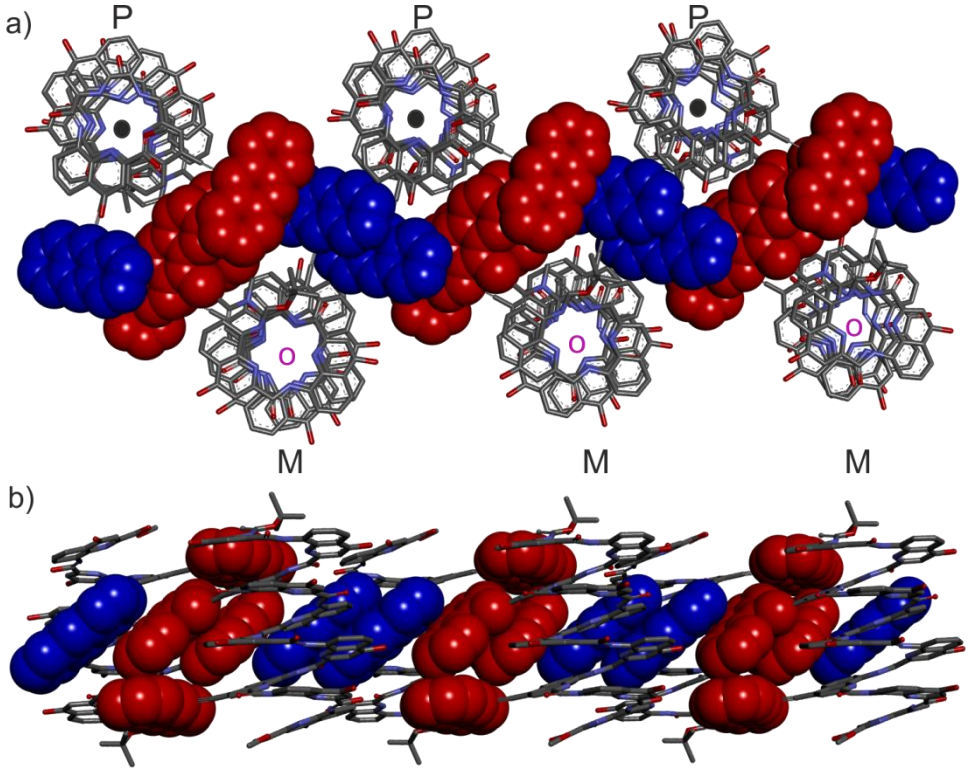

Figure 4-17: The packing pattern of **2b** in the crystal, a) top view through helices, P and M indicate the handedness of the helices, the black dot indicate the helices are standing outward toward the surface (from Boc-amide terminus to ester terminus), the empty circle indicate the helices are standing inward toward the surface; b) side view across the helices.

4.4 Conclusions and perspectives

In conclusion, we have successfully synthesized *oligo*-quinolinecarboxamide foldamers bearing different numbers of acridine units on the side chains. Due to the interactions of acridine side chains, the oligomers showed weak association in solution especially the oligomers with five acridine side chains. However, the association was weak and probably nonspecific in solution. Nevertheless, in the solid state, interactions between helices through acridine units were found. Aromatic interactions such as π-π stacking and CH-π interactions have been observed in the solid state. A continuous ladder of acridine stacking has been observed in **2b**. These observations suggested that the assemblies of these oligomers are strongly guided by the interactions of acridines.

As for perspectives, the acridine guided self-assembly of helical foldamers is weak but probably sufficient to be used to guide the formation of nicely self-organized helices on the surface of solid supports. Pyrene functionalized oligomers (Fig.14-8A) are designed. The pyrene unit attached at the N-terminus of the helical foldamers is used for attaching on surfaces such as highly oriented graphite. Another perspective is to change acridine unit to other functional groups that have stronger π-π stacking ability than acridine such as porphyrin as showed in Fig.4-18B. The ability of porphyrin to form π-stacks may allow formation of intercalated assembly of helical foldamers. A third perspective is the methylation of acridine units to acridium (Fig. 4-18C). The positive charge on acridium may allow it to intercalate with electron rich aromatic compounds.

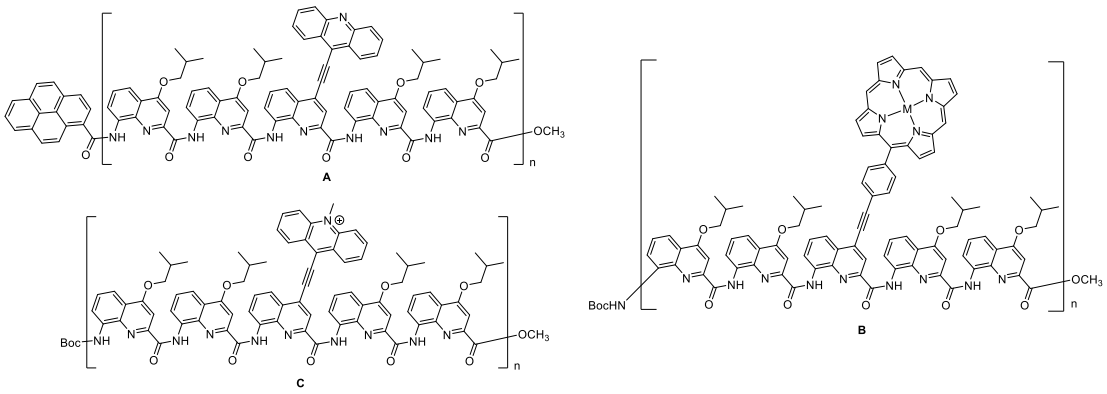

Figure 4-18: Proposed chemical structures for organization of helices on surface (**A**); self-assembly using porphyrin as functional groups (**B**); and methylation of acridine to methyl-acridine (**C**).

4.5 Experimental section

4.5.1 General remarks

All the solvents and reagents were used as received unless otherwise specified. Dry dichloromethane was obtained passing the solvent through a alumina column of solvent drying system. Dry chloroform and DIEA were obtained by refluxing with CaH_2 and the dry solvent was collected after distillation before using. ^{1}H NMR, ^{13}C NMR and 2D NMR were recorded on 300 MHz and 400 MHz Bruker Avance 300 and 400 spectrometer. Reactions were monitored by thin layer chromatography (TLC) on Merck silica gel 60-F254 plates and observed under UV light. Column chromatography purifications were carried out on Merck

GEDURAN Si60 (40-63 μm). ESI mass spectra were obtained from the Mass Spectrometry Laboratory at the European Institute of Chemistry and Biology (UMS 3033 - IECB), Pessac, France.

4.5.2 X-ray crystallography

The single crystals were obtained by slow diffusion of poor solvents such as acetonitrile, hexane or methanol into the stock solution in chloroform. Typically, the crystals were obtained in around 1 to 2 weeks and suitable crystals were picked for x-ray diffraction.

4.5.3 Monomer synthesis

Compound **3** was prepared according to the known procedure[18] with minor changes.

Compound **5**: To a 100 mL flask charged with **4** (1.56 g, 5 mmol), then 10 mL of AcOH and 20 mL of MeOH was added. The mixture was stirred with magnetic stirring bar and was equipped with condenser. Iron powder (1.4 g, 25 mmol) was added slowly in portions to avoid vigorous generation of gases. After completion of addition of iron powder, the reaction was allowed to slowly heat at 65 °C for about 40 minutes. The reaction mixture was cooled down to room temperature after the complete conversion of the starting material by check TLC. The resulting slurry was filtrated through celite and washed thoroughly with dichloromethane. The organic layer was then dried over sodium sulfate, filtrated and the solvent was removed with rotatory evaporation. The resulting orange solid (1.2 g) was not purified and used directly for the next step. ^{1}H NMR (300 MHz, $CDCl_3$) δ: 8.40 (s, 1H), 7.54-7.45 (m,2 H), 6.98 (dd, J = 7.0, 1.7 Hz, 1 H), 5.24 (bs, 2 H), 4.04 (s, 3 H) ppm.

Compound **6**: The crude starting material of compound **5** (1.2 g, 4.27 mmol) and Boc_2O (5.45 g, 25 mmol) were added into a 100 mL flask. Dioxane (15 mL) and DIPEA (5.6 mL) were added and the reaction mixture was then heated at 80 °C for 5 days under N_2 with magnetic stirring. After cooling down to room temperature, solvent was evaporated and the

resulting sluggish mixture was directly applied on a column. The product was eluted with dichloromethane/ethyl acetate (v/v 20/1). Some of the unreacted **5** was recovered from the column and recycled for the reaction. Yield 1.4 g (75% over two steps). ^{1}H NMR (300 MHz, $CDCl_3$) δ: 9.00 (s, 1H), 8.56 (d, J = 8.0 Hz, 1 H), 8.46 (s, 1 H), 7.80 (dd, J = 8.4, 1.3 Hz, 1 H), 7.71 (t, J =8.0 Hz, 1 H), 4.07 (s, 3 H), 1.59 (s, 9 H) ppm.

Compound **7**: To a 50 mL dry flask was added with **6** (1.22 g, 3.21 mmol), **3** (0.85 g, 4.18 mmol), $PdCl_2(PPh_3)_2$ (120 mg, 0.16 mmol), CuI (61 mg, 0.32 mmol) and PPh_3 (84 mg, 0.32 mmol). Then the flask was equipped with condenser and was connected with vacuum line and exchanged with N_2 for three times. A mixture of degassed THF and Et_3N (12 mL, v/v 2/1, THF was from solvent drying system and Et_3N was distilled over CaH_2 before degassing) was added into the flask. The resulting mixture was heated at 75 ℃ for overnight. After cooling down to room temperature, the precipitate was filtrated and washed with methanol. The solid was dried under vacuum. (yield 1.1 g, 68%). ^{1}H NMR (300 MHz, $CDCl_3$) δ: 9.08 (s, 1H), 8.63 (d, J = 8.4 Hz, 2 H), 8.60 (s, 1 H), 8.32 (d, J = 8.6 Hz, 2 H), 8.16 (d, J = 8.4 Hz, 1 H), 7.89 (d, J = 8.6, 1 H), 7.86 (d, J = 8.6 Hz, 1 H), 7.81 (t, J =8.2 Hz, 1 H), 7.75 (d, J = 8.4 Hz, 1 H), 7.72 (d, J = 8.4 Hz, 1 H), 4.14 (s, 3 H), 1.62 (s, 9 H) ppm; ^{13}C NMR (75 MHz, $CDCl_3$) δ: 165.2, 152.8, 148.6, 148.6, 145.0, 137.7, 137.0, 131.2, 130.6, 130.6, 130.4, 130.4, 130.2, 128.5, 127.6, 127.5, 126.6, 126.4, 126.3, 125.8, 124.7, 117.8, 115.9, 99.4, 93.7, 81.2, 53.3, 28.5 ppm.

4.5.4 Oligomer synthesis

Compound **8**: To a 25 mL flask added **7** (200 mg, 0.4 mmol), NaOH (40 mg, 1 mmol), then 4 mL THF and 1 mL MeOH was added. The resulting mixture was stirred at room temperature for about 2 hours. Then the pH was adjusted to around 3 with 5% citric acid. The precipitate was filtrated and washed with water and MeOH. The resulting yellow solid (180 mg, yield 91%) was not purified further and used directly for next step.

General procedure for the coupling: To a dry flask added corresponding acid (1 equivalent), the flask was sealed with septum and filled with N_2. Then 10 mL of dry dichloromethane was added through a syringe. Ghosez reagent (1.5 equivalents) was added slowly with a syringe. The resulting mixture was stirred at room temperature under N_2 for 2 hours. Solvent was removed under high vacuum and the residue solid was further dried under high vacuum for 3 hours. The resulting acid chloride was not purified and no further purification process applied and used directly. The amine (1 equivalent) was added into another dry flask and filled with N_2. Freshly distilled diisopropylehthylamine (2.5 equivalent) was added into the flask with amine compound through a syringe. The acid chloride was then dissolved with appropriate amount of dry chloroform and added into the amine with a syringe. Upon complete transfer of the acid chloride into the amine, the resulting mixture was stirred at room temperature overnight. After completion of the reaction, the solvent was removed and the product was purified either by precipitation with dichloromethane/methanol mixing solvent or silica gel column chromatography or GPC.

Compound **10**: The compound was prepared according to the general coupling procedure and the product was purified by precipitation form dichloromethane/methanol. (Yield 75%) ^{1}H NMR (300 MHz, $CDCl_3$) δ: 12.44 (s, 1 H), 12.41 (s, 1 H), 9.07 (d, J = 7.6 Hz, 1 H), 9.06 (d, J = 7.6 Hz, 1 H), 8.81 (s, 1 H), 8.73 (d, J = 8.3 Hz, 2 H), 8.40 (s, 1 H), 8.35 (d, J = 8.8 Hz, 2 H), 8.08 (d, J = 8.8 Hz, 1 H), 8.06 (d, J = 8.4 Hz, 1 H), 7.96-7.89 (m, 3 H), 7.82 (s, 1 H), 7.81 (d, J = 8.6 Hz, 1 H), 7.78 (d, J = 8.6 Hz, 1 H), 7.74 (t, J = 8.3 Hz, 1 H), 7.68 (t, J = 8.3 Hz, 1 H), 7.58 (d, J = 8.3 Hz, 1 H), 7.42 (t, J = 8.3 Hz, 1 H), 6.72 (s, 1 H), 4.19 (d, J = 6.6 Hz, 2 H), 3.82 (d, J = 6.3 Hz, 2 H), 3.61 (s, 3 H), 2.41-2.21 (m, 3 H), 1.38 (s, 9 H), 1.20 (d, J = 6.6 Hz, 6 H), 1.17 (d, J = 6.9 Hz, 6 H) ppm.

Compound **11**: To a dry flask was added with **10** (40 mg, 0.04 mmol), then 3 mL of dichloromethane was added to dissolve the solid and then 1 mL of TFA was added and the resulting solution was stirred at room temperature for 2 hours. Then the reaction mixture was diluted with dichloromethane and then washed three times with $NaHCO_3$ solution. The organic layer was dried over sodium sulfate and then filtrated and the solvent was removed.

The residue solid was pure enough for subsequent reaction and no further purification. ^{1}H NMR (300 MHz, $CDCl_3$) δ: 12.39 (s, 1 H), 12.35 (s, 1 H), 9.11 (d, J = 8.0 Hz, 1 H), 8.95 (d, J = 7.6 Hz, 1 H), 8.77 (s, 1 H), 8.73 (d, J = 8.6 Hz, 2 H), 8.33 (d, J = 8.9 Hz, 2 H), 8.05 (d, J = 8.5 Hz, 1 H), 7.98 (d, J = 8.4 Hz, 1 H), 7.91 (d, J = 8.6 Hz, 1 H), 7.88 (d, J = 8.8 Hz, 1 H), 7.80-7.69 (m, 6 H), 7.23 (t, J = 7.8 Hz, 1 H), 6.85 (s, 1 H), 6.06 (d, J = 7.7 Hz, 1 H), 4.18 (d, J = 6.4 Hz, 2 H), 3.86 (d, J = 6.4 Hz, 2 H), 3.57 (s, 1 H), 2.38-2.24 (m, 3 H), 1.19 (d, J = 6.3 Hz, 6 H), 1.17 (d, J = 6.3 Hz, 6 H).

Compound **1a**: The compound was prepared according to the general coupling steps. Yield: 240 mg, 76%. ^{1}H NMR (300 MHz, $CDCl_3$) δ: 11.98 (s, 1 H), 11.92 (s, 1 H), 11.83 (s, 1 H), 11.81 (s, 1 H), 8.76 (d, J = 8.4 Hz, 2 H), 8.72 (d, J = 7.8 Hz, 1 H), 8.62 (d, J = 7.8 Hz, 1 H), 8.39 (d, J = 8.4 Hz, 2 H), 8.34 (d, J = 6.9 Hz, 1 H), 8.18 (d, J = 7.5 Hz, 1 H) , 8.12 (d, J = 8.6 Hz, 1 H), 8.07 (s, 1 H), 8.05-7.85 (m, 9 H), 7.74 (t, J = 8.5 Hz, 1 H), 7.71 (t, J = 8.5 Hz, 1 H), 7.53 (t, J = 8.0 Hz, 1 H), 7.45 (s, 1 H), 7.40 (s, 1 H), 7.40 (d, J = 7.6 Hz, 1 H), 7.36 (t, J = 8.0 Hz, 1 H), 7.24 (t, J = 8.0 Hz, 1 H), 6.87 (s, 1 H), 6.63 (s, 1 H), 4.47-4.40 (m, 2 H), 4.26-4.17 (m, 2 H), 3.96 (d, J = 6.2 Hz, 2 H), 3.86-3.81 (m, 2 H), 3.29 (s, 3 H), 2.61-2.27 (m, 4 H), 1.36-1.17 (m, 24 H), 1.13 (s, 9 H) ppm; ^{13}C NMR (75 MHz, $CDCl_3$) δ: 164.0, 163.9, 163.6, 163.3, 162.5, 161.7, 161.2, 161.1, 160.6, 151.6, 150.2, 149.8, 149.1, 148.82, 147.4, 145.5, 139.3, 138.4, 137.9, 137.0, 136.6, 134.4, 134.3, 133.8, 133.7, 133.5, 130.7, 130.4, 130.3, 129.4, 127.8, 127.8, 127.7, 127.3, 127.2, 127.1, 126.9, 126.5, 126.2, 122.6, 122.4, 122.1, 122.0, 121.2, 119.5, 117.4, 117.3, 117.2, 116.6, 116.3, 116.2, 115.6, 114.7, 114.6, 100.5, 99.7, 99.5, 99.3, 98.1, 93.6, 80.6, 75.7, 75.6, 75.3, 75.2, 52.3, 28.4, 28.4, 28.3, 28.3, 27.9, 19.6, 19.5, 19.5, 19.5, 19.4 ppm.

Compound **13**: The procedure was the same as compound **11**, yield quantitative. ^{1}H NMR (300 MHz, $CDCl_3$) δ: 12.00 (s, 1 H), 11.97 (s, 1 H), 11.83 (s, 1 H), 11.71 (s, 1 H), 8.76 (d, J = 8.6 Hz, 2 H), 8.64 (d, J = 8.6 Hz, 1 H), 8.61 (d, J = 8.8 Hz, 1 H), 8.39 (d, J = 8.4 Hz, 2 H), 8.23 (s, 1 H), 8.20 (s, 1 H), 8.12 (d, J = 8.1 Hz, 2 H), 8.06-7,84 (m, 8 H), 7.71 (t, J = 8.1 Hz, 1 H), 7.70 (t, J = 8.4 Hz, 1 H), 7.62-7.56 (m, 2 H), 7.42 (s, 1 H), 7.35 (s, 1 H), 7.35 (t, J = 7.5 Hz, 1 H), 7.07 (t , J = 8.1 Hz, 1 H), 6.87 (s, 1 H), 6.67 (s, 1 H), 5.93 (d, J = 7.8 Hz, 1 H),

4.46-4.32 (m, 2 H), 4.25-4.11 (m, 2 H), 3.96 (d, J = 6.3 Hz, 2 H), 3.85 (q, J = 2.7 Hz, 2 H), 3.32 (s, 2 H), 2.58-2.27 (m, 4 H), 1.35-1.18 (m, 24 H) ppm.

Compound **14**: To a flask added compound **1a** (120 mg, 0.08 mmol) and NaOH (33 mg, 0.8 mmol), then 1.8 mL of THF and 0.2 mL of MeOH was added. The resulting mixture was stirred at room temperature for 2 hours. Upon completion of the reaction, the pH was adjusted to 3. The orange precipitate was filtrated and washed 3 times with methanol and 3 times with water. Then the solid was died to yield orange solid 100 g (84% yield) ^{1}H NMR (300 MHz, $CDCl_3$) δ: 12.08 (s, 1 H), 12.01 (s, 1 H), 11.86 (s, 1 H), 11.80 (s, 1 H), 8.75 (d, J = 8.6 Hz, 2 H), 8.62 (dd, J = 7.8, 1.1 Hz, 1 H), 8.45 (dd, J = 7.8, 1.5 Hz, 1 H), 8.37 (d, J = 8.5 Hz, 2 H), 8.30 (d, J = 7.6 Hz, 1 H), 8.20 (d, J = 8.3 Hz, 1 H), 8.09 (dd, J = 8.5, 1.3 Hz, 1 H), 8.05 (s, 1 H), 8.02 (s, 2 H), 8.02 (dd, J = 8.5, 1.3 Hz, 1 H), 7.95 (dd, J = 8.5, 1.3 Hz, 1 H), 7.93 (dd, J = 8.5, 1.3 Hz, 1 H), 7.87 (dd, J = 8.5, 1.3 Hz, 1 H), 7.84 (dd, J = 8.5, 1.3 Hz, 1 H), 7.82 (dd, J = 8.5, 1.3 Hz, 1 H), 7.76 (s, 1 H), 7.71-7.53 (m, 4 H), 7.50 (s, 1 H), 7.43-7.24 (m, 5 H), 6.87 (s, 1 H), 6.72 (s, 1 H), 4.48-4.38 (m, 2 H), 4.26-4.13 (m, 2 H), 3.96 (dd, J = 6.3, 2.6 Hz, 2 H), 3.80 (d, J = 6.1 Hz, 2 H), 2.45-2.26 (m, 4 H), 1.35-1.14 (m, 24 H), 1.11 (s, 9 H) ppm;

Compound **1b**: The compound was prepared according to the general coupling procedures with minor changes. The acid **14** was activated with Ghosez reagent for overnight. The rest of the procedure was the same. The product was purified with silica gel column chromatography (eluent: DCM/EA 100/3). Yield: 40 mg, 55%. ^{1}H NMR (300 MHz, $CDCl_3$) δ: 11.34 (s, 1 H), 11.25 (s, 1 H), 11.18 (s, 1 H), 11.17 (s, 1 H), 10.98 (s, 1 H), 10.85 (s, 1 H), 10.73 (s, 1 H), 10.56 (s, 1 H), 10.53 (s, 1 H), 8.54 (m, 4 H), 8.29 (d, J = 8.8 Hz, 2 H), 8.26 (d, J = 8.5 Hz, 1 H), 8.19-8.05 (m, 8 H), 7.95 (d, J = 8.4 Hz, 2 H), 7.85 (d, J = 8.3 Hz, 1 H), 7.77 (d, J = 8.3 Hz, 1 H), 7.74-7.65 (m, 8 H), 7.65 (s, 1 H), 7.57-7.28 (m, 18 H), 7.23-7.07 (m, 7 H), 7.00 (s, 1 H), 6.95 (t, J = 7.9 Hz, 2 H), 6.90 (s, 1 H), 6.84 (s, 1 H), 6.55 (s, 1 H), 6.44 (s, 1 H), 6.35 (s, 1 H), 6.34 (s, 1 H), 6.27 (s, 1 H), 6.22 (s, 1 H), 4.15-3.77 (m, 14 H), 3.63 (d, J = 6.2 Hz, 2 H), 3.04 (s, 3 H), 2.55-2.13 (m, 8 H), 1.39-1.03 (m, 48 H), 0.93 (s, 9 H) ppm; ^{13}C NMR (75 MHz, $CDCl_3$) δ: 163.3, 163.2, 162.9, 162.8, 162.7, 162.4, 162.0, 161.1, 160.6, 160.5, 160.1, 159.4, 159.2, 159.2, 159.1, 158.0, 151.4, 149.4, 149.1, 148.7, 148.6, 148.5,

148.5, 147.1, 146.2, 145.0, 138.7, 137.9, 137.4, 137.4, 137.3, 137.2, 136.4, 136.1, 134.1, 133.7, 133.5, 133.3, 133.2, 133.1, 132.9, 132.6, 132.4, 132.1, 130.6, 130.3, 130.2, 129.9, 129.8, 128.8, 128.7, 128.0, 127.6, 127.4, 127.2, 126.9, 126.8, 126.6, 126.6, 126.3, 126.0, 125.8, 122.5, 122.3, 122.2, 122.0, 121.9, 121.6, 121.5, 121.3, 120.2, 119.5, 117.4, 116.9, 116.7, 116.2, 116.1, 115.7, 115.2, 114.5, 114.4, 100.2, 99.8, 99.2, 99.0, 98.8, 98.6, 98.4, 97.7, 93.1, 92.9, 80.2, 75.4, 75.3, 75.0, 74.8, 52.0, 45.9, 28.3, 28.2, 28.1, 28.0, 27.7, 19.7, 19.7, 19.5, 19.5, 19.4, 19.4, 19.3, 19.3, 19.3, 19.2, 8.7 ppm.

The corresponding amine of **1b**: The compound was prepared the same as compound **11**, the yield was considered to be quantitative by NMR and no further purification was done and used directly. ^{1}H NMR (300 MHz, $CDCl_3$) δ: 11.34 (s, 1 H), 11.25 (s, 1 H), 11.20 (s, 1 H), 11.03 (s, 1 H), 11.00 (s, 1 H), 10.88 (s, 1 H), 10.82 (s, 1 H), 10.60 (s, 1 H), 8.58-8.52 (m, 4 H), 8.29-8.20 (m, 5 H), 8.15-8.03 (m, 7 H), 7.97 (q, J = 3.3 Hz, 2 H), 7.84 (d, J = 8.2 Hz, 2 H), 7.76-7.26 (m, 22 H), 7.19 (t, J = 8.2 Hz, 1 H), 7.16 (s, 1 H), 7.13 (t, J = 7.6 Hz, 1 H), 7.10 (t, J = 7.6 Hz, 1 H), 6.84 (s, 1 H), 6.82 (s, 1 H), 6.79 (t, J = 7.6 Hz, 1 H), 6.56 (s, 1 H), 6.43 (s, 1 H), 6.36 (s, 1 H), 6.34 (s, 1 H), 6.30 (s, 1 H), 6.24 (s, 1 H), 5.65 (d, J = 7.6 Hz, 1 H), 4.16-3.78 (m, 14 H), 3.64 (d, J = 6.1 Hz, 2 H), 3.04 (s, 3 H), 2.54-2.13 (m, 8 H), 1.42-1.04 (m, 48 H) ppm.

Compound **1c**: The same procedure as the preparation of compound **1b**. The pure product was obtained by GPC and silica gel column chromatography. yield 25 mg, 44%. ^{1}H NMR (300 MHz, $CDCl_3$) δ: 11.15 (s, 1 H), 11.08 (s, 1 H), 10.99 (s, 1 H), 10.95 (s, 1 H), 10.70 (s, 1 H), 10.50 (s, 1 H), 10.32 (s, 1 H), 10.28 (s, 2 H), 10.22 (s, 1 H), 10.20 (s, 1 H), 10.18 (s, 1 H), 10.06 (s, 1 H), 10.02 (s, 1 H), 8.45-8.42 (m, 2 H), 8.38 (d, J = 8.3 Hz, 2 H), 8.25 (t, J = 8.7 Hz, 3 H), 8.15-7.95 (m, 8 H), 7.89 (dd, J = 8.2, 1.3 Hz, 3 H), 7.82-7.59 (m, 12 H), 7.52 (s, 1 H), 7.48 (d, J = 7.8 Hz, 1 H), 7.46-7.28 (m, 13 H), 7.23-7.04 (m, 14 H), 7.01-6.89 (m, 6 H), 6.84 (t, J = 8.1 Hz, 1 H), 6.83 (s, 1 H), 6.80 (s, 1 H), 6.77 (s, 1 H), 6.70 (s, 1 H), 6.44 (s, 1 H), 6.24 (s, 1 H), 6.23 (s, 1 H), 6.13 (s, 1 H), 6.08 (s, 1 H), 6.04 (s, 1 H), 5.93 (s, 1 H), 5.91 (s, 1 H), 5.88 (s, 1 H), 5.76 (s, 1 H), 4.02-3.53 (m, 24 H), 2.94 (s, 3 H), 2.44-2.04 (m, 12 H), 1.31-0.96 (m, 72 H), 0.85 (s, 9 H) ppm; ^{13}C NMR (75 MHz, $CDCl_3$) δ: 163.2, 163.1, 162.7,

162.6, 162.5, 162.4, 162.2, 162.0, 162.0, 160.9, 160.5, 160.4, 160.0, 159.1, 158.9, 158.8, 158.8, 158.5, 157.7, 151.2, 149.3, 148.9, 148.7, 148.6, 148.4, 148.3, 148.3, 148.2, 148.1, 148.0, 147.7, 151.3, 149.3, 148.9, 148.7, 148.6, 148.4, 148.3, 148.3, 148.2, 148.1, 148.0, 147.7, 146.9, 146.0, 145.9, 144.9, 138.6, 137.8, 137.2, 137.1, 136.9, 136.9, 136.8, 136.7, 136.2, 136.0, 135.8, 133.9, 133.6, 133.3, 133.2, 133.2, 133.1, 133.0, 132.6, 132.4, 132.3, 132.1, 131.9, 131.6, 130.5, 130.4, 130.2, 130.0, 129.8, 129.7, 129.5, 128.7, 128.5, 127.9, 127.5, 127.2, 127.1, 127.0, 126.8, 126.7, 126.5, 126.4, 126.1, 125.7, 125.6, 122.3, 122.2, 122.1, 122.0, 121.9, 121.8, 121.6, 121.5, 121.4, 121.1, 120.2, 117.2, 117.1, 116.8, 116.6, 116.0, 115.6, 115.1, 114.3, 100.2, 100.1, 99.7, 99.1, 98.7, 98.2, 98.6, 93.0, 92.8, 92.5, 80.1, 75.4, 75.3, 75.2, 75.0, 52.0, 28.4, 28.2, 28.2, 28.1, 28.0, 28.0, 27.9, 27.7, 19.9, 19.8, 19.7, 19.7, 19.6, 19.6, 19.5, 19.5, 19.4, 19.4, 19.3, 19.3, 19.3, 19.2 ppm.

Compound **17**: To a 25 mL flask was added with compound 7 (200 mg, 0.4 mmol). Then 6 mL of dichloromethane and 2 mL of TFA was added into the flask. The resulting solution was stirred at room temperature for 2 hours. Then the solvent was removed under high vacuum and the residue solid was added with 5 mL of toluene to co-evaporation under reduced pressure. The solid was dried under high vacuum and used without further purification. To a separate flask was added with 8-Bocamide-2-carboxylic acid-quinoline **15** (214 mg, 0.594 mmol) and 3 mL of dry dichloromethane. Then Ghosez reagent (119 mg, 0.892 mmol) was added into the flask. The resulting solution was stirred at room temperature for 2 hours. Then solvent was removed under high vacuum and the residue solid was dried under high vacuum for 3 hours. Then the solid was dissolved into 3 mL of dry chloroform and transferred into the flask containing the amine and DIEA (230 mg, 1.78 mmol). The resulting mixture was stirred at room temperature under N_2 for overnight. Then the solvent was removed and minimum amount of chloroform was added to dissolve the residue and methanol was added slowly to form a precipitate. The precipitate was filtrated and washed with methanol and then dried under vacuum. Yield a yellow solid 120 mg (40% over two steps). ^{1}H NMR (300 MHz, $CDCl_3$) δ: 12.46 (s, 1 H), 9.07 – 8.98 (m, 1 H), 8.72 (s, 1 H), 8.66 (dd, J = 8.8, 1.4 Hz, 2 H), 8.50 (dd, J = 7.8, 1.3 Hz, 1 H), 8.32 (dd, J = 8.4, 1.2 Hz, 2 H), 8.00 – 7.82

(m, 3 H), 7.81 – 7.70 (m, 2 H), 7.60 (t, J = 8.1 Hz, 1 H), 4.12 (d, J = 7.0 Hz, 2 H), 4.11 (s, 3 H), 2.33 (m, 1 H), 1.51 (s, 9 H), 1.16 (d, J = 7.1 Hz, 6 H) ppm.

Compound **18**: To a 25 mL flask was added with compound **17** (120 mg, 0.16 mmol). Then 2 mL of dichloromethane and 1 mL of TFA was added into the flask. The resulting solution was stirred at room temperature for 2 hours. Then 10 mL dichloromethane was added to dilute the reaction mixture. The solution was then washed with water and $NaHCO_3$ (5%) aqueous solution three times. The organic layer was collected and dried over Na_2SO_4. Then the solvent was removed after filtration to give an orange solid. The solid was dried under high vacuum and used without further purification. To a separate flask was added with **8** (118 mg, 0.24 mmol) and 3 mL of dry dichloromethane. Then Ghosez reagent (48 μL, 0.36 mmol) was added into the flask. The resulting solution was stirred at room temperature for 2 hours. Then solvent was removed under high vacuum and the residue solid was dried under high vacuum for 3 hours. Then the solid was dissolved into 3 mL of dry chloroform and transferred into the flask containing the amine and DIEA (126 μL, 0.72 mmol). The resulting mixture was stirred at room temperature under N_2 for overnight. Then the solvent was removed and minimum amount of dichloromethane was added to dissolve the residue slurry and methanol was added slowly to form a precipitate. The precipitate was filtrated and washed with methanol and then dried under vacuum. Yield a yellow solid 120 mg (67% over two steps). ^{1}H NMR (300 MHz, $CDCl_3$) δ: 12.47 (s, 1 H), 12.45 (s, 1 H), 9.23 (d, J = 7.9 Hz, 1 H), 9.08 (d, J = 7.5 Hz, 1 H), 8.83 (s, 1 H), 8.73 (d, J = 8.4 Hz, 2 H), 8.65 (d, J = 8.6 Hz, 2 H), 8.50 (s, 1 H), 8.34 (d, *J* = 8.7 Hz, 2 H), 8.27 (dd, *J* = 8.4, 1.3 Hz, 1 H), 8.11 (ddd, *J* = 8.5, 4.6, 1.3 Hz, 2 H), 8.00 – 7.82 (m, 6 H), 7.81 – 7.72 (m, 5 H), 7.65 (d, *J* = 7.8 Hz, 1 H), 7.54 (t, *J* = 8.0 Hz, 1 H), 4.21 (d, *J* = 6.5 Hz, 2H), 3.70 (s, 3 H), 2.39 (m, 1 H), 1.41 (s, 9 H), 1.22 (d, *J* = 6.7 Hz, 6 H) ppm.

Compound **2a**: To a 25 mL flask was added with compound **18** (120 mg, 0.10 mmol). Then 3 mL of dichloromethane and 1 mL of TFA was added into the flask. The resulting solution was stirred at room temperature for 2 hours. Then 10 mL dichloromethane was added to dilute the reaction mixture. The solution was then washed with water and $NaHCO_3$ (5%) aqueous

solution three times. The organic layer was collected and dried over Na_2SO_4. Then the solvent was removed after filtration to give an orange solid. The solid was dried under high vacuum and used without further purification. To a separate flask was added with **12** (92 mg, 0.15 mmol) and 3 mL of dry dichloromethane. Then Ghosez reagent (31 μL, 0.23 mmol) was added into the flask. The resulting solution was stirred at room temperature for 2 hours. Then solvent was removed under high vacuum and the residue solid was dried under high vacuum for 3 hours. Then the solid was dissolved into 3 mL of dry chloroform and transferred into the flask containing the amine and DIEA (80 μL, 0.46 mmol). The resulting mixture was stirred at room temperature under N_2 for overnight. Then the solvent was removed and minimum amount of dichloromethane was added to dissolve the residue slurry and methanol was added slowly to form a precipitate. The precipitate was filtrated and washed with methanol and then dried under vacuum. Yield a yellow solid 150 mg (87% over two steps). ^{1}H NMR (300 MHz, $CDCl_3$) δ: 12.08 (s, 1 H), 11.96 (s, 1 H), 11.89 (s, 1 H), 11.85 (s, 1 H), 8.84 – 8.66 (m, 6 H), 8.44 – 8.33 (m, 5 H), 8.29 (d, *J* = 7.6 Hz, 1 H), 8.25 (dd, *J* = 8.4, 1.1 Hz, 1 H), 8.13 (dd, *J* = 8.4, 1.3 Hz, 1 H), 8.09 (s, 1 H), 8.04 (d, *J* = 8.0 Hz, 2 H), 8.00 (d, *J* = 8.0 Hz, 1 H), 7.98 – 7.85 (m, 7 H), 7.84 – 7.74 (m, 3 H), 7.69 (s, 1 H), 7.66 (t, *J* = 8.0 Hz, 1 H), 7.52 (s, 1 H), 7.44 (s, 1 H), 7.42 – 7.34 (m, 2 H), 7.26 (t, J= 8.2 Hz, 1 H), 6.87 (s, 1 H), 4.51 – 4.40 (m, 2 H), 4.24 (dt, *J* = 12.2, 8.2 Hz, 2 H), 3.97 (d, *J* = 6.4 Hz, 2 H), 3.39 (s, 3 H), 2.66 – 2.48 (m, 2 H), 2.39 (dt, *J* = 13.1, 6.5 Hz, 1 H), 1.39 – 1.23 (m, 18 H), 1.12 (s, 9 H) ppm.

Compound **2b**: To a 25 mL flask was added with compound **2a** (150 mg, 0.09 mmol), NaOH (38 mg, 0.94 mmol). Then 2.7 mL of THF and 0.3 mL of MeOH was added into the flask. The resulting red solution was stirred at room temperature for 1.5 hours. Then 5% citric acid aqueous solution was added into the flask to adjust the pH to around 4 and yellow precipitate was formed. The precipitate was filtrated and washed with water. The solid was collected and dried under high vacuum. Then the solid was added into a dry flask and 3 mL of dry dichloromethane was added to dissolve the solid. Then Ghosez reagent (31 μL, 0.23 mmol) was added into the flask. The resulting solution was stirred at room temperature for overnight. Then solvent was removed under high vacuum and the residue solid was dried under high vacuum for 3 hours. Then the solid was dissolved into 3 mL of dry chloroform and transferred

into the flask containing the amine **13** (100 mg, 0.07 mmol) and DIEA (46 μL, 0.26 mmol). The resulting mixture was stirred at room temperature under N_2 for overnight. Then the solvent was removed and minimum amount of dichloromethane was added to dissolve the residue slurry and methanol was added slowly to form a precipitate. The precipitate was then dissolved in chloroform and purified with GPC and followed by silica gel column chromatography to obtain small amount (25 mg, 7% over two steps) of pure **2b** as yellow solid. ^{1}H NMR (300 MHz, $CDCl_3$) δ: 11.37 (s, 1 H), 11.32 (s, 1 H), 11.28 (s, 1 H), 11.20 (s, 1 H), 11.01 (s, 1 H), 10.78 (s, 1 H), 10.65 (s, 2 H), 10.61 (s, 1 H), 8.86 (d, *J* = 8.5 Hz, 2 H), 8.55 (m, 4 H), 8.47 – 8.40 (m, 3 H), 8.27 (d, *J* = 8.8 Hz, 2 H), 8.24 (d, J = 7.6 Hz, 1 H), 8.20 – 8.13 (m, 5 H), 8.09 (t, *J* = 6.4 Hz, 2 H), 8.04 – 7.96 (m, 4 H), 7.94 – 7.82 (m, 4 H), 7.80 – 7.65 (m, 7 H), 7.64 – 7.40 (m, 9 H), 7.39 – 7.30 (m, 4 H), 7.14 (dt, *J* = 14.1, 7.3 Hz, 3 H), 6.98 (d, *J* = 1.7 Hz, 2 H), 6.94 (d, *J* = 7.9 Hz, 1 H), 6.89 (s, 1 H), 6.56 (s, 1 H), 6.51 (s, 1 H), 6.43 (s, 1 H), 6.34 (s, 1 H), 6.16 (s, 1 H), 4.23 – 3.73 (m, 15 H), 3.55 (d, *J* = 6.6 Hz, 2 H), 3.06 (s, 3 H), 2.61 – 2.20 (m, 8 H), 2.06 – 1.94 (m, 1 H), 1.43 – 1.06 (m, 30 H), 0.94 – 0.79 (m, 21H) ppm.

Compound **21**: The compound was prepared according to the general coupling procedure, yield: 300 mg, 75%. ^{1}H NMR (300 MHz, $CDCl_3$) δ: 12.42 (s, 1 H), 9.08 (s, 1 H), 8.98 (dd, J = 7.8, 1.3 Hz, 1 H), 8.85 (s, 1 H), 8.69 (d, J = 8.6 Hz, 2 H), 8.32 (d, J = 8.8 Hz, 2 H), 8.28 (dd, J = 8.8, 1.3 Hz, 2 H), 8.03 (dd, J = 8.6, 1.3 Hz, 1 H), 7.90 (dd, J = 8.8, 1.4 Hz, 1 H), 7.87 (d, J = 8.8 Hz, 1 H), 7.86 (t, J = 8.5 Hz, 1 H), 7.78 (dd, J = 8.6, 1.1 Hz, 1 H), 7.75 (dd, J = 8.3, 1.2 Hz, 1 H), 7.72 (t, J = 8.2 Hz, 1 H), 7.68 (s, 1 H), 4.11 (d, J = 6.4 Hz, 2 H), 4.06 (s, 3 H), 2.38-2.29 (m, 1 H), 1.50 (s, 9 H), 1.18 (d, J = 6.8 Hz, 6 H) ppm.

Compound **22**: To a flask added **21** (300 mg, 0.4 mmol) and NaOH (160 mg, 4 mmol), then 3.6 mL of THF and 0.4 mL of MeOH was added into the flask. The resulting mixture was stirred at room temperature for 2 hours. After completion of the reaction as followed by TLC, the pH was adjusted to 3 with citric acid (5%). The precipitate was filtrated and then precipitated in $CHCl_3$ and methanol to obtain an orange solid after filtration, yield: 180 mg, 62 %. ^{1}H NMR (300 MHz, $CDCl_3$) δ: 11.09 (s, 1 H), 8.82 (d, J = 7.3 Hz, 1 H), 8.46 (br, 1 H), 8.39 (s, 1 H), 8.34 (d, J = 7.8 Hz, 1 H), 8.29 (d, J = 7.8 Hz, 2 H), 8.12 (d, J = 8.2 Hz, 2 H),

8.05 (d, J = 8.2 Hz, 2 H), 7.79 (s, 1 H), 7.68 (t, J = 7.8 Hz, 1 H), 7.67 (t, J = 8.2 Hz, 1 H), 7.60-7.49 (m, 4 H), 4.18 (d, J = 6.8 Hz, 2 H), 2.42-2.31 (m, 1 H), 1.64 (s, 9 H), 1.21 (d, J = 6.4 Hz, 6 H) ppm.

Compound **23**: The compound was prepared according to the general coupling procedure, yield: 55 mg, 46%. ^{1}H NMR (300 MHz, $CDCl_3$) δ: 11.85 (s, 1 H), 11.76 (s, 1 H), 11.63 (s, 1 H), 11.60 (s, 1 H), 11.45 (s, 1 H), 8.84 (d, J = 8.1 Hz, 2 H), 8.76 (d, J = 8.5 Hz, 2 H), 8.70 (d, J = 7.8 Hz, 1 H), 8.42-8.34 (m, 5 H), 8.27 (d, J = 8.1 Hz, 1 H), 8.25 (d, J = 8.1 Hz, 1 H), 8.16 (dd, J = 8.4, 1.3 Hz, 1 H), 8.14 (s, 1 H), 8.12 (d, J = 8.2 Hz, 1 H), 8.08 (dd, J = 7.6, 1.1 Hz, 1 H), 8.04 (dd, J = 8.3, 1.0 Hz, 1 H), 8.02 (dd, J = 8.3, 1.3 Hz, 1 H), 7.98-7.78 (m, 15 H), 7.73 (t, J = 8.2 Hz, 2 H), 7.66 (t, J = 8.1 Hz, 2 H), 7.48 (s, 2 H), 7.46 (t, J = 7.8 Hz, 1 H), 7.46 (t, J = 8.2 Hz, 1 H), 7.43 (t, J = 8.2 Hz, 1 H), 7.39 (t, J = 8.2 Hz, 1 H), 7.36 (t, J = 7.9 Hz, 1 H), 6.79 (s, 1 H), 6.55 (s, 1 H), 6.51 (s, 1 H), 4.50-3.67 (m, 8 H), 3.27 (s, 3 H), 2.64-2.30 (m, 4 H), 1.38-1.01 (m, 24 H) ppm.

The corresponding amine of **23**: The compound was prepared according to the same procedure as compound **11**, the yield was considered to be quantitative and used for next step without any further purification. ^{1}H NMR (300 MHz, $CDCl_3$) δ: 11.87 (s, 1 H), 11.79 (s, 1 H), 11.69 (s, 1 H), 11.55 (s, 1 H), 11.47 (s, 1 H), 8.85 (d, J = 7.7 Hz, 2 H), 8.75 (d, J = 8.3 Hz, 2 H), 8.71 (d, J = 7.7 Hz, 1 H), 8.41 (d, J = 7.8 Hz, 2 H), 8.36 (d, J = 8.8 Hz, 2 H), 8.35 (d, J = 7.9 Hz, 1 H), 8.29 (d, J = 7.7 Hz, 1 H), 8.23 (d, J = 7.4 Hz, 1 H), 8.15 (d, J = 7.2 Hz, 2 H), 8.13 (s, 1 H), 8.09 (d, J = 8.5 Hz, 1 H), 8.08 (d, J = 8.5 Hz, 1 H), 8.00-7.70 (m, 14 H), 7.64 (t, J = 8.0 Hz, 1 H), 7.45 (t, J = 8.0 Hz, 3 H), 7.44 (s, 1 H), 7.20 (t, J = 8.0 Hz, 1 H), 6.82 (s, 1 H), 6.64 (s, 1 H), 6.55 (s, 1 H), 5.97 (d, J = 7.4 Hz, 1 H), 4.47 (m, 1 H), 4.27-4.15 (m, 2 H), 3.95-3.88 (m, 3 H), 3.77-3.67 (m, 2 H), 3.64 (br, 2 H), 3.29 (s, 3 H), 2.62-2.10 (m, 4 H), 1.38-1.24 (m, 18 H), 1.04 (dd, J = 6.6, 1.6 Hz, 6 H) ppm.

Compound **24**: The compound was prepared according to the general coupling procedures. The pure compound was obtained by GPC, yield 58 mg, 95%. ^{1}H NMR (300 MHz, $CDCl_3$) δ: 11.56 (s, 1 H), 11.43 (s, 1 H), 11.36 (s, 1 H), 11.31 (s, 1 H), 11.19 (s, 1 H),

11.01 (s, 1 H), 10.87 (s, 1 H), 8.77 (d, J = 8.2 Hz, 2 H), 8.59 (d, J = 8.6 Hz, 2 H), 8.55 (d, J = 7.8 Hz, 2 H), 8.41 (d, J = 8.6 Hz, 2 H), 8.39 (d, J = 7.2 Hz, 1 H), 8.35 (d, J = 8.6 Hz, 1 H), 8.34 (d, J = 7.8 Hz, 1 H), 8.27 (d, J = 8.9 Hz, 2 H), 8.20 (d, J = 8.5 Hz, 1 H), 8.17 (d, J = 7.8 Hz, 1 H), 8.15 (d, J = 8.6 Hz, 1 H), 8.12 (d, J = 7.8 Hz, 2 H), 8.08 (d, J = 7.8 Hz, 1 H), 7.97-7.93 (m, 6 H), 7.86-7.68 (m, 9 H), 7.64-7.30 (m, 17 H), 7.28 (s, 1 H), 7.05 (s, 1 H), 6.68 (s, 1 H), 6.66 (s, 1 H), 6.59 (s, 1 H), 6.40 (s, 1 H), 4.27-4.16 (m, 3 H), 4.11-3.97 (m, 3 H), 3.88 (d, J = 6.4 Hz, 2 H), 3.59 (d, J = 5.7 Hz, 2 H), 3.12 (s, 3 H), 2.61-2.31 (m, 5 H), 1.43-1.37 (m, 12 H), 1.28-1.21 (m, 12 H), 1.02 (s, 9 H), 0.90 (dd, J = 6.4, 2.5 Hz, 6 H) ppm.

The corresponding amine of **24**: The compound was prepared as the same procedure of compound **11**. The yield was considered to be quantitative and used for next step without any further purification. ^{1}H NMR (300 MHz, $CDCl_3$) δ: 11.58 (s, 1 H), 11.46 (s, 1 H), 11.37 (s, 1 H), 11.27 (s, 1 H), 11.16 (s, 1 H), 11.09 (s, 1 H), 10.96 (s, 1 H), 8.77 (d, J = 7.9 Hz, 2 H), 8.61 (d, J = 7.9 Hz, 2 H), 8.56 (dd, J = 7.9, 2.0 Hz, 2 H), 8.42 (d, J = 8.8 Hz, 2 H), 8.36-8.31 (m, 4 H), 8.27 (d, J = 7.8 Hz, 2 H), 8.20-8.14 (m, 4 H), 8.10 (d, J = 7.9 Hz, 1 H), 8.06 (d, J = 7.6 Hz, 1 H), 8.01-7.92 (m, 5 H), 7.90 (s, 1 H), 7.86 (d, J = 8.6 Hz, 1 H), 7.84 (d, J = 8.4 Hz, 1 H), 7.80 (s, 1 H), 7.75-7.46 (m, 16 H), 7.42 (s, 1 H), 7.41-7.29 (m, 5 H), 7.16 (t, J = 7.9 Hz, 1 H), 7.01 (s, 1 H), 6.69 (s, 1 H), 6.67 (s, 1 H), 6.61 (s, 1 H), 6.41 (s, 1 H), 5.89 (d, J = 7.5 Hz, 1 H), 4.26-4.17 (m, 3 H), 4.11-3.96 (m, 3 H), 3.89 (d, J = 6.1 Hz, 2 H), 3.60 (d, J = 6.3 Hz, 2 H), 3.51 (br, 2 H), 3.13 (s, 3 H), 2.63-2.29 (m, 5 H), 1.42-1.37 (m, 12 H), 1.28-1.21 (m, 12 H), 0.91 (d, J = 6.8 Hz, 6 H) ppm.

Compound **25**: The compound was prepared according to the general coupling procedures. The compound was purified with GPC. Yield 50 mg, 68%. ^{1}H NMR (300 MHz, $CDCl_3$) δ: 11.47 (s, 1 H), 11.42 (s, 1 H), 11.33 (s, 1 H), 11.28 (s, 1 H), 11.10 (s, 1 H), 10.85 (s, 1 H), 10.78 (s, 1 H), 10.76 (s, 1 H), 8.84 (d, J = 7.8 Hz, 2 H), 8.58 (d, J = 7.5 Hz, 2 H), 8.57 (d, J = 8.2 Hz, 2 H), 8.43 (d, J = 8.5 Hz, 2 H), 8.40 (dd, J = 7.1, 2.1 Hz, 2 H), 8.30 (d, J = 7.4 Hz, 1 H), 8.28 (d, J = 8.5 Hz, 2 H), 8.17-8.07 (m, 7 H), 8.01-7.85 (m, 10 H), 7.79 (s, 1 H), 7.76-7.31 (m, 23 H), 7.17 (d, J = 7.8 Hz, 1 H), 7.11 (t, J = 8.2 Hz, 1 H), 6.99 (t, J = 7.8 Hz, 1 H), 6.93 (s, 1 H), 6.64 (s, 1 H), 6.58 (s, 1 H), 6.47 (m, 1 H), 6.38 (s, 1 H), 6.04 (s, 1 H),

4.24-3.84 (m, 7 H), 3.79 (d, J =6.4 Hz, 2 H), 3.64 (t, J = 8.2 Hz, 1 H), 3.58 (d, J = 5.7 Hz, 2 H), 3.10 (s, 3 H), 2.62-2.22 (m, 6 H), 1.41 (d, J = 6.7 Hz, 6 H), 1.38 (d, J = 6.4 Hz, 3 H), 1.34 (d, J = 6.7 Hz, 3 H), 1.28-1.14 (m, 18 H), 0.96 (s, 9 H), 0.90 (dd, J = 6.7, 1.4 Hz, 6 H) ppm.

The corresponding amine of **25**: The compound was prepared according to the same procedure of compound **11**. The yield was considered to be quantitative and used for next step without any further purification. ^{1}H NMR (300 MHz, $CDCl_3$) δ: 11.49 (s, 1 H), 11.34 (s, 1 H), 11.30 (s, 2 H), 11.12 (s, 1 H), 10.92 (s, 1 H), 10.82 (s, 2 H), 8.85 (d, J = 8.7 Hz, 2 H), 8.58 (d, J = 8.7 Hz, 4 H), 8.42 (d, J = 8.7 Hz, 2 H), 8.39 (d, J = 8.2 Hz, 1 H), 8.37 (d, J = 8.2 Hz, 1 H), 8.29 (d, J = 9.4 Hz, 2 H), 8.29 (d, J = 7.7 Hz, 1 H), 8.14-8.08 (m, 7 H), 8.02-7.95 (m, 6 H), 7.92 (s, 1 H), 7.91-7.84 (m, 4 H), 7.80 (s, 1 H), 7.76-7.69 (m, 4 H), 7.67 (d, J = 8.3 Hz, 1 H), 7.61-7.28 (m, 21 H), 7.12 (t, J = 8.2 Hz, 1 H), 6.91 (s, 1 H), 6.84 (t, J = 7.7 Hz, 1 H), 6.65 (s, 1 H), 6.59 (s, 1 H), 6.47 (s, 1 H), 6.38 (s, 1 H), 6.17 (s, 1 H), 5.70 (d, J = 7.2 Hz, 1 H), 4.25-3.58 (m, 12 H), 3.17 (br, 2 H), 3.10 (s, 3 H), 2.61-2.22 (m, 6 H), 1.42-1.12 (m, 30 H), 0.90 (dd, J = 6.8, 1.4 Hz, 6 H) ppm.

Compound **26**: The compound was prepared according to the general coupling procedure. The compound was purified with GPC. Yield 35 mg, 66%. ^{1}H NMR (300 MHz, $CDCl_3$) δ: 11.32 (s, 1 H), 11.22 (s, 1 H), 11.14 (s, 1 H), 11.12 (s, 1 H), 10.90 (s, 1 H), 10.75 (s, 1 H), 10.66 (s, 1 H), 10.58 (s, 1 H), 10.53 (s, 1 H), 10.51 (s, 1 H), 8.65 (d, J =7.5 Hz, 2 H), 8.61 (d, J = 8.7 Hz, 2 H), 8.53 (d, J = 8.7 Hz, 2 H), 8.51-8.47 (m, 2 H), 8.38 (d, J = 7.1 Hz, 1 H), 8.32 (d, J = 8.5 Hz, 2 H), 8.27 (d, J = 8.5 Hz, 2 H), 8.22 (d, J = 7.5 Hz, 1 H), 8.19 (d, J = 7.9 Hz, 2 H), 8.18 (dd, J = 8.3, 1.3 Hz, 1 H), 8.14-8.10 (m, 4 H), 8.03 (d, J = 7.3 Hz, 2 H), 7.98 (d, J = 7.7 Hz, 1 H), 7.96 (d, J = 7.7 Hz, 1 H), 7.91 (d, J = 8.2 Hz, 1 H), 7.89 (s, 1 H), 7.86-7.29 (m, 39 H), 7.24 (s, 1 H), 7.22-7.16 (m, 3 H), 7.15 (s, 1 H), 7.06 (t, J = 8.1 Hz, 1 H), 6.98 (s, 1 H), 6.51 (s, 1 H), 6.49 (s, 1 H), 6.30 (s, 2 H), 6.12 (s, 1 H), 6.04 (s, 1 H), 4.20-3.75 (m, 14 H), 3.52 (d, J = 6.7 Hz, 2 H), 3.03 (s, 3 H), 2.59-2.17 (m, 10 H), 1.41-1.13 (m, 36 H), 0.93 (s, 9 H), 0.84 (d, J = 6.6 Hz, 3 H), 0.83 (d, J = 6.6 Hz, 3 H) ppm.

The corresponding amine of **26**: The compound was prepared as the same procedure of compound **11**. The yield was considered to be quantitative and used for the next step without any further purification. ^{1}H NMR (300 MHz, $CDCl_3$) δ: 11.32 (s, 1 H), 11.23 (s, 1 H), 11.16 (s, 1 H), 11.01 (s, 1 H), 10.91 (s, 1 H), 10.85 (s, 1 H), 10.69 (s, 1 H), 10.63 (s, 1 H), 10.59 (s, 1 H), 10.56 (s, 1 H), 8.65 (d, J = 7.4 Hz, 2 H), 8.63 (d, J =7.4 Hz, 2 H), 8.52 (d, J = 8.5 Hz, 2 H), 8.49 (d, J = 8.9 Hz, 2 H), 8.36 (d, J = 7.8 Hz, 1 H), 8.31 (d, J = 8.9 Hz, 2 H), 8.27 (d, J = 8.7 Hz, 2 H), 8.24-8.12 (m, 8 H), 8.01 (d, J = 8.1 Hz, 1 H), 8.04 (d, J = 7.4 Hz, 1 H), 7.98 (d, J = 8.1 Hz, 2 H), 7.92 (d, J = 8.1 Hz, 1 H), 7.89 (s, 1 H), 7.83 (d, J = 8.5 Hz, 4 H), 7.78-7.28 (m, 36 H), 7.22 (s, 2 H), 7.15 (s, 2 H), 7.15 (t, J = 8.3 Hz, 1 H), 7.07 (t, J = 7.8 Hz, 1 H), 7.03 (t, J = 7.8 Hz, 1 H), 6.93 (s, 1 H), 6.51 (s, 1 H), 6.49 (s, 1 H), 6.32 (s, 1 H), 6.30 (s, 1 H), 6.17 (s, 1 H), 6.14 (s, 1 H), 5.75 (d, J = 8.1 Hz, 1 H), 4.21-3.75 (m, 15 H), 3.63 (t, J = 7.4 Hz, 1 H), 3.52 (d, J = 6.1 Hz, 2 H), 3.27 (br, 2 H), 3.04 (s, 3 H), 2.57-2.32 (m, 7 H), 1.39-1.13 (m, 42 H), 0.84 (d, J = 6.5 Hz, 3 H), 0.83 (d, J = 6.8 Hz, 3 H) ppm.

Compound **27**: The compound was prepared according to the general coupling procedure. The compound was purified with GPC. Yield 30 mg, 66%. ^{1}H NMR (300 MHz, $CDCl_3$) δ: 11.23 (s, 1 H), 11.15 (s, 1 H), 11.00 (s, 2 H), 10.77 (s, 1 H), 10.50 (s, 2 H), 10.46 (s, 2 H), 10.35 (s, 2 H), 10.33 (s, 1 H), 8.56 – 8.47 (m, 4 H), 8.45 – 8.32 (m, 4 H), 8.32 – 7.95 (m, 12 H), 7.89 (q, J = 8.8, 8.1 Hz, 2 H), 7.82 – 7.68 (m, 7 H), 7.68 – 7.54 (m, 2 H), 7.54 – 7.39 (m, 9 H), 7.37 (d, J = 4.0 Hz, 1 H), 7.32 (dd, J = 9.0, 4.3 Hz, 4 H), 7.22 (d, J = 7.0 Hz, 4 H), 7.18 (s, 1 H), 7.15 (s, 1 H), 7.13 (s, 1H), 7.10 (s, 1 H), 7.08 (s, 1 H), 7.05 (s, 1 H), 7.04 (s, 1 H), 7.02 (s, 1 H), 6.99 (s, 1 H), 6.92 (s, 1 H), 6.47 (s, 1 H), 6.37 (s, 1 H), 6.26 (s, 1 H), 6.24 (s, 1 H), 6.13 (s, 1 H), 6.10 (s, 1 H), 5.98 (s, 1 H), 4.14 – 3.19 (m, 10 H), 2.98 (s, 3 H), 2.59 – 2.09 (m, 8 H), 1.39 – 1.08 (m, 72 H), 0.91 (s, 9 H), 0.79 (d, J = 6.7 Hz, 6 H) ppm.

Compound **2c**: The corresponding amine of **27** was obtained by treatment with TFA similar as procedure to make compound **11** and was used without any further purification. The compound was prepared according to the general coupling procedures by reacting with the corresponding amine of **27** with the corresponding acid chloride of **12**. The compound was purified with GPC. Yield 25 mg, 44%. ^{1}H NMR (300 MHz, $CDCl_3$) δ: 11.23 (s, 1 H), 11.52 (s,

1 H), 11.00 (s, 2 H), 10.77 (s, 1 H), 10.50 (s, 2 H), 10.46 (s, 2 H), 10.35 (s, 2 H), 10.33 (s, 1 H), 8.54-8.49 (m, 4 H), 8.42-7.97 (m, 28 H), 7.90 (q, J = 6.8 Hz, 4 H), 7.80-7.30 (m, 42 H), 7.24-6.99 (m, 15 H), 6.92 (s, 1 H), 6.47 (s, 1 H), 6.36 (s, 1 H), 6.26 (s, 1 H), 6.24 (s, 1 H), 6.13 (s, 1 H), 6.10 (s, 1 H), 5.98 (s, 1 H), 4.09-3.71 (m, 17 H), 3.48 (d, J = 6.0 Hz, 2 H), 2.98 (s, 3 H), 2.54-2.17 (m, 12 H), 1.34-1.10 (m, 104 H), 0.91 (s, 9 H), 0.80 (d, J = 6.6 Hz, 3 H), 0.78 (d, J = 6.6 Hz, 3 H) ppm.

References

(1) Dang, B.; Wu, H.; Mulligan, V. K.; Mravic, M.; Wu, Y.; Lemmin, T.; Ford, A.; Silva, D.-A.; Baker, D.; DeGrado, W. F. *Proceedings of the National Academy of Sciences* **2017**, *114*, 10852-10857.

(2) Gradišar, H.; Božič, S.; Doles, T.; Vengust, D.; Hafner-Bratkovič, I.; Mertelj, A.; Webb, B.; Šali, A.; Klavžar, S.; Jerala, R. *Nat. Chem. Biol.* **2013**, *9*, 362.

(3) Churchfield, L. A.; Alberstein, R. G.; Williamson, L. M.; Tezcan, F. A. *J. Am. Chem. Soc.* **2018**, *140*, 10043-10053.

(4) Doyle, L.; Hallinan, J.; Bolduc, J.; Parmeggiani, F.; Baker, D.; Stoddard, B. L.; Bradley, P. *Nature* **2015**, *528*, 585.

(5) Fletcher, J. M.; Harniman, R. L.; Barnes, F. R. H.; Boyle, A. L.; Collins, A.; Mantell, J.; Sharp, T. H.; Antognozzi, M.; Booth, P. J.; Linden, N.; Miles, M. J.; Sessions, R. B.; Verkade, P.; Woolfson, D. N. *Science* **2013**, *340*, 595-599.

(6) Lai, Y.-T.; Cascio, D.; Yeates, T. O. *Science* **2012**, *336*, 1129-1129.

(7) Lakshmanan, A.; Zhang, S.; Hauser, C. A. E. *Trends Biotechnol.* **2012**, *30*, 155-165.

(8) Bai, Y.; Luo, Q.; Liu, J. *Chem. Soc. Rev.* **2016**, *45*, 2756-2767.

(9) Fleishman, S. J.; Whitehead, T. A.; Ekiert, D. C.; Dreyfus, C.; Corn, J. E.; Strauch, E.-M.; Wilson, I. A.; Baker, D. *Science* **2011**, *332*, 816-821.

(10) Woolfson, D. N. In *Adv. Protein Chem.*; Academic Press: 2005; Vol. 70, p 79-112.

(11) Delsuc, N.; Massip, S.; Léger, J.-M.; Kauffmann, B.; Huc, I. *J. Am. Chem. Soc.* **2011**, *133*, 3165-3172.

(12) Tsiamantas, C.; de Hatten, X.; Douat, C.; Kauffmann, B.; Maurizot, V.; Ihara, H.; Takafuji, M.; Metzler-Nolte, N.; Huc, I. *Angew. Chem. Int. Ed.* **2016**, *55*, 6848-6852.

(13) De, S.; Chi, B.; Granier, T.; Qi, T.; Maurizot, V.; Huc, I. *Nat. Chem.* **2017**, *10*, 51.

(14) Rao, L.; Bierbach, U. *J. Am. Chem. Soc.* **2007**, *129*, 15764-15765.

(15) Baruah, H.; Day, C. S.; Wright, M. W.; Bierbach, U. *J. Am. Chem. Soc.* **2004**, *126*, 4492-4493.

(16) Baruah, H.; Wright, M. W.; Bierbach, U. *Biochemistry* **2005**, *44*, 6059-6070.

(17) Jiang, H.; Léger, J.-M.; Huc, I. *J. Am. Chem. Soc.* **2003**, *125*, 3448-3449.

(18) Smeyanov, A.; Schmidt, A. *Synth. Commun.* **2013**, *43*, 2809-2816.

V Helix-helix Assembly Directed by Palladium Coordination

5.1 Introduction

Metal coordination is a bonding event between a metal center and a ligand. The compound formed in this manner is known as metal coordination complex. The metal centers usually have empty electron orbitals which are able to accept electrons from the ligands. The structure of a metal complex is usually described by coordination number and the geometry. Coordination number is the number of atoms/ligands that coordinate to the metal center. The geometry of a metal complex is the spatial arrangement of the ligands which is determined mostly by the electron configuration of the metal center and affected by the nature of the ligands. Linear, trigonal planar, tetrahedral, square planar, trigonal bipyramidal, octahedral are examples of commonly founded geometries in metal complexes.

The metal coordination has been used as a powerful way to form various types of self-assembled structures.[1-4] The metal coordination directed assembly is achieved by proper design of ligands and choice of metal centers. The ligands have multiple coordination sites which are usually pre-organized in space. Ligands, such as pyridine, bipyridine, terpyridine, are covalently linked with spacer that arranges them at the right distances and angles.[5,6] In order to achieve the pre-organization of the ligand groups, rigid spacers are usually used. The choice of metal center is largely based on the requirement of geometry. For a given ligand, the geometry of the coordination is determined by the metal center which defines the angles between the ligands. Palladium (II), for instance, forms square planar coordination geometry with most ligands. Hence, palladium (II) can be used as turn by blocking two adjacent coordination sites or can be used as a vertex to connect four ligands. For example, the self-assembly of pyridine ligands P1 and P3 with *cis*-palladium can form a [3+2+6] molecular cage (fig. 5-1).[7] This cage was formed by using palladium as a vertex which connected the two pyridine ligand at an angle of 90^{o}.

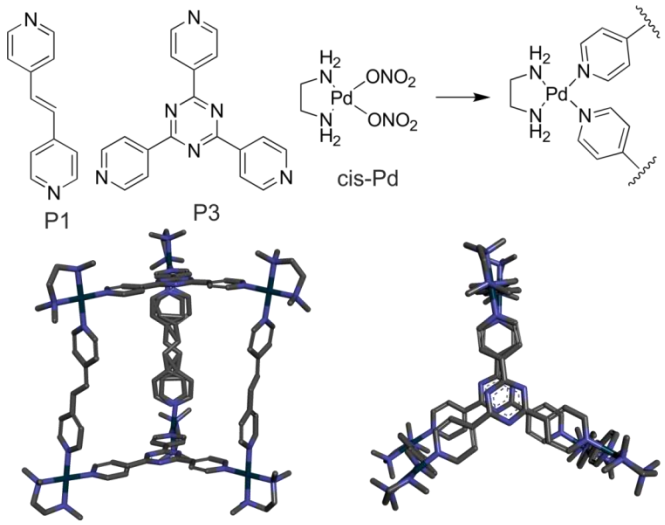

Figure 5-1: The self-assembly of pyridine ligands P1 and P3 with cis-palladium to afford [3+2+6] cage molecule.

Metal binding is a very important strategy to design protein/peptide assemblies also. The importance of metal binding can be seen from a lot of essential enzymes: metalloproteins.[8] The use of metal as a design element to guide the self-assembly of proteins/peptides has leaded to many novel architectures beyond the scope of natural proteins. Metal-three-helix bundles were made by taking advantage of the metal binding of three stranded helical coiled-coils.[9] By employing the strategy called "metal-templated interface redesign", F. Tezcan and coworkers have developed de novo designed metalloprotein assemblies.[10-14] This strategy allowed modular design to combine different proteins and structures to form more sophisticated architectures. Also, functions such as allosteric structure change were achieved using this method.[15,16] Metal binding was easy to be performed and also orthogonal to many intermolecular interactions. Also, metal coordination is dynamic and directional which facilitate the design.

Recently, Sawada and Fujita reported interlocking structures of metal coordination directed folding and assembly of peptides.[17] This study has elegantly demonstrated that metal coordination was able to guide the assembly of short peptide to form complicated structures. In our group, helical folded aromatic oligoamide foldamers have been well established. The formation of helix bundles and assemblies of the aromatic amide foldamers are interesting objects which mimic the α-helix bundles of proteins. Metal coordination is a useful method to direct the self-assembly of proteins/peptides as mentioned above. It would be interesting to

use metal coordination to guide the self-assembly of foldamers to form helix bundles or complex structures as found in metalloproteins and *de novo* designed proteins/peptides. Herein, we developed acridine and pyridine functionalized *oligo*-quinolinecarboxamides and successfully prepared helix-helix assembly driven by metal coordination.

In this chapter, the acridine functionalized oligoamides described in previous chapter are used as a ligand to form helix-helix assembly by coordinating with palladium in the first part. Since these oligomers are asymmetrical, parallel and antiparallel orientations are possible. In the second part, a new design of foldamers which have a C2 symmetric axis at the center is discussed. Pyridine units are introduced as ligand group to enable coordination with palladium. With this new design, the possibility of parallel and antiparallel orientation is eliminated.

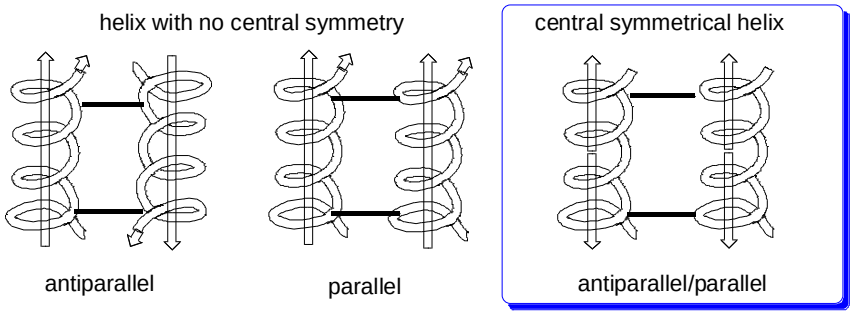

5.2 Compounds design

Oligo-quinoline carboxylic amides might be considered as nice spacers in which the positions and orientations of functional groups can be easily controlled and well predicted based on the 2.5 units per turn helical structures.[18] The side chains of foldamers can be functionalized with various different groups at convenience to fulfil the functions wanted. By carefully choosing the side chains to functionalize, the relative distances and angles between the functional groups are controlled. The properties and functions of the foldamers can be tuned by changing the functional groups of the side chains. The functional groups of the side chains as well as their sequences together define the properties of the foldamers controlled by the outer surfaces.

In order to achieve helix-helix assembly mediated by metal coordination, suitable

ligands are needed to be introduced on the surface of foldamers at proper positions. Acridine, which was introduced in previous chapter, was used in here as a ligand. Another choice of ligand is pyridine. Pyridine was extensively used as ligand to form complexes with various transition metals. In the last past few decades, many types of complexes, including macrocycles, cages and catenenes, have been prepared by using pyridine as ligand.[1,4,6,7,19]

For a given helix, the handedness of it can be P or M. When two asymmetric helices are assembled together, four possible stereoisomers are generated: PP/MM-parallel; PM-parallel; PP/MM-antiparallel and PM-antiparallel which results into complex mixtures of stereoisomers. In order to reduce this complexity, helices with C2 axis are designed. The symmetric compounds not only reduce the number of signals in ^{1}H NMR spectroscopy to half for the ligand itself but also eliminate the possibility to form parallel/antiparallel oriented helix-helix structures. The stereoisomers left possible are the PM and PP/MM isomers. Another consideration of the foldamers' design is the relative orientation of the ligand groups. In order to facilitate the formation of helix-helix assemblies, the spatial angle between the ligands has to be controlled in order to form closed macrocyclic systems and avoid polymerization. For example, angles of 0^{o}, 60^{o} or 120^{o} are preferred which are easier to form closed ring systems. Based on above considerations, we designed sequences as showed in figure 5-2. The pyridine ligand was linked to the quinoline monomer through acetylene similar to the acridine unit. Depending on the positions of pyridine, i.e. *para* or *meta* to the acetylene, that links to quinoline, two monomer, Q^{mp} and Q^{pp}, with pyridine side chain were prepared. Pyridine diamine (P^{n}), pyridine dicarboxylic acid (P^{c}) and phenantroline-2,9-dicarboxylic acid (Phe) were used as the central units to afford a C2 axis in the foldamers. The length of the oligomers was chosen based on the 2.5 units per turn structure of the quinoline carboxylic amide oligomers that after every five units the side chains are pointing to the same side of the helices. Energy minimized models were built for all sequences as presented in Figure 5-3. The sequences **L1** and **L2** share the same pyridine dicarboxylic acid central unit. The pyridine side chains are pointed at the same side of the helix where only very small off-set are observed (fig. 5-3 a and d). The sequences **L3** and **L4** use the pyridine diamine as central unit. Due to the wider curvature of the central pyridine diamine, the pyridine side chains, in this case, are diverging with spatial angle around 120^{o}

are observed (Fig. 5-3 b and e). The sequence **L5** use phenantroline-2,9-dicarboxylic acid as central unit which required one more units to allow the pyridine side chains to be at the same side of the oligomer (Fig. 5-3 c and f). Oligomers with acridine units introduced in previous chapter are also showed in figure 5-2. These oligomers are used here to form helix-helix assembly. S-camphanic amide was introduced at N-terminus of **1b** (S-**1b**) to obtain pure P-helix of **1b**. The use of camphanic acid at N-terminus to induce complete handedness induction of quinoline oligoamides has been reported previously.[20]

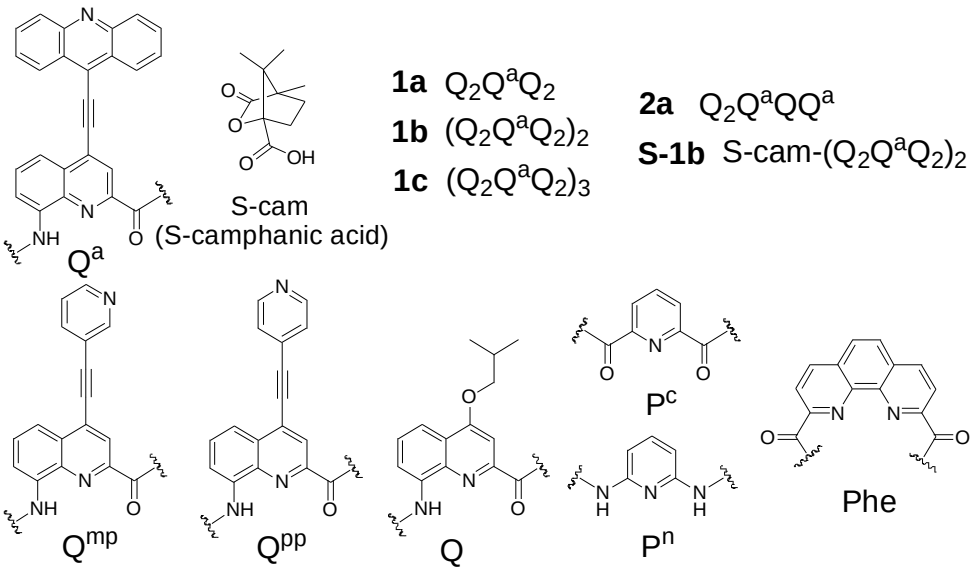

Figure 5-2: residues of monomers and sequences of foldamers.

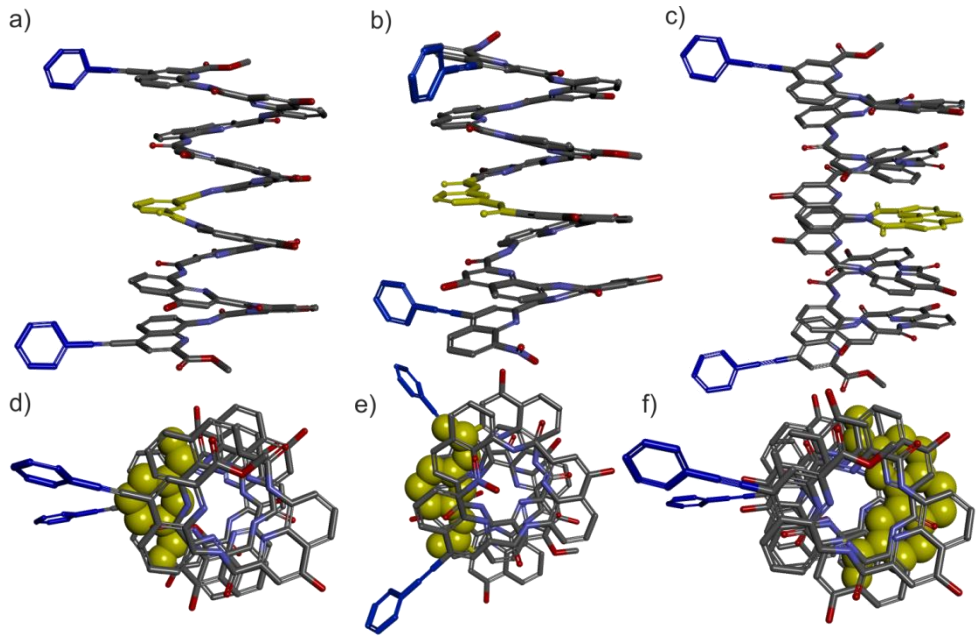

Figure 5-3: Energy minimized molecular models of the designed oligomers with pyridine group at the side chain as coordination site and pyridine-2,6-dicarboxylic acid (**L2**, a and d), pyridine-2,6-diamine (**L4**, b and e) and phenotroline-1-10-dicarboxylic acid (**L5**, c and f) as central units to generate C2 symmetry of the oligomers. The models were produced with Maestro software package, using MFFS force field, chloroform as solvent and PRCG as minimization method.

5.3 Results and discussions

5.3.1 Compounds synthesis

The monomers and oligomers were synthesized according to the schemes 5-1 to 5-7. The monomer with pyridine side chain was prepared using palladium catalyzed Sonogashira cross coupling reaction with good yield. The oligomers were prepared by stepwise coupling reaction of acid chloride and amine to afford the amide. For oligomers **L1** and **L2**, the Q^{pp} and Q^{mp} monomer were first treated with TFA to remove the boc-protecting group. Two times coupling of quinoline carboxylic amide dimer (Q_2) acid to this amine afforded intermediate oligomers Q_4Q^{mp}/Q_4Q^{pp} which were then coupled with pyridine diacidchloride to give the desired foldamers. For oligomers **L3** and **L4**, different strategies were applied. The pyridine diamine was first coupled two times with 2 equivalent of quinoline carboxylic amide dimer (Q_2) acid to give $Q_4P^nQ_4$. This intermediate oligomer was then coupled with Q^{mp} or Q^{pp} acid chloride to yield the desired oligomers. The oligomer **L5** was prepared according to similar

strategy as oligomer **L1** and **L2**. The difference is that for the preparation of oligomer **L5**, Q_5Q^{pp} was first prepared and then this intermediate was coupled with phenantroline-2.9-dicarboxylic acid chloride to obtain **L5**. All the targeted oligomers were characterized with NMR and HRMS to confirm the successful preparation of those oligomers.

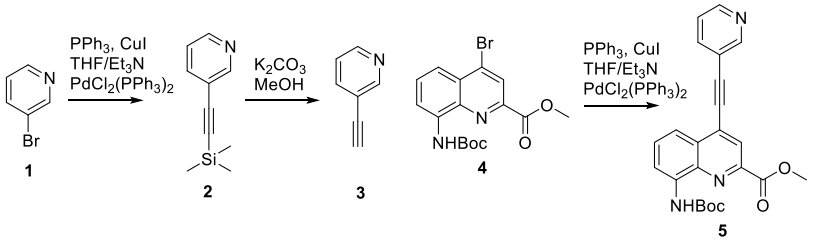

Scheme 5-1: Synthetic route for the monomer **5**.

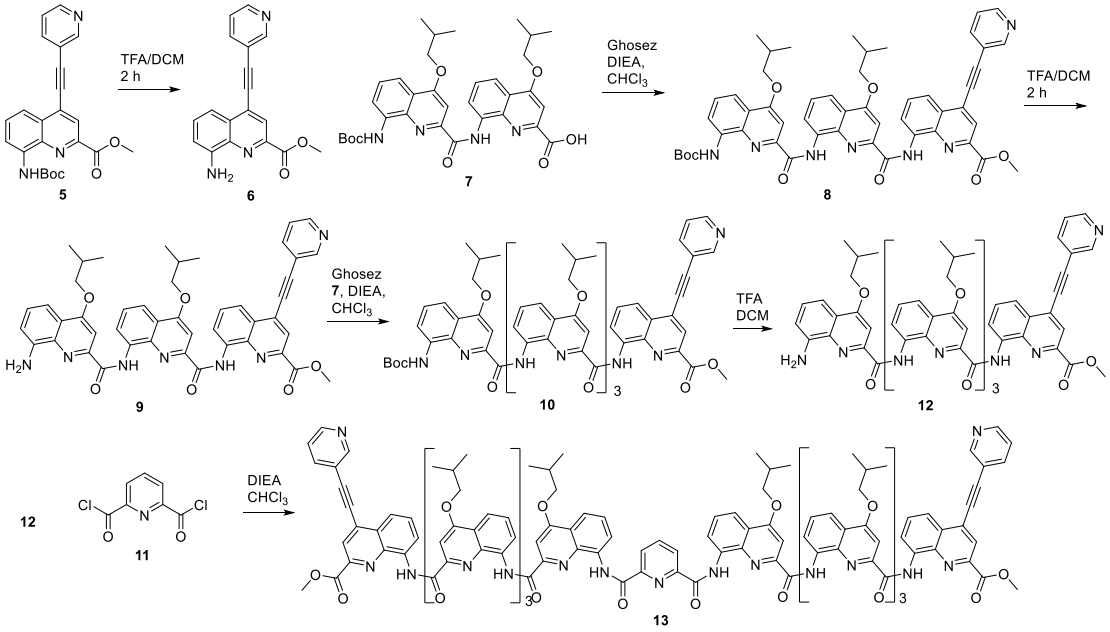

Scheme 5-2: Synthetic route for the oligomer **13** (**L1**).

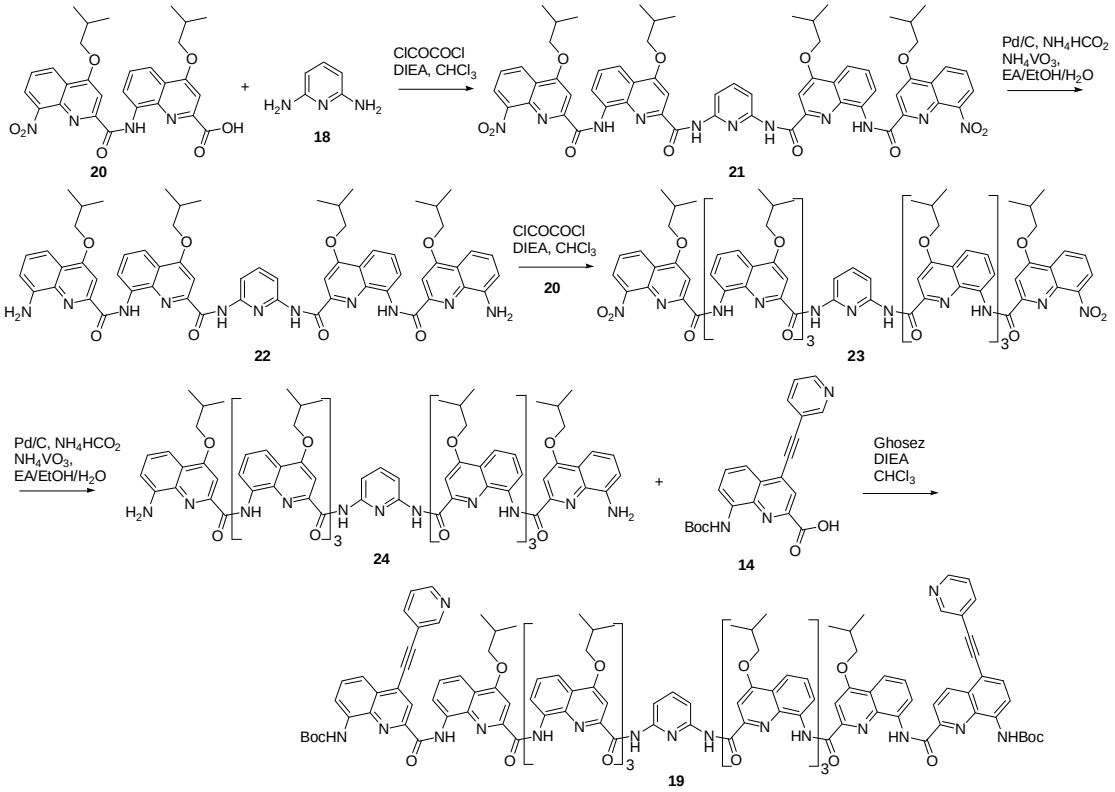

Scheme 5-3: Synthetic route for the oligomer **19** (**L3**).

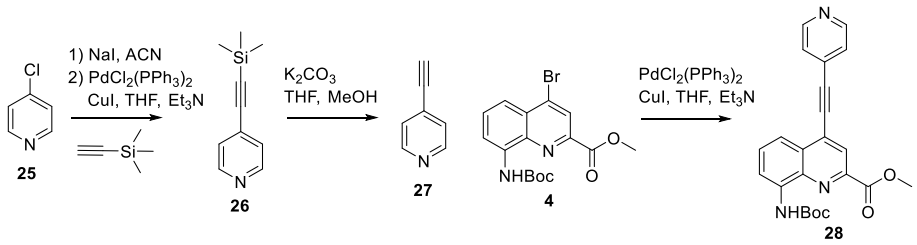

Scheme 5-4: Synthetic router for the monomer **28**.

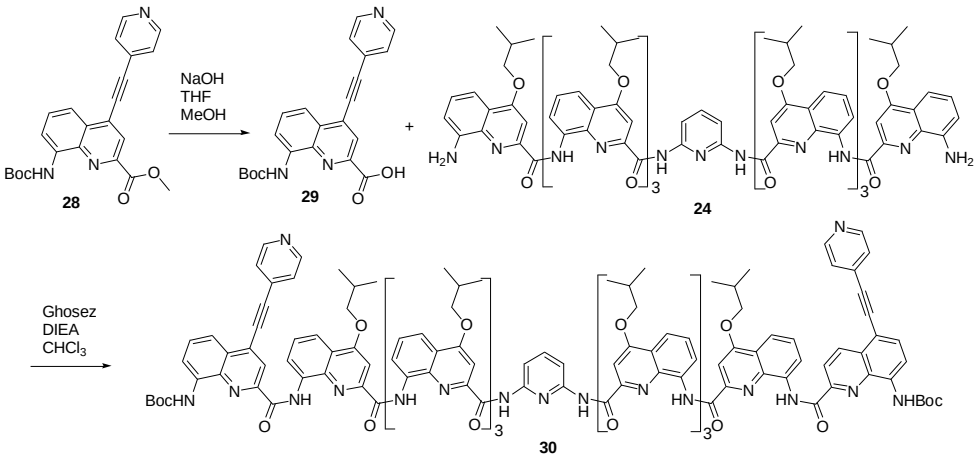

Scheme 5-5: Synthetic route for the oligomer **30** (**L4**).

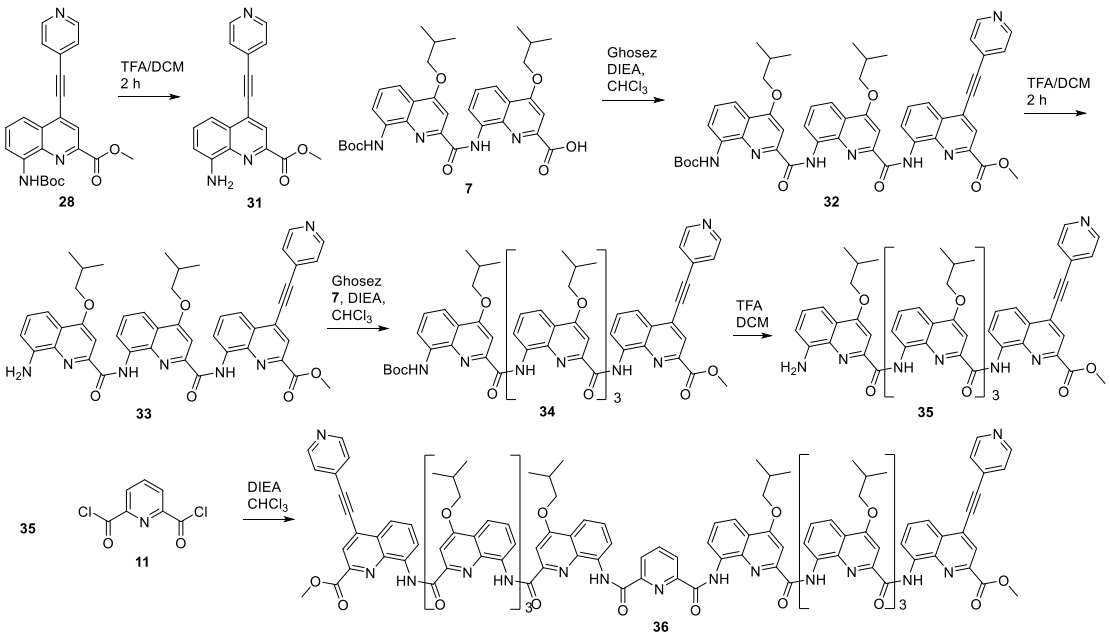

Scheme 5-6: Synthetic route for the compound **36 (L2)**.

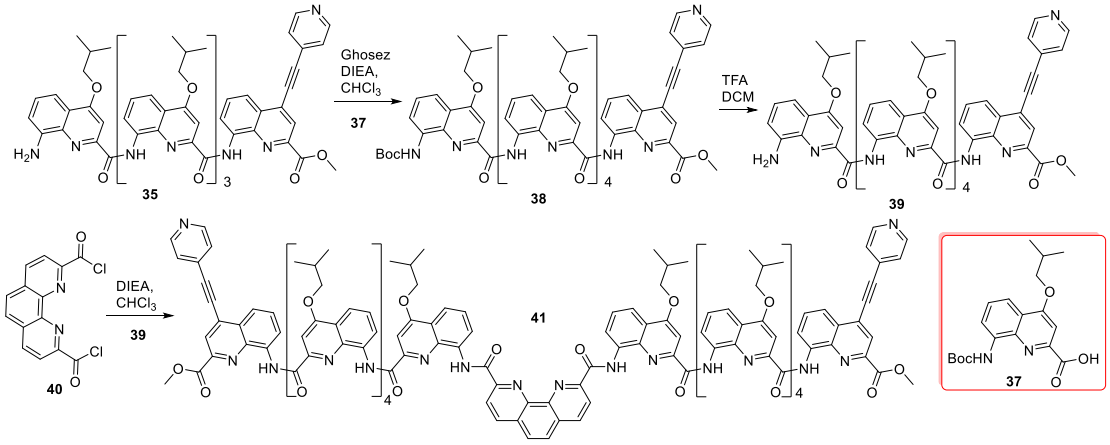

Scheme 5-7: Synthetic route for the compound **41** (**L5**).

5.3.2 Self-assembly of acridine functionalized oligomers with palladium

Acridine has been used as ligand to form complexes with various metal ions. Here, we tried to form helix-helix structure by taking advantage of the metal coordination with the acridine. We started by testing the formation of complex between the acridine and palladium (II). By heating the mixture of 2 equivalents of acridine and 1 equivalent of $PdCl_2(CH_3CN)_2$ at 50 ^oC for about 4 hours in chloroform, the ^1H NMR spectrum showed a clean new set of peaks which was different from the starting material (figure 5-4). The new set of peaks was

assigned to the 2-to-1 complex of $PdCl_2(Acr)_2$. In order to test our assumption that the new peaks are the 2-to-1 complex of the acridine and palladium, we mixed the acridine with palladium salt of different ratios. When more than 2 equivalents of acridine were added, the set of peaks corresponding to the product of complex and the excess of acridine were observed. When less than 2 equivalents of acridine was added, the NMR spectra showed two sets of news peaks which belonged to the 2-to-1 complex and 1-to-1 complex and the peaks corresponding to the acridine are not observed. This observation clearly indicated the formation of complex between acridine and palladium.

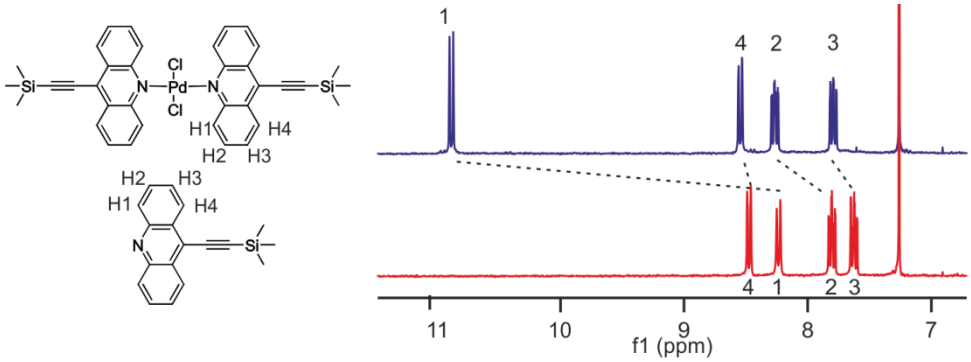

Figure 5-4: The ^{1}H NMR spectra (300 MHz, $CDCl_3$) of acridine (red) and the complex $PdCl_2(Acr)_2$ (blue).

The shifts of signals after formation of complex were made clear by full assignment of the acridine and the complex signals using 2D NMR spectra. As showed in figure 5-4, the signal of H^1 proton of the acridine unit shifted from 8.23 ppm to 10.89 ppm, a 2.67 ppm of chemical shifts variations which can be explained by the position of those protons are close to the coordination sites and thereby face the major surrounding environment differences. Other signals also displayed significant chemical shifts variations. The signals of protons 2, 3, and 4 shifted from 7.81, 7.63 and 8.47 ppm to 8.27, 7.80 and 8.55 ppm respectively.

After this preliminary study, we started to test metal coordination of the acridine functionalized oligomers. A solution of **1a** and $PdCl_2(CH_3CN)_2$ in $CDCl_3$ was heated at 60 ^oC for three days to form the expected 2-to-1 complex. The kinetics to form the complex was slower compared to the acridine itself which might be due to the size of the foldamer and steric hindrance. NMR analysis showed that after complexation, a new peak appeared at 11.11 ppm in the ^{1}H NMR spectrum which is a clear indication of the complex formation. The slow reaction kinetics allowed following the process with NMR spectroscopy. After 30 minutes of

mixing the oligomer with palladium salt (2 to 1 ratio), a clear distinct doublet appeared at 10.55 ppm which we attribute to the formation of the intermediate 1-to-1 complex. This distinct new peak was assigned to the acridine H^1 proton at the side chain based on previous assignment of the acridine complex with palladium alone. Upon further incubating the reaction mixture, the doublet at 11.11 ppm slowly glowed while the doublet at 10.55 ppm disappeared concomitantly. This change in the NMR spectra was consistent with a two steps formation of the complex. First step is the formation of 1-to-1 complex and the second is the formation of 2-to-1 complex. Upon formation of the 2-to-1 complex, the size of the molecule is doubled; nevertheless, the amide peaks in ^{1}H NMR spectrum were not shifted dramatically to upper field which indicated weak helix-to-helix interactions. Other peaks in ^{1}H NMR spectrum were mostly showing only small chemical shifts variations except for those protons from the acridine unit. The complex showed only one set of peaks probably due to the fast rotation around the coordinating bond and also fast handedness inversion at the NMR time scale. For each helix, the handedness can be either P or M. The P/M helices can exchange with each other through inversion of handedness. Upon connecting two helices together, PP/MM and PM diastereomers can be formed. The two diastereomers may display different NMR spectrum. Similar as the P/M handedness inversion, the PP/MM and PM diastereomers also exchange with each other. In the case here, the one set of signals observed maybe the average signal of PP/MM and PM due to their fast exchange. The HRMS showed the peaks of expected mass of the 2-to-1 complex (m/z 3123.06 was found) which has the isotope distribution match with the calculated one. The formation of 2-to-1 complex was also confirmed by DOSY NMR spectroscopy (fig. 5-6). As showed in the figure, the diffusion coefficient of the complex was bigger than **1a** which indicated that the complex has bigger size than **1a** alone.

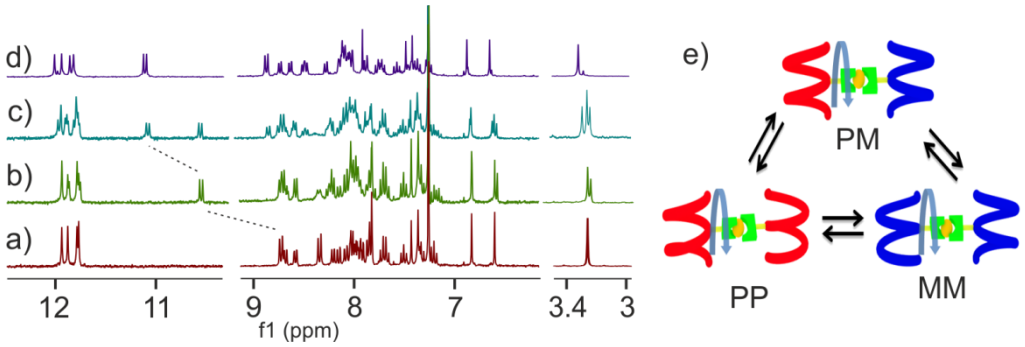

Figure 5-5: The changes of ^{1}H NMR spectra (300 MHz, $CDCl_3$) of **1a** after mixing with 1 equivalent of $PdCl_2(CH_3CN)_2$, a) **1a**; b) 0.5 hours c) 30 hours and d) 140 hours after mixing **1a** and $PdCl_2(CH_3CN)_2$; e) carton representation of PM and PP/MM exchange, red color represent P-helix, blue color represent M-helix.

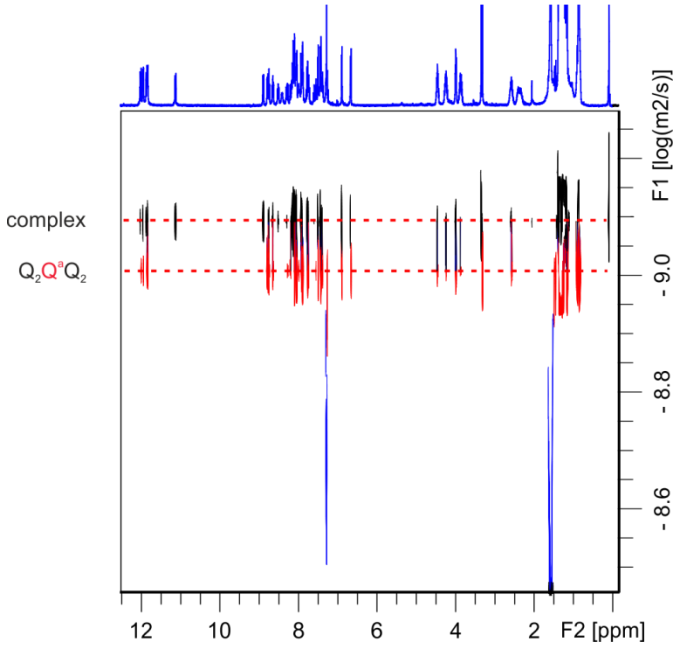

Figure 5-6: DOSY NMR spectra of **1a** and the complex between **1a** and Pd (II), the red peaks corresponding to **1a** and the black corresponding to the complex.

The crystal structure of the complex showed the expected 2-to-1 complex (fig. 5-7). Two molecules were observed in the unit cell. The two molecules displayed different orientation between the two helices connected through the palladium coordination. One has an angle of around 180^{o} between the axis of two helices and the other has an angle around 30^{o} (fig. 5-7b and 5-7c). The two different relative angles between the two helices in the same crystals were merely two snap shots of the numerous orientations between the two helices due to the fast rotation around the coordination bond. The handedness of the two helices in the crystals is P/M which might result from the preferential crystallization of the P/M over P/P and M/M.

The distance between the two helices was around 1.7 nm which was too far to allow any interactions between the two helices. The coordination geometry of the palladium metal was square planar as expected; however, the two acridine rings were not exactly parallel with each other. The triple bonds which connected the acridine and the helices substantially deviated from linearity which produced a wave shape of the link between helices. The reason behind this distortion might be the packing of crystal and illustrate the flexibility of the linker.

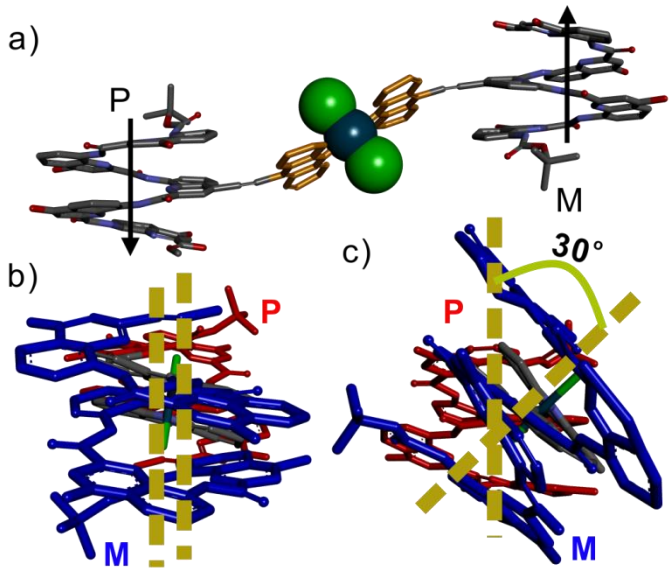

Figure 5-7: The crystal structure of Pd-**1a** complex, a) view from the side of the helix; b) and c) side view of two molecules found in the same unit cell, the line indicate the axis of the helix.

After the success of the formation of a complex with an oligomer with only one acridine side chain, oligomers with more acridine side chains were tested. The oligomer **1b** which bears two acridines on the same side of the helix was expected to form a macrocycle with two palladium atoms. The oligomer **1b** and palladium salt were mixed in a 1 to 1 ratio in chloroform. The complexation was slow also, after overnight reaction, still small amount of **1b** can be found. At this time, the NMR spectrum was complicated. The complicated NMR spectrum indicated many species formed at this time (fig. 5-9 showed possible species of incomplete complexation). After heating the solution for around 4 days, the peaks corresponding to **1b** disappeared and new sets of peaks appeared in the NMR spectra. The reaction was very slow which was not surprising given the fact that **1a** already showed slow kinetics to form the complexes with palladium. Four sets of new peaks correspond to the expected 2-to-2 complex were observed in the NMR spectrum after complete conversion.

This multiple sets of peaks can be rationalized as follows: the handedness of each of the helix can be P or M, and the orientation of the helix can be parallel or antiparallel. Due to the formation of macrocycle, the rotation of the helices around the coordination bonds were restricted which gives two steric isomers: parallel and antiparallel. The handedness inversion was slow in longer oligomers which also give two isomers: P and M helices. These two reasons caused the four isomers of the 2-to-2 complexes (fig. 5-9 the species of complete complexation). The multiple sets of signals of the macrocyclic complex made the analysis of the spectra complicated. However, the four peaks of the methyl group from the methylester of the terminus of the oligomer were clearly seen as equal ratio which indicated that there is no preference of any of the four isomers. Unlike in the case of **1a** that distinct new peak was observed, in the case of **1b**, the macrocyclic complex of **1b** and palladium showed complicated NMR spectrum due to the existence of isomers and also overlapping of some signals. The signal peaks of the complex from the H^1 proton of the acridine side chain was overlapping with amide protons of the oligomers. Despite the complicated NMR, the clear changes in the NMR spectra indicated the formation of expected complexes. DOSY NMR spectroscopy (fig. 5-10) further confirmed the size of the complex was bigger than **1b** since it had lower diffusion coefficient as showed in the figure 5-10. The high resolution mass spectroscopy showed the expected mass peak (m/z 2990.987, z = 2) corresponding to the 2-to-2 macrocyclic complex. The experimental isotope distribution also matched with calculated one. In order to test our hypothesis that P/M handedness of the helices was one of the reasons for the four sets of products observed, we prepared oligomer with 1s-camphanic amide functionalized at the N-terminus of the **1b** which was known to be completely P-helix (S-**1b**). The complex formed of S-**1b** with palladium was prepared similarly to the previously described procedure and showed only two sets of peaks by NMR. (fig. 5-11) The observation of only two sets of complexes formed from single handed helix proved that the assumption of P/M steroisomer was correct.

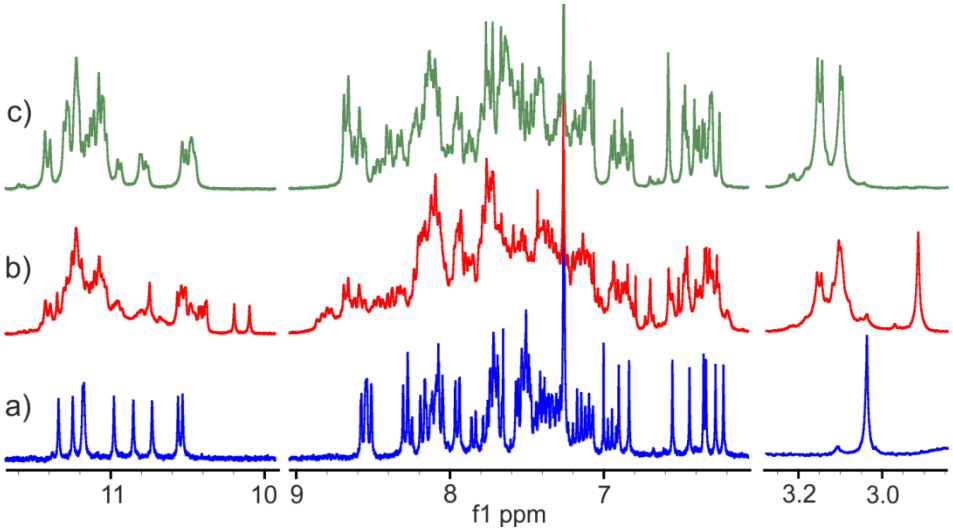

Figure 5-8: Parts of ^{1}H NMR spectra showing the amide, aromatic and methyl ester regions of a) **1b**; b) 18 hours after mixing **1b** with $PdCl_2(CH_3CN)_3$ and c) complete complexation of **1b** with palladium.

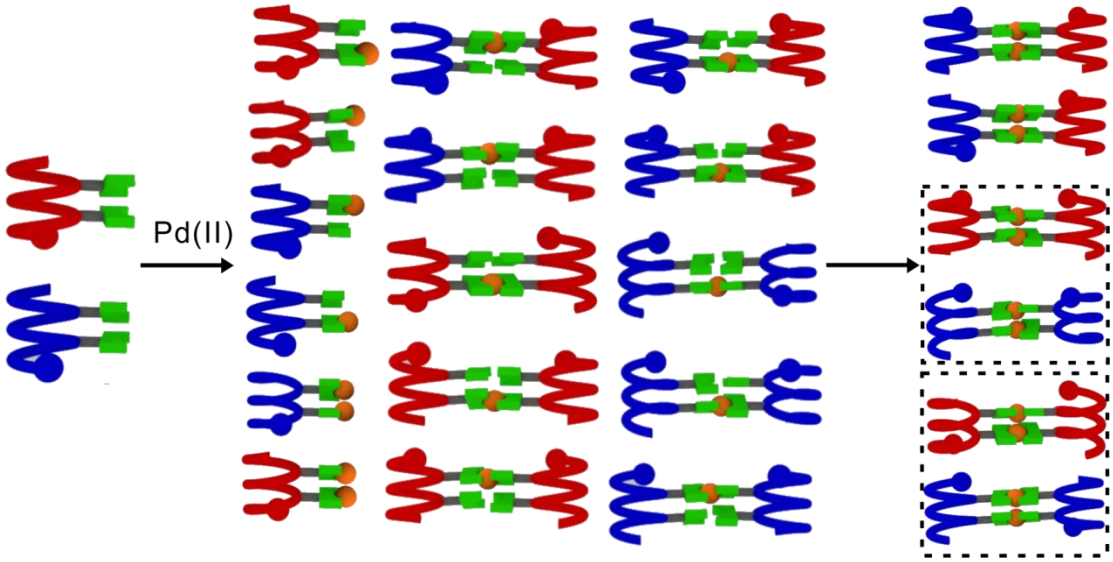

Figure 5-9: The possible complexes of incomplete complexation and the possible isomers of complete complexation of **1b** and $PdCl_2(CH_3CN)_2$, red color represent P-helix and blue color represent M-helix.

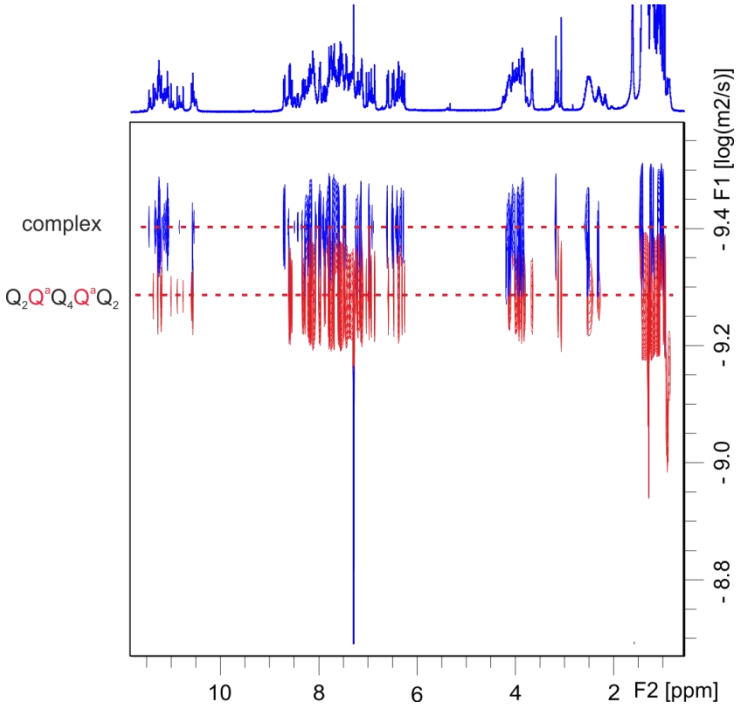

Figure 5-10: DOSY NMR spectra of **1b** and the complex between **1b** and Pd (II), the red peaks corresponding to **1a** and the blue corresponding to the complex.

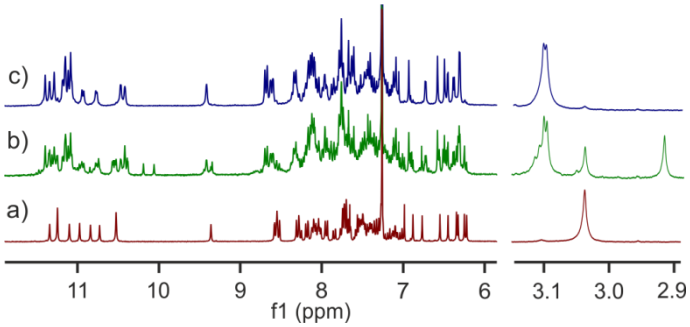

Figure 5-11: Parts of ^{1}H NMR spectra of S-**1b** and the complex Pd-S-**1b** showing the amide, aromatic and side chain regions, a) S-**1b**; b) intermediate state of the formation of complex of Pd-S-**1b**; c) the complex Pd-S-**1b**.

Single crystal of the macrocyclic complex Pd-**1b** was obtained by slow diffusion of acetonitrile into the stock solution in chloroform. The crystal structure is presented in figure 5-12. In the crystal, the stereoisomer of P/M helices with anti-parallel orientation was found. The two helices were connected with two palladium atoms to form a metal coordinated macrocycle as expected. The distance between the two helices was around 1.78 nm so that the two helices were well separated in space. This long distance is probably the cause for the lack of chiral communication between the two helices. The acridine ligands connected with palladium were not in the same plan with each other. The angles formed by the two planes of the acridines were 30^o and 35^o respectively. (fig. 5-12c) Small distortions of the acetylene

linkages were found in order to form the macrocyclic complexes. Compared to the crystal structure of **1b** alone, small differences in the structures of the helices and orientation of the acridines have been observed by overlaying the crystal structures of **1b** and the complex. The structural differences can be viewed as induced fit due to complexation. From the side view, the two palladium atoms were not aligning parallel with the helices. Instead, a small angle can be found between the two palladium atoms and the axis of helices (around 20^{o}, fig. 5-12e). This misalignment was probable caused by the small offset between the acridine side chains. The acridine planes have angle around 40^{o} with respect to the axis of the helix (fig. 5-12d). Within the macrocycle, not much space was left by the acridine ligands. From the side view, the acridine actually bent towards each other probably to allow more efficient stacking effects.

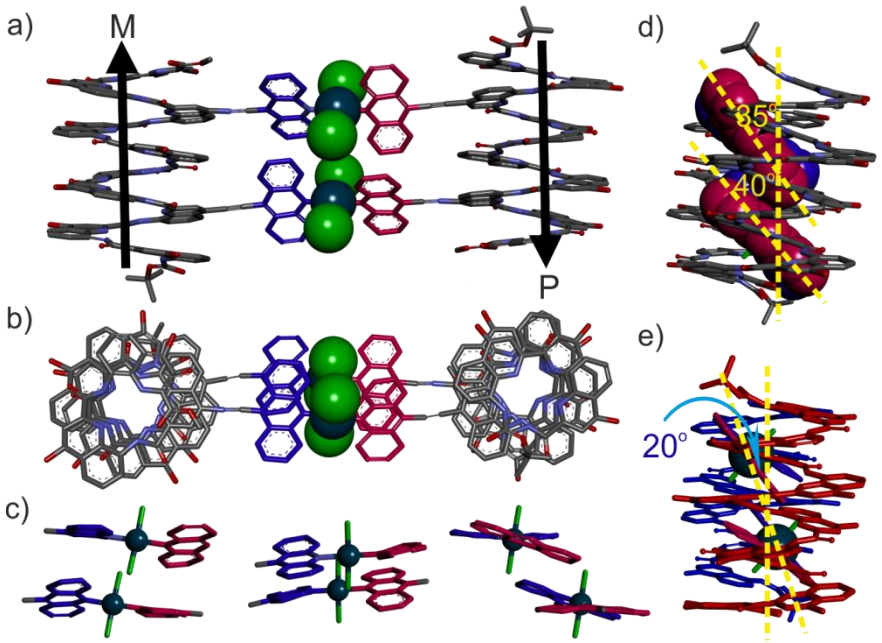

Figure 5-12: Crystal structure of Pd-**1b**, a) view from the top of helix; b) view from the side of the helix; c) and d) view form the side where two helices were overlapped.

The crystal packing of the complex was also interesting. As mentioned earlier, the quinoline oligomers formed a 2.5 units per turn helical structure where a C5 screw axis existed. Hence the shape of quinoline oligomers can be represented by a five star. However, pentagon itself is not possible to fill a plane without leaving gaps. The geometry of quinoline oligomers was reflected in the crystal packing that normally they packed loosely to leave as less amount of space as possible and no particular pattern presented. The packing of Pd-**1b**,

however, was different that they organized in a way to leave periodic solvent channels. As showed in the figure below, from the view of crystal a-axis, parallelogram shaped channels were found produced by the packing of the macrocycle. The solvent channels were also seen from the c-axis view. The unique packing pattern formed a supramolecular sponge that large pores left. The unique packing pattern was probably resulted from few factors. The metal coordination macrocycle enforced the two helices to be at anti-parallel orientation which created a C2 axis through the two helices. The acridine side chains also affected the packing. From the view, the acridine side chains and the helices were separated from each other. The packing of macrocycles was AB type that all the helices were aligned.

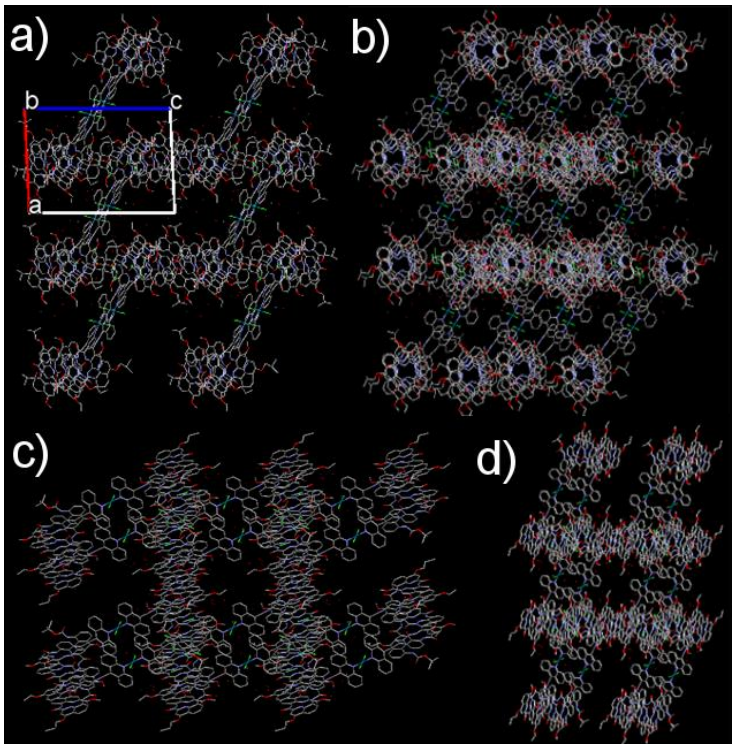

Figure 5-13: The crystal packing pattern of Pd-**1b** at different view.

The longer oligomer **1c** was also tested for the formation of complexes with palladium. As showed in figure 5-14, after complexation with palladium, the ^{1}H NMR spectrum became very broad and complicated. In the methyl ester region, four major new sets of peaks were observed similar with **1b** which indicated that four stereoisomers were formed. It was speculated that two helices were complexed with palladium to form a [2+3] complex with three ladders of acridines. The formation of [2+3] complex was also supported by mass spectrum where a peak at m/z 2210.7291 (z = 4) was found. This mass peak matched with

two helices complex with three palladium atoms.

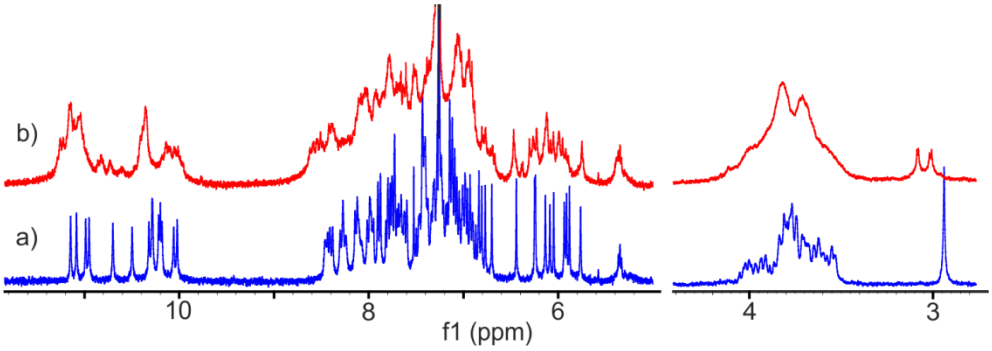

Figure 5-14: Parts of ^{1}H NMR spectra of **1c** and the complex Pd-**1c** showing the amide, aromatic and side chain regions, a) **1c**; b) the complex Pd-**1c**.

The sequence of **2a** (Q2QaQQa) was also used to make complex with palladium. As showed in the figure below, the formation of complex was slow. After mixing the foldamer with palladium salt, new peaks slowly appeared. After 50 minutes, new peaks appeared at 10.5 ppm and very tiny new peaks appeared at 11.1 ppm and at 3.3 ppm. The new peaks appeared at 10.5 ppm were attributed to 1-to-1 complex that formed faster and the peaks at 11.1 ppm were attributed to macrocycle. The peaks at 10.5 ppm slowly disappeared after longer incubation time and only the broad peaks at 11.1 ppm remain. After such time, no starting material was left. The changes of NMR spectra signals indicated formation of complexes. However, the final product formed was complicated due to multiple stereoisomers as showed by the broad signals. Mass spectrometry indicates that a 3-to-3 complex was favored. The isotope distribution matched with the calculation. The formation of larger macrocycle was possible because of the acridine side chains were on two different faces of the helices. The possibility to form larger macrocycle by introducing the acridine side chains at two different faces of the helices was very inspiring for the design of more complicated metal coordination directed assembly of helices. However, the complexity caused by the handedness and steric orientation rendered difficulty of analysis.

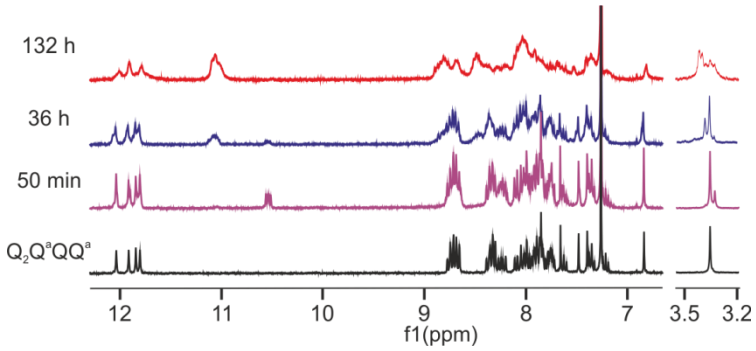

Figure 5-15: The changes of ^{1}H NMR spectra (300 MHz, $CDCl_3$) of **2a** after mixing with 1.5 equivalent of $PdCl_2(CH_3CN)_2$, the bottom was the spectrum of **2a**, and upper ones were after the time specified.

5.3.3 Self-assembly of pyridine functionalized oligomers with palladium

In order to perform preliminary studies, the intermediate oligomer **10** (Q_4Q^{mp}) which was half size of the symmetrical **L1** ($Q^{mp}Q_4P^cQ_4Q^{mp}$) was mixed with $PdCl_2(CH_3CN)_2$ in chloroform. The ^{1}H NMR spectrum after mixing with 0.5 equivalent of $PdCl_2(CH_3CN)_2$ changed immediately as seen in figure 5-16. The singlet at 9.05 ppm of compound **10** which was the signal of H^2 proton of the pyridine side chain shifted to lower field (9.15 ppm). Also, the peaks at 8.70 ppm became separated and shifted to lower field. Other significant changes in the aromatic regions can also be observed, however, it's difficult to follow all the chemical shifts variations due to signal overlapping. The methyl ester protons' signal (3.21 ppm) showed slight lower field shift. The amide region, however, almost remained unchanged. The overall changes in the ^{1}H NMR spectroscopy clearly indicated the complex formation. Only one set of signals corresponding to the complex was observed indicated fast exchange between different stereoisomers (i.e. PP/MM and PM similar as in the case of **1a**).

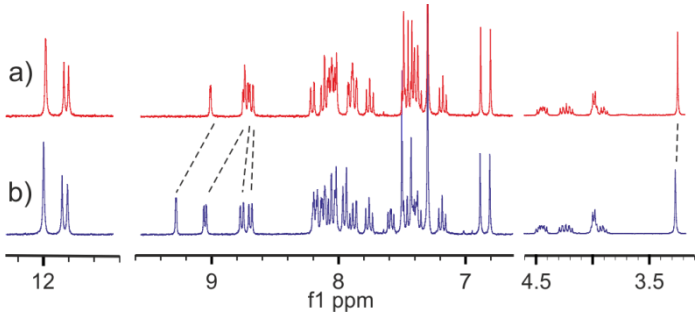

Figure 5-16: Parts of ^{1}H NMR spectra (300 MHz, $CDCl_3$), a) compound **10** and b) the complex

(**10**)$_2$-$PdCl_2$ showing the amide, aromatic and side chain regions.

The complexation of the symmetric foldamers with metal ions such as palladium was tested by mixing foldamers with palladium salt. The pyridine functionalized foldamers **L1**-**L5** were mixed with 1 equivalent of $PdCl_2(CH_3CN)_2$ in chloroform, the color of the solution turned from yellow to light orange after heated at 50 ^oC for around 30 minutes. The NMR spectroscopy of the solution after mixing with palladium was checked. As showed in figures 5-17 to 5-21, clear changes were observed in all cases. Substantial chemical shifts differences were observed between the complexes and the foldamers alone. However, due to the complexity of the proton resonances of the foldamers, it was difficult to track all the changes. Nevertheless, some of the signals were possible to follow. For example, the protons of the pyridine side chains are influenced by the palladium upon complexation and hence great chemical shifts variations were expected. Indeed, in the cases of **L1** and **L3**, the H^2 proton of the pyridine side chain shifted from to 8.85 ppm and 8.87 ppm to 9.17 ppm and 9.18 ppm respectively. In the cases of **L2** and **L4**, since the pyridine side chains were connected in para position, these protons appeared as two doublets at 8.72 ppm, 7.47 ppm and 8.69 ppm, 7.51 ppm. Two proton resonances at lower field of those protons shifted to 8.99 ppm and 9.00 ppm in the complexes. The other two resonances were difficult to follow due to overlap with aromatic signals. For foldamer **L1** and **L2**, the methyl ester resonances slightly shifted to upper field and appeared as two peaks in the complexes. The two peaks of the methyl ester resonances in the complexes clearly indicated two stereoisomers of the complexes formed which were attributed as PM and PP/MM similar as in the case of **1b**. This phenomenon was also observed in **L3**. In the case of **L4**, the proton NMR spectrum was broad which probably indicated less defined objects are formed. In the case of **L5**, two major stereoisomers are formed, but there were some other species formed as indicated by small signals in the NMR spectrum. The major signals were attributed to PP/MM and PM similar as **L2**. This observation clearly indicated slow helical inversion of the foldamers which was in agreement with the handedness inversion kinetic study performed previously.[21] The handedness inversion of the foldamers is slow due to the length of the oligomer that the rate of handedness inversion slowed down with increasing the length of the oligomers. The

formation of macrocycle upon complexation might further decrease the rate of handedness inversion. Other parts in the NMR spectra of the complexes can also observe similar split into two peaks upon complexation. For example, in the amide region, two sets of amide peaks were observed in all cases.

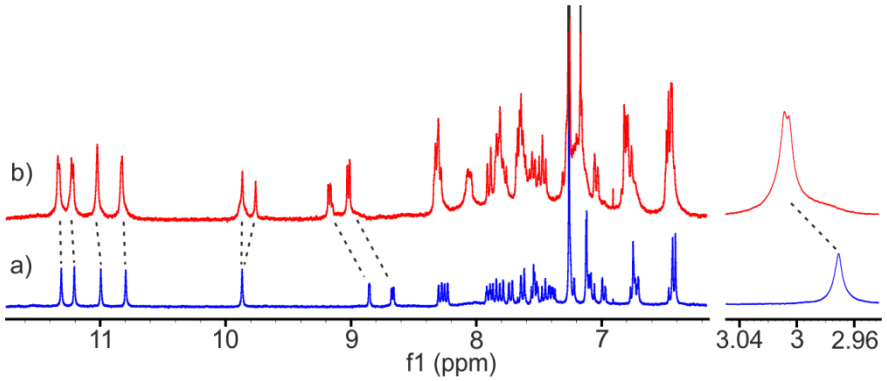

Figure 5-17: Parts of ^{1}H NMR spectra (300 MHz, $CDCl_3$) of **L1** and the complex **L1**-$PdCl_2$ showing the amide, aromatic and methyl ester regions; a) compound **L1** and b) the complex **L1**-$PdCl_2$.

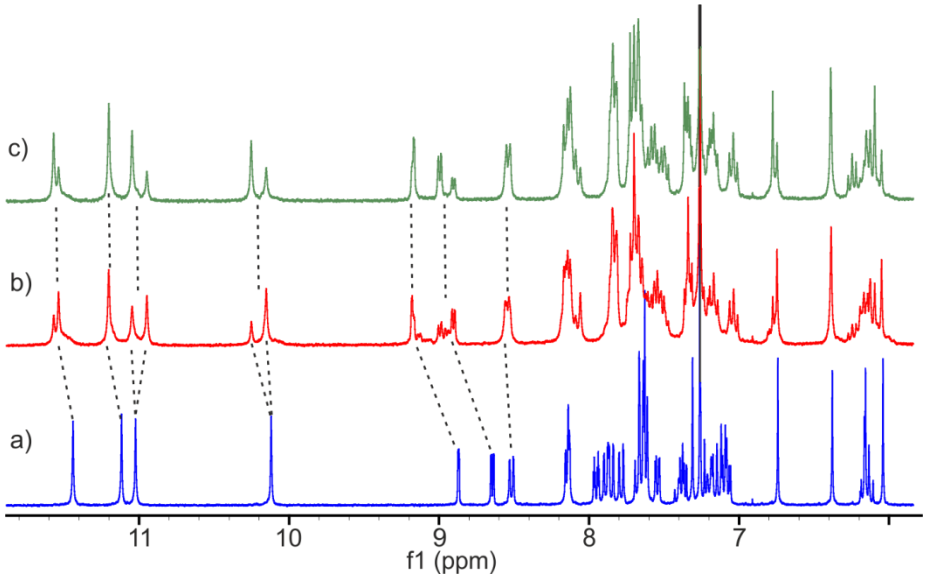

Figure 5-18: Parts of ^{1}H NMR spectra (300 MHz, $CDCl_3$) of **L3** and the complex **L3**-$PdCl_2$ showing the amide and aromatic regions; a) compound **L3** and b) the complex **L3**-$PdCl_2$ (4 hours after mixing **L3** and palladium) and c) the complex **L3**-$PdCl_2$ (1 month after mixing **L3** and palladium).

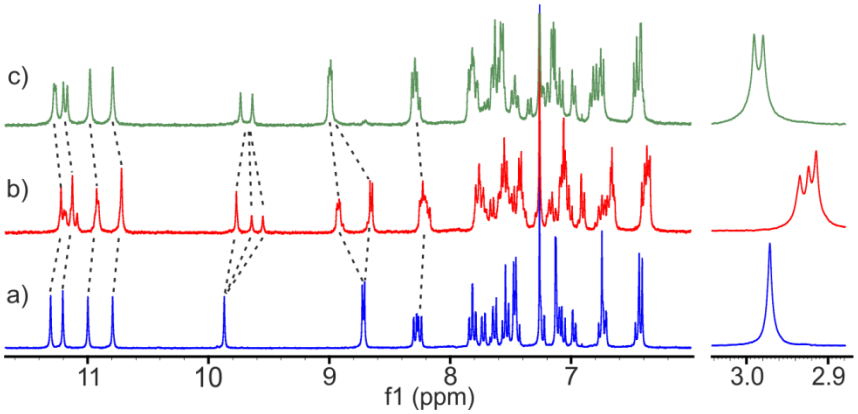

Figure 5-19: Parts of ^{1}H NMR spectra (300 MHz, $CDCl_3$) of **L2** and the complex **L2**-$PdCl_2$ showing the amide, aromatic and methyl ester regions; a) compound **L2** and b) the incomplete complexation **L2**-$PdCl_2$ and c) the complex **L2**-$PdCl_2$.

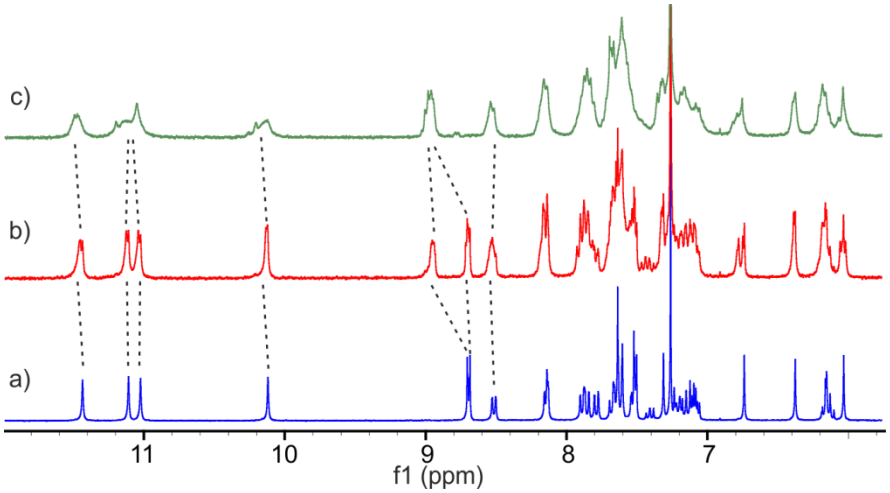

Figure 5-20: Parts of ^{1}H NMR spectra (300 MHz, $CDCl_3$) of **L4** and the complex **L4**-$PdCl_2$ showing the amide and aromatic regions; a) compound **L4** and b) the incomplete complexation **L4**-$PdCl_2$ and c) the complex **L4**-$PdCl_2$.

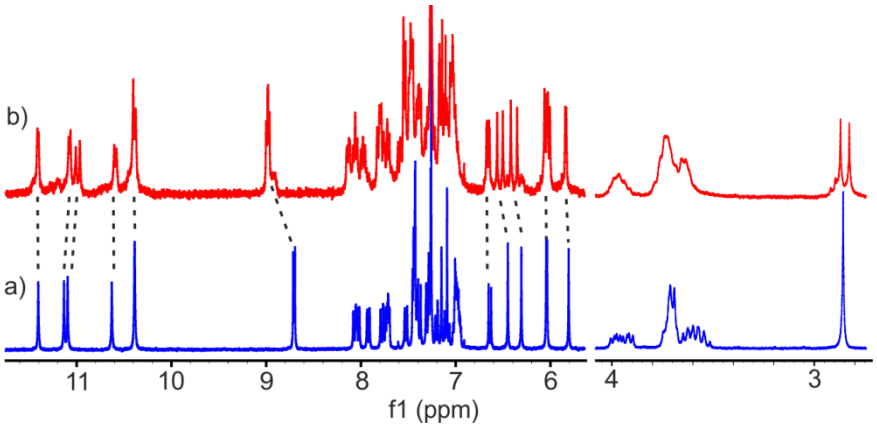

Figure 5-21： Parts of ^{1}H NMR spectra (300 MHz, $CDCl_3$) of **L5** and the complex **L5**-$PdCl_2$ showing the amide, aromatic and side chain regions; a) compound **L5** and b) the complex **L5**-$PdCl_2$.

The foldamers used here were racemic and hence the complexes formed should be optically non-active. Nevertheless, some chiral selections were observed in the complexes. As

calculated from the integrations of one amide resonance that clearly separated from others, the ratios of the PM and PP/MM isomers were not exactly 1 to 1 ratio. Diastereomeric excess of 20%, 5% and 43% were found for foldamers **L1, L2** and **L3** respectively. The origin of bias between PM and PP/MM was not very clear by now, but we suspected that steric hindrance is slightly different between PM and PP/MM isomers that causes the selectivity between PM and PP/MM.

The complexes should contain two foldamer molecules which result in doubling the size of the complexes compared with the foldamers alone. The increase in molecular size was supported by DOSY spectroscopy which measures the diffusion coefficient of a compound in solution. As showed in figure 5-22 to 5-24, in the DOSY spectra, two lines were observed in which the line with lower diffusion coefficient corresponding to the complex and the line with higher diffusion coefficient corresponding to the foldamer ligand alone. These observations clearly indicated that the complexes have larger size than the foldamer alone. All the complexes showed lower diffusion coefficient compared to the corresponding foldamer ligand as reference. The lower diffusion coefficients of all complexes clearly support the formation of complexes with at least of two foldamer ligands. In the case of **L4** and **L5**, the complexes formed were less defined and the DOSY spectra were not recorded.

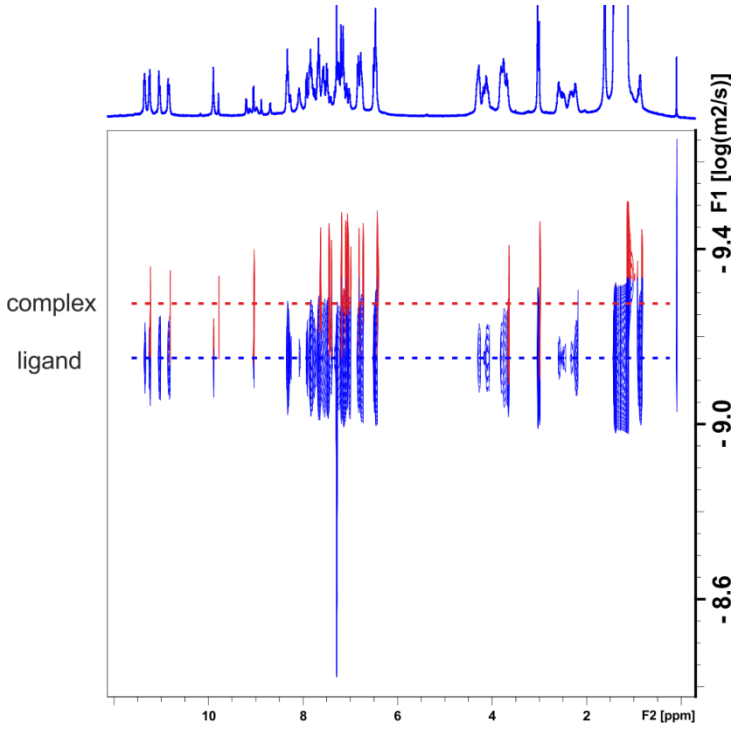

Figure 5-22: DOSY NMR spectra (400 MHz) of the **L1** and complex **L1**-$PdCl_2$ in chloroform at 298 K,

the blue line indicated **L1** and the red line indicated the complex.

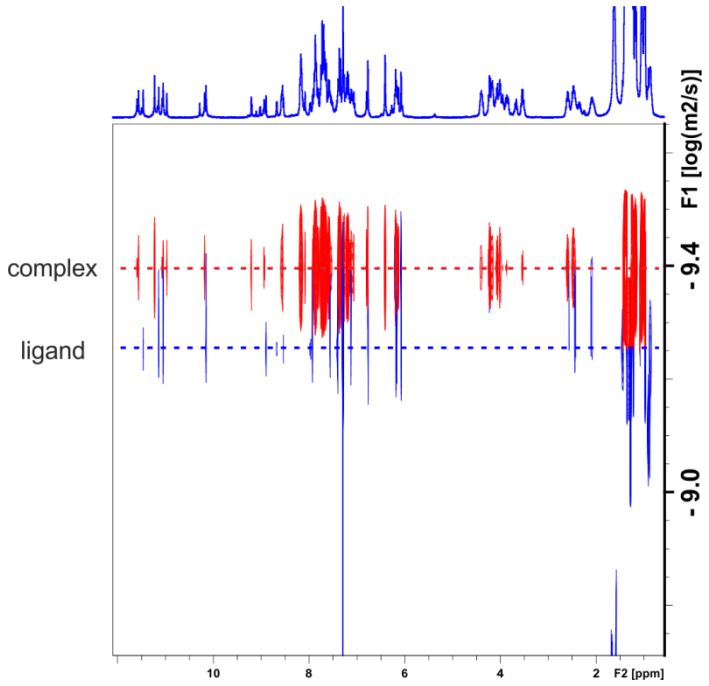

Figure 5-23: DOSY NMR spectra (400 MHz) of the **L3** and complex **L3**-$PdCl_2$ in chloroform at 298 K, the blue line indicated **L3** and the red line indicated the complex.

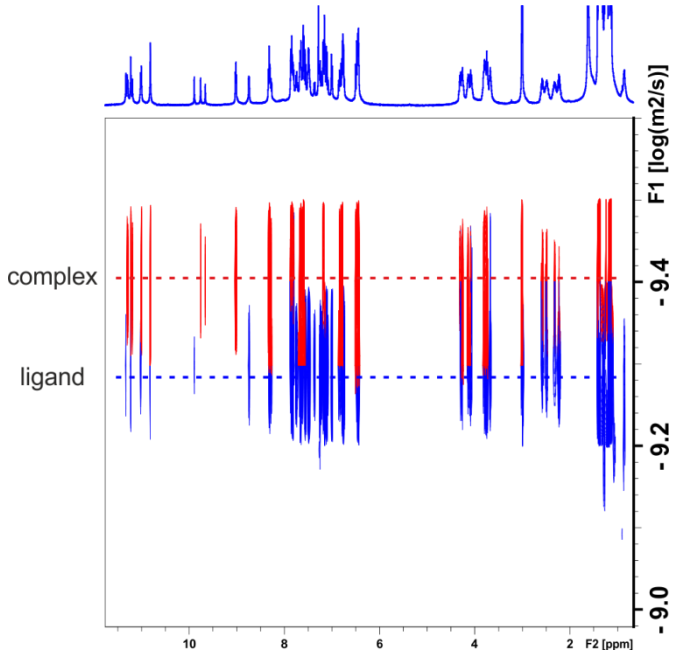

Figure 5-24: DOSY NMR spectra (400 MHz) of the **L2** and complex **L2**-$PdCl_2$ in chloroform at 298 K, the blue line indicated **L2** and the red line indicated the complex.

The formation of complexes was also confirmed by HRMS spectroscopy that the peaks corresponding to the complexes were observed. The calculated molecular weights were 5699.7754 for **L1**-$PdCl_2$ and **L2**-$PdCl_2$ and 5928.0068 for **L3**-$PdCl_2$ and **L4**-$PdCl_2$ respectively. The mass peaks observed at 1902.7 (3+), 1902.7 (3+) and 11979.7 (3+) for

L1-$PdCl_2$, **L2**-$PdCl_2$ and **L3**-$PdCl_2$ respectively. The observed mass peaks matched with the [2+2] complex. For the complex **L4**-$PdCl_2$, the expected molecular mass of [2+2] complex was not observed which might indicated that the [2+2] complex might not formed or not stable. This observation also matched with the broad peaks observed in the NMR spectroscopy. For the observed molecular mass, the isotope distributions of the observed mass peaks also matched with the calculated one which again confirmed the formation of expected [2+2] complexes.

While the formation of expected complexes of the foldamers and palladium as we designed was successful, the foldamer **L3** showed some behaviors that fall out of our design. As discussed above, foldamer **L3** formed the expected [2+2] complexes with palladium similar as other foldamers. However, when we repeated the complexation reaction at higher concentration (10 mM solution in chloroform), one set of additional broad signals was observed which was not seen at lower concentration (1 mM solution in chloroform). The ratio of the broad signals increased as increasing the reaction concentration. The appearance of new set of signals at higher concentration indicated other species were formed and they were preferred at higher concentration. Hence, higher order of aggregate was suspected to form at higher concentration.

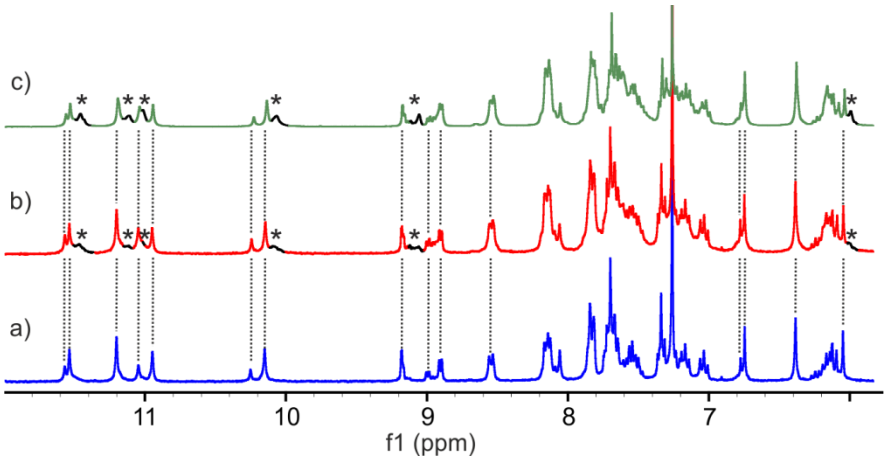

Figure 5-25: Part of ^{1}H NMR spectra (300 MHz) of **L3**-$PdCl_2$ at different concentration in $CDCl_3$ after reaction, a) 1 mM; b) 4 mM and c) 10 mM.

Luckily, single crystal of the complexes **L3**-$PdCl_2$ was obtained by slow diffusion of acetonitrile into the chloroform solution in about 2 to 3 days. The structure was showed in figure 5-26. As displayed in the figure, a 2-to-2 metal macrocycle complex was formed as

designed. The two helices stand almost parallel with each other as showed in the front view of the structure. Off-set between the two helices was observed which allowed better accommodation of all the side chains. The top view showed that the overall shape of the complex was pseudo hexagonal which was made possible by the meta-substituted pyridine ligand and also the angles between the two pyridine defined by the helix shape of the foldamers. The two helices were PM which was one of the stereoisomer expected. The other stereoisomer (PP/MM) was not observed in the crystal.

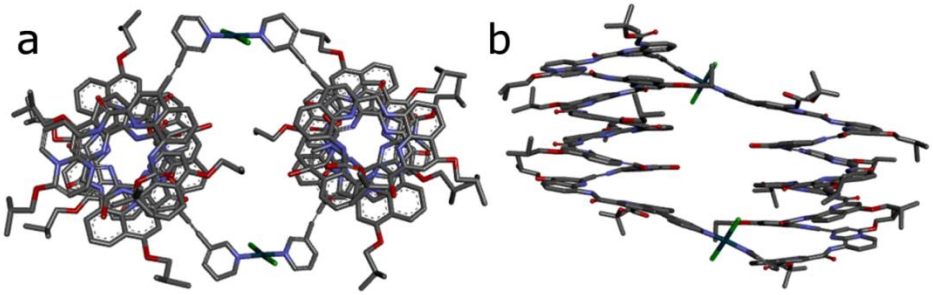

Figure 5-26: Crystal structure of **L3**-$PdCl_2$ showing the a) top view from the helices; b) front view from the helices, all the proton atoms were removed for clarity.

Since in the crystal of **L3**-$PdCl_2$ only contains PM isomer of 2-to-2 macrocyclic complex, the assignment of the different sets of signals in proton NMR spectra was possible. Immediately after dissolving the crystal of **L3**-$PdCl_2$ in chloroform, the recorded proton NMR spectrum was compared with the spectrum of complexation reaction. As displayed in figure 5-27b, the NMR spectrum of the crystal immediately after dissolving showed only one set of signals. By comparing with the spectrum of complexation reaction, the minor set of signals in the complexation reaction can be assigned as PM helices as found in the crystal structure. The major set of signals was then naturally assigned to PP/MM helices. This assignment was also supported by the DOSY spectrum which indicated that the two sets of signals corresponding to complexes have same diffusion coefficient, i.e. similar size of the compounds. The PP/MM stereoisomer was the major one formed after complexation and the ratio of PP/MM to PM was around 3 to 1 indicated by the integration in proton NMR spectrum.

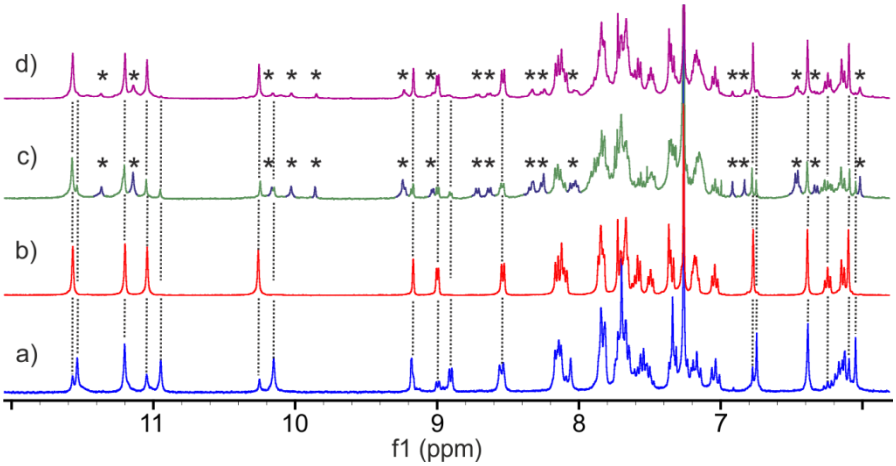

Figure 5-27: Part of ^{1}H NMR spectra (300 MHz, $CDCl_3$) showing the amide and aromatic regions of the complex **L3**-$PdCl_2$ a) the complexation reaction at 1 mM concentration; b) 5 minutes after dissolving the single crystals of the complex in chloroform; c) 5 minutes after dissolving the new types of crystals and d) the mother liquid of the mixtures that gave the new types of crystals, the spectra was recorded after removing solvent and redissolved in chloroform.

Under the same crystallization condition that gave the crystal of **L3**-$PdCl_2$ presented in figure 5-26, another form of crystals appeared after longer period (about one week after the set-up). This new form of crystal had more deep color than the previous one and the shape was completely different. To our disappointment, this crystal diffracted only at low resolution which made the solving structure impossible. Nevertheless, the ^{1}H NMR was able to be measured immediately after dissolving the crystals. As showed in figure 5-27c of the ^{1}H NMR spectra, this form of crystal showed new set of peaks that was not seen before in the reaction mixture. Three new peaks appeared at 10.15, 10.3, and 9.86 ppm which may correspond to amide protons. The three peaks might indicate that this new species may be composed by three non-equal foldamers or is a mixture. The new forms of crystals were obtained in different batch reactions and they always gave the three peaks with similar ratio which favored the assumption of single specie with three non-equal foldamers. By checking DOSY NMR, lower diffusion coefficient than the 2-to-2 macrocyclic complex of **L3**-$PdCl_2$ was found for this specie which indicated this specie has larger size than 2-to-2 complex of **L3**-$PdCl_2$. After incubating the solution in chloroform at 60 ^{o}C, the new specie slowly converted to the two 2-to-2 species. The kinetics for the conversion was slow and took around 13 hours to complete conversion as observed by NMR spectrum. The converting of the new specie to the 2-to-2 complex of **L3**-$PdCl_2$ clearly indicated that the new specie was merely

another form of complex of the foldamer **L3** and palladium.

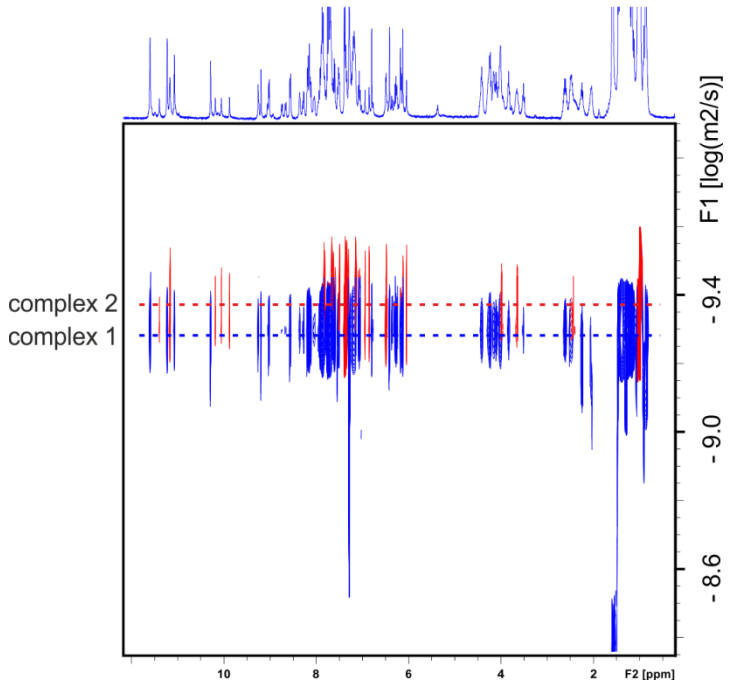

Figure 5-28: DOSY NMR spectra (400 MHz) of two types of complexes of **L3**-$PdCl_2$ in chloroform at 298 K, the blue line indicated the [2+2] complex found in crystal structure and the red line indicated the new type of complex.

In order to understand the equilibrium of the complexes formed by foldamer **L3** and palladium ion, three tubes of the complexes at same concentration (1 mM) were incubated in chloroform/acetonitrile mixing solvent. The ratios of the solvents were different between the three tubes. The volume percentages of acetonitrile of the solutions in the three tubes were 10%, 20% and 50% respectively. After overnight incubation which was presumably considered enough to reach equilibrium, the ratios of two species were different. The ratios of PM specie increased as the content of acetonitrile increased. Then the solvent were changed to pure chloroform and incubated for overnight, the ratios of the two 2-to-2 complexes in three tubes changed back to originally observed. If acetonitrile was added again, the ratio of PM specie was increased again. We noticed that at higher acetonitrile content, some precipitations were observed. The precipitate was found to be PM helices as indicated by ^1H NMR measured immediately after dissolving the solid in chloroform. These experiments justified that PM and PP/MM helices interconvert with each other and the equilibrium can be controlled by solvents where PP/MM was favored in chloroform while PM was favored by acetonitrile. The completely shifting of equilibrium to PM in acetonitrile was probably driven

by lower solubility of PM helices in acetonitrile. At higher concentration or after long time of crystallization conditions, species of larger sized complexes were formed as discussed above which added another equilibrium species into the system. The overall equilibrium can be represented as in figure 5-30. The two stereoisomers of 2-to-2 complexes undergo equilibrium. The equilibrium state was able to be controlled by solvents. The 2-to-2 complexes were also equilibrating with higher order aggregates. Since each helix is either P or M, much more complicated stereoisomers are possible in higher order of aggregates than the 2-to-2 complexes.

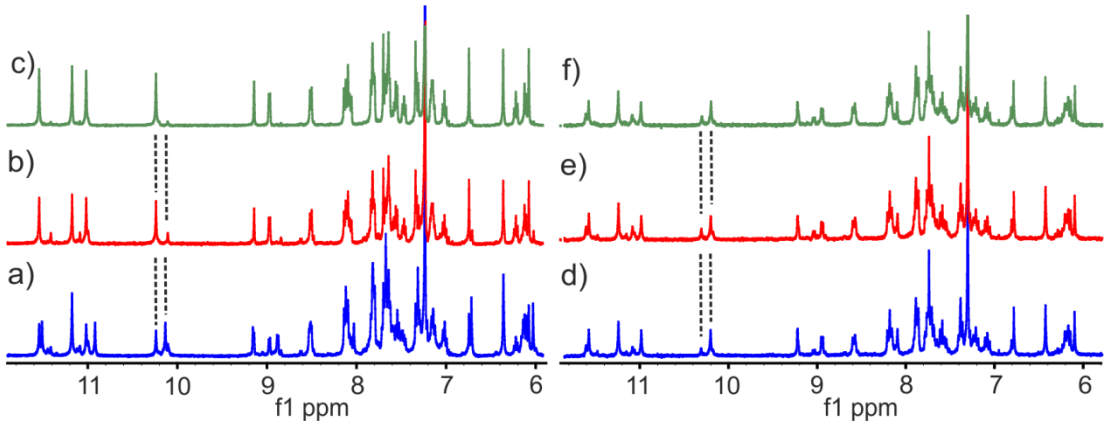

Figure 5-29： Parts of ^{1}H NMR spectra of 1 mM solution of **L3** and $PdCl_2(CH_3CN)_2$ (1 to 1 molar ratio) after incubation in a) $CDCl_3/CD_3CN$ (9/1 v/v) for 17 hours; b) $CDCl_3/CD_3CN$ (7/3 v/v) for 17 hours; c) $CDCl_3/CD_3CN$ (5/5 v/v) for 17 hours and d) $CDCl_3/CD_3CN$ (9/1 v/v) for 17 hours and then remove all solvents and incubated in $CDCl_3$ for 1 day; e) $CDCl_3/CD_3CN$ (7/3 v/v) for 17 hours and then remove all solvents and incubated in $CDCl_3$ for 2 days; f) $CDCl_3/CD_3CN$ (5/5 v/v) for 17 hours and then remove all solvents and incubated in $CDCl_3$ for 3 days.

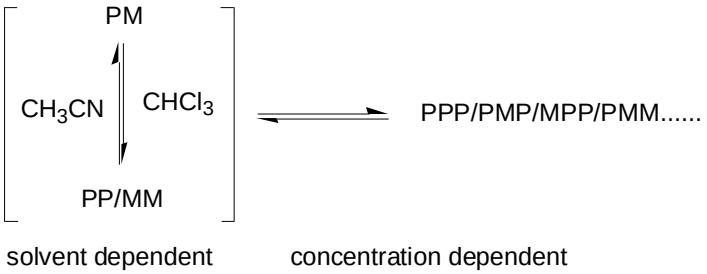

Figure 5-30: Equilibrium between PM, PP/MM and higher order complexes, the equilibrium between the PM and PP/MM was solvent dependent and the equilibrium the PM/PP/MM and higher order complexes were concentration dependent.

One of the stereoisomers of the complexes from foldamers **L1**, **L2** and **L3** could be obtained in a pure form after slow precipitation or crystallization with acetonitrile. The pure stereoisomers were incubated in chloroform to follow the kinetics of equilibrium. At room

temperature, the kinetics was found to be very slow that no obvious changes were observed in the NMR spectra after few hours' incubation. The kinetics for the sequence **L1** and **L3** was found to be faster at higher temperature (60 ^{o}C). After about 15 hours' incubating of the **L1**-$PdCl_2$, the ratio stopped changing as observed by NMR spectroscopy which indicated the ratio is at the equilibrium. For oligomer **L3**, it took around 24 hours to reach equilibrium state at 60 ^{o}C. However, for oligomer **L2**, the kinetics was even slow at higher temperature (60 ^{o}C) and it took few weeks of heating to reach the equilibrium. The kinetic profiles were plotted in figure 5-31. The PP/MM and PM interconverting reaction was a first order reaction. Based on this model, we were able to extract the kinetics constant of PM and PP/MM isomerization for all three compounds. For the complexes formed form oligomers **L1**, **L2** and **L3** with palladium, the kinetics constants were found to be 0.12 h^{-1}, 0.01 h^{-1} and 0.13 h^{-1} respectively. For complex **L2**-$PdCl_2$, the kinetic constant was one order magnitude smaller than the other two.

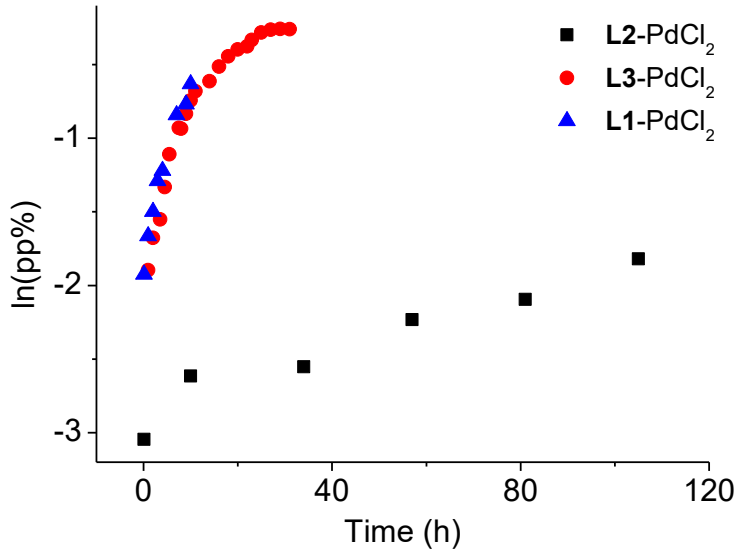

Figure 5-31: Kinetics for the equilibrium of PM and PP/MM helices of **L1**/**L2**/**L3**-$PdCl_2$ starting from pure single stereoisomers incubated in chloroform at 60 ^{o}C.

The obvious differences of the kinetics probable can be explained by the mechanism of P/M equilibrium in the systems. As showed in figure 5-32 of the proposed mechanism of P/M equilibrium, three mechanisms were considered. One possible mechanism does not require any dissociation of the coordinating bond and one helix undergo handedness inversion while

keeping the metal macrocycle intact (path 3). The other two mechanisms require either partial (path 1) or complete (path 2) dissociation of the coordination bonds first, and then helical handedness inversion and re-association of the coordination are proceeded to complete the P/M interconverting. The differences in the kinetic constants probably rule out path 3 mechanism where no dissociation happened. This is based on the observation previously of the dependence of helical handedness inversion rate on the length of oligomers.[21] In the cases considered here, all the oligomers here are the same length hence similar handedness inversion kinetics were expected based on the first mechanism. The other two mechanisms which involve breaking and reforming of coordinating bond were difficult to differentiate based on current data.

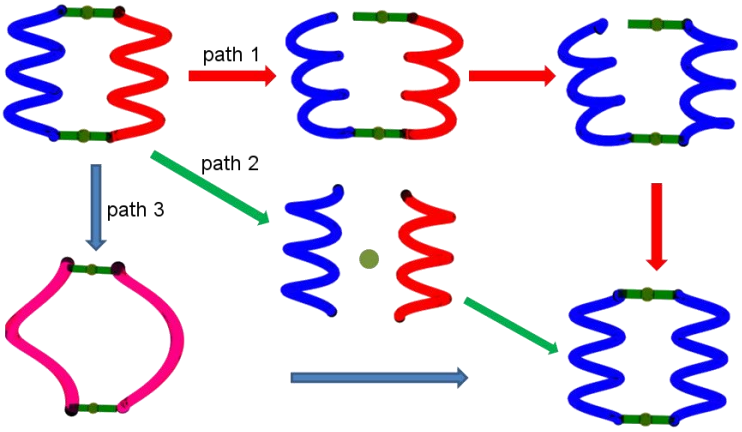

Figure 5-32：Possible mechanism for the handedness inversion of PP/MM and PM helices.

5.4 Conclusions and perspectives

In conclusion, we have successfully designed and prepared acridine and pyridine functionalized oligoamide foldamers at the side chain. In the case of acridine functionalized oligomers, four sets of signals were observed after formation of macrocyclic [2+2] complexes with palladium. The four sets of signals are assigned to parallel-PP/MM, parallel-PM and antiparallel-PP/MM, antiparallel-PM. In the case of pyridine functionalized oligomers, the symmetrical unit at the center of those oligomers generates C2 symmetry of these oligomers. Upon formation of complexes with palladium (II) ion, macrocyclic [2+2] complexes were successfully prepared. Due to the C2 symmetry of the foldamers, the parallel and antiparallel

oriented isomers were ruled out and only PP/MM and PM stereoisomers of the complexes could be obtained. The PP/MM and PM stereoisomers were in equilibrium in solution. Some more complicated equilibrium was observed in the complex formed between **L3** where higher order complexes were formed. The successful formation of helix-helix structures by metal coordination paved a new way to design helical assembly.

For perspectives, more complicated helix-helix assemblies were encouraged to be made based not only the side chain functionalization but also on the main chain of foldamer sequences. For example, ligand groups such as pyridine can be introduced on the main chain. A possible design is showed in the below figure. Two quinoline oligoamides are attached on a Tröger's base which served as turn unit. Nicotinic acid, isonicotiic acid or 2-picolinic acid can be attached to enable coordination with suitable metals. This design is possible to make square shaped assembly of quinoline oligoamide foldamers.

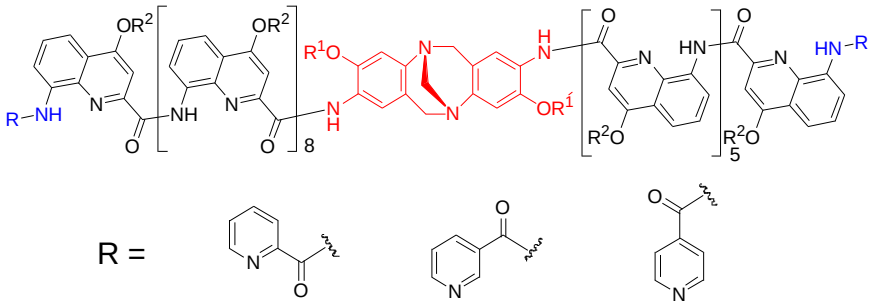

Figure 5-33: Chemical structure of ligand attached on the main chain.

5.5 Experiments

5.5.1 General remarks

All the solvents and reagents were used as received unless otherwise specified. Dry dichloromethane was obtained passing the solvent through a alumina column of solvent drying system. Dry chloroform and DIEA were obtained by refluxing with CaH_2 and the dry solvent was collected after distillation before using. ^{1}H NMR, ^{13}C NMR and 2D NMR were recorded on 300 MHz and 400 MHz Bruker Avance 300 and 400 spectrometer. Reactions were monitored by thin layer chromatography (TLC) on Merck silica gel 60-F254 plates and observed under UV light. Column chromatography purifications were carried out on Merck

GEDURAN Si60 (40-63 μm). ESI mass spectra were obtained from the Mass Spectrometry Laboratory at the European Institute of Chemistry and Biology (UMS 3033 - IECB), Pessac, France.

5.5.2 X-ray crystallography

The single crystals were obtained by slow diffusion of poor solvents such as acetonitrile, hexane or methanol into the stock solution in chloroform. Typically, the crystals were obtained in around 1 to 2 weeks and suitable crystals were picked for X-ray diffraction.

5.5.3 Monomer and oligomers synthesis

The compound **2** and **3** was prepared according to reported procedures.[22]

Compound **5**: To a 50 mL flask was charged with compound **4** (520 mg, 1.37 mmol), **3** (170 mg, 1.65 mmol), $PdCl_2(PPh_3)_2$ (48 mg, 0.068 mmol), PPh_3 (36 mg, 0.14 mmol), CuI (13 mg, 0.068 mmol) and equipped with condenser. The flask was then exchanged with Ar three times. The degassed solvent THF/Et_3N (v/v 1/1, mL) was added into the flask through a syringe. The mixture was then heated at 75 ^oC under inert atmosphere for overnight. After cooling down to room temperature, the solvent was removed and residue was purified with silica gel chromatogram. The product was eluted with DCM/EA (v/v 10/1). The product was obtained as yellow solid after remove solvent and dry under vacuum. Yield: 350 mg, 85%. ^1H NMR (300 Mhz, $CDCl_3$): δ = 9.03 (s, 1 H), 8.91 (d, J = 1.3 Hz, 1 H), 8.66 (dd, J = 5.1, 1.7 Hz, 1 H), 8.56 (d, J = 7.6 Hz, 1 H), 8.36 (s, 1 H), 7.97-7.93 (m, 2 H), 7.71 (t, J = 8.2 Hz, 1 H), 7.38 (dd, J = 7.8, 4.8 Hz, 1 H), 4.09 (s, 3 H), 1.60 (s, 9 H) ppm; ^{13}C NMR (75 MHz, $CDCl_3$): δ = 165.3, 152.8, 152.7, 150.0, 145.0, 139.0, 137.7, 136.9, 130.8, 130.6, 128.7, 124.4, 123.4, 117.9, 115.8, 96.2, 88.1, 81.2, 53.2, 28.5 ppm.

Compound **6**: Compound **5** (100 mg, 0.25 mmol) was dissolved in about 3 mL of dry DCM and then about 1 mL of TFA was added in to the solution. The mixture was then stirred at

room temperature for about 2 hours. The mixture was then diluted with DCM and washed three times with $NaHCO_3$ saturated aqueous solution. The organic layer was combined and dried over Na_2SO_4. The solvent was removed after filtration and dried under high vacuum to yield the desired amine. The compound was pure enough as indicated by NMR for the subsequent reaction and no further purification required. ^{1}H NMR (300 MHz, $CDCl_3$): δ = 8.90 (d, J = 1.3 Hz, 1 H), 8.65 (dd, J = 4.8, 1.7 Hz, 1 H), 8.31 (s, 1 H), 7.94 (dt, J = 7.8, 1.7 Hz, 1 H), 7.63 (dd, J = 8.3, 1.3 Hz, 1 H), 7.52 (t, J = 7.6 Hz, 1 H), 7.37 (dd, J = 8.0, 5.0 Hz, 1 H), 6.99 (dd, J = 7.6, 1.3 Hz, 2 H), 4.05 (s, 3 H) ppm.

Compound **8**: To a 25 mL dry flask was added with **7** (164 mg, 0.27 mmol), then the flask was exchanged with N_2 three times. Dry DCM (3 mL) was added into the flask through a syringe to dissolve the solid. Ghosez reagent (55 μL, 0.41 mmol) was added into the solution and the mixture was stirred at room temperature for 2 hours. Then the solvent was removed under high vacuum and the residue solid was dried for further 3 hours under high vacuum. The acid chloride was then dissolved into 2 mL of dry chloroform and transferred into the amine **6** (75 mg,0.25 mmol) under N_2 atmosphere. Dry DIEA (86 μL, 0.49 mmol) was added into the mixture. Then the mixture was stirred under N_2 for overnight. Then solvent was evaporated and the residue was purified with flash silica gel chromatogram to afford the pure product as reddish solid after removing solvent. Yield 160 mg (73 %).^{1}H NMR (300 MHz, $CDCl_3$): δ = 12.44 (s, 1 H), 12.37 (s, 1 H), 9.13 (d, J = 7.8 Hz, 1 H), 9.00 (dd, J = 7.6, 1.1 Hz, 1 H), 8.94 (d, J = 1.3 Hz, 1 H), 8.70 (dd, J = 4.9, 1.6 Hz, 1 H), 8.33 (s, 1 H), 8.05 (d, J = 8.4 Hz, 2 H), 7.99 (dt, J = 7.9, 1.8 Hz, 1 H), 7.82 (t, J = 7.9 Hz, 1 H), 7.80 (s, 1 H), 7.76 (dd, J = 8.3, 1.2 Hz, 1 H), 7.73 (d, J = 7.9 Hz, 1 H), 7.72 (s, 1 H), 7.48 (s, 1 H), 7.42 (m, 2 H), 7.25 (t, J = 8.0 Hz, 1 H), 4.19 (d, J = 6.6 Hz, 2 H), 4.16 (d, J = 6.7 Hz, 1 H), 3.53 (s, 3 H), 2.45-2.29 (m, 2 H), 1.35 (s, 9 H), 1.22 (d, J = 6.6 Hz, 6 H), 1.20 (d, J = 6.6 Hz, 6 H) ppm; ^{13}C NMR (75 MHz, $CDCl_3$): δ = 164.2, 163.8, 163.4, 163.3, 163.2, 152.7, 151.8, 150.8, 150.4, 149.9, 143.8, 139.1, 139.0, 138.4, 136.9, 135.6, 134.7, 134.1, 130.5, 130.1, 128.3, 128.2, 127.4, 123.5, 123.4, 122.6, 121.9, 119.9, 119.4, 117.5, 117.4, 116.4, 115.0, 114.4, 99.2, 98.4, 95.9, 87.9, 80.7, 75.6, 52.5, 28.4, 28.2, 19.4, 19.4 ppm.

Compound **9**: This compound was prepared according to the same procedure as compound **6**. ^{1}H NMR (300 MHz, $CDCl_3$): δ = 12.39 (s, 2 H), 9.05 (dd, J = 7.7, 1.2 Hz, 1 H), 9.02 (dd, J = 7.7, 1.1 Hz, 1 H), 8.95 (q, J = 0.9 Hz, 1 H), 8.69 (dd, J = 4.9, 1.6 Hz, 1 H), 8.08 (dd, J = 8.4, 1.2 Hz, 1 H), 8.03 (dd, J = 8.4, 1.2 Hz, 1 H), 7.99 (dt, J = 7.9, 2.0 Hz, 1 H), 7.87 (t, J = 7.8 Hz, 1 H), 7.78 (s, 1 H), 7.70 (t, J = 7.9 Hz, 1 H), 7.69 (s, 1 H), 7.62 (s, 1 H), 7.45 (dd, J = 8.3, 1.2 Hz, 1 H), 7.42 (ddd, J = 7.8, 5.0, 1.0 Hz, 1 H), 7.07 (t, J = 7.8 Hz, 1 H), 5.93 (dd, J = 7.5, 1.1 Hz, 1 H), 4.18 (d, J = 6.5 Hz, 2 H), 4.12 (d, J = 6.5 Hz, 2 H), 3.97 (br, 2 H), 3.50 (s, 3 H), 2.42-2.29 (m, 2 H), 1.19 (d, J = 6.7 Hz, 12 H) ppm.

Compound **10**: This compound was synthesized the same way as compound **8**. Yield 242 mg (69 %).^{1}H NMR (300 MHz, $CDCl_3$): δ = 11.94 (s, 2 H), 11.80 (s, 1 H), 11.76 (s, 1 H), 8.97 (d, J = 1.3 Hz, 1 H), 8.71 (dd, J = 4.9, 1.6 Hz, 1 H), 8.69 (dd, J = 7.7, 1.2 Hz, 1 H), 8.65 (dd, J = 7.7, 1.0 Hz, 1 H), 8.17 (dd, J = 8.6, 1.3 Hz, 2 H), 8.10-7.98 (m, 6 H), 7.89-7.82 (m, 3 H), 7.72 (t, J = 7.9 Hz, 1 H), 7.45 (d, J = 7.8 Hz, 1 H), 7.45 (s, 1 H), 7.42 (s, 1 H), 7.38 (s, 1 H), 7.35 (d, J = 7.9 Hz, 2 H), 7.14 (t, J = 8.0 Hz, 1 H), 6.84 (s, 1 H), 6.76 (s, 1 H), 4.45-4.36 (m, 2 H), 4.25-4.11 (m, 3 H), 3.95 (d, J = 6.1 Hz, 2 H), 3.86 (m, 1 H), 3.21 (s, 3 H), 2.60-2.33 (m, 4 H), 1.35-1.23 (m, 24 H), 1.08 (s, 9 H) ppm; ^{13}C NMR (75 MHz, $CDCl_3$): δ = 163.9, 163.8, 163.3, 163.2, 162.9, 161.4, 161.4, 161.2, 152.8, 151.6, 150.4, 149.9, 149.8, 149.4, 148.8, 143.7, 139.1, 138.5, 138.3, 138.0, 137.8, 136.9, 135.1, 134.2, 133.9, 133.6, 133.0, 130.0, 128.4, 127.5, 127.1, 126.7, 123.5, 123.5, 122.5, 122.4, 122.1, 121.4, 120.2, 119.5, 117.4, 117.1, 116.9, 116.3, 116.2, 116.1, 115.7, 114.6, 99.4, 99.3, 98.0, 97.4, 95.8, 88.0, 80.4, 75.7, 75.6, 75.4, 75.3, 52.2, 45.9, 28.4, 28.4, 28.4, 28.3, 27.9, 19.6, 19.6, 19.6, 19.5, 19.5, 19.4, 8.8 ppm.

Compound **12**: This compound was prepared according to the same procedure as compound **6**. ^{1}H NMR (300 MHz, $CDCl_3$): δ = 11.99 (s, 1 H), 11.95 (s, 1 H), 11.82 (s, 1 H), 11.67 (s, 1 H), 8.98 (d, J = 1.4 Hz, 1 H), 8.71 (dd, J = 5.0, 1.6 Hz, 1 H), 8.67 (dd, J = 7.8, 1.0 Hz, 1 H), 8.56 (dd, J = 7.5, 1.0 Hz, 1 H), 8.14 (dd, J = 8.3, 1.0 Hz, 1 H), 8.11-8.00 (m, 4 H), 7.97 (dd, J = 8.4, 1.2 Hz, 1 H), 7.90 (dd, J = 8.3, 1.2 Hz, 1 H), 7.84 (t, J = 7.9 Hz, 1 H), 7.69 (t, J = 7.9 Hz, 1 H), 7.54 (dd, J = 8.2, 0.9 Hz, 1 H), 7.47-7.42 (m, 1 H), 7.43 (s, 1 H), 7.42 (t, J = 7.9 Hz, 1 H), 7.39 (s, 1 H), 7.34 (s, 1 H), 7.32 (t, J = 8.2 Hz, 1 H), 6.98 (t, J = 7.6 Hz, 1 H), 6.88 (s, 1 H),

6.83 (s, 1 H), 5.85 (dd, J = 7.4, 0.9 Hz, 1 H), 4.44-3.84 (m, 8 H), 3.57 (br, 2 H), 3.25 (s, 3 H), 2.59-2.30 (m, 4 H), 1.34-1.22 (m, 24 H) ppm.

Compound **13** (**L1**): Amine **12** (224 mg, 0.176 mmol) was added into a dry flask and exchanged with N_2 three times. Dry DIEA (46 μL, 0.264 mmol) was added into the flask with a syringe. 2,6-pyridinediacidchloride (17 mg, 0.083 mmol) was dissolved in 2 mL dry chloroform and added into the flask. The resulting mixture was stirred under N_2 for overnight. Then solvent was evaporated and the residue was purified with silica gel chromatography to afford the pure product as yellow solid after removing solvent. Yield: 115 mg (48 %).^{1}H NMR (300 MHz, $CDCl_3$): δ = 11.31 (s, 2 H), 11.21 (s, 2 H), 10.99 (s, 2 H), 10.80 (s, 2 H), 9.87 (s, 2 H), 8.85 (d, J = 1.4 Hz, 2 H), 8.67 (dd, J = 4.8, 1.6 Hz, 2 H), 8.29 (d, J = 7.9 Hz, 2 H), 8.24 (d, J = 7.8 Hz, 2 H), 7.90 (dt, J = 7.8, 1.9 Hz, 2 H), 7.85 (dd, J = 8.4, 1.2 Hz, 2 H), 7.80 (dd, J = 8.4, 1.0 Hz, 2 H), 7.73 (dd, J = 8.2, 1.2 Hz, 2 H), 7.63 (d, J = 8.1 Hz, 2 H), 7.53 (t, J = 7.8 Hz, 2 H), 7.53 (d, J = 7.2 Hz, 2 H), 7.45 (t, J = 7.7 Hz, 2 H), 7.39 (dd, J = 7.8, 4.7 Hz, 2 H), 7.23 (dd, J = 8.2, 1.0 Hz, 2 H), 7.12 (s, 2 H), 7.12 (s, 2 H), 7.10 (d, J = 4.5 Hz, 2 H), 7.08 (t, J = 8.0 Hz, 2 H), 6.98 (dd, J = 7.6, 1.2 Hz, 2 H), 6.77-6.71 (m, 6 H), 6.44 (t, J =7.8 Hz, 2 H), 6.43 (s, 2 H), 6.41 (s, 2 H), 4.30-3.61 (m, 16 H), 2.97 (s, 6 H), 2.60-2.15 (m, 8 H), 1.39-1.09 (m, 48 H) ppm; ^{13}C NMR (75 MHz, $CDCl_3$): δ = 163.0, 162.9, 162.7, 162.7, 160.9, 160.8, 159.9, 159.9, 159.0, 152.7, 149.8, 149.6, 148.7, 148.6, 148.1, 148.1, 143.2, 139.0, 137.9, 137.8, 137.1, 136.8, 136.7, 134.5, 133.3, 132.2, 131.9, 131.8, 129.7, 129.5, 128.0, 127.0, 126.4, 126.1, 123.4, 123.1, 121.9, 121.6. 121.4, 121.2, 119.8, 119.5, 117.1, 116.9, 116.5, 116.3, 116.1, 115.9, 115.7, 115.4, 113.9, 99.9, 99.1, 97.5, 97.1, 95.4, 87.9, 75.4, 75.2, 75.2, 75.0, 52.0, 28.5, 28.3, 28.2, 28.2, 19.7, 19.6, 19.5, 19.5, 19.4, 19.3 ppm.

Compound **21**: To a dry flask was added with the acid **20** (560 mg, 1.05 mmol), the flask was exchanged with N_2 three times and then 4 mL of dry $CHCl_3$ was added to dissolve the solid. Oxalyl chloride (0.45 mL, 5.25 mmol) was added into the solution with a syringe. The resulting mixture was stirred at room temperature under N_2 for 2 hours. Then the solvent was removed under high vacuum and the residue solid was kept under vacuum for additional 3 hours. To another dry flask was added with the 2,6-pyridinediamine (55 mg, 0.5 mmol) and

the flask was then exchanged with N_2 three times. Dry DIEA (262 μL, 1.5 mmol) was added into the flask was a syringe. The dry acid chloride of **20** was dissolved into 3 mL of dry chloroform and transferred into the flask with amine. The mixture was stirred at room temperature under N_2 for overnight. Then solvent was removed and the residue solid was redissolved into minimum amount of dichloromethane and then methanol was added till large amount of precipitate formed. The solid was filtrated and washed three times with methanol and then dried under high vacuum to afford yellow solid. Yield: 500 mg (87.8 %).^{1}H NMR (300 MHz, $CDCl_3$): δ = 11.20 (s, 2 H), 9.55 (s, 2 H), 8.96 (dd, J = 7.5, 1.0 Hz, 2 H), 8.12-8.07 (m, 6 H), 7.96 (dd, J = 8.7, 7.3 Hz, 1 H), 7.84 (s, 2 H), 7.77 (s, 2 H), 7.70 (t, J = 8.0 Hz, 2 H), 7.11 (dd, J = 8.3, 1.4 Hz, 2 H), 6.41 (t, J = 8.0 Hz, 2 H), 4.29 (d, J = 5.8 Hz, 4 H), 4.22 (d, J = 6.5 Hz, 4 H), 2.41 (m, 2 H), 2.18 (m, 2 H), 1.24 (d, J = 6.8 Hz, 12 H), 1.14 (d, J = 6.6 Hz, 12 H) ppm; ^{13}C NMR (75 MHz, $CDCl_3$): δ = 163.9, 163.5, 162.0, 161.4, 152.9, 149.0, 141.1, 140.9, 139.9, 138.4, 134.0, 128.3, 127.8, 127.7, 123.7, 123.4, 122.2, 118.6, 116.8, 110.1, 99.6, 98.8, 75.8, 75.7, 28.4, 28.2, 19.6, 19.5 ppm.

Compound **22**: To a dry flask was added with compound **21** (500 mg, 0.439 mmol), ammonium formate (2.77 g, 43.93 mmol), and ammonium metavanadate (45 mg, 0.386 mmol). Then ethyl acetate (25 mL), ethanol (6 mL) and water (1.25 mL) were added into the flask. Then Pd/C (10%, 100 mg) was added into the flask and start stirring at room temperature. Then a condenser of suitable size was equipped and then exchanged with N_2 three times. The mixture was then heated at 75 ^{o}C for overnight. After cooling down to room temperature, an amount of 40 mL of dichloromethane was added to dilute the solution. Then the mixture was filtrated through a pack of celite to remove the Pd/C. The solution was then washed with 5% ammonium chloride solution two times. The organic layer was combined and dried over sodium sulfate. After filtration and remove the solvent, the product was obtained as a yellow solid. The product was pure enough for subsequent reaction and no further purification needed. Yield: quantitative.^{1}H NMR (300 MHz, $CDCl_3$): δ = 10.83 (s, 2 H), 9.74 (s, 2 H), 9.01 (dd, J = 7.6, 1.0 Hz, 2 H), 8.16 (d, J = 7.9 Hz, 2 H), 8.04 (dd, J = 8.6, 1.2 Hz, 2 H), 7.98 (t, J = 8.2 Hz, 1 H), 7.74 (s, 2 H), 7.67 (t, J = 8.0 Hz, 2 H), 7.58 (s, 2 H), 6.31 (dd, J = 6.9, 1.7 Hz, 2 H), 6.19-6.09 (m, 4 H), 4.30 (br, 4 H), 4.20 (d, J = 6.5 Hz, 8 H),

2.40 (m, 2 H), 2.17 (m, 2 H), 1.23 (d, J = 6.7 Hz, 12 H), 1.14 (d, J = 6.7 Hz, 12 H) ppm.

Compound **23**: This compound was prepared according to the same procedure as compound **21**. Yield: 780 mg (84 %).^{1}H NMR (300 MHz, $CDCl_3$): δ = 11.47 (s, 2 H), 11.28 (s, 2 H), 10.35 (s, 2 H), 8.48 (s, 2 H), 8.43-8.39 (m, 4 H), 8.20 (dd, J = 7.3, 1.3 Hz, 2 H), 8.15 (d, J = 8.1 Hz, 2 H), 7.94 (d, J = 7.7 Hz, 2 H), 7.89 (d, J = 8.4 Hz, 2 H), 7.79 (m, 1 H), 7.74 (t, J = 8.3 Hz, 2 H), 7.60 (t, J = 7.7 Hz, 2 H), 7.34 (s, 2 H), 7.22-7.12 (m, 8 H), 6.91 (s, 2 H), 6.38 (s, 2 H), 6.17 (t, J = 8.2 Hz, 2 H), 6.10 (dd, J = 8.4, 1.5 Hz, 2 H), 4.34-3.96 (m, 14 H), 3.41 (t, J = 8.4 Hz, 2 H), 2.56-2.39 (m, 6 H), 2.02 (m, 2 H), 1.34-1.23 (m, 36 H), 1.14 (d, J = 6.8 Hz, 6 H), 1.06 (d, J = 6.6 Hz, 6 H) ppm; ^{13}C NMR (75 MHz, $CDCl_3$): δ = 163.3, 163.0, 162.9, 162.5, 161.1, 161.0, 160.4, 159.7, 153.6, 150.8, 148.5, 147.7, 147.7, 145.1, 139.3, 138.8, 138.2, 137.9, 137.8, 134.5, 133.4, 133.3, 127.6, 126.5, 126.4, 126.2, 125.5, 124.0, 123.8, 122.1, 121.9, 121.2, 117.2, 117.0, 116.8, 116.7, 116.2, 114.3, 109.1, 100.3, 99.4, 98.0, 97.1, 75.8, 75.5, 75.5, 74.6, 28.5, 28.4, 28.4, 28.1, 19.9, 19.6, 19.6, 19.6, 19.5 ppm.

Compound **24**: The compound was prepared according to the same procedure of compound **22**. Yield: quantitative.^{1}H NMR (300 MHz, $CDCl_3$): δ = 11.69 (s, 2 H), 11.44 (s, 2 H), 10.33 (s, 2 H), 8.59 (s, 2 H), 8.44 (d, J = 7.4 Hz, 2 H), 8.13-8.08 (m, 4 H), 7.85-7.77 (m, 7 H), 7.63 (t, J = 8.0 Hz, 2 H), 7.38 (dd, J = 8.3, 1.0 Hz, 2 H), 7.18 (s, 2 H), 7.17 (t, J = 7.9 Hz, 2 H), 7.08 (s, 2 H), 6.90 (s, 2 H), 6.77 (t, J = 7.6 Hz, 2 H), 6.49 (s, 2 H), 6.20 (d, J = 2.5 Hz, 2 H), 6.19 (s, 2 H), 5.53 (d, J = 7.4 Hz, 2 H), 4.25-3.96 (m, 14 H), 3.45 (t, J = 8.1 Hz, 2 H), 3.26 (br, 4 H), 2.50-2.38 (m, 6 H), 2.00-1.94 (m, 2 H), 1.34-1.24 (m, 36 H), 1.13 (d, J = 6.7 Hz, 6 H), 1.06 (d, J = 6.6 Hz, 6 H) ppm.

Compound **14**: To a dry flask was added with compound 5 (80 mg, 0.2 mmol) and NaOH (80 mg, 2 mmol). Then THF (1.8 mL) and MeOH (0.2 mL) were added into the flask. The resulting mixture was stirred at room temperature for 1.5 hours. Then citric acid (5%) was added to adjust the pH to around 3. The precipitate was filtrated and washed with distilled water twice. The solid was dried under high vacuum. Yield: quantitative.^{1}H NMR (300 MHz, $CDCl_3$): δ = 8.92 (dd, J = 2.0, 0.9 Hz, 1 H), 8.73 (s, 1 H), 8.68 (dd, J = 4.9, 1.6 Hz, 1 H), 8.59

(d, J = 8.1 Hz, 1 H), 8.49 (s, 1 H), 8.02 (dd, J = 8.3, 1.1 Hz, 1 H), 7.97 (dt, J = 7.9, 1.8 Hz, 1 H), 7.77 (t, J = 8.1 Hz, 1 H), 7.40 (ddd, J = 7.9, 4.9, 1.0 Hz, 1 H), 1.62 (s, 9 H) ppm.

Compound **19** (**L3**): The compound was prepared according to the same procedure as compound **21** except that the acid **14** was activated with Ghosez reagent to corresponding acid chloride. Yield: 200 mg (76 %).^{1}H NMR (300 MHz, $CDCl_3$): δ = 11.44 (s, 2 H), 11.12 (s, 2 H), 11.02 (s, 2 H), 10.12 (s, 2 H), 8.87 (dd, J = 2.1, 0.7 Hz, 2 H), 8.64 (dd, J = 4.9, 1.6 Hz, 2 H), 8.52 (dd, J = 7.6, 1.1 Hz, 2 H), 8.14 (dd, J = 8.2, 1.0 Hz, 2 H), 8.14 (s, 2 H), 7.95 (dt, J = 7.9, 1.8 Hz, 2 H), 7.89 (dd, J = 7.5, 1.1 Hz, 2 H), 7.85 (dd, J = 8.5, 1.3 Hz, 2 H), 7.78 (dd, J = 8.4, 1.2 Hz, 2 H), 7.69-7.61 (m, 10 H), 7.54 (dd, J = 6.8, 2.1 Hz, 2 H), 7.40 (t, J = 8.2 Hz, 1 H), 7.37 (ddd, J = 7.9, 4.9, 0.9 Hz, 2 H), 7.31 (s, 2 H), 7.26-7.06 (m, 9 H), 6.74 (s, 2 H), 6.38 (s, 2 H), 6.19-6.10 (m, 4 H), 6.04 (s, 2 H), 4.35 (dd, J = 8.9, 6.4 Hz, 2 H), 4.20-4.12 (m, 4 H), 4.03 (dd, J = 8.8, 6.4 Hz, 2 H), 3.92 (dd, J = 8.7, 6.8 Hz, 2 H), 3.82 (dd, J = 8.9, 6.2 Hz, 2 H), 3.64 (dd, J =8.7, 7.0 Hz, 2 H), 3.52 (t, J = 8.4 Hz, 2 H), 2.60-2.27 (m, 6 H), 2.12-2.03 (m, 2 H), 1.38-1.14 (m, 48 H), 0.95 (s, 18 H) ppm; ^{13}C NMR (75 MHz, $CDCl_3$): δ = 163.6, 163.0, 162.8, 162.5, 161.1, 160.5, 159.8, 159.5, 158.9, 152.8, 151.4, 150.3, 149.6, 149.1, 147.9, 147.8, 147.2, 147.1, 139.3, 139.1, 137.6, 136.6, 137.5, 137.3, 135.5, 134.6, 133.2, 133.0, 132.9, 132.6, 130.9, 128.6, 128.5, 126.8, 126.7, 126.3, 125.5, 123.3, 122.3, 121.8, 121.8, 121.4, 121.0, 119.7, 118.2, 117.2, 116.7, 116.4, 116.1, 116.0, 115.7, 115.4, 115.1, 114.7, 108.5, 99.6, 97.8, 98.8, 97.6, 95.8, 88.8, 80.6, 75.6, 75.4, 75.3, 74.6, 28.5, 28.3, 28.2, 27.7, 20.0, 19.7, 19.6, 19.6, 19.5, 19.5 ppm.

Compound **26** and **27** were prepared according to reported procedures.[22]

Compound **28**: The compound was prepared according to the same procedure as compound **5**. Yied: 92%. ^{1}H NMR (300 MHz, $CDCl_3$): δ = 9.02 (s, 1 H), 8.71 (dd, J = 4.4, 1.7 Hz, 2 H), 8.57 (d, J = 7.8 Hz, 1 H), 8.37 (s, 1 H), 7.92 (dd, J = 8.3, 1.5 Hz, 1 H), 7.72 (t, J = 8.1 Hz, 1 H), 7.52 (dd, J = 4.2, 1.4 Hz, 2 H), 4.09 (s, 3 H), 1.60 (s, 9 H) ppm; ^{13}C NMR (75 MHz, $CDCl_3$): δ = 165.2, 152.8, 150.2, 145.0, 137.7, 136.9, 131.0, 130.1, 129.7, 125.8, 124.6, 117.8, 115.8, 96.3, 88.8, 81.2, 53.2, 28.5 ppm.

Compound **29**: This compound was prepared according to the same procedure as compound **14**. Yield: 230 mg (93%).^{1}H NMR (300 MHz, $CDCl_3$): δ = 8.73 (dd, J = 4.5, 1.3 Hz, 2 H), 8.66 (br, 1 H), 8.61 (d, J = 7.6 Hz, 1 H), 8.50 (s, 1 H), 8.00 (dd, J = 8.3, 1.1 Hz, 1 H), 7.78 (t, J = 8.1 Hz, 1 H), 7.54 (dd, J = 4.4, 1.5 Hz, 2 H), 1.62 (s, 9 H) ppm.

Compound **30** (**L4**): This compound was prepared according to the same procedure as compound **19**. Yield: 190 mg (74 %).^{1}H NMR (300 MHz, $CDCl_3$): δ = 11.43 (s, 2 H), 11.11 (s, 2 H), 11.02 (s, 2 H), 10.12 (s, 2 H), 8.69 (dd, J = 4.4, 1.6 Hz, 4 H), 8.51 (d, J = 7.6 Hz, 2 H), 8.14 (d, J = 8.2 Hz, 2 H), 8.14 (s, 2 H), 7.89 (d, J = 7.6 Hz, 2 H), 7.85 (dd, J = 8.4, 1.2 Hz, 2 H), 7.79 (dd, J = 8.4, 1.0 Hz, 2 H), 7.69-7.60 (m, 9 H), 7.54-7.50 (m, 5 H), 7.41 (t, J = 7.9 Hz, 1 H), 7.31 (s, 2 H), 7.23-7.05 (m, 9 H), 6.74 (s, 2 H), 6.38 (s, 2 H), 6.19-6.10 (m, 4 H), 6.03 (s, 2 H), 4.35 (dd, J = 8.6, 6.4 Hz, 2 H), 4.21-4.12 (m, 4 H), 4.03 (m, 2 H), 3.93 (m, 2 H), 3.82 (m, 2 H), 3.64 (m, 2 H), 3.52 (t, J = 8.3 Hz, 2 H), 2.59-2.27 (m, 6 H), 2.07 (m, 2 H), 1.38-1.14 (m, 48 H), 0.95 (s, 18 H) ppm; ^{13}C NMR (75 MHz, $CDCl_3$): δ = 163.6, 163.0, 162.8, 162.5, 161.1, 160.5, 159.6, 159.5, 158.9, 151.4, 150.3, 150.2, 150.1, 149.1, 147.9, 147.8, 147.2, 147.1, 139.1, 137.6, 137.6, 137.5, 137.3, 135.5, 134.7, 133.2, 133.0, 132.9, 132.6, 130.5, 130.4, 128.7, 128.4, 126.9, 126.7, 126.3, 126.0, 125.5, 122.3, 122.1, 121.8, 121.4, 121.0, 118.1, 117.2, 116.7, 116.5, 116.0, 115.7, 115.4, 115.1, 114.8, 108.4, 99.6, 97.8, 97.6, 95.9, 89.7, 80.6, 75.6, 75.4, 75.3, 74.6, 28.5, 28.3, 28.2, 27.7, 20.0, 19.7, 19.6, 19.6, 19.5, 19.5 ppm.

Compound **31**: This compound was prepared according to the same procedure as compound **6**. Yield: quantitative.^{1}H NMR (300 MHz, $CDCl_3$): δ = 8.70 (dd, J = 4.3, 1.6 Hz, 2 H), 8.32 (s, 1 H), 7.60 (dd, J = 8.3, 1.4 Hz, 1 H), 7.54 (d, J = 7.3 Hz, 1 H), 7.51 (dd, J = 4.5, 1.6 Hz, 2 H), 6.99 (dd, J = 7.4, 1.4 Hz, 1 H), 5.25 (br, 2 H), 4.06 (s, 3 H) ppm.

Compound **32**: This compound was prepared according to the same procedure as compound **8**. Yield: 1.1 g (65 %).^{1}H NMR (300 MHz, $CDCl_3$): δ = 12.43 (s, 1 H), 12.36 (s, 1 H), 9.14 (dd, J = 7.5, 1.0 Hz, 2 H), 9.00 (dd, J = 7.6, 1.1 Hz, 2 H), 8.75 (dd, J = 4.4, 1.6 Hz, 2 H), 8.32 (s, 1 H), 8.06 (d, J = 8.5 Hz, 1 H), 8.03 (d, J = 8.6 Hz, 1 H), 7.83 (t, J = 7.9 Hz, 1 H), 7.80 (s, 1 H), 7.77-7.69 (m, 3 H), 7.55 (dd, J = 4.6, 1.6 Hz, 2 H), 7.49 (s, 1 H), 7.42 (d, J = 6.9 Hz, 1 H),

7.24 (t, J = 8.1 Hz, 1 H), 4.19 (d, J= 6.7 Hz, 2 H), 4.16 (d, J = 6.5 Hz, 2 H), 3.53 (s, 3 H), 2.43-2.32 (m, 2 H), 1.35 (s, 9 H), 1.22 (d, J = 5.7 Hz, 6 H), 1.20 (d, J = 5.7 Hz, 6 H) ppm; ^{13}C NMR (75 MHz, $CDCl_3$): δ = 164.2, 163.8, 163.4, 163.2, 163.1, 151.8, 150.8, 150.4, 150.3, 143.8, 139.0, 138.4, 136.9, 135.7, 134.7, 134.1, 130.7, 130.2, 129.6, 128.3, 128.2, 127.4, 125.8, 123.6, 122.6, 121.9, 119.8, 117.5, 117.4, 116.5, 115.0, 114.4, 99.2, 98.4, 96.0, 88.7, 80.8, 75.6, 52.6, 28.4, 28.3, 19.4, 19.4 ppm.

Compound **33**: This compound was prepared the same way as compound **6**. Yield: quantitative.^{1}H NMR (300 MHz, $CDCl_3$): δ = 12.39 (s, 2 H), 9.05 (dd, J = 7.5, 1.0 Hz, 1 H), 9.02 (dd, J = 7.8, 1.3 Hz, 1 H), 8.75 (dd, J = 4.4, 1.5 Hz, 2 H), 8.06 (dd, J = 4.8, 1.1 Hz, 1 H), 8.03 (dd, J = 4.9, 1.3 Hz, 1 H), 7.88 (t, J = 7.8 Hz, 1 H), 7.78 (s, 1 H), 7.71 (t, J = 8.0 Hz, 1 H), 7.69 (s, 1 H), 7.63 (s, 1 H), 7.56 (dd, J = 4.4, 1.6 Hz, 2 H), 7.45 (dd, J = 8.3, 1.1 Hz, 1 H), 7.06 (t, J = 7.9 Hz, 1 H), 5.92 (dd, J = 7.5, 1.1 Hz, 1 H), 4.18 (d, J = 6.6 Hz, 2 H), 4.12 (d, J = 6.6 Hz, 2 H), 3.97 (br, 2 H), 3.50 (s, 3 H), 2.40-2.32 (m, 2 H), 1.19 (d, J = 6.8 Hz, 12 H) ppm.

Compound **34**: This compound was prepared according to the same procedure of compound **8**. Yield: 1.78 g (89 %).^{1}H NMR (300 MHz, $CDCl_3$): δ = 11.94 (s, 2 H), 11.80 (s, 1 H), 11.76 (s, 1 H), 8.77 (dd, J = 4.4, 1.5 Hz, 2 H), 8.70 (d, J = 7.8 Hz, 1 H), 8.65 (d, J = 7.9 Hz, 1 H), 8.14 (dd, J = 8.4, 1.1 Hz, 1 H), 8.09 (d, J = 8.4 Hz, 1 H), 8.07-7.98 (m, 4 H), 7.88-7.82 (m, 3 H), 7.72 (t, J = 8.2 Hz, 1 H), 7.58 (dd, J = 4.4, 1.6 Hz, 2 H), 7.44 (s, 1 H), 7.42 (s, 1 H), 7.38 (s, 1 H), 7.37-7.31 (m, 3 H), 7.14 (t, J = 8.2 Hz, 1 H), 6.84 (s, 1 H), 6.77 (s, 1 H), 4.45-4.36 (m, 2 H), 4.25-4.14 (m, 3 H), 3.97-3.92 (m, 3 H), 3.89-3.83 (m, 1 H), 3.21 (s, 3 H), 2.58-2.49 (m, 2 H), 2.41-2.31 (m, 2 H), 1.35-1.23 (m, 24 H), 1.08 (s, 9 H) ppm; ^{13}C NMR (75 MHz, $CDCl_3$): δ = 164.0, 163.8, 163.3, 163.2, 162.8, 161.5, 161.4, 161.2, 151.6, 150.3, 150.3, 149.8, 149.4, 148.8, 143.7, 138.4, 138.3, 138.0, 137.8, 136.9, 135.2, 134.2, 133.9, 133.6, 133.0, 130.3, 130.1, 129.4, 128.4, 127.5, 127.1, 127.0, 126.7, 125.9, 123.8, 122.5, 122.4, 122.1, 121.4, 120.1, 117.5, 117.2, 116.9, 116.3, 116.2, 116.1, 115.7, 114.6, 99.4, 99.3, 98.0, 97.4, 95.9, 88.8, 80.4, 75.7, 75.6, 75.4, 75.3, 52.3, 28.4, 28.4, 28.4, 28.3, 28.1, 27.9, 19.6, 19.6, 19.6, 19.5, 19.5, 19.4 ppm.

Compound **35**: This compound was prepared according to the same procedure of compound **6**. Yield: quantitative. ^{1}H NMR (300 Mhz, $CDCl_3$): δ = 11.99 (s, 1 H), 11.96 (s, 1 H), 11.82 (s, 1 H), 11.67 (s,1 H), 8.77 (dd, J = 4.4, 1.6 Hz, 2 H), 8.68 (dd, J = 7.7, 1.1 Hz, 1 H), 8.57 (dd, J = 7.7, 1.2 Hz, 1 H), 8.13-8.09 (m, 3 H), 8.03 (dd, J = 7.6, 1.1 Hz, 1 H), 7.98 (dd, J = 8.3, 1.1 Hz, 1 H), 7.90 (dd, J = 8.5, 1.1 Hz, 1 H), 7.85 (t, J = 8.1 Hz, 1 H), 7.70 (t, J = 8.2 Hz, 1 H), 7.58 (dd, J = 4.3, 1.5 Hz, 2 H), 7.54 (dd, J = 8.2, 1.1 Hz, 1 H), 7.44 (s, 1 H), 7.41 (t, J = 8.2 Hz, 1 H), 7.40 (s, 1 H), 7.34 (s, 1 H), 7.32 (t, J = 7.9 Hz, 1 H), 6.99 (t, J = 7.6 Hz, 1 H), 6.88 (s, 1 H), 6.84 (s, 1 H), 5.86 (dd, J = 7.4, 1.0 Hz, 1 H), 4.44-4.39 (m, 1 H), 4.34-4.29 (m, 1 H), 4.24-4.19 (m, 1 H), 4.13-4.08 (m, 1 H), 4.00-3.94 (m, 3 H), 3.90-3.85 (m, 1 H), 3.57 (br, 2 H), 3.26 (s, 1 H), 2.59-2.32 (m, 4 H), 1.34-1.22 (m, 24 H) ppm.

Compound **36** (**L2**): This compound was prepared according to the same procedure as compound **13**. Yield: 120 mg (19 %). ^{1}H NMR (300 MHz, $CDCl_3$): δ = 11.30 (s, 2 H), 11.20 (s, 2 H), 11.00 (s, 2 H), 10.79 (s, 2 H), 9.87 (s, 2 H), 8.72 (dd, J = 4.5, 1.4 Hz, 4 H), 8.29 (d, J = 7.5 Hz, 2 H), 8.25 (d, J = 7.7 Hz, 2 H), 7.83 (dd, J = 8.2, 1.0 Hz, 2 H), 7.80 (dd, J = 8.2, 1.1 Hz, 2 H), 7.72 (dd, J = 8.1, 1.1 Hz, 2 H), 7.63 (d, J = 8.2 Hz, 3 H), 7.54 (t, J = 7.6 Hz, 4 H), 7.46 (dd, J = 4.5, 1.5 Hz, 4 H), 7.45 (t, J = 7.8 Hz, 2 H), 7.24 (dd, J = 8.2, 1.0 Hz, 2 H), 7.13-7.09 (m, 6 H), 7.08 (t, J = 8.2 Hz, 2 H), 6.97 (dd, J = 7.5, 1.1 Hz, 2 H), 6.77-6.71 (m, 6 H), 6.44 (t, J = 7.7 Hz, 2 H), 6.44 (s, 2 H), 6.41 (s, 2 H), 4.25 (m, 4 H), 4.07 (m, 4 H), 3.80-3.61 (m, 8 H), 2.97 (s, 6 H), 2.60-2.15 (m, 8 H), 1.37 (t, J = 6.0 Hz, 12 H), 1.30 (t, J = 6.5 Hz, 12 H), 1.19 (t, J = 7.1 Hz, 12 H), 1.14 (d, J = 6.6 Hz, 6 H), 1.10 (d, J = 6.8 Hz, 6 H) ppm; ^{13}C NMR (75 MHz, $CDCl_3$): δ = 163.0, 162.9, 162.7, 162.7, 162.6, 160.8, 160.8, 159.9, 159.9, 159.0, 150.2, 149.6, 148.8, 148.6, 148.1, 148.0, 143.2, 137.9, 137.8, 137.7, 137.1, 136.8, 136.6, 134.6, 133.3, 132.2, 131.9, 131.7, 130.2, 129.9, 128.9, 127.9, 127.0, 126.3, 126.1, 125.8, 123.3, 121.9, 121.6, 121.4, 121.2, 119.7, 117.1, 116.9, 116.6, 116.3, 116.2, 115.9, 115.7, 115.4, 114.0, 99.9, 99.0, 97.5, 97.1, 95.5, 88.7, 75.4, 75.2, 75.2, 75.0, 52.0, 28.5, 28.3, 28.2, 28.2, 19.7, 19.5, 19.5, 19.4, 19.4, 19.3 ppm.

Compound **38**: This compound was prepared according to the same procedure as compound **8**. Yield: 270 mg (72%). ^{1}H NMR (300 MHz, $CDCl_3$): δ = 11.83 (s, 1 H), 11.70 (s, 1 H), 11.58 (s,

1 H), 11.55 (s, 1 H), 11.34 (s, 1 H), 8.77 (dd, J = 4.3, 1.5 Hz, 2 H), 8.63 (dd, J = 7.7, 1.2 Hz, 1 H), 8.31 (d, J = 7.8 Hz, 1 H), 8.24 (d, J = 7.7 Hz, 1 H), 8.13 (d, J = 8.6 Hz, 1 H), 8.04 (dd, J = 8.3, 1.1 Hz, 1H), 8.01-7.92 (m, 4 H), 7.80 (s, 1 H), 7.73-7.58 (m, 4 H), 7.55 (dd, J = 4.5, 1.5 Hz, 2 H), 7.43 (s, 1 H), 7.38-7.29 (m, 4 H), 7.07 (t, J = 8.0 Hz, 1 H), 6.99 (s, 1 H), 6.86 (s, 1 H), 6.77 (s, 1 H), 6.43 (s, 1 H), 4.43 (m, 1 H), 4.20 (m, 1 H), 4.12-4.05 (m, 2 H), 4.01-3.83 (m, 6 H), 3.18 (s, 3 H), 2.60-2.35 (m, 5 H), 1.35-1.22 (m, 24 H), 1.11 (d, J = 6.7 Hz, 6 H), 1.05 (s, 9 H) ppm; ^{13}C NMR (75 MHz, $CDCl_3$): δ = 163.8, 163.3, 163.1, 163.0, 162.8, 161.6, 161.4, 161.1, 160.8, 159.4, 151.6, 150.4, 150.3, 149.5, 149.3, 148.9, 148.8, 143.5, 138.5, 138.0, 137.9, 137.7, 136.7, 134.8, 134.1, 133.9, 133.6, 133.4, 132.7, 130.4, 130.1, 129.1, 128.1, 127.2, 127.0, 126.6, 125.8, 123.6, 122.7, 122.2, 122.2, 122.0, 121.8, 119.7, 117.4, 117.2, 117.1, 116.7, 116.6, 116.3, 116.2, 116.1, 115.6, 114.7, 114.5, 99.8, 98.8, 98.3, 98.1, 97.8, 95.6, 88.9, 80.4, 75.7, 75.5, 75.4, 75.4, 75.4, 75.3, 52.2, 28.5, 28.4, 28.4, 28.3, 28.1, 27.8, 19.7, 19.6, 19.6, 19.6, 19.5, 19.5, 19.4, 19.3 ppm.

Compound **39**: This compound was prepared according to the same procedure as compound **6**. Yield: quantitative.^{1}H NMR (300 MHz, $CDCl_3$): δ = 11.86 (s, 1 H), 11.73 (s, 1 H), 11.65 (s, 1 H), 11.45 (s, 1 H), 11.43 (s, 1 H), 8.76 (dd, J = 4.4, 1.5 Hz, 2 H), 8.64 (dd, J = 7.7, 1.2 Hz, 1 H), 8.36 (dd, J = 7.8, 1.2 Hz, 1 H), 8.20 (dd, J = 7.6, 1.1 Hz, 1 H), 8.11 (dd, J = 8.3, 1.2 Hz, 1 H), 8.04-7.98 (m, 4 H), 7.95 (dd, J = 8.4, 1.2 Hz, 1 H), 7.70 (t, J = 7.9 Hz, 1 H), 7.62 (t, J = 8.0 Hz, 1 H), 7.54 (dd, J = 7.8, 1.2 Hz, 1 H), 7.54 (dd, J = 4.6, 1.5 Hz, 2 H), 7.40 (t, J = 7.9 Hz, 1 H), 7.38 (s, 1 H), 7.37 (dd, J = 3.1, 2.0 Hz, 1 H), 7.34 (s, 1 H), 7.31 (t, J = 7.8 Hz, 1 H), 6.99 (s, 1 H), 6.91 (t, J = 8.0 Hz, 1 H), 6.87 (s, 1 H), 6.79 (s, 1 H), 6.56 (s, 1 H), 5.81 (dd, J = 7.4, 1.1 Hz, 1 H), 4.42 (m, 1 H), 4.20 (m, 1 H), 4.11 (m, 1 H), 4.05-3.98 (m, 3 H), 3.93-3.80 (m, 4 H), 3.39 (br, 2 H), 3.19 (s, 3 H), 2.59-2.25 (m, 5 H), 1.34-1.22 (m, 24 H), 1.09 (d, J = 6.7 Hz, 6 H) ppm.

Compound **41** (**L5**): This compound was prepared according to the same procedure as compound **13**. Yield: 35 mg (13 %).^{1}H NMR (300 MHz, $CDCl_3$): δ = 11.40 (s, 2 H), 11.13 (s, 2 H), 11.09 (s, 2 H), 10.63 (s, 2 H), 10.39 (s, 2 H), 8.70 (dd, J = 4.6, 1.5 Hz, 4 H), 8.06 (d, J = 7.6 Hz, 2 H), 8.03 (d, J = 7.6 Hz, 2 H), 7.92 (d, J = 8.4 Hz, 2 H), 7.78 (d, J = 8.4 Hz, 2 H),

7.74-7.69 (m, 4 H), 7.52 (d, J = 7.6 Hz, 2 H), 7.45-7.37 (m, 12 H), 7.30 (d, J = 8.1 Hz, 4 H), 7.20 (dd, J = 7.6, 1.0 Hz, 2 H), 7.15 (s, 2 H), 7.09 (s, 2 H), 7.09 (t, J = 7.4 Hz, 2 H), 7.02-6.94 (m, 8 H), 6.64 (d, J = 8.1 Hz, 2 H), 6.45 (s, 2 H), 6.31 (s, 2 H), 6.04 (s, 2 H), 6.03 (s, 2 H), 5.81 (s, 1 H), 4.00-3.90 (m, 4 H), 3.75-3,52 (m, 16 H), 2.86 (s, 6 H), 2.47-2.13 (m, 10 H), 1.36 (d, J = 6.6 Hz, 6 Hz), 1.29-1.21 (m, 18 H), 1.16-1.08 (m, 36 H) ppm; ^{13}C NMR (75 MHz, $CDCl_3$): δ = 162.8, 162.6, 162.6, 162.5, 161.5, 161.5, 160.9, 160.6, 159.3, 158.7, 158.7, 158.6, 150.2, 148.5, 148.3, 148.0, 147.6, 147.4, 147.1, 143.1, 141.3, 137.9, 137.7, 137.2, 137.1, 136.7, 136.2, 135.5, 134.4, 133.2, 132.7, 132.6, 132.1, 131.9, 130.3, 129.9, 128.7, 127.9, 127.6, 126.6, 126.1, 126.0, 125.9, 125.7, 123.3, 121.9, 121.6, 121.2, 120.7, 120.7, 119.4, 119.0, 117.1, 117.0, 117.0, 116.7, 116.5, 116.4, 115.9, 115.7, 115.2, 115.0, 98.4, 97.8, 97.6, 96.9, 95.3, 88.8, 75.2, 75.1, 52.0, 28.3, 28.3, 28.2, 27.9, 20.0, 19.7, 19.6, 19.6, 19.5, 19.4, 19.3 ppm.

References

(1) Fujita, M.; Fujita, N.; Ogura, K.; Yamaguchi, K. *Nature* **1999**, *400*, 52-55.

(2) Inokuma, Y.; Arai, T.; Fujita, M. *Nat. Chem.* **2010**, *2*, 780.

(3) Northrop, B. H.; Yang, H.-B.; Stang, P. J. *Chem. Commun.* **2008**, 5896-5908.

(4) Seidel, S. R.; Stang, P. J. *Acc. Chem. Res.* **2002**, *35*, 972-983.

(5) Albrecht, M. *Chem. Rev.* **2001**, *101*, 3457-3498.

(6) Chakrabarty, R.; Mukherjee, P. S.; Stang, P. J. *Chem. Rev.* **2011**, *111*, 6810-6918.

(7) Yamauchi, Y.; Yoshizawa, M.; Fujita, M. *J. Am. Chem. Soc.* **2008**, *130*, 5832-5833.

(8) Hellinga, H. W. *Curr. Opin. Biotechnol.* **1996**, *7*, 437-441.

(9) Mocny, C. S.; Pecoraro, V. L. *Acc. Chem. Res.* **2015**, *48*, 2388-2396.

(10) Salgado, E. N.; Radford, R. J.; Tezcan, F. A. *Acc. Chem. Res.* **2010**, *43*, 661-672.

(11) Brodin, J. D.; Ambroggio, X. I.; Tang, C.; Parent, K. N.; Baker, T. S.; Tezcan, F. A. *Nat. Chem.* **2012**, *4*, 375.

(12) Song, W. J.; Tezcan, F. A. *Science* **2014**, *346*, 1525-1528.

(13) Song, W. J.; Yu, J.; Tezcan, F. A. *J. Am. Chem. Soc.* **2017**, *139*, 16772-16779.

(14) Churchfield, L. A.; Alberstein, R. G.; Williamson, L. M.; Tezcan, F. A. *J. Am. Chem. Soc.* **2018**, *140*, 10043-10053.

(15) Churchfield, L. A.; Medina-Morales, A.; Brodin, J. D.; Perez, A.; Tezcan, F. A. *J. Am. Chem. Soc.* **2016**, *138*, 13163-13166.

(16) Churchfield, L. A.; Tezcan, F. A. *Acc. Chem. Res.* **2019**, *52*, 345-355.

(17) Sawada, T.; Yamagami, M.; Ohara, K.; Yamaguchi, K.; Fujita, M. *Angew. Chem. Int. Ed.* **2016**, *55*, 4519-4522.

(18) Jiang, H.; Léger, J.-M.; Huc, I. *J. Am. Chem. Soc.* **2003**, *125*, 3448-3449.

(19) Cook, T. R.; Vajpayee, V.; Lee, M. H.; Stang, P. J.; Chi, K.-W. *Acc. Chem. Res.* **2013**, *46*, 2464-2474.

(20) Kendhale, A. M.; Poniman, L.; Dong, Z.; Laxmi-Reddy, K.; Kauffmann, B.; Ferrand, Y.; Huc, I. *The Journal of Organic Chemistry* **2011**, *76*, 195-200.

(21) Delsuc, N.; Kawanami, T.; Lefeuvre, J.; Shundo, A.; Ihara, H.; Takafuji, M.; Huc, I. *ChemPhysChem* **2008**, *9*, 1882-1890.

(22) Bonakdarzadeh, P.; Topić, F.; Kalenius, E.; Bhowmik, S.; Sato, S.; Groessl, M.; Knochenmuss, R.; Rissanen, K. *Inorg. Chem.* **2015**, *54*, 6055-6061.